Functional Evaluation of Smad4 Disruption in Mouse Intestinal Adenoma



Mirvat Surakhy

Jesus College

University of Oxford

A thesis submitted for the degree of

Doctor of Philosophy

Trinity 2015

Acknowledgements

First of all I would like to express gratitude for God for the confidence, power and endurance he gave me throughout my life and studying period.

Second and foremost I want to express my deeply-felt and sincere gratitude to Professor Bass Hassan, for giving me the opportunity to join his research group at the Sir William Dunn Dunn School of Pathology. My thanks also go to my departmental advisor Dr. Kevin Maloy and my college advisor Prof. Paul Riley for their guidance throughout my degree.

Of course, this work would not exist without the support of all the colleagues in the Hassan lab. With special thanks to David Barnes for his assistance and RNA-seq analysis and to Andrea Baines for all the support she gave. Thanks to Julia, a former student in the lab, who has started the project. Thanks to all the lab members (former and ex-members); Susanna, Sabina, Emma, Jen, Claudia, Hans, Harriet, Mehak and Sermet for their support, help and being nice friends.

Thanks to all the people in the Dunn School with special thanks to the PSB staff especially Linda Randall and Nicky Hamp for all their support, Prof Elizabeth Robertson for the mouse model, Richard Stillion for his expertise in preparing the histological slides and the required staining and Alan Wainman for his assistance with the microscopes when required.

I would like to acknowledge the Islamic Development bank (IDB) for their generous scholarship, the Dunn School for financial support and to Cancer Research UK for providing core lab funding.

Huge thanks to my husband and my children; Ibrahim, Ala', Aya and lovely Dania who have supported me and for being patient during the long hours of being away from them. My thanks also to Mum, Dad, brothers and sisters for their moral support.

Functional Evaluation of Smad4 Disruption in Mouse Intestinal Adenoma

Submitted for the degree of Doctor of Philosophy

Mirvat Surakhy, Jesus College, Trinity 2015

Abstract

Human colorectal cancer (CRC) is one of the most common types of cancer. Aberrant activation of the Wnt pathway, typically via adenomatous polyposis coli (*Apc*) loss of function, acts as the initiating event for adenoma formation. However, alterations in additional pathways are associated with progression towards CRC. For example, 10-15% of carcinomas downregulate the transforming growth factor-β (TGF-β) pathway due to SMAD4 mutations in either the MH1 domain, the linker or the MH2 domain. The growth advantages of Smad4 mutations and their contribution to the switch from a tumour suppressor effect of TGF-β to a tumour promoter are as yet poorly understood. The aim of this thesis was to evaluate the functional consequences of Smad4 loss of function on intestinal tumorigenesis in the context of active Wnt signalling in mouse conditional models of human CRC.

Apc$^{fl/fl}$*Smad4*$^{fl/fl}$*Lgr5-EGF-IRES-CreERT2* (*Smad4*$^{fl/fl}$) mouse models were generated by breeding, and tamoxifen mediated Cre-activation allowed conditional deletions to be made in the intestinal stem cell compartment. The functional consequences of Smad4 MH1 loss of function on adenoma growth were evaluated using intestinal adenoma culture. The effects of TGF-β1 on Smad4 disrupted organoids were also evaluated. Comprehensive gene expression was then performed to evaluate changes in transcriptome profiling according to Smad4 status in the presence or absence of TGF-β1.

Mice that had both *Apc* and *Smad4* genes disrupted in the Lgr5 compartment showed enhanced survival, reduced small intestinal adenoma burden, and large caecal tumours. Dysplastic histology with signs of inflammation were observed within tumours. *In vitro*, *Smad4*$^{fl/fl}$ adenomas displayed slow growth that was rescued with the Rock inhibitor, Y-27632. Gene set enrichment analysis (GSEA) of RNA-Seq showed that these adenomas might be autoregulating the TGF-β pathway by upregulating *Tgfb1* expression, differentially regulating genes associated with differentiation, inflammation, in addition to enhancing the Wnt pathway by upregulating β-*catenin*. The upregulation of Muc2 expression in these adenomas was validated from *Smad4*$^{fl/fl}$ tissue sections. Gene ontology analysis suggested that Smad4 disruption affects the cytostatic function of TGF-β by differentially regulating genes involved in the cell cycle and proliferation. In *Smad4*$^{fl/fl}$ adenomas, resistance to TGF-β tumour suppressor effect was confirmed by a higher IC_{50}, higher fraction of proliferative cells, *c-Myc* upregulation, and Survivin modulation following TGF-β1 treatment. Smad4 disruption had no effect on epithelial-mesenchymal transition under the concentration of TGF-β1 used but was associated with enhanced migration in Matrigel.

In conclusion, Smad4 disruption in intestinal adenomas affects control of the tumour microenvironment and creates suitable conditions for inflammation. It alters tumour sensitivity to TGF-β1 and thus interferes with the tumour suppressor and tumour promoter effects of the TGF-β pathway. Further validation is required to determine whether the observed phenotypes are dependent on Smad2/3 transcriptional activity, concentration of TGF-β1 used, and can be rescued with Smad4 complementation.

Contents

1 Introduction **3**
1.1 Introduction . . . 3
1.2 The intestinal epithelium and homeostasis . . . 4
1.3 The Wnt pathway . . . 7
1.3.1 Wnt proteins, agonists and regulators . . . 7
1.3.2 Wnt/β-catenin signalling . . . 8
1.3.3 Wnt pathway in intestinal tumorigenesis . . . 8
1.4 Transforming growth factor-β pathway . . . 11
1.4.1 TGF-β Receptors . . . 12
1.4.2 Smad proteins . . . 14
1.4.2.1 Smad functional domains . . . 14
1.4.2.2 Smad interaction . . . 18
1.4.3 TGF-β pathway regulation . . . 19
1.4.4 Non-canonical TGF-β signalling . . . 20
1.4.5 TGF-β/BMP in intestinal homeostasis and disease . . . 21
1.4.5.1 *Smad4* mutations in CRC . . . 21
1.4.5.2 Mutations in the TGF-β and BMP pathway other than *Smad4* . . . 22
1.4.6 Tumour microenvironment and TGF-β . . . 23
1.4.7 Mucinous adenocarcinoma . . . 23
1.5 Modelling intestinal tumorigenesis . . . 25
1.5.1 Mouse models . . . 26
1.5.1.1 Mouse intestinal models altered in the TGF-β pathway . . . 27
1.5.2 *In vitro* intestinal organoid culture and cell lines . . . 28
1.6 Aims . . . 30

2 Materials and methods **32**
2.1 Genetically modified mice . . . 32
2.1.1 Animal husbandry . . . 32
2.1.2 Genetic models and strain background . . . 32
2.1.3 Mouse breeding . . . 32
2.1.3.1 Breeding strategy for Smad4 adenoma model and adenoma culture 33
2.1.3.2 Breeding for *Igf2r*$^{I1565Amaternal/+paternal}$ (*Igf2r*$^{I1565Am/+p}$) adenoma model 33
2.1.3.3 Breeding to generate adenoma using genetic manipulation . . . 33
2.1.4 Tamoxifen injection . . . 34
2.1.5 Mouse dissection . . . 34
2.1.5.1 Intestinal tissue for adenoma count and histology . . . 34
2.1.6 Intestinal tissue collection for culture . . . 39
2.1.6.1 Intestinal tissue collection for adenoma culture . . . 39
2.1.6.2 Intestinal tissue collection for crypt culture . . . 39
2.2 Identification and Genotyping . . . 39
2.2.1 Material collection . . . 39
2.2.2 Genomic DNA isolation . . . 40

2.2.3 Genotyping by polymerase chain reaction (PCR) . . . 40
2.2.4 Gel electrophoresis . . . 40
2.2.5 DNA sequencing . . . 41
2.2.6 DNA quality and quantity assessment . . . 41
2.3 Intestinal adenoma counting and scoring . . . 41
2.4 General histology and tissue staining . . . 42
2.5 Adenoma culture . . . 42
2.5.1 Adenoma extraction . . . 42
2.5.2 Adenoma counting . . . 43
2.5.3 Adenoma culture in Matrigel . . . 43
2.5.3.1 Supplements for adenoma growth measurement . . . 43
2.5.3.2 Supplement for protein and RNA extraction . . . 44
2.5.4 Adenoma freezing and thawing . . . 44
2.5.4.1 Freezing growing adenomas . . . 44
2.5.4.2 Freezing adenomas directly after extraction . . . 46
2.5.4.3 Adenoma thawing and culture . . . 46
2.5.5 Passaging adenomas in culture . . . 46
2.6 Intestinal crypt culture . . . 47
2.6.1 Intestinal crypt isolation and culture . . . 47
2.6.1.1 Crypt culture supplements . . . 48
2.6.2 Genetic manipulation of intestinal organoids . . . 48
2.6.3 Passaging crypt derived organoids . . . 49
2.7 Tissue and cell labelling . . . 49
2.7.1 Tissue processing . . . 49
2.7.1.1 Immunohistochemistry . . . 49
2.7.1.2 Immunofluorescence . . . 50
2.7.2 Cell labelling . . . 50
2.7.2.1 Immunofluorescence . . . 50
2.7.3 F-actin labelling . . . 52
2.7.4 Nuclear labelling and mounting . . . 52
2.7.5 EdU labelling . . . 52
2.7.6 Image acquisition and analysis . . . 53
2.8 AlamarBlue for adenoma growth . . . 53
2.9 Western blots . . . 54
2.9.1 Protein extraction . . . 54
2.9.1.1 Protein extraction from organoids . . . 54
2.9.1.2 Protein extraction from cell lines . . . 55
2.9.2 Protein quantification . . . 55
2.9.3 SDS-PAGE electrophoresis and immunoblotting . . . 55
2.9.4 Western blot analysis . . . 56
2.10 RNA preparation for RNA-seq and miRNA-seq . . . 56
2.10.1 RNA extraction . . . 57
2.10.2 RNA quality and quantity assessment . . . 57
2.10.3 RNA concentration . . . 57
2.10.4 RNA-seq and miRNA processing . . . 58
2.11 Cell lines . . . 58
2.12 Constructs for the luciferase assay . . . 59
2.12.1 Long-term storage of plasmids . . . 59
2.12.2 Miniprep and maxiprep . . . 59
2.13 Statistical analysis . . . 60

3 *In vivo* models for TGF-β and IGF2 in intestinal tumorigenesis **61**
3.1 Introduction . . . 61
3.1.1 Pathways altered in intestinal tumorigenesis . . . 63
3.1.1.1 Wnt/β-catenin pathway . . . 63
3.1.1.2 Function of TGF-β/Smad4 pathway . . . 64
3.1.1.3 PI3K, RAS-MAPK Igf2/Igf2r pathway . . . 67
3.2 Rationale for study . . . 68
3.3 Materials and methods . . . 68
3.3.1 Mouse models . . . 68
3.3.2 Mouse breeding . . . 69
3.3.3 Genotyping . . . 69
3.3.4 Tamoxifen injection and mouse dissection . . . 69
3.3.5 Intestinal tissue collection, adenoma count and histology . . . 69
3.4 Results . . . 69
3.4.1 *In vivo* $Apc^{fl/fl}$ $Smad4^{fl/fl}$ *Lgr5-CreERT2* adenoma model . . . 69
3.4.1.1 Improved survival, development of large caecal tumour and reduced small intestinal adenoma burden in $Apc^{fl/fl}$ $Smad4^{fl/fl}$ mice . . . 70
3.4.1.2 $Apc^{fl/fl}$ $Smad4^{fl/fl}$ tumours lack Smad4 protein . . . 72
3.4.1.3 Histopathology of $Apc^{fl/fl}$ $Smad4^{fl/fl}$ tumours . . . 72
3.4.1.4 Does inflammation trigger adenoma formation? . . . 76
3.4.2 *In vivo* $Apc^{fl/fl}$ $Igf2r^{I1565Am/+p}$ *Lgr5-CreERT2* adenoma model . . . 80
3.4.2.1 Deviation from Mendelian ratio in progeny of $Igf2r^{I1565Am/+p}$ mating . 80
3.4.2.2 Decreased survival of $Apc^{fl/fl}$ $Igf2r^{I1565Am/+p}$ animals following tamoxifen injection . . . 81
3.4.2.3 $Apc^{fl/fl}$ $Igf2r^{I1565Am/+p}$ *Lgr5-CreERT2* histology . . . 83
3.5 Discussion . . . 85
3.5.1 $Apc^{fl/fl}$ $Smad4^{fl/fl}$ adenoma model . . . 85
3.5.2 $Apc^{fl/fl}$ $Igf2r^{I1565Am/+p}$ adenoma model . . . 87

4 Intestinal Organoid Culture **89**
4.1 Introduction . . . 89
4.2 Rationale for study . . . 91
4.3 Materials and methods . . . 91
4.3.1 Mouse models . . . 91
4.3.2 Mouse breeding . . . 91
4.3.3 Genotyping . . . 91
4.3.4 Mouse dissection and tissue collection . . . 92
4.3.5 Adenoma culture . . . 92
4.3.6 Crypt culture and genetic manipulation . . . 92
4.3.7 Immunolabelling . . . 92
4.3.8 Growth and proliferation assay . . . 92
4.3.9 Image acquisition . . . 92
4.4 Results . . . 97
4.4.1 $Apc^{fl/fl}$ *Lgr5-CreERT2* adenoma growth is Noggin independent . . . 97
4.4.2 Crypt culture and mouse intestinal organoid growth is Noggin dependent . . . 99
4.4.3 Genetic manipulation of conditional crypt culture and adenoma formation *in vitro* . . . 101
4.4.3.1 Expression of *Rosa26-YFP* and upregulation of Wnt/β-catenin following intestinal organoid manipulation . . . 103
4.4.4 Adenoma culture optimisation . . . 106
4.4.4.1 TryplE Express is better for adenoma extraction . . . 106
4.4.4.2 Viability assay to measure adenoma growth . . . 106
4.4.4.3 Storage and passage of growing adenoma . . . 108

4.4.4.4 Freshly extracted adenomas can be frozen directly and recovery of cryopreserved adenomas can be enhanced with TGF-β inhibitor and Rock inhibitor . . . 108
4.4.4.5 Enhanced growth of passaged adenomas by Rock inhibitor and TGF-β inhibitor . . . 109
4.5 Discussion . . . 114
4.5.1 Organoid culture optimisation shows different Noggin requirements . . . 114
4.5.2 Adenoma formation *in vitro* from conditional crypt culture . . . 115
4.5.3 *Apc*$^{fl/fl}$*Lgr5-CreERT2 in vitro* adenoma model optimisation . . . 117
4.5.3.1 AlamarBlue: a cell viability assay to measure adenoma growth . . . 117
4.5.3.2 Adenoma storage and passage . . . 118

5 TGF-β/Smad4 signalling 121
5.1 Introduction . . . 121
5.1.1 TGF-β tumour suppressor effect . . . 122
5.1.2 TGF-β tumour promoter effect . . . 124
5.2 Rationale for the study . . . 126
5.3 Materials and methods . . . 127
5.3.1 Mouse models . . . 127
5.3.2 Mouse breeding . . . 127
5.3.3 Genotyping . . . 127
5.3.4 Mouse dissection and tissue collection . . . 127
5.3.5 Adenoma culture . . . 127
5.3.6 Crypt culture and genetic manipulation . . . 127
5.3.7 Immunolabelling . . . 128
5.3.8 Growth and proliferation assay . . . 128
5.3.9 Image acquisition . . . 128
5.4 Results . . . 128
5.4.1 Cultured adenoma and genetically manipulated intestinal organoids lack *Smad4* 128
5.4.1.1 *Lgr5-CreERT2* and *Villin-CreERT2* adenoma characterisation . . . 129
5.4.2 Slow growth of *Apc*$^{fl/fl}$*Smad4*$^{fl/fl}$ adenomas . . . 133
5.4.3 Y-27632 rescued the slow growth of *Apc*$^{fl/fl}$*Smad4*$^{fl/fl}$ adenomas . . . 135
5.4.4 Effect of passage and freezing on *Apc*$^{fl/fl}$*Smad4*$^{fl/fl}$ growth . . . 136
5.4.5 Characterisation of Wnt signalling in *Apc*$^{fl/fl}$*Smad4*$^{fl/fl}$ adenoma . . . 140
5.4.6 MH1 deletion in *Apc*$^{fl/fl}$*Smad4*$^{fl/fl}$ following Cre-mediated recombination . . . 140
5.4.7 Nuclear localisation of R-Smads with TGF-β1 treatment in *Apc*$^{fl/fl}$ *Smad4*$^{fl/fl}$ adenomas . . . 142
5.4.8 TGF-β1 induced growth inhibition of the adenomas . . . 146
5.4.9 Smad4 is not required for EMT . . . 153
5.4.10 Effect of TGF-β1 on Wnt/β-catenin pathway . . . 154
5.5 Discussion . . . 164
5.5.1 *In vitro* adenomas mimic the *in vivo* adenomas . . . 164
5.5.2 *Apc*$^{fl/fl}$*Smad4*$^{fl/fl}$ slow growth . . . 164
5.5.3 MH1 deletion in Smad4 protein after Cre-mediated recombination . . . 166
5.5.4 Nuclear localisation of R-Smad in *Apc*$^{fl/fl}$*Smad4*$^{fl/fl}$ adenomas with TGF-β1 treatment . . . 167
5.5.5 The effect of TGF-β1 on *Smad4*$^{+/+}$ and *Smad4*$^{fl/fl}$ adenomas . . . 168
5.5.5.1 TGF-β1 induced growth inhibition in adenomas . . . 169
5.5.5.2 Smad4 is not required for EMT . . . 170
5.5.5.3 Effect of TGF-β/Smad4 on the Wnt/β-catenin pathway . . . 171

6 RNA-seq and microRNA-seq **174**
6.1 Introduction . . . 174
6.1.1 Smad DNA-binding and transcription regulation . . . 175
6.1.2 Crosstalk between TGF-β and Wnt/β-catenin pathways . . . 176
6.1.2.1 MicroRNA . . . 177
6.1.3 RNA-seq . . . 178
6.2 Rationale for the study . . . 179
6.3 Materials and methods . . . 179
6.3.1 Adenoma culture and passage . . . 179
6.3.2 RNA experiment preparation . . . 179
6.3.3 RNA analysis . . . 179
6.3.4 Rationale for using Gene Set Enrichment Analysis . . . 181
6.3.4.1 Gene Set Enrichment Analysis as applied to the RNA-Seq data from this project . . . 182
6.3.4.2 MiRNA-seq analysis . . . 183
6.4 Results . . . 184
6.4.1 Differentially expressed genes at the basal level in $Apc^{fl/fl}Smad4^{fl/fl}$ adenomas 184
6.4.1.1 Mucin pools in tissue sections from $Apc^{fl/fl}Smad4^{fl/fl}$ mice . . . 191
6.4.2 Gene regulation in response to TGF-β1 treatment . . . 193
6.4.2.1 Transcriptome of $Apc^{fl/fl}Smad^{+/+}$ adenomas . . . 193
6.4.2.2 *Smad4* is a tumour suppressor . . . 205
6.4.3 Survivin modulation with TGF-β1 as validation to the RNA-seq data . . . 206
6.4.4 Promoter analysis for the identification of Smad4 target genes in differentially regulated genes . . . 219
6.4.4.1 Smad4 dependent and independent genes . . . 219
6.4.4.2 *Serpine1* and Smad4 dependency . . . 220
6.4.5 MiRNA in intestinal adenomas . . . 220
6.5 Discussion . . . 226
6.5.1 Differentially regulated genes at the basal level . . . 226
6.5.1.1 c-Myc enrichment . . . 226
6.5.1.2 TGF-β pathway autoregulation and possible link to inflammation with Smad4 deletion . . . 226
6.5.1.3 *Smad4* deletion increased β-*Catenin* expression . . . 228
6.5.1.4 Upregulation of mucin family members in $Apc^{fl/fl}Smad4^{fl/fl}$ . . . 228
6.5.2 Normal response to TGF-β1 in $Smad4^{+/+}$ adenomas . . . 230
6.5.3 Differential regulation of the cytostatic and apoptotic effect of TGF-β1 . . . 230
6.5.3.1 Novel genes in RNA-seq data . . . 232
6.5.3.2 Modulation of *Birc5* in response to TGF-β1 . . . 232
6.5.4 Are miRNAs contributors to intestinal tumorigenesis? . . . 233

7 Discussion and Future Directions **235**
7.1 Summary . . . 235
7.2 Discussion and future directions . . . 236
7.2.1 Altered tumour position in $Apc^{fl/fl}Smad4^{fl/fl}$*Lgr5-CreERT2* is a possible link to inflammation . . . 236
7.2.2 Are motility and migration Smad4 dependent or pathway dependent? . . . 239
7.2.3 Is the phenotype in this study related to Smad4 MH1 deletion . . . 240
7.3 Are R-Smads regulating genes in the absence of Smad4? . . . 241
7.4 Future work . . . 243
7.4.1 Preliminary results . . . 244
7.4.1.1 Nuclear localisation of R-Smad and Colo205 lacks truncated Smad4 244
7.4.2 EMT, β-catenin and and Survivin in Colo205 . . . 246
7.4.3 Discussion . . . 246

A Appendix **248**

Bibliography **255**

List of Figures

1.1 Mammalian small intestine and colon . . . 6
1.2 Wnt/β signalling . . . 9
1.3 TGF-β signalling pathway . . . 15
1.4 Smad transcription factors . . . 17
1.5 TGF-β and BMP in intestinal homeostasis and disease . . . 24

2.1 Experimental breeding to generate *Apc*$^{fl/fl}$, *Smad4*$^{fl/fl}$, *Lgr5-CreERT2*, *Rosa26-YFP* adenoma model. . . . 35
2.2 Experimental breeding to generate *Apc*$^{fl/fl}$, *Igf2r*$^{I1565Am/+p}$, *Lgr5-CreERT2* adenoma model. . . . 36
2.3 Experimental breeding to generate *Apc*$^{fl/fl}$, *Smad4*$^{fl/fl}$, *Villin-CreERT2*, *Rosa26-YFP* adenoma model. . . . 37

3.1 Intestinal tumorigenesis . . . 62
3.2 *Apc*$^{fl/fl}$*Smad4*$^{fl/fl}$ mice had better survival with large caecal tumour and reduced small intestinal adenoma burden . . . 71
3.3 Absence of Smad4 protein from caecal tumours of *Smad4*$^{fl/fl}$ mice . . . 73
3.4 Apc Smad4 Lgr5-Cre small intestine histology . . . 74
3.5 *Apc Smad4 Lgr5-CreERT2* caecal histology with crypt abscesses . . . 75
3.6 F4/80^{+} and CD11b^{+} cells in the stroma . . . 77
3.7 CD3 infiltrate . . . 78
3.8 Active TGF-β pathway in the epithelium and stroma in tissue sections from *Smad4*$^{fl/fl}$ mice . . . 79
3.9 Survival, adenoma count and distribution in *Apc*$^{fl/fl}$*Igf2r*^{I1565A}*Lgr5-CreERT2* adenoma model . . . 82
3.10 *Apc*$^{fl/fl}$ *Igf2r*$^{I1565Am/+p}$ *Lgr5-CreERT2* histology . . . 84

4.1 Intestinal adenoma culture flow chart. . . . 93
4.2 Intestinal adenoma passage flow chart. . . . 94
4.3 Intestinal crypt culture and genetic manipulation flow chart . . . 95
4.4 Intestinal crypt derived organoids passaging. . . . 96
4.5 *Apc*$^{fl/fl}$*Lgr5-Cre* in 3D culture . . . 98
4.6 Crypt culture and mouse intestinal organoid growth is Noggin dependent . . . 100
4.7 Genetic manipulation of conditional intestinal organoids and adenoma formation in 5 days. . . . 102
4.8 Expression of *Rosa26-YFP* following intestinal organoid manipulation . . . 104
4.9 Cytoplasmic β-catenin in *Apc*$^{fl/fl}$*Villin-CreERT2* adenomas . . . 105
4.10 Effect of different extraction enzymes on adenoma growth . . . 107
4.11 Growing adenomas can be passaged and frozen . . . 110
4.12 Recovery of fresh frozen adenomas . . . 111
4.13 10% DMSO enhanced the viability of frozen adenoma . . . 111
4.14 TGF-β inhibitor and Rock inhibitor enhanced the recovery of frozen adenoma . . . 112
4.15 Passage of *Apc*$^{fl/fl}$ adenoma . . . 113

5.1 Cultured adenoma and genetically manipulated intestinal organoids lack *Smad4* . . 130
5.2 Upregulation of Muc2 in *Apc*$^{fl/fl}$*Smad4*$^{fl/fl}$*Lgr5-CreERT2* adenomas 131
5.3 Similar proportion of EdU incorporation in the different adenoma models 132
5.4 Slow growth of *Apc*$^{fl/fl}$*Smad4*$^{fl/fl}$ adenoma that is Noggin independent 134
5.5 Y-27632 rescued the slow growth of *Apc*$^{fl/fl}$*Smad4*$^{fl/fl}$ adenoma growth 137
5.6 Significant effect of Y-27632 on the recovery of *Smad4*$^{fl/fl}$ growth without EGF 138
5.7 Effect of freezing and passaging on *Smad4*$^{fl/fl}$ adenoma growth 139
5.8 MH1 deletion in *Smad4*$^{fl/fl}$ following Cre-mediated recombination 141
5.9 TGF-β1 signalling in *Apc*$^{fl/fl}$*Smad4*$^{fl/fl}$ adenomas 143
5.10 Nuclear localisation of R-Smads with TGF-β1 stimulation 144
5.11 Y-27632 did not block p-R-Smad in response to TGF-β1 145
5.12 TGF-β1 induced growth inhibition of the adenomas that can be rescued with SB-505124 148
5.13 Morphological changes of adenoma following TGF-β1 treatment 149
5.14 Decrease in adenoma proliferation with TGF-β1 150
5.15 Positive cleaved caspase-3 labelling in *Smad4*$^{+/+}$ and *Smad4*$^{fl/fl}$ adenomas with TGF-β1 151
5.16 Transformed adenomas expressed Rosa26-YFP 152
5.17 TGF-β1 upregulated fibronectin within 12h 155
5.18 Morphological changes after 24h TGF-β1 156
5.19 Morphological changes after 48h TGF-β1 157
5.20 Morphological changes after 72h TGF-β1 158
5.21 Morphological changes after 96h TGF-β1 159
5.22 Cadherin switch with TGF-β1 160
5.23 Vimentin and F-actin labelling following TGF-β1 treatment 161
5.24 Changes in the expression of Wnt/β-catenin genes by TGF-β1. 162
5.25 Cytoplasmic and nuclear β-catenin with E-cadherin loss following TGFβ-1 treatment. 163

6.1 Flow chart summarises the different steps conducted for the RNA-seq and miRNA-seq experiments 180
6.2 Differentially expressed genes in adenomas from RNA-seq data with fold difference at the basal level 186
6.3 Identification of common genes in different sets. 189
6.4 Mucins in *Apc*$^{fl/fl}$*Smad4*$^{fl/fl}$. 192
6.5 Early and late response genes differentially regulated in *Smad*$^{+/+}$ adenomas with TGF-β1 treatment 195
6.6 Differential regulation of gene expression represented by Venn diagrams 207
6.7 Heat maps of *Smad4*$^{fl/fl}$ compared to *Smad4*$^{+/+}$ 208
6.8 Survivin modulation by TGF-β1 in *Smad4*$^{fl/fl}$ adenomas 218
6.9 Core enriched genes promoter analysis 221
6.10 Steps implemented for the identification of Smad4 independent genes 222
6.11 Significant miRNA expression in adenomas 225
6.12 Venn diagrams for DEG in *Smad4*$^{fl/fl}$ adenomas compared to *Smad4*$^{+/+}$ at 0h, 1h and 12h of TGF-β1 234

7.1 TGF-β signalling in Colo205 245
7.2 EMT and Survivin following TGF-β1 treatment 247

A.1 Wnt/β-catenin upregulated genes in *Apc*$^{fl/fl}$ adenomas 251
A.2 Optimisation of AB viability assay to measure adenoma growth 252
A.3 Adenoma growth is independent on Matrigel batch. 253
A.4 Confocal images for Wnt/β-catenin genes expression 254

List of Tables

1 List of abbreviations 1

1.1 *Apc* mouse models 13

2.1 Genetic models and strain background 33
2.2 Symptom and sign score sheet (humane end point monitoring) 38
2.3 Reagents for crypt and adenoma culture 45
2.4 Primary antibodies for immunofluorescence and immunohistochemistry 51
2.5 Secondary antibodies for immunofluorescence and immunohistochemistry 52
2.6 Antibodies for western blots 56

3.1 Characteristic phenotypes of different mouse models for intestinal tumorigenesis with *Smad4* mutations. 66
3.2 Mendelian segregation of progeny from *Igf2r*^{I1565A} mating 81

6.1 Description of the top 50 DEG in *Apc*$^{fl/fl}$*Smad4*$^{fl/fl}$ adenomas at the basal level compared to *Apc*$^{fl/fl}$*Smad4*$^{+/+}$ 187
6.2 Gene set enrichment in *Apc*$^{fl/fl}$*Smad4*$^{+/+}$ compared to *Apc*$^{fl/fl}$*Smad4*$^{fl/fl}$ at the basal level 188
6.3 Gene set enrichment in *Apc*$^{fl/fl}$*Smad4*$^{fl/fl}$ compared to *Apc*$^{fl/fl}$*Smad4*$^{+/+}$ at the basal level 188
6.4 Leading edge genes upregulated in *Apc*$^{fl/fl}$*Smad4*$^{fl/fl}$ at basal level compared to *Apc*$^{fl/fl}$ *Smad4*$^{+/+}$ 190
6.5 Description of the top 50 differentially regulated genes in *Apc*$^{fl/fl}$*Smad4*$^{+/+}$ after 1h TGF-β1 treatment compared to 0h 196
6.6 Gene set enrichment in *Apc*$^{fl/fl}$*Smad4*$^{+/+}$ at 0h after TGF-β1 treatment compared to 1h 197
6.7 Gene set enrichment in *Apc*$^{fl/fl}$*Smad4*$^{+/+}$ at 1h after TGF-β1 treatment compared to 0h 197
6.8 Leading edge genes upregulated in *Apc*$^{fl/fl}$*Smad4*$^{+/+}$ after 1h TGF-β1 treatment compare to 0h 198
6.9 Description of the top 50 differentially regulated genes in *Apc*$^{fl/fl}$*Smad4*$^{+/+}$ after 12h TGF-β1 treatment compared to 0h 199
6.10 Gene set enrichment in *Apc*$^{fl/fl}$*Smad4*$^{+/+}$ at 0h after TGF-β1 treatment compared to 12h 200
6.11 Gene set enrichment in *Apc*$^{fl/fl}$*Smad4*$^{+/+}$ at 12h after TGF-β1 treatment compared to 0h 200
6.12 Leading edge genes upregulated in *Smad4*$^{+/+}$ after 12h TGF-β1 treatment compare to 0h 201
6.13 Leading edge genes downregulated in *Apc*$^{fl/fl}$*Smad4*$^{+/+}$ after 12h TGF-β1 treatment compare to 0h 202
6.14 Leading edge genes induced in *Apc*$^{fl/fl}$*Smad4*$^{+/+}$ adenomas after 1h TGF-β1 treatment and maintained expression 203
6.15 Leading edge genes repressed in *Apc*$^{fl/fl}$*Smad4*$^{+/+}$ adenomas after 1h TGF-β1 treatment and maintained repression 204

6.16 Description of the top 50 differentially regulated genes in *Apc*$^{fl/fl}$*Smad4*$^{fl/fl}$ compared to *Apc*$^{fl/fl}$*Smad4*$^{+/+}$ following 1h TGF-β1 treatment 209
6.17 Gene set enrichment in *Apc*$^{fl/fl}$*Smad4*$^{+/+}$ compared to *Apc*$^{fl/fl}$*Smad4*$^{fl/fl}$ after 1h TGF-β1 treatment 210
6.18 Gene set enrichment in *Apc*$^{fl/fl}$*Smad4*$^{fl/fl}$ compared to *Apc*$^{fl/fl}$*Smad4*$^{+/+}$ after 1h TGF-β1 treatment 210
6.19 Leading edge genes upregulated in *Apc*$^{fl/fl}$*Smad4*$^{+/+}$ compared to *Apc*$^{fl/fl}$ *Smad4*$^{fl/fl}$ following 1h of TGF-β1 treatment 211
6.20 Leading edge genes upregulated in *Apc*$^{fl/fl}$*Smad4*$^{fl/fl}$ compared to *Apc*$^{fl/fl}$*Smad4*$^{+/+}$ after 1h TGF-β1 treatment 213
6.21 Description of the top 50 differentially regulated genes in *Apc*$^{fl/fl}$*Smad4*$^{fl/fl}$ compared to *Apc*$^{fl/fl}$*Smad4*$^{+/+}$ following 12h TGF-β1 treatment 214
6.22 Gene set enrichment in *Apc*$^{fl/fl}$*Smad4*$^{+/+}$ compared to *Apc*$^{fl/fl}$*Smad4*$^{fl/fl}$ at 12h after TGF-β1 treatment 215
6.23 Gene set enrichment in *Apc*$^{fl/fl}$*Smad4*$^{fl/fl}$ compared to *Apc*$^{fl/fl}$*Smad4*$^{+/+}$ at 12h after TGF-β1 treatment 215
6.24 Leading edge genes upregulated in *Apc*$^{fl/fl}$*Smad4*$^{+/+}$ compared to *Apc*$^{fl/fl}$*Smad4*$^{fl/fl}$ after 12h TGF-β1 treatment 216
6.25 Leading edge genes upregulated in *Apc*$^{fl/fl}$*Smad4*$^{fl/fl}$ compared to *Apc*$^{fl/fl}$*Smad4*$^{+/+}$ following 12h TGF-β1 treatment 217
6.26 Smad4 independent genes that are expressed in *Apc*$^{fl/fl}$Smad4$^{fl/fl}$ in response to 1hr TGF-β1 treatment 223
6.27 Smad4 independent genes that are repressed in *Apc*$^{fl/fl}$Smad4$^{fl/fl}$ in response to 1hr TGF-β1 treatment 224

A.1 PCR primers 249
A.2 PCR mix, cycling conditions for genes of interest 250

Table 1: List of abbreviations

Abbreviation	Description
AB	AlamarBlue
AB red	AlamarBlue reduction
AFD	Advanced DMEM AFD/F12
Alk	Activin receptor-like kinases
AMH	Anti-Müllerian hormone
APC	Adenomatous polyposis coli
ARE	Activin responsive element
ATF2	Activating transcription factor 2
ATF3	activating transcription factor 3
BMP	Bone morphogenic protein
BMPR1	BMP receptor 1
CBCs	crypt base columnar cells
CC3	Cleaved caspase-3
ChIP-Chip	Chromatin immunoprecipitation with DNA microarray
CIN	Chromosomal instability
Co-Smad	Common mediator Smad
CRC	Colorectal cancer
D	Day
DAB	3,3-diaminobenzidine
DAPI	4',6-Diamidino-2-Phenylindole
DEG	Differentially expressed genes
DMSO	Dimethyl sulfoxide
DPC4	Deleted in pancreatic cancer locus 4
E	EGF
ECM	Extracellular matrix
EdU	5-ethynyl-2'-deoxyuridine
EGF	Epidermal growth factor
EMT	Epithelial-mesenchymal transition
ENR	EGF, Noggin, R-spondin
EtOH	Ethanol
FAP	Familial adenomatous polyposis
FCS	Fetal Calf Serum
FDR	False discovery rate
FPKM	Fragments per kilobase per million mapped reads
Fz	Frizzled
GDFs	Growth and differentiation factors
GO	Gene ontology
GSEA	Gene set enrichment analysis
H	Hour
H&E	Haematoxylin and eosin
HATs	Histone acetyltransferase
hESc	human embryonic stem cells
HNPCC	Hereditary non-polyposis colorectal cancer
H_2O_2	Hydrogen peroxide
4-OHT	4-Hydroxy Tamoxifen
IκK	I kappa B kinase
IF	Immunofluorescence
IHC	Immunohistochemistry
I-Smads	Inhibitory Smads
Igf2	Insulin like growth factor 2
Igf2r	Insulin like growth factor 2 receptor
siRNA	Interfering RNA
IL-6	Interleukin-6

Continued on following page

Abbreviation	Description
ISCs	Intestinal stem cells
JP	Juvenile polyposis
Lef	Lymphoid enhancing factor
Lgr5	Leucine-rich repeat-containing G-protein coupled receptor 5
LOH	Loss of heterozygosity
LRP5/6	Lipoprotein receptor related protein 5/6
MDSCs	Myeloid-derived suppressor cells
MH	Mad homology
miRNA	MicroRNA
Mom1	Modifier of Min 1
MSI	Microsatellite instability
MSS	Microsatellite-stable
Muc2	Mucin 2
N	Noggin
NAC	*N*-acetylcysteine
NBF	Neutral buffered formalin
N-Cadherin	Neural cadherin
NES	Nuclear export signal
NLS	Nuclear localisation signal
PAS	Periodic acid Schiff
PBS	Phosphate buffered saline
PCR	polymerase chain reaction
PFA	Paraformaldehyde
PI3K	Phosphatidylinositol 3-kinase
Pla2g2a	Phospholipase A2
PM	Post-mortem
R	R-spondin1
RB	Retinoblastoma
RNA-seq	RNA sequencing
RNAi	Stable RNA interference
ROS	Reactive oxygen species
R-Smads	Receptor-regulated Smads
RSPO	R-spondin
SARA	Smad anchor for receptor activation
SBE	Smad binding element
SCF	Skp1-Cμl-F-box
Ser/Thr	Serine/threonine
SIM	Smad interaction motif
Smurf1	Smad ubiquitin regulatory factor 1
SSA/Ps	Sessile serrated polyps/Adenomas
TA	Transit-amplifying cells
TBS	Tris buffered saline
TBST	TBS-Tween20
TCF	T-cell factor
TF	Transcription factor
TFE3	Transcription factor E3
TGF-β	Transforming growth factor-β
TGFβR-II, Tgfb2r	TGFβ receptor 2
TIF1γ	Transcription intermediary factor
TSS	Transcription start site
TTF-1	Thyroid transcription factor-1

Continued from previous page.

Chapter 1

Introduction

1.1 Introduction

Human colorectal cancer (CRC) is one of the most common types of cancer affecting mainly elderly people. Each year more than 1.2 million new cases are diagnosed worldwide (Ferlay et al., 2010). The mortality rate of this disease is approximately 33% as a result of metastases (Walther et al., 2009; Fearon, 2011). The hereditary component of CRC has been estimated to be as high as 30% based on its occurrence in related individuals (Fearon, 2011). There are two main familial syndromes; familial adenomatous polyposis (FAP) and hereditary non-polyposis colorectal cancer (HNPCC) syndromes (Fearon, 2011). FAP is characterised by multiple adenomatous polyps (>100) and carcinomas of the colon and rectum (Fearon, 2011). In most cases it is initiated as a result of active Wnt pathway due to germline mutations in the *adenomatous polyposis coli* (*APC*) gene (Powell et al., 1992; Fodde et al., 2001). The progression from adenoma to carcinoma requires alterations in additional pathways and takes another 20-40 years. In a similar route to FAP, sporadic CRC develops either through *Apc* loss of function, β-catenin gain of function or R-spondin gene fusion (Fearon, 2011; Seshagiri et al., 2012). HNPCC is a cancer predisposition syndrome without extensive polyposis and is mainly related to germline inactivation of one of the mismatch repair genes (*MSH2* and *MLH1*) which cause microsatellite instability (MSI). The initiated lesion (adenoma) greatly increases the mutation rate and within 3-5 years can progress to carcinoma (Fearon, 2011; Young et al., 2013).

The cells of origin of CRC are in the intestinal epithelium, a highly proliferative, and self-

renewing tissue (Cheng and Leblond, 1974). The proliferation and differentiation of this epithelium is highly controlled by different pathways such as Wnt/β-catenin, transforming growth factor-β (TGF-β) superfamily, and Notch pathways. Alterations in these pathways in addition to environmental factors are both identified as risk factors in CRC (Medema and Vermeulen, 2011). Understanding the molecular mechanisms of CRC may lead to targeted therapy for advanced stages. However, due to the diversity of mutations and heterogeneity in individual tumours, the current challenge is to determine the mechanisms of driver events. An obstacle to mechanistic understanding is the lack of models for the disease that recapitulate the human CRC phenotype.

The TGF-β superfamily and receptor pathways are important for intestinal homeostasis. Mutations of these pathway lead to intestinal diseases and cancer (Massagué, 2008; Wakefield and Hill, 2013; Network et al., 2012). This thesis evaluates the effects of alterations in the TGF-β pathway due to mutations in *Smad4* on intestinal tumorigenesis in the context of active Wnt pathway, using mouse models.

1.2 The intestinal epithelium and homeostasis

The intestine is composed of a single layer of epithelial cells organised into finger-like protrusions called villi, and invasions called the crypts of Lieberkühn. The villi provide a large surface area for absorption (van der Flier and Clevers, 2009), and start to form at embryonic day 15 (Crosnier et al., 2006). This compartment also consists of differentiated cells such as enterocytes (absorpative for nutrient uptake), goblet cells (producing mucin, and phospholipase A2) (Fijneman et al., 2008), and enteroendocrine (producing hormones), tuft cells (producing enzymes involved in prostaglandin synthesis) (Crosnier et al., 2006; Krausova and Korinek, 2014). Within the crypts there are transit-amplifying cells (TA) and at the base of the crypts, the intestinal stem cells (ISCs), and Paneth cells. Paneth cells produce bactericidal products (lysozyme and defensins) (Porter et al., 2002). Recently, it has been shown that Paneth cells ($CD24^{+}$) are the niche for stem cells (*Lgr5*) and produce

EGF, TGF-α, Wnt3a and D114 (Notch ligand), that are important for stem cell maintenance (Sato et al., 2011) (Figure 1.1).

Two areas within the crypts -the crypt base columnar cells (CBCs) and the +4 cells - are composed of cells that are defined as ISCs. The identification of both areas was based on mouse models with lineage-tracing reporters and the ability of these cells to produce the variety of epithelial cells present in crypts. *Lgr5-GFP-IRES-CreERT2*/*Lgr5-LacZ* mouse models showed that CBC cells located between the Paneth cells are stem cells. The Lgr5 (Leucine-rich repeat-containing G-protein coupled receptor 5) marker is a Wnt/β-catenin target gene (Barker et al., 2007). *Bmi1*^{CreER}*Rosa26-lacZ*$^{+}$ transgenic mouse model showed that Bmi1 positive cells mark the +4 cells. These cells are located just above the Paneth cells (Sangiorgi and Capecchi, 2008). Further evidence supports that these two markers are ISCs. Bmi1 positive cells are considered to be reserves for the stem cell pool, and can give rise to Lgr5 cells in cases of injury (Tian et al., 2011). Moreover, Lgr5^{high} positive cells can grow into organoids in 3D culture systems (Sato et al., 2009). Sox9, CD133, Msi1 are other reported markers for the CBC stem cells and Tert, Wip1 and Dcamkl1 are reported for +4 cells (Barker, 2014).

Intestinal homeostasis including self-renewal, continuous migration of cells upward to the villous tip and anoikis (shedding of dead cells at the villi top), are highly regulated by the crypt niche and the Wnt, TGF-β, and Notch pathways (Sancho et al., 2004; Clevers and Nusse, 2012). Mutations in these regulatory pathways cause marked change in the distribution of cells along the crypt-villous axis and predispose patients to cancer (Sancho et al., 2004; Crosnier et al., 2006). For instance, the Notch pathway is important for cell fate decision between enterocytes and secretory lineages as its activation results in goblet cell depletion (Medema and Vermeulen, 2011).

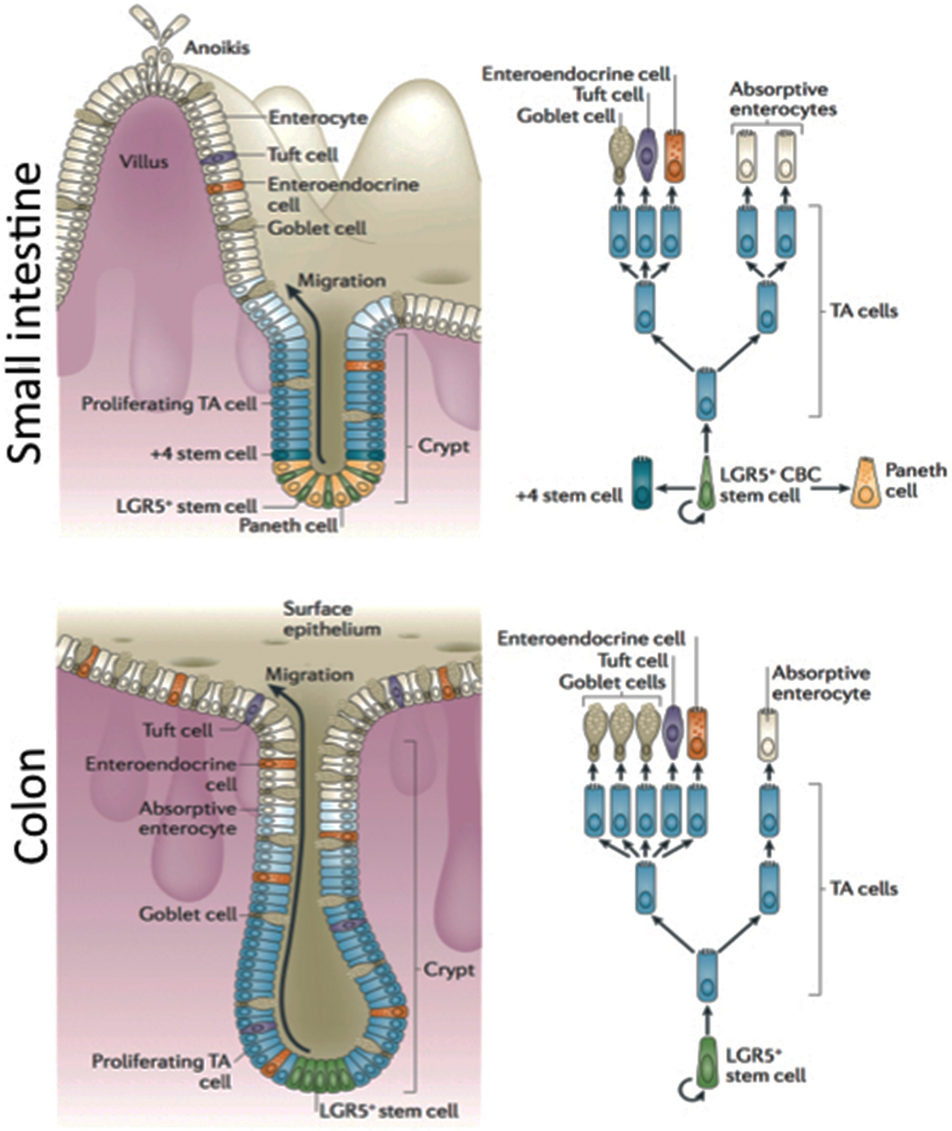

Figure 1.1: **Mammalian small intestine and colon.** Small intestine contains crypt and villous compartments. ISCs reside within the crypts. Stem cell division leads to a population of cells in the TA compartment that undergoes 4-5 divisions before differentiation. Differentiated cells (except Paneth cells) migrate towards the villous compartment and undergo anoikis with turnover occurring every 3-5 days. Paneth cells occupy the bottom of the crypt and are intercalated with CBC stem cells. New Paneth cells are supplied from the TA cells every 3-6 weeks. The colon lacks the villous compartment and the differentiated cells are within the crypt. Colonic TA cells are in the lower half of the crypt. Epithelial turnover occurs every 5-7 days (Barker, 2014). Paneth cells are absent from the colon, the presence of $CD24^+$ cells between the colonic Lgr5 stem cells might be Paneth cell equivalents (Sato et al., 2011). Adapted from (Barker, 2014). TA: transit-amplifying.

1.3 The Wnt pathway

1.3.1 Wnt proteins, agonists and regulators

Most mammals have 19 Wnt genes encoding proteins of approximately 40 KDa, such as Wnt1, Wnt3a and Wnt8. These are involved in the regulation of different developmental pathways (Clevers and Nusse, 2012). Characterisation of these proteins showed that they are lipid modified, which is crucial for effective signalling and may be important for Wnt secretion. Wnt ligands bind to a heterodimeric receptor complex, composed of a Frizzled (Fz) and a lipoprotein receptor related protein 5/6 (LRP5/6) protein (Clevers and Nusse, 2012).

Norrin and R-spondins are other proteins known as Wnt agonists that bind to the receptor Fz/LRP complex. In the context of intestinal biology, R-spondins are important Wnt agonists. R-spondins are small secreted proteins consisting of four family members R-spondin1-4. Rapid onset of intestinal crypt proliferation involving β-catenin stabilisation was seen in mice injected with human R-spondin1 (Kim et al., 2005). R-spondin1 is an important recombinant protein for intestinal organoid culture (Sato et al., 2009). Moreover, R-spondin gene fusions (RSPO2 and RSPO3) occur in 10% of colon tumours with normal *APC* and *CTNNB1* (Seshagiri et al., 2012) providing further evidence of the importance of this agonist and the Wnt pathway in CRC. RSPO2 and RSPO3 gene fusion increases their expression and the expression of their receptors Lgr5/Lgr4 (Seshagiri et al., 2012). Different mechanisms of how R-spondins activate the Wnt pathway have been proposed. R-spondins may bind to their receptors through the association with the Fz-LRP5/6 complex (de Lau et al., 2011), or interact with the extracellular domain of transmembrane E3 ubiquitin ligase protein ZNRF3 and its homologue ring finger 43 (RNF43), to promote association between ZNRF3 and LGR4, resulting in degradation of ZNRF3 (Hao et al., 2012). Wnt signalling is negatively regulated by DKK, which binds to the LRP receptor and inhibits Wnt signalling (Nusse, 2012), and by RNF43 and ZNRF3 which degrade the frizzled receptor by ubiquitination (Koo et al., 2012; Hao et al., 2012).

1.3.2 Wnt/β-catenin signalling

Signalling through β-catenin is known as the Wnt canonical pathway. It regulates several biological processes, such as cell fate determination, proliferation, and stem cell maintenance (Clevers, 2006). Different hereditary syndromes and cancer are associated with alterations in this pathway (Clevers and Nusse, 2012). Signal transduction in this pathway is based on titrating away Axin -the negative regulator- offering a stoichiometric rather than a catalytic mechanism for signal transduction, unlike other pathways in which the signals are propagated by protein kinases (Clevers and Nusse, 2012). In the inactive state, the cytoplasmic destruction complex -composed of protein kinases GSK-3β and CK1, the tumour suppressor protein APC, and the scaffolding protein Axin- binds to β-catenin. β-catenin then becomes phosphorylated by CK1 and GSK-3β at a series of highly conserved serine/threonine (Ser/Thr) N-terminus residues for ubiquitination by the proteasome β-TrCP (Clevers, 2006; Clevers and Nusse, 2012). Binding of the ligand to its receptor deactivates the complex and prevents β-catenin phosphorylation and degradation. The mechanism was thought to be related to the binding of Axin to the phosphorylated LRP receptor, disassembling the destruction complex, and stabilising β-catenin (Clevers and Nusse, 2012). The new model for Wnt signalling is based on binding of the destruction complex to phosphorylated LRP. The complex is still capable of binding and phosphorylating β-catenin until saturation after which β-catenin cannot bind. The degradation of β-catenin is then inhibited (Figure 1.2A). Newly synthesised β-catenin accumulates in the nucleus (Li et al., 2012) and is involved in gene regulation by binding to the T-cell factor/lymphoid enhancing factor (TCF/LEF) transcription factors (TFs) (Clevers and Nusse, 2012). In addition to the role of β-catenin and its regulation by the Wnt pathway, β-catenin is also regulated by adhesion complexes containing cadherins and α-catenin (Nusse, 2012).

1.3.3 Wnt pathway in intestinal tumorigenesis

Mutations in components of the destruction complex lead to aberrant activation of the pathway resulting in cancer mainly affecting the colon (Clevers and Nusse, 2012). Approximately 93% of CRC cases have mutations in this pathway (Network et al., 2012) which is

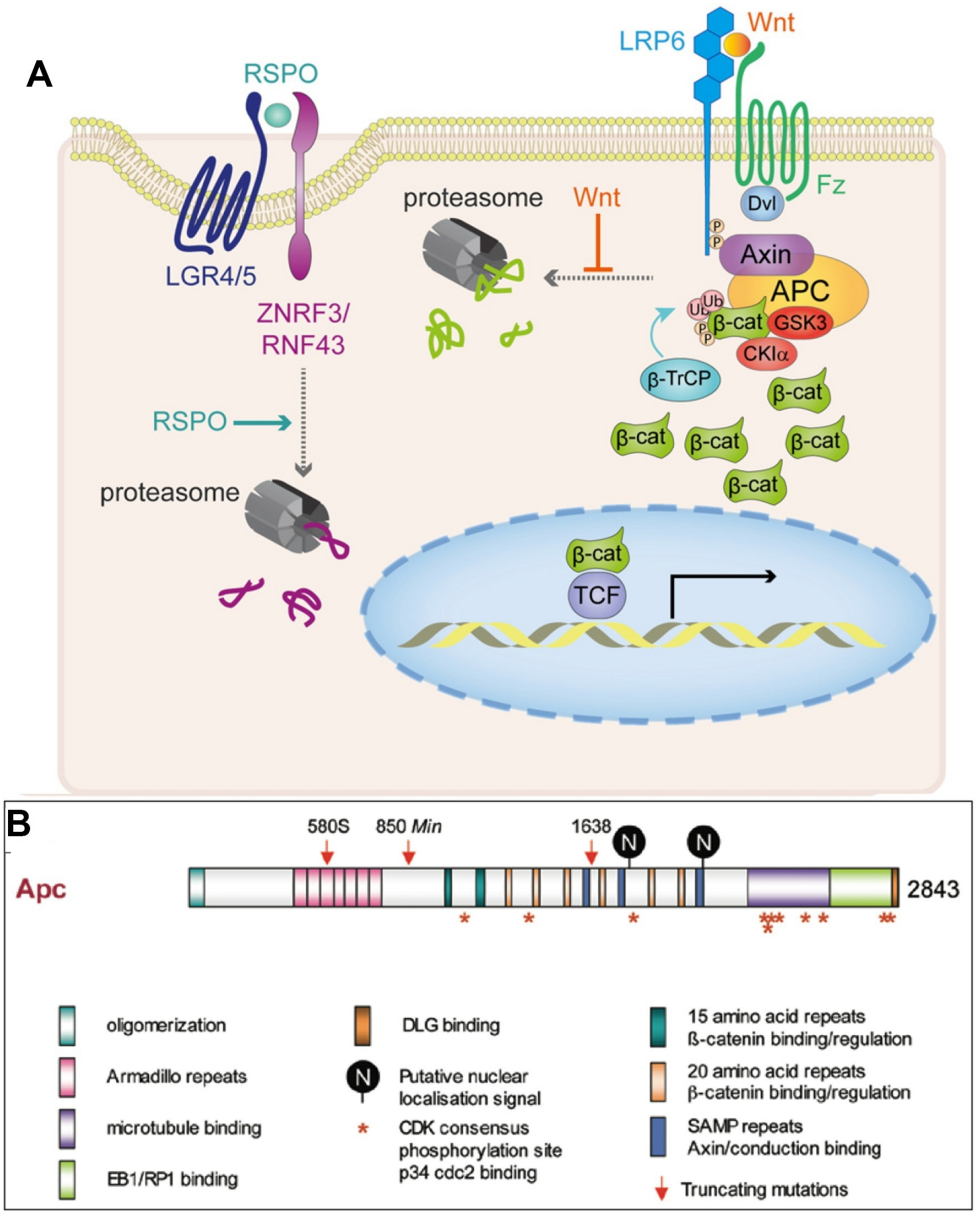

Figure 1.2: **Wnt/β signalling.** (A) A new model describes the Wnt signalling and its regulation by R-spondin (RSPO). In the presence of Wnt the destruction complex binds to the active LRP receptor, β-catenin binds until complex saturation, but its proteasomal degradation is abrogated. β-catenin is then stabilised and enters the nucleus, where it is associated with TCF/LEF TFs and involved in gene regulation. RSPO binds to its receptors Lgr5/Lgr4 and to the negative Wnt regulators ZNRF3/RNF43, which allows proteasomal degradation of ZNRF3/RNF43. In the absence of Wnt signal the β-catenin is phosphorylated and degraded by the proteasome β-TrCP. Adapted from (Krausova and Korinek, 2014). (B) Apc protein structure showing the binding sites for β-catenin, Axin with the Apc protein. Mutations introduced to the *Apc* gene (Apc^{580S}, Apc^{Min}, $Apc^{\Delta 1638}$) affect its binding to β-catenin, leading to β-catenin stabilisation. Adapted from (Sansom, 2009).

important for the initiation step and driving the formation of benign adenomas (Morin et al., 1997; Clevers and Nusse, 2012). The most commonly mutated gene is *APC* (70-80%) (Fearon, 2011) while 10% of cases have inactivating mutations in *CTNNB1* (β-catenin) which prevent its degradation (Morin et al., 1997; Giles et al., 2003) and others have mutations in *AXIN2* (Liu et al., 2000; Network et al., 2012). Mutations in other components of the Wnt pathway have also been reported, for instance, 10% of cases have mutations in R-spondin family members (Seshagiri et al., 2012). Mutations in *TCF7L2*, *SOX9*, DKK family members and overexpression of the Wnt receptor frizzled *FZD10* (17%) (Network et al., 2012).

Mutations in the Wnt pathway result in stabilisation of β-catenin, which enters the nucleus and is involved in gene regulation with TCF/LEF TFs (Clevers and Nusse, 2012). Several genes important for proliferation, prevention of differentiation, tumorigenesis, stemness and impaired migration of the cells along the crypt-villous axis such as *c-Myc* (He et al., 1998), *cyclin D1* (Tetsu and McCormick, 1999) *Axin2*, (Lustig et al., 2002) *CD44* (Wielenga et al., 1999), *Lgr5* (Barker et al., 2007), *Sema3c*, *EphB3* and *Tiam1* (Sansom et al., 2004) are Wnt/β-catenin target genes. *Birc5*- the inhibitor of apoptosis- known also as *Survivin* is a Wnt target gene and is required for the regulation of cell death and cell proliferation. It is expressed during embryonic development and re-expressed in different cancers including CRC (Kim et al., 2003).

Most of the mouse models for the initiation steps in CRC are based on *Apc* mutations which mimic FAP (Table 1.1). This hereditary form of CRC is characterised by the development of hundreds to thousands of colorectal adenomas (Nishisho et al., 1991). Differences in mutations of *Apc* affect the phenotype. Apc is a large protein that has multiple binding sites for β-catenin and Axin, and the site of mutations and the extent of the truncation affects the phenotype (Fodde et al., 2001) (Figure 1.2B). The nature of the germline mutation in these patients has been reported to affect the loss of the normal allele of *Apc*. For example, the more distal the germline mutation, the more proximal the somatic mutation (Medema and Vermeulen, 2011). This pattern is to provide a specific level of β-catenin signalling for

optimal tumorigenesis in a model named ”just-right signalling” (Albuquerque et al., 2002). This model was proposed after analysis of 133 polyps from six different FAP patients for *Apc* mutations, suggesting that the function of the *Apc* gene must be affected to a specific degree for sufficient nuclear β-catenin accumulation, as excessive β-catenin accumulation in the nucleus results in cell death and inability to form tumours (Albuquerque et al., 2002).

The phenotype of $Apc^{Min/+}$ mice is influenced by the strain background which is responsible for variation in polyp number due to the presence of certain modifiers (McCart et al., 2008). *Phospholipase A2 (Pla2g2a)* is a gene which acts by altering the cellular microenvironment within the intestinal crypt (MacPhee et al., 1995). It encodes secretion of Pla2g2a by Paneth cells in the small intestine (Mulherkar et al., 1993) and by goblet cells in the large intestine (Fijneman et al., 2008). The modifier of Min 1 (*Mom1*) is found in strains such as AKR and is responsible for the presence of high levels of Pla2g2a in the intestinal lumen providing a protective layer against intestinal microbes and is associated with decreased polyp formation. The decreased expression of Pla2g2a in C57BL/6J mice allows the proliferation of microbes which facilitate polyp formation and transformation (MacPhee et al., 1995). Pla2g2a may modulate the intestine immune homeostasis and prevents chronic inflammation by suppressing interferon-induced genes (Fijneman et al., 2009).

1.4 Transforming growth factor-β pathway

The TGF-β superfamily of cytokines is divided into two main branches. The first branch includes TGF-β, Activins and Nodal. The second includes the bone morphogenic proteins (BMPs), anti-Müllerian hormone (AMH) and growth and differentiation factors (GDFs). The classification is based on sequence similarity, the type 1 receptor they activate and the downstream signalling (Shi and Massagué, 2003; Massagué, 2012). They control numerous cellular processes by regulating genes involved in cell proliferation, cell differentiation, apoptosis, cell fate and migration (Massagué, 1998, 2012). These cytokines signal through a heteromeric complex of Ser/Thr kinase receptors. The ligand brings the constitutively ac-

tive type II receptor to type I receptor and activates it by phosphorylation which is required for signal propagation through Smad TF family members to the nucleus. The activated type I receptor phosphorylates R-Smads which bind to Co-Smad (Smad4) and translocate to the nucleus (Massagué, 2012). The activated TFs can regulate the transcriptional output of active genes and can open repressive chromatin. Smad TFs act as hubs for the consolidation of regulatory inputs and modulate the TGF-β signalling in a context dependent manner (Massagué, 2012) (Figure 1.3). TGF-β pathway is highly regulated by phosphorylation and ubiquitination. Mutation in this pathway predisposes patients to different diseases including cancer (Massagué, 2012; Wakefield and Hill, 2013).

1.4.1 TGF-β Receptors

Type II receptors -the activator receptor- consist of five members; TGF-β binds exclusively to TGFβ receptor II (TGFβR-II). BMP, Nodal and Activin bind and share activin receptor type 2A (ACTR-IIA) and activin receptor type 2B (ACTR-IIB). BMPR-II is another receptor for BMP, wheres AMH binds to AMHR-II. Type I receptors - the signal propagating receptor- consist of seven members known as activin receptor-like kinases (Alk1-7). TGF-β binds to TGFBR1 (Alk5 or TβR1). Activin and Nodal bind to activin receptor type 1 (ACVR1) (Alk2), ACVR1B (known as Alk4) and ACVR1C (Alk7). BMPs and AMH bind to BMP receptor 1 (BMPR1)A (Alk3) and BMPR1B (Alk6). BMP9 and BMP10 binds to ACVRL1 (Alk1) (Figure 1.3) (Massagué, 2012).

TGF-β1, TGF-β2 and TGF-β3 are three different isoforms of TGF-β present in mammals and signal through the same receptors. TGF-β1 and 3 have higher affinity to the receptors than TGF-β2 (Wrana et al., 1992). TGF-β1 is present in high concentration in platelets, bone, and placenta (Dennis and Rifkin, 1991). It is also most frequently upregulated in tumour cells and is used in most of the studies that evaluates the role TGF-β in tumorigenesis (Derynck et al., 2001).

Table 1.1: *Apc* mouse models

Mouse model	Mutation and deletion site	Phenotype	Death point	Reference
Apc^{Min*}	Truncation at a.a[1] 850, germline	Multiple polyps (30-100) in the small intestine	4-6 months	(Su et al., 1992)
$Apc^{\Delta 716}$	Truncation at a.a 716, germline	Multiple polyps (300) mainly in the small intestine	4-6 months	(Oshima et al., 1995)
$Apc^{\Delta 1638N}$	Truncated protein at a.a 1638	Few upper gastrointestinal adenoma (<10)	1 year	(Fodde et al., 1994)
$Apc^{\Delta 1638T}$	Truncated protein at a.a 1638	Normal	Normal	(Smits et al., 1999)
Apc^{580S}	Truncated protein at a.a 580, LoxP sites flanking exon 14, based on Cre	Adenoma after Cre activation by adenovirus in the colon	4 weeks following Cre activation	(Shibata et al., 1997)
$Apc^{fl/fl}$ *Ah-Cre*	Same as Apc^{580S}, in the intestinal epithelium	Adenoma throughout the intestine	3 weeks after Cre-activation	(Sansom et al., 2004)
$Apc^{fl/fl}$ *Villin-CreERT2*	Same as Apc^{580S}, in the intestinal epithelium	Massive proliferation with the crypt compartment with dysplastic features	4 days	(Andreu et al., 2005)
Lgr5-EGFP-IRES-CreERT2	Same as Apc^{580S}, in the *Lgr5* stem cells	Macroscopic adenoma within the intestine, rare large adenoma	3-5 weeks after Cre activation	(Barker et al., 2009)

*: This model was first introduced by ethylnitrosourea mutagenesis and mice developed multiple intestinal neoplasia (Moser et al., 1990). [1]a.a: amino acids

1.4.2 Smad proteins

Smad proteins are classified into three functional groups; receptor-regulated Smads (R-Smads), common mediator Smad (Co-Smad), and inhibitory Smads (I-Smads). Five members belong to the R-Smads group and are separated mainly according to the type 1 receptors that activate them. Alk4, 5, 7 activate Smad2 and Smad3 and hence are considered TGF-β R-Smads. On the other hand, Alk1, 2, 3, 6 activate Smad1, Smad5 and Smad8 and they are considered BMP R-Smads (Schmierer and Hill, 2007; Heldin and Moustakas, 2012). TGF-β usually signals through Alk5, however, it has been reported that TGF-β can activate Smad1 and Smad5 by signalling through different type 1 receptors. For instance, TGF-β can signal via Alk1 in endothelial cells (Goumans et al., 2002) and in normal epithelial cells and fibroblasts via Alk2, 3 resulting in mixed R-Smad complexes (Daly et al., 2008). In mammary tumour epithelial cells, TGF-β signals through its receptor, Alk5, activates Smad1 and Smad5 and leads to migration (Liu et al., 2009). Smad4 (known as Mothers against decapentaplegic homolog 4 and also as Deleted in pancreatic cancer locus 4 (DPC4)) is a co-Smad and acts as a common partner for all R-Smads. I-Smads are Smad6 and Smad7, they are induced in response to TGF-β and BMP (Massagué et al., 2005; Schmierer and Hill, 2007). They act as negative regulators for the signalling pathway mainly by interfering with Smad-receptor interactions or Smad-Smad interactions (Massagué et al., 2005).

1.4.2.1 Smad functional domains

R-Smads and Smad4 proteins consists of two highly conserved globular domains named Mad homology (MH) 1 at the N-terminus and MH2 at the C-terminus, separated by a less well-conserved serine and proline-rich linker region (Massagué, 1998; Massagué et al., 2005; Massagué, 2012; Gaarenstroom and Hill, 2014) (Figure1.4).

The MH1 domain is involved in DNA binding through a conserved identical hairpin structure present in all members except Smad2 (Massagué et al., 2005; Heldin and Moustakas,

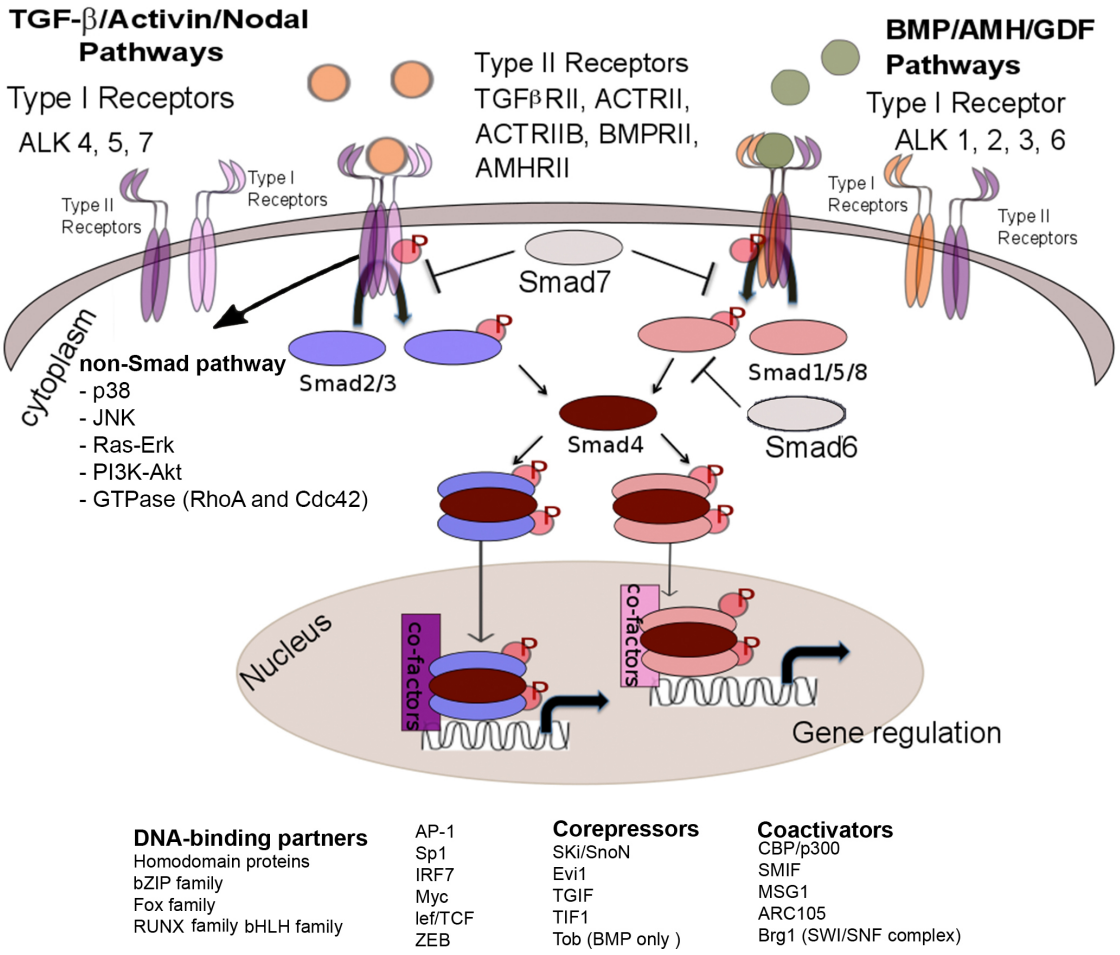

Figure 1.3: **TGF-β signalling pathway.** The core signalling pathway is through Smads. TGF-β superfamily of cytokines signals through a heteromeric complex of Ser/Thr kinase receptors. The ligands bring the constitutively active type II receptor to a type I receptor. Type II receptors phosphorylate and activate the type I receptor in the complex. The activated type I receptor phosphorylates and activates R-Smads which associate with Smad4 and translocate to the nucleus. R-Smad-Smad4 complexes in association with other specific DNA-binding TFs are directly involved in the transcription of target genes. Type II receptors can activate other pathways known as non-Smad signalling pathways (Wrana, 2013).

2012). Smad2 has an insert of 30 amino acids directly prior to the hairpin structure that prevents DNA recognition (Shi et al., 1998). At the N-terminus of this domain, Smads have a nuclear localisation signal (NLS) domain that is constitutively active (Pierreux et al., 2000). I-Smads lack the MH1 domain (Massagué, 2012; Gaarenstroom and Hill, 2014).

The linker region is important for Smad regulation. It contains a PY motif for recognition by the WW domain in the Smurf ubiquitin ligase and is a site for phosphorylation by different kinases (Massagué et al., 2005; Heldin and Moustakas, 2012). In addition, Smad4 has a nuclear export signal (NES) at the linker that is recognized by the nuclear exporter CRMI (Pierreux et al., 2000; Watanabe et al., 2000). Smad4 has 48-amino acid segment within the linker known as the Smad4 activation domain (SAD). SAD is required for the activation of Smad4-dependent signalling responses (de Caestecker et al., 1997). SAD has an intrinsic, p300-dependent, transcriptional activity that is important for the physical interaction between SAD and the NH2 terminus of p300/CBP (de Caestecker et al., 2000; Chacko et al., 2001). p300, CBP, and P/CAF have histone acetyltransferase (HAT) activity, which facilitate Smad contact with DNA and with other transcriptional partners (Ten Dijke et al., 2002). Although Smad4 mutants lacking SAD are able to form complexes with other R-Smads and associated TFs, they are unable to activate transcription (de Caestecker et al., 2000). For several years, SAD was believed to be present only in Smad4 until Wang *et al*. in 2005 showed that Smad3 also has a SAD domain in the linker region that physically and functionally interacts with p300 (Wang et al., 2005). Moreover, p-Smad2 can bind to p300 only on chromatin templates and not on naked DNA (Ross et al., 2006). The presence of this domain, and the ability of Smad2 to recruit p300 on chromatin might uncover important roles for Smad3 and Smad2 in the pathology when Smad4 is deficient.

The MH2 domain is required for R-Smad C-terminal phosphorylation by the activated type 1 receptors at an SSXS conserved motif at the C-terminus, Smad-Smad interaction and is the site for binding of many different transcriptional activators or repressors (Schmierer and Hill, 2007; Massagué, 2012; Gaarenstroom and Hill, 2014).

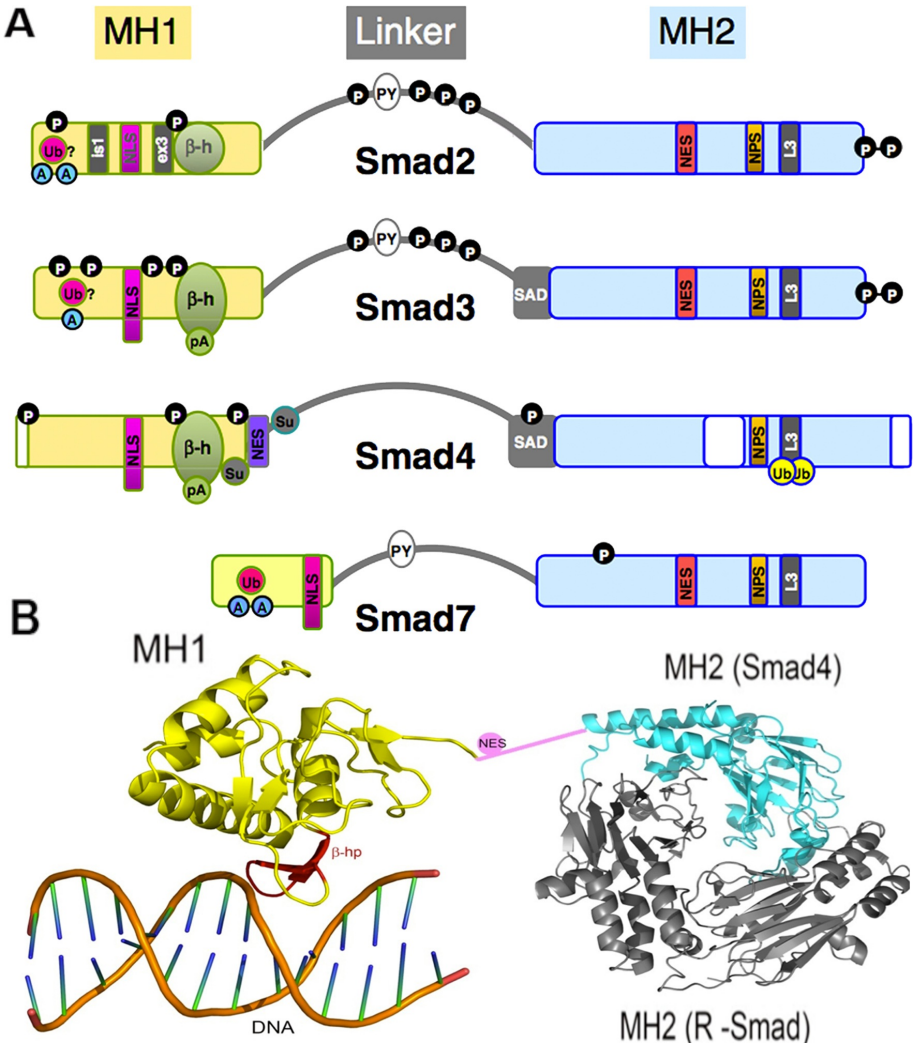

Figure 1.4: **Smad transcription factors**. (A) Cartoon representing the different domains (MH1 and MH2) and the linker in Smads and their post-translational modifications. Smad2 has insert 1 (*is1*) and insert 2 (*ex3*) which prevent NLS (shaded pink), DNA binding (circular hairpin (β-h)) and blocks the interaction with poly (ADP-ribose) polymerase-1 (PARP-1). Smad3, 4 lack *is1* and *ex3* and thus have a functional NLS (pink, bold and elongated) and can bind DNA (β-h, oval) . Smad7 lacks a distinct MH1 domain. Linker has a PY motif for recognition by the WW domain in the Smurf ubiquitin ligase. Between the linker and the MH2 domain, Smad3 and Smad4 have Smad activation domain (SAD) which mediates the interaction with repressors and activators. The MH2 domain has nucleopore signal (NPS) that mediates nuclear import and export. The L3 loop which is conserved in all Smads, is the site for Smad interaction and the ubiquitination site for Smad4. NES is within the MH2 domain for Smad2, 3, 7. Smad4 has NES in the linker region. Phosphorylation (P) in the MH1 domain regulates the binding of Smads to the DNA and at the linker for ubiquitination of Smad2, 3. P-P in the C-terminus of MH2 domain in Smad2, 3 is the phosphorylation site with the activated receptor. Acetylation (A) in MH1 domain regulates DNA binding and stability. (Ub) is the ubiquitination site and the exact location is not determined for Smad4, 7 and R-Smads. Adapted from (Heldin and Moustakas, 2012). (B) crystal structure of Smad4 showing the MH1 domain binding to the DNA and the interaction with R-Smads in the MH2 domain.

1.4.2.2 Smad interaction

Without a signal, Smad4 continuously shuttles between the cytoplasm and the nucleus. Treatment with Leptomycin B suppresses the nuclear export mechanism and Smad4 accumulates inside the nucleus (Pierreux et al., 2000; Watanabe et al., 2000). R-Smads are also continuously shuttling but they prefer residing in the cytoplasm (Inman et al., 2002). Here, they are bound to a membrane-associated protein named Smad anchor for receptor activation (SARA), which presents them to the activated type I receptors for phosphorylation (Tsukazaki et al., 1998). Upon stimulation, Smad4 binds to phosphorylated R-Smads forming heterotrimeric or heterodimeric complexes (Inman and Hill, 2002; Massagué, 2012). These complexes are either formed in the cytoplasm and translocated to the nucleus by the NLS of Smad4 that interact with importin-α (Pierreux et al., 2000; Xiao et al., 2003) or are formed directly in the nucleus (Massagué et al., 2005). It has been reported that Smad3, but not Smad2, has a conserved N-terminal basic motif which acts as a NLS, allowing constitutive nuclear localisation and is essential for Smad3 nuclear import in response to TGF-β stimulation (Xiao et al., 2000). Smad2 nuclear import is mediated by a direct interaction with CAN/Nup214 via MH2 domain (Xu et al., 2002). With TGF-β1 stimulation p-Smad2, 3 are transported via importin 7 and 8 (Xu et al., 2007). The formed complexes mask the NES in Smad4 allowing the complex to reside in the nucleus (Pierreux et al., 2000; Watanabe et al., 2000). Recently, it has been reported that the Smad2, 3, 4 complexes bind to TAZ following TGFβ stimulation, a process important for their nucleocytoplasmic shuttling and nuclear localisation by binding to the MH1 domain of Smad2 and the absence of TAZ prevents nuclear accumulation of Smad complexes (Varelas et al., 2008). Once Smad4-R-Smad complexes are in the nucleus, they bind to a DNA motif, CAGA, known as Smad-binding element (SBE) to regulate gene transcription with the help of other partners and cofactors (more details of how Smad regulates transcription will be in Chapter 6) (Massagué, 2012).

1.4.3 TGF-β pathway regulation

The TGF-β pathway is highly regulated by phosphorylation, dephosphorylation, sumoylation, acylation, ubiquitination and deubiquitination. Briefly, linker phosphorylation is required for binding of the HECT E3 ligase Nedd4L which targets the R-Smads for degradation (Gao et al., 2009). p-R-Smads are dephosphorylated in the nucleus, thus dissociated from the complex and returned to the cytoplasm for another phosphorylation cycle as long as the receptor is active (Inman et al., 2002). Thus, linker phosphorylation provides an additional level of control (Inman, 2011).

Ski and SnoN are negative regulators of the TGF-β signalling pathway and are expressed in response to TGF-β1 stimulation (Massagué and Gomis, 2006; Deheuninck and Luo, 2009). They interact with p-R-Smads-Smad4 at the promoters of TGF-β target genes and repress their activation by recruiting and binding different repressors as such as N-CoR, mSin3A (Luo, 2004). Moreover, binding of Ski to Smad4 results in the disruption of the p-R-Smads-Smad4 complexes (Deheuninck and Luo, 2009). They are considered as onco-proteins and in a context dependent manner they either promote transformation or promote tumour suppression (Deheuninck and Luo, 2009). They are also overexpressed in different cancers (Deheuninck and Luo, 2009). *SKI* amplification in human CRC is predicted to reduce relapse-free and overall survival and its deletion is not correlated with prognosis (Buess et al., 2004). Overexpression of Ski or SnoN in TGF-β responsive cells blocks TGF-β induced growth arrest and promotes proliferation (Luo, 2004; Deheuninck and Luo, 2009). Downregulation of SnoN expression by small interfering RNA (siRNA) in human lung, pancreatic or breast cancer cells inhibits tumour growth (Deheuninck and Luo, 2009) .

Ubiquitination of Smad4 by E3 ligase and β-TrCP promotes the degradation of wild type Smad4. Ubiquitination by Skp2 degrades mutated Smad4 in cancer (Heldin and Moustakas, 2012). Smad7 binds to Smad ubiquitin regulatory factor 1 (Smurf1) and Smurf2- E3 ubiquitin ligase- for the degradation of type 1 receptor and is required for BMP pathway

regulation (Heldin and Moustakas, 2012; Inoue and Imamura, 2008). *Smurf1* is a TGF-β-Smad4 dependent late response gene (Levy and Hill, 2005).

Deubiquitination -where a ubiquitin moiety can be removed by deubiquitinating enzymes (DUBs) such as USP15- is another mechanism of TGF-β pathway regulation (Eichhorn and Iyengar, 2013). USP15 is a DUB for R-Smad and opposes their ubiquitination, a mechanism important for full TGF-β responsiveness. USP15 is important for Smad complex association with DNA and Smad3 mono-ubiquitination is inhibited in Smad4 depleted cells (Inui et al., 2011).

Sumoylation is another post translational modification that has been reported for Smad4 to prevent its degradation and acylation of Smads is important for their stabilisation (Heldin and Moustakas, 2012).

1.4.4 Non-canonical TGF-β signalling

While signalling through Smads is the main pathway for TGF-β, TGF-β can also activate other pathways known as non-canonical TGF-β pathways. Bound TGFβR-II can also activate other pathways such as mitogen activated protein kinase (MAPK), ERK1/ERK2 , phosphatidylinositide 3-kinases (PI3K) and RHOA. The activation is cell-type and context-specific and the exact mechanisms for activation remain to be defined (Massagué, 2012; Wrana, 2013).

TGF-β signalling regulates several genes. Although Smad4 is an important partner in these complexes, there are TGF-β responses that are Smad4 dependent and others that are Smad4 independent. It has been reported in hematopoietic stem cells that transcription intermediary factor 1γ (TIF1γ), also known as TRIM33, can replace Smad4 and mediate erythrocyte differentiation, while Smad4 mediates growth inhibition of the same cells (He et al., 2006) in response to TGF-β. TIF1γ can also bind to Smad2, Smad3 in mesenchymal, and epithelial cells in response to TGF-β1. Moreover, Smad2 and Smad3 complex

with both Smad4 and TIF1γ (He et al., 2006). In the lung epithelial cells, Smad3 binds with thyroid transcription factor-1 (TTF-1) in the presence and absence of TGF-β3 and competes with Smad4 for interaction with Smad3 at all Smad-binding sites in the genome (Isogaya et al., 2014).

1.4.5 TGF-β/BMP in intestinal homeostasis and disease

TGF-β and BMP pathways are important for maintaining intestinal homeostasis (Figure 1.5). TGF-β type II receptors and ligands are present and expressed in the muscularis, the lamina propria and the differentiated compartment of both the small intestine and colon (Winesett et al., 1996; Sancho et al., 2004). BMP pathway is also involved in the regulation of intestinal homeostasis. BMP ligands, their receptors and the SMADs are expressed both in epithelial and mesenchymal cells whereas BMP antagonists are expressed mainly in mesenchymal cells (Hardwick et al., 2008). BMPR1A has a gradient distribution along the crypt-villous axis and is expressed at ICS (He et al., 2004). BMP acts in an opposing gradient to the Wnt pathway. BMP signalling is active at the crypt-villous border to promote differentiation and cell fate decision towards secretory cells, a process mediated by BMP2 and BMP4 expressed by mesenchymal cells. At the crypt base, BMP signalling is regulated by different BMP antagonists expressed by mesenchymal cells such as Gremlin, Noggin, and Chordin-like 1 to control stem cell renewal. In the proliferative zone there is no BMP signalling as these cells have low expression of Alk3 (He et al., 2004; Medema and Vermeulen, 2011; Wakefield and Hill, 2013).

1.4.5.1 *Smad4* mutations in CRC

SMAD4 mutations have been reported in 10-15% of colorectal cancer and are associated with worse overall survival (Kozak et al., 2015; Fearon, 2011). Loss of Smad4 expression was found to be present in 7.3% of stage I, 5.9% of stage II, 12.3% of stage III and 20% of stage IV CRC and in 43% of patients with metastasis (Kozak et al., 2015). Loss of heterozygosity (LOH) on chromosome 18 -where SMAD4 and SMAD2 are located- occurs

in 70% of CRC tumours (Fearon, 2011) and 50-60% of them are related to *SMAD4* allele loss (Woodford-Richens et al., 2001). A recent study has characterised SMAD2, SMAD3, and SMAD4 mutations in CRC from 744 patients with primary CRCs and 36 CRC cell lines. Somatic mutations of *SMAD4* were detected in 78 of primary CRC cases. Most of the mutations were missense (66.7%), followed by nonsense (19.2%), splice site (5.1%), frameshift (3.8%) and in-frame insertion/deletion mutations (3.8%) (Fleming et al., 2013). The hot spot mutation area is within the conserved R-SMAD binding surface in the MH2 domain (Fleming et al., 2013). Missense mutations were also reported in the MH1 domain of *SMAD4*, with no evidence for clustering along the DNA-binding interface. *In silico* analysis showed that A118V, R100G, R100T, G65R, and L98F mutations were expected to alter protein stability (Fleming et al., 2013) and K45N mutation was expected to alter the conserved NLS (Xiao et al., 2003). Fewer mutations in this study were reported in the linker and were predicted to be benign, but might affect the regulatory phosphorylation sites (Fleming et al., 2013). In this study, no differences between males, females, and the site of tumour (right colon, left colon or rectum) were observed (Fleming et al., 2013).

1.4.5.2 Mutations in the TGF-β and BMP pathway other than *Smad4*

Mutations in these pathways also lead to intestinal diseases and cancer (Massagué, 2008; Achyut and Yang, 2011). TGFβR-II mutations occur in approximately 30% of CRCs (Lao and Grady, 2011), and are mainly associated with MSI due to frameshift mutations at a poly-adenosine (poly(A)10) tract in exon 4 in 80% of the cases (Iacopetta et al., 1998).

SMAD2 and *SMAD3* mutations occur also in CRC with a similar distribution between the domains as in *SMAD4*. Mutation of SMAD2 occurs in 3.4% (Fleming et al., 2013) and SMAD3 in around 5% (Leary et al., 2008; Fleming et al., 2013).

Germline mutations in *BMPR1A* or *SMAD4* have been found in patients with juvenile polyposis (JP) -rare autosomal dominant adenomatous polyposis syndrome- and increased susceptibility to CRC (Hardwick et al., 2008; Wakefield and Hill, 2013).

1.4.6 Tumour microenvironment and TGF-β

Homeostasis is preserved in normal tissues by continuous basal release of TGF-β by local sources. In cases of tissue injury increased TGF-β release by platelets and various stromal components is important to prevent uncontrolled regenerative cell proliferation and inflammation (Massagué, 2008). In cases of tumours, TGF-β is frequently present in the tumour microenvironment -which consists of non-cancer cells, stromal tissue, soluble factors, signalling molecules, and extracellular matrix. TGF-β could be released by the cancer cells or other various cells in the tumour stroma (Massagué, 2008). The tumour microenvironment contains inflammatory cells such as F4/80$^+$, CD11b$^+$, B-cells, T-cells, cancer associated fibroblasts and endothelial progenitor cells (Achyut and Yang, 2011). Such stromal components create an environment that promotes tumour progression by providing different growth factors, cytokines, proteases and adhesion molecules. TGF-β is among these secreted cyokines. TGF-β initially signals to prevent pre-malignant progression, however, tumour cells could benefit from TGF-β for tumour progression once the tumour acquires more genetic alterations (Massagué, 2008, 2012). In cases where alterations are in the TGF-β pathway, it has been proposed that colonic cancer cells are behaving in an invasive manner appropriate for an immune reaction (Taketo, 2012). Moreover, it has been recently reported that high levels of TGF-β isoforms in stromal cells increases the chance of tumour recurrence after therapy (Calon et al., 2012).

1.4.7 Mucinous adenocarcinoma

Mucinous carcinoma is a histological subtype of colorectal cancer defined according to the WHO by pools of extracellular mucin covering $\geq$50% of tumour area (Bosman et al., 2010). It accounts for 11-15% of the cases with a tendency to occur at late stages (Green et al., 1993; Consorti et al., 2000; Kakar et al., 2004; Langner et al., 2012). Tumours in which extracellular mucin consist of <50% of the tumour area are designated as adenocarcinomas with mucinous component (Bosman et al., 2010). In most of the cases it is related to the MSI status of the patients (Kakar et al., 2004). *Smad4* mutations are frequently associ-

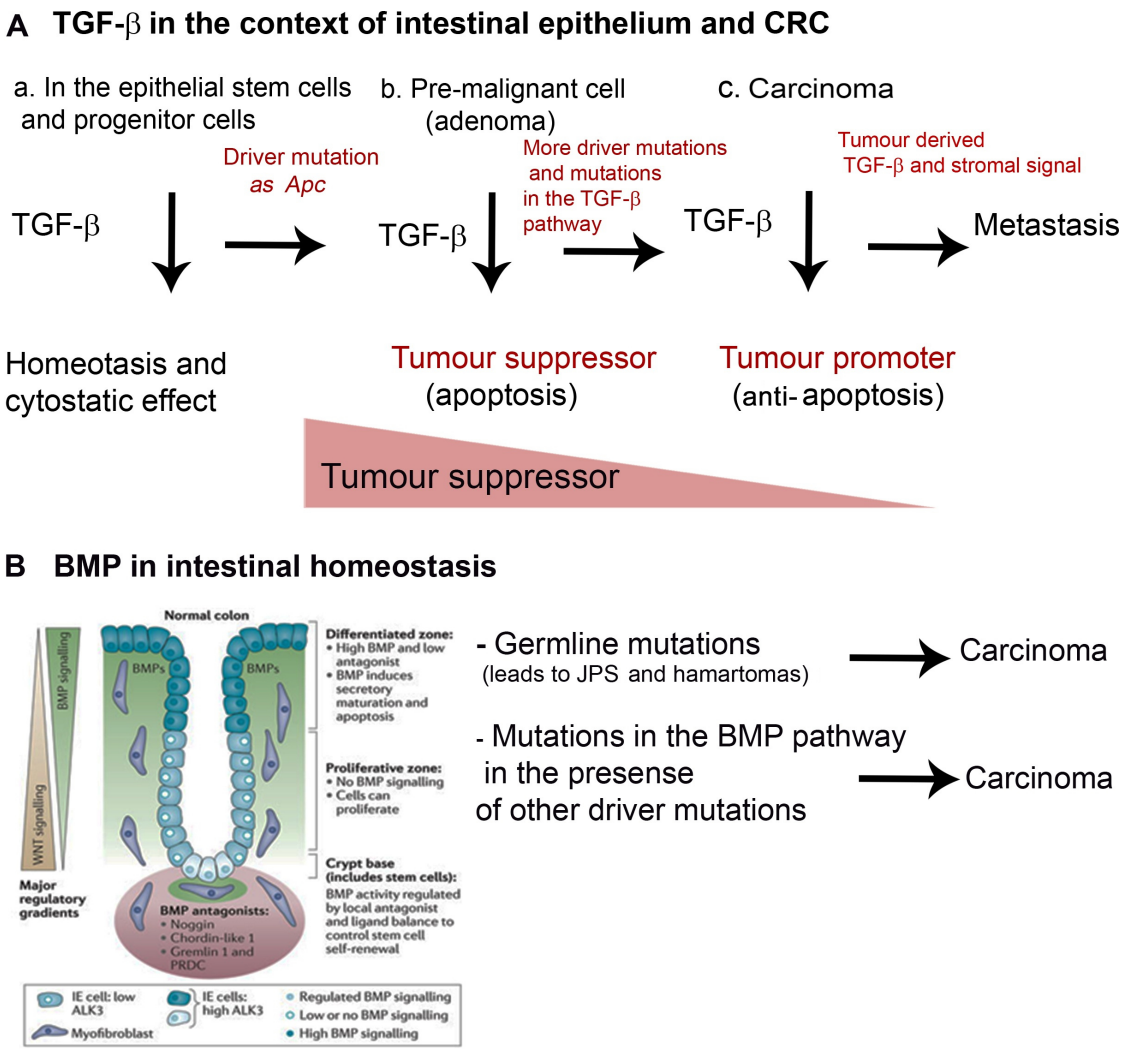

Figure 1.5: **TGF-β and BMP in intestinal homeostasis and disease**. Both pathways are important for intestinal homeostasis and mutations in these pathways predispose CRC. (A) TGF-β paradoxically acts as a tumour suppressor at early stages of intestinal tumorigenesis and at late stages it has a tumour promoter effect. The exact molecular mechanisms of the switch are yet to be defined (Massagué, 2012). (B) BMP pathway is important for the differentiation of the epithelial cells, acting in an opposite gradient to Wnt pathway. The base of the crypt is protected from BMPs by different antagonists. Mutations in this pathway also lead to intestinal tumorigenesis. Adapted from (Wakefield and Hill, 2013).

ated with mucinous histology both in human and mice (Takaku et al., 1998; Freeman et al., 2012). Increased mucin production is also reported in sessile serrated polyps/Adenomas (SSA/Ps) (Delker et al., 2014). The mucinous cancers with microsatellite-stable (MSS) or showing low levels of microsatellite-instability (MSI-L) are classified to be high-grade lesions, whereas tumours with high microsatellite-instability (MSI-H) are classified to be low-grade lesions (Kakar et al., 2004; Bosman et al., 2010; Langner et al., 2012). Mucinous adenocarcinomas occurred mainly in the right colon, and presented with large tumour size (Langner et al., 2012).

Mucins are glycosylated proteins with high molecular weight that can either secrete gel-forming mucins (MUC2, MUC5AC, MUC5B, and MUC6) or transmembrane mucins that have juxtamembrane domains with homology to the EGF family (MUC1, MUC3A, MUC3B, MUC4, MUC12, MUC17) (Byrd and Bresalier, 2004; Hollingsworth and Swanson, 2004). The colon normally contains different types of mucins with MUC2 being the most abundant and expressed in goblet cells. MUC4 is expressed in both goblet and columnar cells, whereas MUC3 appears to be expressed within enterocytes. MUC1, MUC5AC, and MUC6 are not normally expressed in the colonic mucosa (Taliano et al., 2013). The deregulation of mucin expression in adenocarcinoma with apparent glycosylation of the mucin core proteins is important for the natural selection of the tumour cells (Hollingsworth and Swanson, 2004). They contribute to tumour cell survival in invasion and metastasis by capturing different growth factors and cytokines. The anti-adhesive properties of mucins allows tumour cells to detach from the tumour mass and invade, with the adhesive effect of mucins the tumour cells can attach to the endothelial cells and also allows them to escape immune surveillance (Hollingsworth and Swanson, 2004).

1.5 Modelling intestinal tumorigenesis

The major complication of CRC is metastasis. Therefore, understanding the consequences of mutations involved in the initiation and progression stages is of great importance. In

CRC different pathways are altered with certain mutations being drivers and others being passengers. *P53, KRAS, PIK3CA, SMAD4, TCF7L2, FBXW7, NRAS* and *PTEN* genes are highly mutated as shown by high-throughput genomic studies for human CRC (Network et al., 2012; Seshagiri et al., 2012) and considered as drivers. Interestingly, the same conserved pathways that have been shown to be altered in human CRC (Network et al., 2012; Seshagiri et al., 2012) were also altered in mouse screen models using the Sleeping Beauty transposon system (Starr et al., 2009; March et al., 2011). March *et al.* reported that within mice carrying mutations in *Apc*, individual cells within tumours gain diverse mutations in order to evolve to carcinomas (March et al., 2011). Seshagiri, S. and her colleagues showed 356 similar genes to be altered between human and mouse model screens (Seshagiri et al., 2012). Among these genes, *APC, SMAD4, PTEN, FBXW7, TP53* and *KRAS* have been reported to be highly mutated in both of them and considered as driver mutations (March et al., 2011; Seshagiri et al., 2012). Therefore, understanding the molecular mechanisms and the functional consequences of these driver mutations and their pathways on the initiation and progression of CRC is of great importance for the development of effective therapy. Different approaches can be used to model CRC such as genetically modified mice, high throughput methods for human colorectal cancer, organoid culture and xenografts (Young et al., 2013). In this thesis mouse models and intestinal organoid culture will be used to model intestinal tumorigenesis when the tumour suppressor of the TGF-β pathway, *Smad4*, is mutated in the context of active Wnt signalling.

1.5.1 Mouse models

Mouse models are one of the tools used for modelling CRC for several decades due to the lack of *in vitro* models that recapitulate the normal behavior of tumour cells. They have increased our understanding of this cancer as they provide controlled *in vivo* studies and the effect of a mutation can be assessed on a whole organism. Different mouse models for the initiation step with *Apc* gene mutations have been used. Also, crypt stem cells (Lgr5) have been described to be the cells-of-origin of intestinal cancer (Barker et al., 2009) (described in section 1.3.3 and Table 1.1). Different mouse models have evaluated

the effect of mutations in the TGF-β pathway on intestinal cancer as well (section 1.5.1.1). Most of these models are based on germline mutations. They showed that downregulation of this pathway is important for tumour progression although there were some variable outcomes. For that, more models directed towards the stem cells are required to evaluate the effect of this pathway on intestinal tumorigenesis. Due to the nature of CRC, the main disadvantages of the mouse models are the long generation time required for combined gene mutations accompanied with the high cost.

1.5.1.1 Mouse intestinal models altered in the TGF-β pathway

Conditional deletion of *Tgfbr2* in an *Apc1638*$^{N/+}$ mouse model increased the number of intestinal adenomas. This mutation enhanced the expression and activity of matrix metalloproteinases MMP-2 and MMP-9 and the secretion of TGF-β1 (Muñoz et al., 2006). Mice with *Smad2*$^{-/-}$ genotype died at an early embryonic stage, and *Smad2*$^{+/-}$ mice do not develop intestinal neoplasia (Hamamoto et al., 2002). In a *cis*-compound *Apc*$^{580D/+}$*Smad2*$^{-/+}$ heterozygous mice, accelerated malignant progression of intestinal tumors was observed compared to *Apc*$^{580D/+}$ mice (Hamamoto et al., 2002). Mice with *Smad3*$^{-/-}$ genotype are viable (Zhu et al., 1998; Sodir et al., 2006). *Smad3*$^{-/-}$ mice developed colorectal adenocarcinoma that metastasis to lymph nodes within 6 months (Zhu et al., 1998), but was not reported in a similar mouse model (Ashcroft et al., 1999). When *Smad3*$^{-/-}$ was crossed with *Apc*$^{Min/+}$, tumour burden increased with rapid onset of invasive tumorigenesis in the distal colon compared to adenoma development in the small intestine of the control group, with *Apc*$^{Min/+}$*Smad3*$^{+/+}$ genotype, suggesting that the distal colon is more prone to tumour initiation and progression when both pathways are altered (Sodir et al., 2006). *Smad4*$^{+/-}$ mice developed JP at 1.5 years (Takaku et al., 1999) and invasive adenocarcinoma when crossed with *Apc*$^{\Delta 716/+}$ (Takaku et al., 1998) (Table 3.1). Germline mutations in *Bmpr1a* in mice results in embryonic lethality and conditional mice for *Bmpr1a*$^{fl/fl}$*Mx1-cre* develop multiple polyps filled with mucin and inflammatory cells within the stroma which is characteristic of JP syndrome (He et al., 2004).

1.5.2 *In vitro* intestinal organoid culture and cell lines

In mouse models, direct experimental manipulation, molecular consequences and functional analysis to understand cancer biology and develop target therapy is not easy due to the complex nature of the whole organism. Such experiments are mainly based on cell lines that are derived from cancer (Li and Clevers, 2012; Krausova and Korinek, 2014). The cell lines differ genetically from primary tissue, gaining new mutations in order to adjust to their new environment (Borrell, 2010). Additionally, these cell lines lack the systems that can recapitulate the normal behavior of tumour cells (Vecsey-Semjen et al., 2002). Recently, new approaches to study intestinal biology via intestinal organoid culture have been introduced (Ootani et al., 2009; Sato et al., 2009). Ootani *el al.* used an air-liquid interface with stromal component to culture intestines from newborn mice in a collagen-based gel. These cultures showed prolonged intestinal epithelial cells that expanded into spheres with proliferation, multi-lineage differentiation and maintenance of both stem cell compartments (Lgr5 and Bim1). This culture does not require specific growth factors due to the presence of the stroma. These organoids also respond to Wnt inhibitor DKK by growth inhibition, enhanced growth with R-spondin1 treatment and differentiation to goblet cells upon Notch pathway blocking with a γ-secretase inhibitor (Ootani et al., 2009). In Hans Clevers lab, single $Lgr5^{high}$ and crypts have been used to grow intestinal organoids (Sato et al., 2009). This culture system is based on defined growth factors which are important to maintain the intestinal stem cell niche. For instance, R-spondin1 is important to stimulate the Wnt pathway, Noggin is required for the inhibition of the BMP pathway and EGF is important for the EGFR dependent proliferation of these organoids. The organoids are supported by extracellular matrix (ECM) provided by Matrigel allowing cell-cell and cell-ECM interactions in a way that mimics aspects of the *in vivo* situation (Sato et al., 2009). Under these conditions organoids can be grown as miniguts characterised by central lumen and villous-like epithelium with multiple crypts. The organoids are genetically stable (Sato et al., 2009). This culture system has been expanded to human normal colonic and adenoma culture and mouse adenoma culture (Sato et al., 2011).

Whilst our project was ongoing and the *in vitro* intestinal crypt manipulation was already performed, primary intestinal organoids with *Apc*$^{fl/fl}$ *Villin-CreETR*, in an air-liquid interface with stromal component, was genetically manipulated in culture to generate adenoma. The transformation of intestinal adenomas to adenocarcinoma required multi-hits of the commonly muted genes in CRC *P53, Kras* and *Smad4* in addition to the *Apc*. Gene mutations were generated using retroviral expression of short hairpin RNAs (shRNAs) (Li et al., 2014).

Hans Clever's lab used CRISPR/Cas9-mediated genome editing to introduce mutations in *APC, P53, KRAS and SMAD4* to human small intestinal organoid stem cells in Matrigel cultures. Mutations sequentially starting from the *APC* gene and based on functional selection strategies were introduced to obtain clonal, mutant organoids. For instance, to select clones with *Apc* mutations, R-spondin1 was withdrawn. Clones growing in the presence of nutlin-3 had mutations in *P53*. EGF withdrawal was used for *KRAS* mutant clone selection, and Noggin withdrawal was used for *Smad4* mutant clone selection (Drost et al., 2015). *APC* and *P53* mutations alone were sufficient to acquire chromosomal instability (CIN). Clones with different mutations were injected subcutaneously in to immunodeficient mice. Those lacking functional APC, KRAS and P53 developed tumours that were well-differentiated carcinomas with relatively limited invasive growth. Those lacking functional APC, KRAS, P53 and Smad4 produced tumours that were poorly differentiated with invasive carcinomas (Drost et al., 2015). Another group used the same approach with genome editing to knockdown the driver mutations in human colorectal carcinogenesis; *APC, KRAS, PIK3CA, Smad4* and *P53*. For Smad4 clone selection, they withdrew Noggin and TGF-β inhibitor and added either TGF-β1 or BMP4 to the medium (Matano et al., 2015). In this study, the mutations in the driver genes are insufficient for the gene expression and re-programming that occurs during the transition to CRC. Genetic stability was maintained in these genetically modified organoids as no aneuploidy or copy number variation was observed (Matano et al., 2015) and more epigenetic alterations and CIN might be required for the malignant transformation (Matano et al., 2015).

Two of these studies showed that multi-hits are required for adenocarcinoma formation and in one of them no transformation occurred. In the study by Li *et al.*, the transformation was in the presence of stromal components. These variable results require further investigation of other factors required for transformation. In addition to genetic alteration, microenvironment, inflammation, and diet might also affect the progression in CRC. For that, the use of organoid culture and microenvironment controlled for certain factors that modify tumour progression is of great importance. For instance, the effect of TGF-β, BMPs, and interleukins might be studied individually as well as in combination in order to understand the effect of alterations in the TGF-β pathway. Here CRISPR was not utilised, but intestinal organoid culture under defined growth conditions with a conditional approach to abrogate gene function by Cre-mediated recombination.

1.6 Aims

Downregulation of TGF-β pathway and upregulation of PI3K and RAS-MAPK pathways are frequently altered in human CRC. Different members of these pathway are mutated and are considered to be driver mutations such as *Smad4* in TGF-β and overexpression of Insulin like growth factor 2 (IGF2), which act downstream of the PI3K and RAS-MAPK pathways (Network et al., 2012). Smad4 effect on intestinal tumorigenesis has been studied *in vivo* only in a few models with variable outcomes. However, different *in vitro* studies have evaluated the effect of Smad4, some of which have used CRC cell lines. These studies were mainly in 2D culture. Although these cell lines are important for functional analysis, such culture systems lack cell to cell interactions, and organisation and are harboring different mutations other than *Smad4*. Mannose-6-phosphate/IGF2R binds IGF2 for degradation and is also involved in the activation of latent TGF-β1. Mutations in IGF2R will lead to increase in Igf2 level leading to aberrant activation of PI3K and RAS-MAPK pathways. It also prevent latent TGF-β activation that is required for a functional TGF-β pathway. Therefore, the aims of this work are:

1. To evaluate functional consequences of Smad4 loss of function on Apc dependent ade-

noma formation *in vivo*

2. To evaluate the functional consequences of Igf2r loss of function on Apc dependent adenoma formation *in vivo*

3. To optimise intestinal organoid culture methodology

4. To genetically manipulate intestinal crypt culture and to form adenomas *in vitro*

5. To evaluate the effect of TGF-β1 on Smad4 disrupted adenoma

6. To interrogate changes in gene expression under defined conditions of Smad4 deletion in the presence and absence of TGF-β1.

Chapter 2

Materials and methods

2.1 Genetically modified mice

2.1.1 Animal husbandry

Animals were housed in isolator cages, in the Pathology Support Building (PSB) -Sir William Dunn School of Pathology- with 12 hour (h) dark/light cycle and fed on normal chow and water. Animals were ear notched between postnatal day 8-12 for identification and genotyping purposes. All procedures were approved by the UK Home Office and implemented under Home Office Project license (30/2695) and Personal licence (L25ED4F2A) following the University of Oxford ethical committee approval.

2.1.2 Genetic models and strain background

The genetically modified mice used in this study and their strain backgrounds are listed in Table 2.1

2.1.3 Mouse breeding

The generation of conditional mouse alleles for both *in vivo* and *in vitro* experiments followed the subsequent strategies.

Table 2.1: Genetic models and strain background

Genetic model	Mutation	Nomenclature	MGI identifier	Background (number of generations)	Reference
Apc$^{fl/fl}$	LoxP sites flanking exon 14 of *Apc*	Apc^{tm1Tno}	3764940	C57BL/6J (>10)	(Shibata et al., 1997)
Lgr5-EGFP-IRES-CreERT2	Tamoxifen inducible Cre in the *Lgr5* compartment	Lgr5$^{tm1(cre/ERT2)Cle}$	3764660	C57BL/6J (>10)	(Barker et al., 2007)
Smad4$^{fl/fl}$	LoxP sites flanking exon 2 of *Smad4*	Smad4^{tm1Rob}	3624262	C57BL/6J (>10)	(Chu et al., 2004)
Villin-CreERT2 (*vil-Cre-ERT2*)	Tamoxifen inducible Cre in the Villin compartment	Tg(Vil-cre/ERT2)23Syr	3053826	D2B2 (backcrossed >10 generations on C57BL/6J)	(El Marjou et al., 2004)
Rosa26-YFP (LoxP-STOP-LoxP)	Reporter gene that is Cre recombinase dependent	Gt(ROSA)26-Sor$^{tm1(EYFP)Cos}$	2449038	C57BL/6J (>10)	(Srinivas et al., 2001)
Igf2r^{I1565A}	Domin 11 knock in mutation that reduces Igf2 affinity	Igf2r^{I1565A}-Art		C57BL/6J (>10)	Hassan lab (unpublished data)

2.1.3.1 Breeding strategy for Smad4 adenoma model and adenoma culture

Breeding was between the models *Apc*$^{fl/fl}$, *Smad4*$^{fl/fl}$, *Lgr5-EGFP-IRES-CreERT2* and *Rosa-26-YFP* to generate mice homozygous for *Apc* and either wild type, heterozygous or homozygous for *Smad4* in both sexes according to Figure 2.1.

2.1.3.2 Breeding for *Igf2r*$^{I1565Amaternal/+paternal}$ (*Igf2r*$^{I1565Am/+p}$) adenoma model

Breeding of *Igf2r*^{I1565A} mouse model was performed in two stages according to Figure 2.2. Igf2r is imprinted on the paternal allele, meaning that the phenotype will be manifest on the maternal allele. Breeding of the genetically modified allele through the maternal line would be experimental to turn on the allele and phenotype whereas breeding through the paternal allele would not be associated with a phenotype.

2.1.3.3 Breeding to generate adenoma using genetic manipulation

Breeding was between the models *Apc*$^{fl/fl}$, *Smad4*$^{fl/fl}$, *Villin-CreERT2* and *Rosa26-YFP* to generate mice homozygous for *Apc* and mice either wild type or homozygous for *Smad4* in both sexes according to the strategy shown in Figure 2.3. Mice from section 2.1.3.1 were also used.

2.1.4 Tamoxifen injection

Mice with a positive *Lgr5-CreERT2* genotype were injected intraperitoneally with 2 doses of 5mg tamoxifen (Sigma, T5648) each dissolved in corn oil on 2 consecutive days (24 hours apart). Mice were aged $\geq$8 weeks and weighed $\geq$25 grams. Animals were monitored after injection, weight and general appearance were recorded and scored according to Table 2.2. Humane end point was met by the criteria in the table.

2.1.5 Mouse dissection

Dissection for both tamoxifen treated or untreated mice was performed in the laminar flow hood. The abdomen was opened by midline abdominal incision, after which the intestine was isolated, and processed as below.

2.1.5.1 Intestinal tissue for adenoma count and histology

Isolated small intestines were divided equally into proximal, middle and distal sections. On the absorptive side of Benchkote (Whatman), the intestines were opened longitudinally using scissors, and washed with cold phosphate buffered saline (PBS) (PAA, H15-002). The colon was also opened longitudinally and washed with PBS. The washed intestines were then rolled, placed in 50ml Falcon tubes and fixed in 10% (v/v) neutral buffered formalin (NBF) for 24h at room temperature, then washed in PBS and preserved in 70% (v/v) ethanol at 4°C.

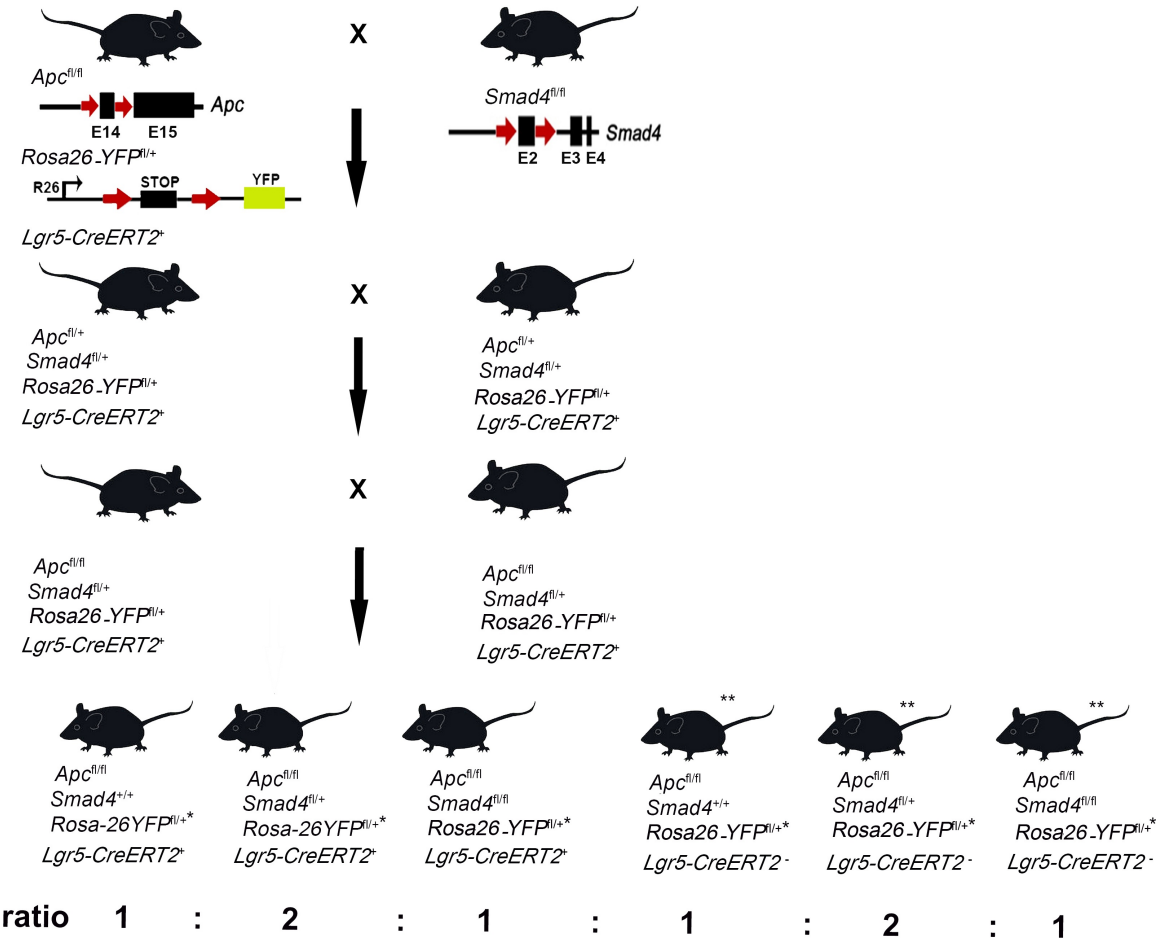

Figure 2.1: **Experimental breeding to generate *Apc*$^{fl/fl}$, *Smad4*$^{fl/fl}$, *Lgr5-CreERT2*, *Rosa26-YFP* adenoma model.** Simplified diagram representing the breeding strategy to generate experimental mice. A mouse model with *Apc*$^{fl/fl}$, *Lgr5-CreERT2*, *Rosa-26YFP* alleles was generated after multi-step breeding and was crossed with a *Smad4*$^{fl/fl}$ mouse model. The last line represents the genotype of the experimental mice. **YFP*$^{fl/+}$ genotype is represented for simplicity. Mice with *YFP*$^{+/+}$ and *YFP*$^{fl/fl}$ were also generated. ***Cre* negative mice were also generated but were not used in experiments. Ratios represent the expected Mendelian ratio for the genotypes.

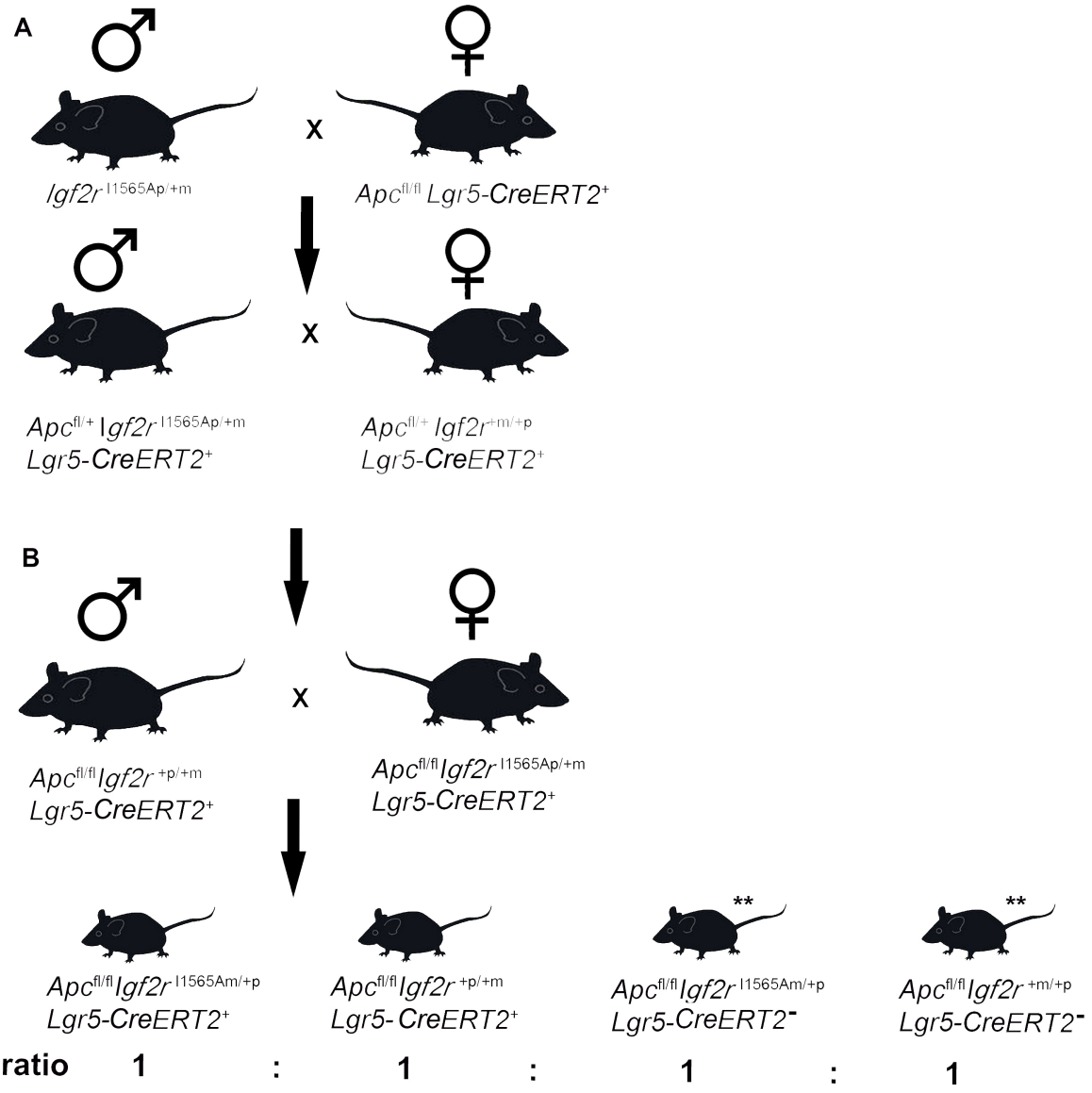

Figure 2.2: **Experimental breeding to generate *Apc*$^{fl/fl}$, *Igf2r*$^{l1565Am/+p}$, *Lgr5-CreERT2* adenoma model.** Simplified diagram representing a sex dependent breeding strategy to generate experimental mice. (A) Paternal transmission of *Igf2r*^{l1565A} to generate mice with *Apc*$^{fl/fl}$*Igf2r*$^{l1565Ap/+m}$*Lgr5-CreERT2*. (B) Maternal transmission of *Igf2r*^{l1565A} to generate experimental mice *Apc*$^{fl/fl}$*Igf2r*$^{l1565Am/+p}$*Lgr5-CreERT2* and their controls. ***Cre* negative mice were also generated but were not used in experiments. Ratios represent the expected Mendelian ratio for the genotypes.

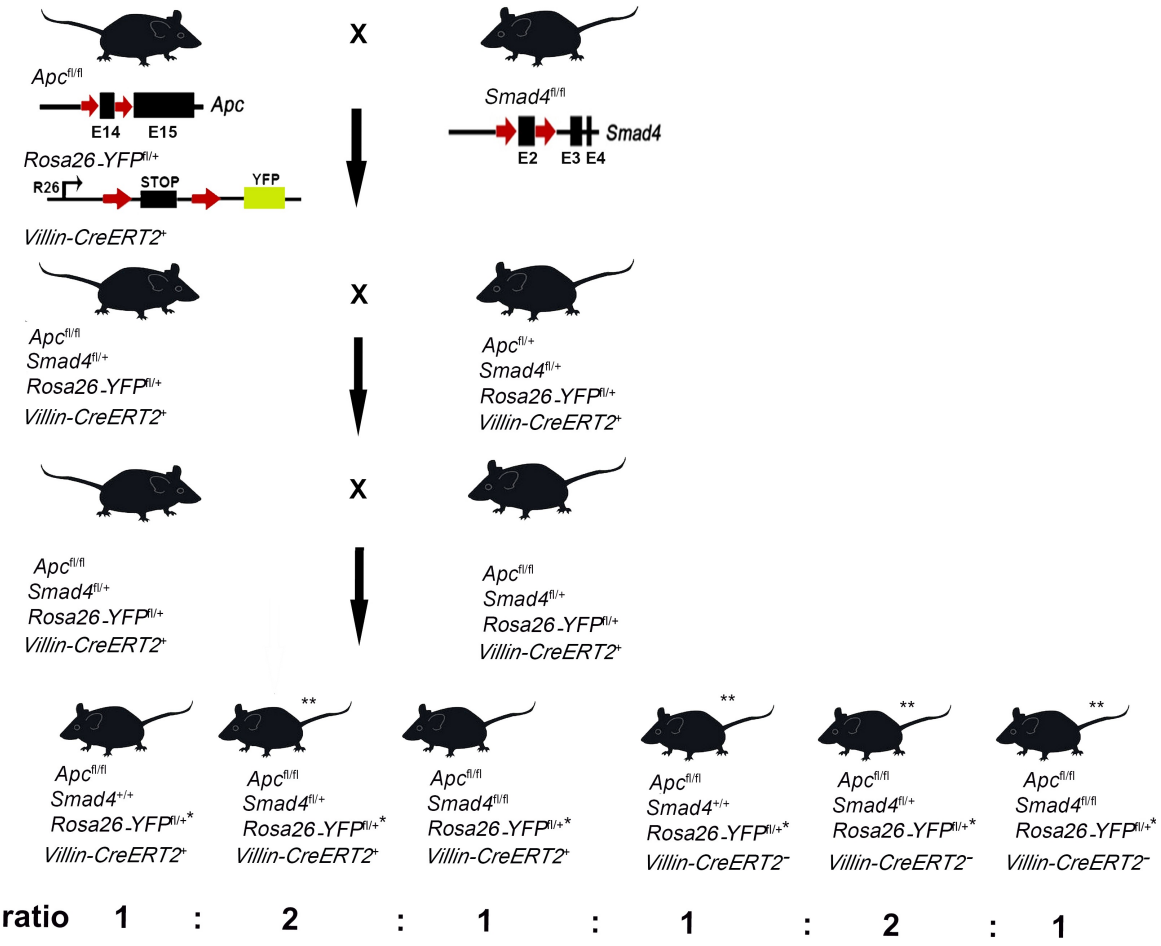

Figure 2.3: **Experimental breeding to generate *Apc*$^{fl/fl}$, *Smad4*$^{fl/fl}$, *Villin-CreERT2*, *Rosa26-YFP* adenoma model.** Simplified diagram representing the breeding strategy to generate experimental mice. A mouse model with *Apc*$^{fl/fl}$ *Villin-CreERT2Rosa-26YFP* alleles was generated after multi-step breeding and was crossed with *Smad4*$^{fl/fl}$ mouse model. The last line represents the genotype of the experimental mice. **YFP*$^{fl/+}$ genotype is represented for simplicity. Mice with *YFP*$^{+/+}$ and *YFP*$^{fl/fl}$ were also generated. ***Cre* negative mice were also generated but were not used in experiments. Ratios represent the expected Mendelian ratio for the genotypes.

Table 2.2: Symptom and sign score sheet (humane end point monitoring)

Sign		score
Body condition	Well-conditioned	0
	Under-conditioned: segmentation of vertebrae evident. Dorsal pelvic bones palpable	2
	Emaciated: skeletal structure extremely prominent. Little or no flesh cover and vertebrae distinctly segmented	3
Weight	Normal	0
	Reduced by <10%	1
	Reduced by 10-15%	2
	Reduced by >15%	3
Respiratory rate	Normal	0
	Reduced by <10%	1
	Reduced by <10-20%	2
	Reduced by >20 or 10-20% accompanied by nasal discharge	3
Evoked response	Normal	0
	less alert	2
	Violent, very weak, very still or hunched	3
Tumour appearance	No abnormality	0
	Distended abdomen, tumour lump 0.5-1cm, anaemia (pale/translucent hind paws)	2
	Tumour >1.5cm, any ulceration, any abdominal distension affecting normal movement, rectal bleeding or fresh blood in cage	3
Total		
Interpretation		
Score 3 in any category	Animal is distressed and should be humanely killed	
Total score >5	The animal should be monitored closely (at least twice daily) and humane killing considered if no improvement within 24 hours.	

2.1.6 Intestinal tissue collection for culture

Tissue collection for culture was performed according to Sato et al. (Sato et al., 2009) with modifications from the Sansom lab (Beatson institute, UK).

2.1.6.1 Intestinal tissue collection for adenoma culture

The caecum of tamoxifen treated mice was opened longitudinally using scissors. The tumour was excised using scissors and placed in cold PBS on ice. The caecal tumours were chosen for sampling as occurrence of small intestinal adenoma in the experimental mice was rare.

2.1.6.2 Intestinal tissue collection for crypt culture

For *in vitro* intestinal crypt culture, the intestine was opened longitudinally, the villi from the small intestine (tamoxifen untreated mice) were scraped gently with a coverslip, and the intestine ($\sim$15cm) was placed in cold PBS on ice.

2.2 Identification and Genotyping

2.2.1 Material collection

Assistance with genotyping was performed by Dr. Emma Carter and Dr. Jennifer Hughes. Genotyping was performed for mice and intestinal organoids in culture. For mice, ear notches were taken between postnatal day 8-12 under sterile conditions (1M NaOH solution was used as disinfectant between ear notches) in a laminar flow cabinet. Post-mortem (PM) samples were taken from the ears of experimental mice as additional controls, and samples were stored at 4°C until needed for DNA extraction. For intestinal organoids growing in Matrigel, medium was removed (one well of 24 or 48 well plate), organoids were washed once with 500µl cold PBS (Ca^{+2} and Mg^{+2} free) and then 1ml cold 5mM EDTA-PBS was added. Organoids were then scraped from the well using a 200µl pipette

tip. Organoids were placed in a centrifuge tube on ice for 15 minutes with agitation from time to time to dissolve the Matrigel. The organoids were centrifuged at 328g, and the DNA was either extracted directly from the pellet or the pellet was preserved at -20°C.

2.2.2 Genomic DNA isolation

DNA was extracted by the HotSHOT extraction method (Truett et al., 2000). Freshly prepared alkaline lysis reagent DPG1 solution (25mM NaOH, 0.2mM EDTA in distilled water, pH 12.0) was added to the tissues (250µl for ear clip and 70µl for organoids) and incubated on a dry hot plate (Dri-Block OB-3, Techne) at 95°C for 1h. An equal amount of DPG2- (neutralizing reagent- 40mM Tris-HCl) was added, vortexed and centrifuged at 16,000g (Biofuge, Heraeus) for 6 minutes. The supernatant was transferred to a new centrifuge tube and stored at 4°C prior to PCR.

2.2.3 Genotyping by polymerase chain reaction (PCR)

Genotyping was performed by polymerase chain reaction (PCR) using the HotStartTaq *Plus* DNA Polymerase kit (Qiagen, 203605). PCRs were prepared in CoralLoad PCR buffer which is ready to load onto electrophoresis gels. PCR primers (Sigma) and PCR conditions are listed in Tables A.1 and A.2, respectively. DNA was amplified using either the Bio-Rad MJ Mini Personal Thermal cycler or MJ Research Dyad Thermal Cycler.

2.2.4 Gel electrophoresis

PCR products were visualised by gel electrophoresis. UltraPure Agarose (Invitrogen, 16500) was dissolved in 0.5M TBE buffer (45mM Tris-borate and 1mM EDTA) at a concentration between 1.5%-2% (w/v) by boiling in a microwave for 2 minutes. The agarose solution cooled and 2µg ml^{-1} of Ethidium Bromide (Sigma, E1510) was added. Agarose solution was poured in the casting chamber to set. 5µl of 100bp DNA ladder (Bioline) and 10µl of sample were loaded in to wells under 0.5M TBE buffer. The gel was run at

80V (PowerPac, Bio-Rad) for 25-30 minutes and visualised by UV transillumination using a Syngene bioimaging system.

2.2.5 DNA sequencing

For DNA sequencing, 50µl PCRs were prepared in each of four tubes. PCR products were visualised by gel electrophoresis. Expected bands were cut using a UV-light. The bands were weighed and the products were cleaned using Zymoclean Gel DNA Recovery kit (D4001) as per the manufacturer's protocol. DNA quantity and quality was assessed (described below). DNA samples associated with 3.2pM primers were sent to Source BioScience LifeSciences for Sanger DNA sequencing. DNA sequencing results (".abl" files) were aligned using Geneious software.

2.2.6 DNA quality and quantity assessment

DNA quantity and quality was assessed using a Nanodrop -1000 spectrophotometer (Thermo scientific). The absorbance was measured at 230nm (A_{230}), 260nm (A_{260}) and 280nm (A_{280}) against distilled water. DNA quantity was calculated and purity with respect to protein contamination measured by comparing ratios of A_{260}/A_{280} automatically and considered pure if the ratio is $\sim$1.8. A_{260}/A_{230} ratio is a secondary ratio to estimate the DNA purity against other contaminants and considered pure if the ratio is 2.0-2.2.

2.3 Intestinal adenoma counting and scoring

Small intestinal and colonic adenomas were scored for number, diameter, and distribution using a dissecting microscope (Nikon SMZ800) and sizing calliper. The calliper sizes were determined by wrapping a wire around drill bits of known diameter generating a range of different sizes to measure adenomas. All adenoma analysis was performed by a single investigator. The length and diameter of the intestine was measured to generate adenoma count per cm^2.

2.4 General histology and tissue staining

Histological procedures were carried out in the core Histology Facility, Sir William Dunn School of Pathology by Richard Stillion (R.S.). Briefly, formalin fixed intestine rolled in a swiss-roll shape was placed in a cassette. The cassettes were processed with an automated buffered system and embedded in wax. Tissue blocks were sectioned at 5µm thickness. Sections were stained by R.S. with haematoxylin and eosin (H&E) and Alcian blue/Periodic acid Schiff (PAS) stain, as required.

2.5 Adenoma culture

Adenoma and crypt culture was carried out according to a protocol from Professor Owen Sansom's lab (Beatson Institute, Glasgow) which was an updated version of a published protocol from Professor Hans Clevers' lab (Sato et al., 2009) (Sato et al., 2011). The protocol was further modified according to my optimisation (Figure 4.1, 4.2). The reagents used are listed in Table 2.3.

2.5.1 Adenoma extraction

Adenomas collected in section 2.1.6.1 were then cut into tiny pieces using scissors, washed 3 times with cold PBS and centrifuged at 328g (Beckman GPR centrifuge, GH-3.7 rotor) for 3-5 minutes before incubation in 5mM EDTA for 10 minutes. The tube was shaken vigorously and the resulting adenoma suspension washed twice with cold PBS followed by centrifuging (328g for 3-5 minutes). The cell pellet was resuspended with 5ml of 1X TryplE Express- a highly purified recombinant cell dissociation trypsin-like enzyme- (Invitogen, 12604), and incubated at $37\,^{\circ}\mathrm{C}$ for 30 minutes. The tube was again shaken vigorously and the supernatant containing dissociated adenomas was collected in a 50ml Falcon tube. The remaing undissociated adenomas were washed and broken down by 2-5 times hard pipetting with 5ml ADF1 medium. Supernatant were collected in a 50ml Falcon tube and the collected adenomas were passed through a 40µm cell strainer (BD Falcon, 352340).

The filtered adenomas were then washed twice with ADF1 at 328g for 5 minutes. The pellet was finally mixed with 1ml ADF1 and the number of cells was counted as described below.

2.5.2 Adenoma counting

To determine cell count and viability for the extracted adenoma, 19µl of the homogeneous adenoma solution was mixed with 1µl of solution 13 (AO.DAPI)- acridine orange (AO), 30µg ml^{-1}. 4',6-Diamidino-2-Phenylindole (DAPI) 100µg ml^{-1} -(Chemometec A/S, 910-3013). Approximately 9µl were then loaded into a NC-Slide A8 (Chemometec, 942-0003) and counted by cell counter (Nucleocounter, NC-3000). Both viable and dead cells are stained with AO and dead cells are stained with DAPI allowing the determination of viable cells with Nucleocounter software.

2.5.3 Adenoma culture in Matrigel

Viable cells suspended in ADF1 were then mixed with Matrigel (50%, v/v), and seeded either onto a 24 well cell culture plate with autoclaved coverslips (6000 cells in 40µl per well), a 48 well plate (6000 cells in 15µl per well or 9000 cells in 25µl per well) or a 96 well plate (5000 cells in 10µl per well) according to the experiment. The seeded plate was incubated (upside down for the 48 and the 96 well plates) at 37°C to allow Matrigel polymerisation. After polymerisation, ADF2, growth factors and inhibitors were added (500µl for the 24 well plate, 250µl for the 48 well plate and 100µl for the 96 well plate).

2.5.3.1 Supplements for adenoma growth measurement

The effects of different growth factors and inhibitors on adenoma growth were tested. Different concentrations of EGF (0.81-81.0nM), Noggin (0.216 and 2.16nM), Y-27632 (0.1-10µM), and/or SB-505124 (0.01-1.00µM) were added every other day starting from the day of culture (D0). Recombinant TGF-β1 (0.039-3900pM) was added to culture on D2

(R&D, 240-B-002). Controls included adenomas embedded in Matrigel and supplemented with ADF2 (negative control), and Matrigel with no cells supplemented with ADF2 and a vehicle for normalization.

2.5.3.2 Supplement for protein and RNA extraction

After seeding on a 48 well plate, ADF2 with 8.1nM EGF, 10µM Y-27632 and 1µM SB-505142 was added. The medium was changed on D2, the cells were washed once with 250µl warm PBS and replaced with 250µl freshly warmed ADF2 medium. EGF was then added and growth factors or inhibitors were added according to the experiment.

2.5.4 Adenoma freezing and thawing

2.5.4.1 Freezing growing adenomas

Growing organoids were frozen according to (Sato et al., 2011). Briefly, the medium was replaced with cold Recovery Cell Culture Freezing Medium (Life Technologies, 12648-010). Adenoma were dissociated using a 200µl pipette, then collected in labelled cryogenic vials. The samples were frozen gradually (-1°C min^{-1}) at -80°C using a Cryo 1°C Freezing Container (Nalgene). After 24h the samples were transferred to long term storage at -80°C. As an optimisation step, Recovery Cell Culture Freezing Medium could be replaced by Cryo-SFM (PromoCell, C-29912) or 10% DMSO with 90% ADF2 (mixed and placed on ice for at least 30 minutes prior to use).

Table 2.3: Reagents for crypt and adenoma culture

Reagent (supplier)	Working conc.[1]	Preparation	Final conc.
Advanced DMEM/F12 media (ADF) (Invitrogen, 12634)[2]	1x	ADF1: 5ml of 200mM L-Glutamine, 5ml of 1M HEPES, and 5ml of 100X Pen/Strep[3] were added to a 500ml ADF bottle. Stored in 48.5ml aliquots at -20°C	1x
Growth factor reduced Matrigel (BD Bioscience, 536231)	1x	Thaw overnight on ice in the fridge. Dilute according to the experiment with cold cell suspension immediately prior to seeding in per-cooled Eppendorf tube and keep on ice	0.7x or 0.5x
N2 (Invitrogen, 17502)	100x	500µl to 47.7ml ADF1 immediately before use	1x
B27 (Invitrogen, 12587)	50x	1ml to 47.7ml ADF1 immediately before use	1x
Epidermal growth factor (EGF) (Peprotech, AF-100-15)	1µg ml^{-1}	Powder resuspended in PBS/0.1% BSA to make 1µg $µl^{-1}$ stock. 10µl of the stock is further diluted in 10ml PBS/0.1%BSA. Use 50µl ml^{-1} with ADF2[4]	8.1nM (50ng ml^{-1})
Bovine serum albumin (BSA) (Sigma)	25%	5 grams dissolved in 20ml PBS. Sterilise using 0.45 µm syringe filter. Store in 800µl aliquots at -20 °C. Add one aliquot to 47.7ml ADF1	0.4%
Y-27632, ROCK Inhibitor (Tocris, 1254)	1mM	1mg vial is dissolved in 3.13ml dH_2O. Use 10µl for 1ml ADF2 medium	10µM
SB-505124, TGF-β inhibitor (Sigma, S4696)	1mM	5mg vial is dissolved in 14.91 DMSO. Use 1µl for 1m ADF2 medium	1µM
Noggin (N), BMP inhibitor (Peprotech, 250-38)	5µl ml^{-1}	Powder resuspended in PBS/0.1%BSA. Use 20µl for 1ml ADF2 medium	2.16nM (100ng ml^{-1})
mR-spondin (R) (R&D Systems, 3474-RS)	25ng $µl^{-1}$	Powder resuspended in PBS. Use 20µl for 1ml ADF2	500ng ml^{-1}

[1]conc.:concentration, [2]ADF dose not have insulin as a component and no serum is required as a supplement [3]Pen/Strep: Penicillin-Streptomycin,[4]ADF2: ADF1 supplemented with N2, B27, and BSA as described in the Table.

2.5.4.2 Freezing adenomas directly after extraction

Adenomas extracted from mice in section 2.5.1 can also be cryopreserved (Figure 4.1). 10% (v/v) dimethyl sulfoxide (DMSO) (Sigma) was mixed with 50% (v/v) foetal calf serum (FCS) (Biosera, UK) and kept on ice for 30 minutes. The mixture was then added dropwise to the freshly isolated adenomas in 40% (v/v) ADF2, the mixture kept on ice and rapidly split into 0.5ml aliquots (6.0-4.0x10^5 cells per vial) in labelled cryogenic vials (Thermo Scientific, 03755-71). Extracted adenoma from the same mouse was preserved in more than one aliquot. The samples were then frozen and stored as indicated above.

2.5.4.3 Adenoma thawing and culture

Cryopreserved adenomas were thawed quickly at 37°C, and 10ml of warm ADF1 was added dropwise to the thawed sample in a 15ml Falcon tube (Figure 4.1). The diluted sample was centrifuged at 115g for 5 minutes and the supernatant was discarded. The best growth was obtained when the pellet was resuspended directly with 50-60µl ADF1, transferred to a prechilled Eppendorf tube, placed on ice, mixed with an equal volume of Matrigel and seeded as mentioned above in a 96 well plate. For certain experiments, thawed adenomas (preserved in section 2.5.4.2) were counted, seeded at a cell density of 5000 cells per well in a 96 well plate and supplemented as indicated above. The formed organoids can be passaged on D5-D7 according to section 2.5.5 described below. The addition of 10µM Y-27632 and 1µM SB-505124 to the cell suspension prior to the addition of Matrigel enhances the growth of thawed adenomas.

2.5.5 Passaging adenomas in culture

In 15ml Falcon tubes pre-coated with 1% (w/v) BSA/PBS and kept for 20 minutes on ice, the organoids were washed once with cold PBS (same volume as the growing medium). Cold EDTA-PBS (5mM EDTA in PBS) was added to the wells (twice the volume of their growing medium). The plate was placed on ice and the organoids were scraped gently from the wells, were collected without pipetting and placed in a pre-coated 15ml Falcon tube. The

tube was placed on ice for 15 minutes with gentle shaking from time to time to dissolve the Matrigel and then washed twice with cold PBS (115g for 5 minutes). Warm TryplE Express was added to the organoids (e.g 1ml per 5 wells of 48 well plate), incubated at 37°C for 15 minutes, and pipetted several times with a 200µl pipette to produce dispersed adenomas. The adenomas were then washed twice with warm ADF1 (5X the volume of TryplE) and centrifuged at 328g for 5 minutes. The organoids were split in 1:3 or 1:5 ratio for protein, or immunofluorescence and seeded as indicated above either on 48 or 24 well plates. For growth assays and RNA, adenomas were counted as in section 2.5.2, seeded as indicated above (5000 cells per 96 well plate and 9000 cells per 48 well plate) and culture was supplemented as in section 2.5.3.1 and 2.5.3.2.

2.6 Intestinal crypt culture

2.6.1 Intestinal crypt isolation and culture

The small intestine collected in section (2.1.6.2) was chopped into 5mm pieces using scissors, and transferred into a 50ml Falcon tube. The pieces were washed 8-10 times (by gravity) with cold PBS using a 10ml pipette tube. They were then incubated in 2mM EDTA in PBS for 30 minutes on ice (EDTA binds free Magnesium to loosen crypts from the surrounding tissue). The pieces were then washed gently with cold PBS alone and the supernatant was discarded. 10ml of fresh PBS was then added, pipetted mechanically and the supernatant was collected in a 15ml Falcon tube. This step was repeated 3 more times, and each supernatant was collected in a separate tube. 20µl of the fraction from each tube was examined under the microscope and the samples with crypt enriched fractions were then combined (mainly fractions 2-4). The crypts were suspended in ADF1 up to 50ml and centrifuged at 328g (Beckman GPR centrifuge, GH-3.7 rotor) for 5 minutes. The pellet was washed 2-3 more times before being suspended in 10ml ADF1, passed through a 70µm cell strainer (BD Bioscience, 352350) and flushed with 5ml ADF1. The crypt suspension was transferred to a fresh 15ml Falcon tube, centrifuged at 100g for 2 minutes and washed 2-3 times with ADF1. The pellet was mixed with 1ml ADF1 and the number of

crypts were counted using a haemocytometer (10µl cell suspension with 10µl Trypan-blue (Sigma, 3050)). 150 crypts were mixed with 70% Matrigel in 50µl final volume per well. Crypts in Matrigel were seeded onto autoclaved coverslips (13mm) in a pre-warmed 24 well cell culture plate (Costar, 3524). The plate was incubated at 37°C for 15-20 minutes for Matrigel polymerisation (Figure 4.3).

2.6.1.1 Crypt culture supplements

To each well 500µl of ADF2 with crypt growth factors, ENR (8.1 nM EGF (E), 500ng ml^{-1} R-spondin1 (R), and 2.16nM Noggin (N)), were added according to each experiment. In addition, 1mM *N*-acetylcysteine (NAC) (Sigma) was added according to the experiment. The plate was incubated at 37°C, 5% CO_2. Growth factors were supplemented every other day and the entire medium was changed twice a week. Passage of cultures was carried out after one week depending on the experiment.

2.6.2 Genetic manipulation of intestinal organoids

Intestinal organoids were generated from *Apc*$^{fl/fl}$*Smad4*$^{+/+}$ *Villin-CreERT2 Rosa26-YFP*, *Apc*$^{fl/fl}$*Smad4*$^{fl/fl}$ *Villin-CreERT2 Rosa26-YFP*, *Apc*$^{fl/fl}$ *Lgr5-CreERT2 Rosa26-YFP* mice according to section 2.1.3.3. At D3, crypts were incubated with 500nM 4-hydroxy-tamoxifen (4-OHT) (Millipore, 579002) dissolved in 100% EtOH (test), vehicle (negative control) with 5µl EtOH for 12h at 37°C, 5% CO_2 and some kept without any treatment (normal crypts). The wells were washed twice with PBS and new medium was added. The test and the vehicle treated organoids were supplemented with EN only (no R) and the normal crypts with ENR. The growth factors were added every other day, at D5 after treatment, organoids were either characterised by immunofluorescence or passaged.

2.6.3 Passaging crypt derived organoids

Intestinal crypt derived organoids were collected and placed in 15ml Falcon tubes pre-coated with 1% BSA/PBS on ice for 20 minutes for Matrigel to dissolve (Figure 4.4). Organoids were then pipetted mechanically with a 200µl pipette, washed twice with cold PBS and a final wash with ADF1 medium followed by centrifuging at 328g for 5 minutes. The pellet was mixed with 70% Matrigel (splitting ratio was 1:3). Then the same steps as for crypt culture were performed. Both test and negative control of passaged organoids in section 2.6.2, were supplemented with 8.1nM E, and 2.16nM N every other day (no R). Untreated organoids were supplemented as in section 2.6.1.1. The formed adenomas and controls were then characterised by immunofluorescence (Figure 4.4).

2.7 Tissue and cell labelling

2.7.1 Tissue processing

Paraffin embedded sections were processed either by immunohistochemistry (IHC) or immunofluorescence (IF). In both methods, sections were rehydrated in xylene (2X 5 minutes), EtOH series 100% twice, 95%, 80%, 70% and 50% (v/v) for 3 minutes each followed by washing with dH_2O.

2.7.1.1 Immunohistochemistry

Sections were permeabilised with 1% (v/v) Tween-20 in dH_2O for 30 minutes followed by washing with dH_2O for 5 minutes. Endogenous peroxidase activity was quenched with 3% (v/v) hydrogen peroxide (H_2O_2) in dH_2O at room temperature for 15 minutes before washing twice in Tris buffered saline (TBS, pH7.4) for 3 minutes. Antigen retrieval with 10mM sodium citrate buffer-pH6 was performed at 125°C for 2 minutes and 85°C for 10 minutes in a pressure cooker (Biocare medical). Slides were cooled on the bench for 15-20 minutes and washed x3 in TBS for 3 minutes followed by permeabilisation and blocking for 1h in 0.5% (v/v) TBS-Tween-20 (TBST) + 10% (v/v) serum in TBST (depending on the

source of the secondary antibody) in a humidified chamber. Sections were then incubated with primary antibody (Table 2.4) in 0.3% (v/v) TBST + 5% (v/v) serum overnight at 4°C in a humidified chamber. Following x3 washing with TBS for 3 minutes, sections were incubated for 2h with species-specific biotinylated secondary antibody (Table 2.5). After washing x3 with TBS, signal amplification was performed using the Vectastain kit (Vector Laboratories), and labelling was visualised with 3,3-diaminobenzidine (DAB) (Vector Laboratories) as per manufacturer's instructions before nuclear counterstaining with haematoxylin (Gibbs) for 15 seconds. Slides were rinsed with dH_2O and washed x2 with TBS for 1 minute. Slides were dehydrated through water, EtOH series and xylene before mounting with DPX (Sigma, 06522).

2.7.1.2 Immunofluorescence

Following the hydration steps in section 2.7.1.1, antigen retrieval and cooling was carried out as in IHC, followed by washing x3 both in dH_2O and TBS for 3 to 5 minutes, respectively. Blocking, permeabilisation and incubation with primary antibody (Table 2.4) were the same as in IHC. Following washing, sections were incubated with the appropriate Alexa Fluor antibody (Table 2.5) for 1h in a dark humidified chamber. Slides were then washed and nuclei were labelled with 200µl of DAPI (0.5µg ml^{-1} DAPI in TBS) for 10 minutes at room temperature in the dark. Slides were washed x3 in TBS for 3 minutes in the dark and mounted with prolong anti-fade (Life technology, P36930).

2.7.2 Cell labelling

2.7.2.1 Immunofluorescence

Organoids or cells growing on coverslips in 24 well plates were used for IF according to a protocol adapted from (Lee et al., 2007) with certain modifications according to the protocol used in the Hassan Lab. The medium was aspirated and the wells were washed x2 with 500µl cold PBS. The culture was fixed for 10 minutes with 4% (w/v) paraformaldehyde (PFA) (Sigma), pH7.4 in PBS at room temperature. The fixation was stopped with 1ml of

Table 2.4: Primary antibodies for immunofluorescence and immunohistochemistry

Antibody (Clone)	Antibody dilution	Host &Isotype	Catalog number	Company
Axin 2	1:200	Rabbit	ab32197	Abcam
β-catenin	1:200	Mouse IgG_1	610154	BD Bioscience
CD11b	1:400	Rabbit	ab75467	Abcam
CD3	1:100	Rabbit	ab5690	Abcam
CD44 (8E2F3)	1:200	Mouse IgG_1	NBP1-47386	Novus Biologicals
Chromogranin A	1:300	Rabbit	1773-1	Epitomics
C-myc	1:200	Rabbit	ab11917	Abcam
Cleaved caspase3 (Asp175)(5A1E)	1:200	Rabbit N/A	9664	Cell Signaling
E-cadherin	1:300	Mouse IgG_{2a}	610182	BD Bioscience
Fibronectin	1:200	Rabbit IgG	ab23750	Abcam
F4/80 (Cl:A3-1)	1:400	Rat IgG_{2b}	MCA497RT	Serotech
GFP	1:500	Chicken IgY	ab13970	Abcam
Ki67	1:300	Rabbit	RM-9106-SI	Thermo Scientific
Lysozyme (EC 3.2.1.17)	1:1000	Rabbit	A0099	Dako
Mucin 2 (H-300)	1:500	Rabbit IgG	sc-14334	Santa Cruz
N-cadherin (EPR1792Y)	1:200	Rabbit	04-1126	Millipore
Smad2 (D43B4) XP	1:100	Rabbit IgG	5339	Cell Signaling
Smad3 (C67H9)	1:100	Rabbit IgG	9523	Cell Signaling
Smad4 (B-8)	1:100	Mouse IgG_1	sc-7966	Santa Cruz
Survivin (71G4B7)	1:500	Rabbit	2808S	Cell Signaling
p-Smad2 (Ser465/467)	1:2000	Rabbit N/A	AB3849	Millipore
Vimentin	1:200	Rabbit IgG	ab45939	Abcam
Villin (c-19)	1:200	Goat IgG	sc-7672	Santa Cruz

100mM glycine (Sigma) in PBS for 10 minutes, and washed once with PBS (fixed samples can be preserved for 1 day at 4°C). Before immunolabelling, coverslips were washed x3 with 200µl of 100mM glycine for 3 minutes at room temperature. Each sample was blocked with 200µl per well of IF buffer (0.2% (v/v) Triton X-100, 0.1% (w/v) BSA, 0.05% (v/v) Tween-20 in PBS) and 10% (v/v) serum, either goat (Vector Laboratories, S-1000) or rabbit (Vector Laboratories, S-5000) depending on the source of the secondary antibody for 1h. Incubation was continued with the primary antibody of interest diluted in IF buffer with 3% (v/v) serum (200µl per well) at 4°C overnight (>12h). Primary antibodies used in this study and their dilutions are listed in Table 2.4. The samples were washed x3 with IF buffer at room temperature on a shaker. Samples were incubated with the appropriate secondary antibody (Table 2.5) diluted in IF buffer (200µl per well) and kept at room temperature in the dark for 1h on a shaker followed by washing once with IF buffer and twice with PBS for 3 minutes each at room temperature. Nuclei were counter labelled with DAPI as described below.

Table 2.5: Secondary antibodies for immunofluorescence and immunohistochemistry

Antibody	Antibody dilution	Catalog number	Company
AF[1]-488 goat anti-mouse IgG_1	1:500	A21121	Invitrogen
AF-488 anti-rabbit IgG $F(ab')_2$	1:500	4412	Cell Signaling
AF-594 goat anti-mouse IgG_{2a}	1:500	A21135	Invitrogen
AF-555 goat anti-mouse IgG_{2a}	1:500	A21137	Invitrogen
AF-647 goat anti-mouse IgG_1	1:500	A21240	Invitrogen
AF-647 goat anti-mouse IgG_{2a}	1:500	A21241	Invitrogen
AF-647 goat anti-rabbit IgG	1:500	A21245	Invitrogen
Goat pAb to chk IgY	1:200	ab96952	Abcam
Biotinylated goat anti-rabbit	1:400	E0432	Dako
Biotinylated goat anti-mouse	1:400	E0433	Dako
Biotinylated rabbit anti-rat	1:400	E0468	Dako

[1]AF: Alexa Fluor.

2.7.3 F-actin labelling

After the steps in 2.7.2.1 coverslips were incubated with 200µl per well Alexa Fluor-488 Phalloidin (1:50 (v/v)) (A12379, Invitrogen). After 2 hours at room temperature in the dark the samples were washed x3 for 3 minutes each in PBS before the nuclei were counter labelled with DAPI.

2.7.4 Nuclear labelling and mounting

The nuclei were counter labelled with DAPI (0.5µg ml^{-1} in PBS) for 10 minutes at room temperature in the dark. The coverslips were then washed twice with PBS for 3 minutes each in the dark. The coverslips were transferred upside down to slides labelled and mounted with prolong anti-fade.

2.7.5 EdU labelling

Organoid proliferation was assessed with thymidine analogue 5-ethynyl-2'-deoxyuridine (EdU) incorporation assay using Click-iT EdU Alexa Fluor-555 Imaging Kit (Invitrogen, C10338). EdU is incorporated in to DNA during active DNA synthesis and detection is based on a click reaction, a copper catalysed reaction between an azide (coupled to the

Alexa Fluor dye) and alkyne (found in the ethynyl moiety of EdU). Organoids growing on coverslips were incubated with EdU (20µM EdU working solution was prepared in culture medium and incubated with growing organoids at a final concentration of 10µM) for 2h at 37°C, 5% CO_2. Organoids were fixed in 4% (w/v) PFA, pH 7.4 in PBS for 10 minutes at room temperature. The labelling was performed according to the manufacturer's instructions. Nuclei were counter labelled with DAPI and mounted with prolong anti-fade as described above (section 2.7.4). Confocal images were then taken as described below.

2.7.6 Image acquisition and analysis

H&E and IHC slides were viewed by brightfield- fluorescent microscopy (Olympus BX60). Images were acquired by CCD camera and Nuance 2.10 software (CRI, Massachusetts). DAPI labelled slides were observed and analysed with the same microscope. Confocal images were taken with Olympus FluoView FV100 and associated software (The Dunn School Bioimaging Facility- Sir William Dunn school of Pathology). Labelled slides (EdU, IHC or IF) were analysed using ImageJ 1.48 software (Schneider et al., 2012).

2.8 AlamarBlue for adenoma growth

AlamarBlue (AB) (AbD Serotec, BUF012B), was used to measure adenoma growth. AB is a cell proliferation assay based on measuring cellular metabolism. It contains a non-toxic, cell permeable blue indicator dye with low fluorescence called resazurin (oxidized form). Resazurin is used as an oxidation-reduction indicator and colorimetric changes occur based on the reducing environment of the living cell. The reduced form resorufin is pink and highly fluorescent, and the intensity of fluorescence produced is proportional to the number of living cells respiring. Thus, AB acts as a direct indicator to quantitatively measure cell viability and cytotoxicity.

Adenomas were treated with growth factors and/or inhibitors according to the experiment.

10µl of AB per 100µl medium was added on D3 and incubated at 37°C, 5% CO_2. Absorbance was measured after 24h at 570nm and 600nm using a plate reader, Spectramax M5 (MTX Lab Systems). Percentage of AB reduction was calculated using the equation:

$$\frac{(O2 \times A1) - (O2 \times A2)}{(R1 \times N2) - (R2 \times N1)} \times 100$$

where O1=molar extinction coefficient (E) of oxidized AB at 570 nm; O2=E of oxidized AB at 600 nm, R1=E of reduced AB (Red) at 570 nm; R2=E of reduced AB at 600 nm; A1=absorbance of test wells at 570 nm; A2=absorbance of test wells at 600 nm; N1=absorbance of negative control well (medium plus AB without cells) at 570 nm; N2=absorbance of negative control well (medium plus AB without cells) at 600 nm.

2.9 Western blots

2.9.1 Protein extraction

2.9.1.1 Protein extraction from organoids

Organoids growing in 48 well plates (8 wells per condition) were extracted from Matrigel as described in (Lee et al., 2007) with modifications. The medium was removed and organoids embedded in Matrigel washed once with 250µl cold PBS. The PBS was aspirated and 500µl of ice-cold PBS-EDTA (5mM EDTA, 1.5mM NaF and 1mM Na_3VO_4-freshly prepared) was added. The plate was placed on ice and the organoids were scraped gently from the wells with the aid of pipette tips. Organoids were collected from wells without pipetting and placed in a 15ml Falcon tube. The tube was placed on ice for 15 minutes with gentle shaking from time to time. The PBS-EDTA was removed from the tube by centrifugation at 115g for 5 minutes. The supernatant was aspirated carefully and completely. 200µl ice-cold RIPA buffer (150mM NaCl, 50mM Tris-HCl pH 8, 1% (w/v) Triton X-100, 0.5% (w/v) Sodium deoxycholate, 0.1% (w/v) SDS) supplemented with protease inhibitor cocktail (Thermo Scientific, 78440) was added, mixed, transferred to a labelled pre-chilled 1.7ml centrifuge tube and kept on ice for 30 minutes. The tube was centrifuged for 20 minutes at 16,000g (Biofuge,Heraeus) at 4°C. The supernatant was transferred to a pre-chilled

centrifuge tube and preserved at -80°C.

2.9.1.2 Protein extraction from cell lines

Cells were grown in 10cm petri dishes (90% confluent). Medium was removed from the culture dish and the monolayer of cells was washed with cold PBS. Ice-cold RIPA buffer and protease inhibitor were added evenly over the cells while the plate was on ice. Cell lysates were collected and processed as in section 2.9.1.1

2.9.2 Protein quantification

Protein level was determined using the CB-X protein assay kit (G Biosciences, 786-12X) following the manufacturer's protocol with sample cleaning step. The assay uses a protein dye that is an improvement of the Bradford Coomassie dye reagent. The change of the dye colour from brown to blue is in proportion to the amount of protein present in the sample. The concentration was determined according to a standard curve created with the provided BSA solution in the range between 0 and 1mg ml^{-1}. The absorbance was measured at 595nm against dH_2O using the plate reader Spectramax M5.

2.9.3 SDS-PAGE electrophoresis and immunoblotting

Protein lysate was denaturated by boiling in 6x Laemlli buffer (Alfa Aesar, J61337) for 5 minutes on a dry plate at 95°C. Then 5µg protein per sample was resolved by SDS-PAGE gel electrophoresis using the Bio-Rad Mini Protean 3 electrophoresis system. Protein was transferred onto PVDF membrane (Immobilon-P, Millipore IPVH00010) and the membrane blocked with either 5% (w/v) non-fat dry milk (Sigma, 70166) or 5% (w/v) BSA, according to the antibody data sheet, in 0.1% (v/v) TBST for 1h at room temperature with agitation. It was then, incubated with primary antibody (Table 2.6) diluted in 5% BSA or milk- 0.1% TBST overnight with agitation in a cold room. The membrane was washed x3 for 5 minutes with 0.1% TBST before incubation with secondary antibody- goat anti-rabbit horseradish

Table 2.6: Antibodies for western blots

Antibody (Clone)	Antibody dilution	Host &Isotype	Catalog number	Company
Axin2	1:600	Rabbit	ab32197	Abcam
α-tubulin	1:2000	Rabbit IgG	2144	Cell Signaling
β-actin	1:25000	Rabbit IgG	ab8227-50	Abcam
β-catenin	1:4000	Mouse IgG_1	610154	BD Bioscience
Cleaved caspase3 (Asp175)(5A1E)	1:1000	Rabbit N/A	9664	Cell Signaling
c-Myc	1:200	Rabbit IgG	sc-764	Sacta Cruz
Fibronectin	1:1000	Rabbit IgG	ab23750	Abcam
N-cadherin (EPR1792Y)	1:50000	Rabbit	04-1126	Millipore
Smad2 (D43B4) XP	1:1000	Rabbit IgG	5339	Cell Signaling
Smad3 (C67H9)	1:1000	Rabbit IgG	9523	Cell Signaling
Smad4 (B-8)	1:500	Mouse IgG_1	sc-7966	Santa Cruz
Survivin (71G4B7)	1:1000	Rabbit	2808S	Cell Signaling
p-Smad2 (Ser465/467)	1:1000	Rabbit N/A	AB3849	Millipore
p-Stat3 (Tyr705) (D3A7) XP	1:2000	Rabbit IgG	9145	Cell Signaling
Vimentin	1:1000	Rabbit	10366-1-AP	Proteintech

peroxidase (HRP) (Dako, P0448) or goat anti-mouse HRP (Dako, P0447)- in 5% (w/v) BSA or milk- 0.1% TBST for 2h at room temperature with agitation. The membrane was washed x3 in 0.1% TBST and immunodetection was performed using Promega ECL (Promega, W1015) -an enhanced luminol-based chemiluminescent substrate for the detection of HRP conjugates on immunoblots- following the manufacturer's instructions and developed by either Amersham Hyper-film (28-9068-35) or Roche chemiluminescent film (11666916001) using an X-ograph imaging system.

2.9.4 Western blot analysis

Loading control and test from scanned western blots was aligned horizontally on Photoshop (CS5) and analysed using ImageJ 1.48 software (Schneider et al., 2012). Data were sorted in Excel and analysed in GraphPad Prism version 6.0.

2.10 RNA preparation for RNA-seq and miRNA-seq

Adenomas from passage 3, seeded at 9000 cells per 25µl density in a 48 well plate and treated as in section 2.5.5 were used for this experiment. Samples from three different time points (0h, 1h, 12h post TGF-β1 treatment) were taken. Three biological replicates from each genotype were used and RNA was pooled from 8 wells per treatment. As a quality

control, samples were collected for genotyping at each passage.

2.10.1 RNA extraction

Prior to RNA extraction, the working station, pipettes, racks and centrifuge were cleaned with RNase Zap wipes (Ambion, life technology, AM9786) and washed with 0.1% DEPC treated water (Sigma) to minimize RNA degradation. RNA extraction was performed using Quick-RNA MiniPrep (Zymo Research, R1054) as per manufacturer's protocol. Briefly, following the incubation period, medium was removed completely and 65µl of RNA lysis buffer was added to each well (8 wells per condition), lysates were collected in pre-labelled RNase-DNase free 1.7ml centrifuge tubes (Axygen, MCT-175-C), and processed directly with in-column DNase I treatment. Sample clearing and gDNA removal was excluded due to the low adenoma input (step checked before excluding). RNA was eluted in 80µl DNase/RNase free water preheated to 95°C. Extracted RNA was either stored directly at -80°C or assessed for quantity and quality before storage.

2.10.2 RNA quality and quantity assessment

RNA quantity and quality was assessed using a Nanodrop-1000 spectrophotometer, by measuring the absorbance at A_{230}, A_{260}, and A_{280} against RNase-free water. RNA quantity is calculated by the instrument software. RNA quality is measured by comparing ratio of A_{260}/A_{280} and $A_{260}/_{230}$ and considered pure if the ratios were $\sim$2.0 and 2.0-2.2, respectively.

2.10.3 RNA concentration

RNA concentration was performed using RNA Clean & concentrator^{TM}-5 (Zymo Research, R1015) following the manufacturer recommendations. This is based on the use of a unique single-buffer system and Clean-Spin column technology that allows for selective recovery of RNA with different sizes based on the required assay and RNA elution in small volume

(>6µl) . However, a high quality concentrated RNA was found to be obtained when the spin column was opened and centrifuged for 2 minutes $\geq$12,000g to dry before being transferred to an RNase-free tube for RNA elution. The eluted RNA quantity and quality was assessed by the Nanodrop and preserved at -80°C.

2.10.4 RNA-seq and miRNA processing

Sequencing was performed in the Wellcome Trust Center for Human Genetics (WTCHG)-University of Oxford. mRNA was ribo-depleted and converted to cDNA. Directional multiplexed mRNA and miRNA Libraries were then prepared. A single lane of paired end sequencing (100nt) and a single rapid mode run of 50bp single end sequencing using Illumina platform were performed for mRNA and miRNA, respectively.

2.11 Cell lines

The cell lines utilised were Colo205, HT29 and NIH3T3. Colo205 and HT29 are colorectal cancer cell lines and have different mutations in the *SMAD4* gene. Colo205 mutation spectra are *Smad4* (del 1-904pb), *BRAF* (V600E), *TP53* (26 bp del) and *APC* (T1556fs (insertion A)) (Chang et al., 2011). HT29 mutation spectra are *SMAD4* (C931T), *APC* (G2557T), *TP53* (C818T) and FLT3 (G680A) . NIH3T3, a mouse embryonic fibroblast cell line, has an intact *Smad4* gene. Colo205 cells (ECACC, 87061208) were grown in RPMI-1640 (Sigma, R8758) supplemented with 1% Pen/Strep (v/v) (Gibco, 15140-122), 2mM L-Glutamine (Gibco, 25030) and 10% (v/v) FCS. HT29 cells were grown in EMEM (Lonza, LA-0009E) supplemented with 1% Pen/Strep, 2mM L-Glutamine and 10% FCS. NIH3T3 cells were grown in DMEM (Sigma, D6429) supplemented with 1% Pen/Strep, 2mM L-Glutamine and 10% FCS. For immunolabelling experiments, cells were grown on coverslips in 24-well plates with $4x10^4$ cells per well and processed as in section 2.7.2. Protein extraction was described in section 2.9.1.2

2.12 Constructs for the luciferase assay

pBV-Luc/Del-6 was a gift from Joan Massague (Addgene plasmid # 14969).
p3TP-lux was a gift from Joan Massague & Jeff Wrana (Addgene plasmid # 11767).
c-myc promoter (4x TBE2-mut) was a gift from Bert Volgestein (Addgene plasmid # 16600).
SBE4-luc was a gift from Bert Volgestein (Addgene plasmid # 16495).
pBabe-puro-Smad4-Flag was a gift from Sam Thiagalingam (Addgene plasmid # 37041).
M50 Super 8x TOPFlash was a gift from Randall Moon (Addgene plasmid # 12456).
M51 Super 8x FOPFlash was a gift from Randall Moon (Addgene plasmid # 12457).

2.12.1 Long-term storage of plasmids

Glycerol stocks for long-term storage of plasmids were made as per Addgene's instructions (https://www.addgene.org/plasmid-protocols/create-glycerol-stock/). 50% Glycerol (Fisher chemical, G/0650/08) was prepared in distilled water and filter sterilised using a 0.22µM filter (Millex GP, SLGP033RS). Stocks were preserved at -80°C.

2.12.2 Miniprep and maxiprep

For plasmid verification, minipreps were prepared using QIA prep spin Miniprep Kit (Qiagen, 27106) as per manufacturer's instructions. After plasmid verification by DNA sequencing (described in section 2.2.5), maxipreps were prepared using HiSpeed Plasmid Maxi Kit (Qiagen, 12662) as per manufacturer's instructions. DNA preparation using Qiagen kits are based on alkaline lysis procedure of the transformed *E.coli* followed by binding of plasmid DNA to an Anion-Exchange Resin. Washing with a medium-salt buffer removes RNA, proteins, dyes, and impurities. Plasmid DNA is eluted in a high-salt buffer and precipitated with isopropanol for concentration and desalting. DNA prepared from miniprep and maxiprep were assessed for quantity and quality using a Nanodrop spectrometer as described earlier (section 2.2.6). The prepared DNA was stored at -20°C.

2.13 Statistical analysis

Data were sorted in Excel and analysed in GraphPad Prism version 6.0 (GraphPad Software, Inc). Survival data were analysed by log-rank test. Statistical analysis for groups of two was performed using unpaired student's t-test. For groups of three or more, analysis was performed with one-way ANOVA. Tukey's multiple comparison test was performed for general comparisons, however, Sidak's multiple comparison test was performed for specific comparisons. Data were presented as mean$\pm$SD or 10-90 percentile. Chi-square test was performed for Mendelian segregation of alleles. Experimental differences were considered statistically significant when $p \leqslant 0.05$. RNA-seq analysis is described in section 6.3.3.

Chapter 3

In vivo models for TGF-β and IGF2 in intestinal tumorigenesis

3.1 Introduction

Intestinal tumorigenesis is initiated mainly as a result of aberrant activation of the Wnt/β-catenin pathway (Morin et al., 1997) often due to mutations that inactivate *Apc* (Fodde and Smits, 2001; Clevers and Nusse, 2012). The progression from adenoma to carcinoma through clonal evolution involves alterations in different pathways; for instance, there is loss of function in TGF-β and p53 pathways and gain of function in PI3K and RAS-MAPK pathways (Network et al., 2012; Seshagiri et al., 2012) (Figure 3.1). Mouse models are one of the important tools used to model human cancer and to study gene function and pathways involved in tumour progression, although there are species-species differences and only limited ability to recapitulate the human phenotype (Cheon and Orsulic, 2011). Several mouse models have been generated for the initiating event in intestinal tumorigenesis which have greatly improved our understanding of this step and the role of the Wnt pathway in this disease. Nevertheless, more models are still needed for understanding later stages of this cancer. In the context of activated Wnt pathway due to mutations in *Apc*, the focus of this chapter will be on understanding the effects of downregulation of TGF-β signalling due to *Smad4* mutation and upregulation of PI3K and RAS-MAPK pathways due to increase Igf2 supply due to loss of function of *Igf2r* from the maternal allele.

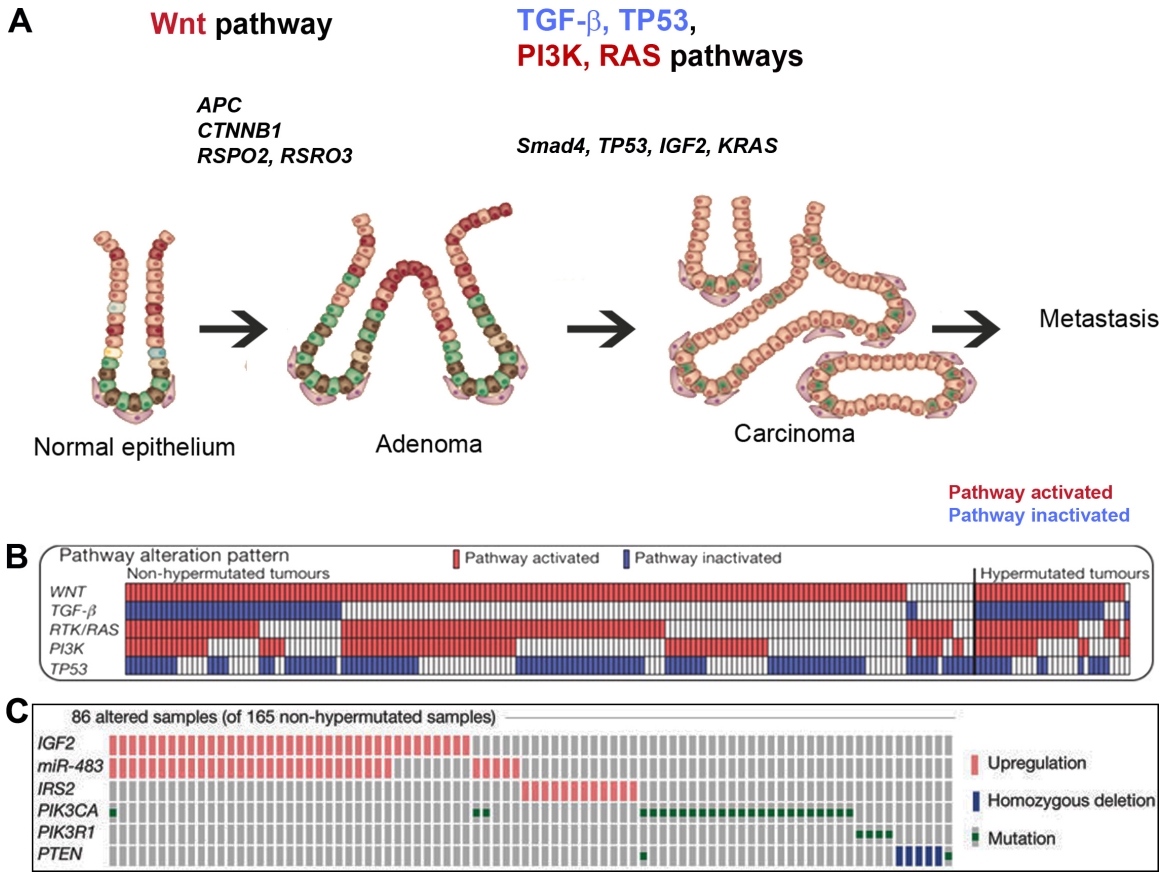

Figure 3.1: **Intestinal tumorigenesis.** Mutations that activate the Wnt pathway drive the transformation of normal epithelium to adenoma. The progression from adenoma to carcinoma requires alteration in different pathways either upregulation or downregulation. Genes shown in the figure are examples of those being altered in CRC. (A) adapted from (Vermeulen and Snippert, 2014) with modification. (B) Progression from adenoma to carcinoma is based on clonal evolution. (C) *IGF2* amplification and overexpression in 86 patients compared to other mutations in PI3K pathway. (B, C) Adapted from (Network et al., 2012).

3.1.1 Pathways altered in intestinal tumorigenesis

3.1.1.1 Wnt/β-catenin pathway

Wnt signalling is important for maintaining intestinal stem cells (Clevers and Nusse, 2012). Mutations in this pathway (93% of cases) are frequently involved in the initiation of intestinal tumorigenesis (Morin et al., 1997; Network et al., 2012). Germline mutations in *APC* underlie FAP -an inherited form of CRC- and predispose patients to CRC in 100% of cases if untreated (Nishisho et al., 1991; Fearon, 2011). In sporadic CRC, mutations in the *APC* gene that lead to premature truncation of the APC protein are reported in 70-80% of cases (Fearon, 2011). Consequently, the coordinated phosphorylation and destruction of β-catenin are disrupted. APC will no longer be able to bind β-catenin for proteasomal degradation. Free β-catenin is accumulated in the nucleus and forms a constitutive complex with the intestinal TCF/LEF TFs leading to aberrant Wnt pathway activation (Korinek et al., 1997; Sansom et al., 2004; Clevers and Nusse, 2012). In cases where *APC* is normal, the Wnt pathway is activated due to mutations of *CTNNB1* (10%) (Giles et al., 2003). Recently, the involvement of R-spondin family members, RSPO2 and RSPO3, due to gene fusions found in 10% of colon tumours and has been reported to be a driver for CRC (Seshagiri et al., 2012). RNA-seq carried out in this experiment showed that the expression of RSPO2 and RSPO3 was elevated together with their receptors Lgr4/Lgr5 (Seshagiri et al., 2012). Alterations in other members of the Wnt pathways such as *AXIN2, FBXW7* and *ARID* have also been reported (Network et al., 2012).

Different mouse models with different mutations in the *APC* gene have been used to study FAP (Fodde and Smits, 2001) such as Apc^{Min} and $Apc^{\Delta 716}$ (Table 1.1). In models with germline mutations, loss of the second *Apc* allele through LOH is required for polyp formation as $Apc^{-/-}$ knockout mice are unable to survive (Sancho et al., 2004). A conditional model using the Cre/loxP site technology has been introduced by Shibata *et al.* This model overcomes lethality and time needed for LOH permitting the study of the *Apc* gene in a spatiotemporal manner (Shibata et al., 1997). Moreover, the introduction of tamoxifen inducible Cre-recombinase under tissue specific promoters allows the study of *Apc* function

in specific compartments within the intestine including the intestinal stem cell (Table 1.1). A marked difference between mouse and human is the site of the polyp and disease progression. Human patients develop more polyps in the large intestine and few in the small intestine and these polyps progress to invasive adenocarcinoma. *Apc* mutant mice develop large numbers of polyps in the small intestine and fewer in the large intestine and do not progress to adenocarcinoma (Karim and Huso, 2013). A process could be related to the *Cdx2* gene. Cdx2 is an important transcription factor involved in the development, differentiation and physiology of the intestines. A shift of polyps distribution resembling the human phenotype was obtained when the cross was between the models *Cdx2*$^{-/+}$ and *Apc*$^{\Delta 716}$ (Aoki et al., 2003).

3.1.1.2 Function of TGF-β/Smad4 pathway

The TGF-β pathway has tumour suppressor and tumour promoter functions (Massagué, 2012). In sporadic CRCs, mutations in different members of this pathway have been reported, for instance *SMAD4, TGFBR2, SMAD3*, and *SMAD2* (Network et al., 2012; Fleming et al., 2013). The tumour suppressor *Smad4* is crucial for embryonic development as *Smad4*$^{-/-}$ knockout mice are not viable (Sirard et al., 1998; Takaku et al., 1999). Germline mutations in *SMAD4* have been found in patients with juvenile intestinal polyposis and increased susceptibility to CRC (Hardwick et al., 2008; Wakefield and Hill, 2013). *SMAD4* mutations occur in 10% of CRCs and 35% of colorectal invasive tumours showed *SMAD4* mutations (Miyaki et al., 1999). Smad4 mutations are associated with mucinous histology (Freeman et al., 2012). Only a few *in vivo* studies have evaluated the effect of Smad4 on intestinal tumorigenesis (Takaku et al., 1998; Kitamura et al., 2007, 2009; Freeman et al., 2012) (Table 3.1). In three of them, *Smad4*$^{-/+}$ has been crossed with *Apc*$^{\Delta 716/+}$ model (*cis*-*Apc*$^{\Delta 716/+}$*Smad4*$^{-/+}$). This cross transformed adenomas to aggressive carcinomas (Takaku et al., 1998), a process related to the recruitment of immature myeloid cells to the invasion site (Kitamura et al., 2007). Moreover, it has been shown that deletion of *Mmp7* reduces both number and size of tumours in *Apc*$^{\Delta 716/+}$*Smad4*$^{-/+}$ (Kitamura et al., 2009). When the *Smad4*$^{fl/fl}$ mouse model was bred with *Apc*$^{\Delta 1638N/+}$*K19-CreERT2* the deletion was in GIT

stem cells and tumour burden was increased due to an increase in β-catenin with no invasion (Freeman et al., 2012). These studies show phenotypic differences and the exact molecular mechanisms following Smad4 disruption on intestinal tumorigenesis remains unclear at the time these studies were initiated. These models did not show metastasis and therefore did not recapitulate the exact phenotype of human CRC. This could be due to the shorter life span of mice mainly as the LOH for *Apc* takes time to occur. Recently, the effect of Smad4 disruption on intestinal tumorigenesis was evaluated using intestinal organoid culture (detailed in section 1.5.2). *Smad4* mutations with *Apc* mutations were not able to drive adenocarcinoma and more hits were required (Li et al., 2014; Drost et al., 2015; Matano et al., 2015). Therefore, there is a need for a more comprehensive *in vivo* study on the role of Smad4 in intestinal tumorigenesis. The question I set out to address was whether disruption of Smad4 in the context of active Wnt signalling using the *Lgr5-CreERT2* model, enhances intestinal tumorigenesis?

Table 3.1: Characteristic phenotypes of different mouse models for intestinal tumorigenesis with *Smad4* mutations.

Mouse model	Mutation and deletion sites	Phenotype	Death point	Reference
Smad4$^{-/+}$	Germline	Normal up to one year. Then, multiple polyps were formed in the duodenum and stomach. Polyps were similar to those found in human JPS[1]	1.5 years	(Takaku et al., 1999)
cis-*Apc*$^{\Delta 716/+}$*Smad4*$^{-/+}$	*cis*-compound heterozygous. Exon 1 of *Smad4*, germline	Large polyps (1.0- 2.0mm) with 82 polyps compared to 676 polyps in the small intestine of the *Apc*$^{\Delta 716/+}$. Presence of heterogeneous types of cells, mucinous cells and sub-mucosal invasions, stromal proliferation, intussusception in the small intestine	14-20 weeks	(Takaku et al., 1998)
cis-*Apc*$^{\Delta 716/+}$*Smad4*$^{-/+}$ *Ccr1*$^{-/-}$	Germline	Similar results to Takaku *et al.* 1998 mouse model but with no invasion due to the deletion of the CC chemokine receptor 1 (Ccr1)		(Kitamura et al., 2007)
cis-*Apc*$^{\Delta 716/+}$*Smad4*$^{-/+}$ *Mmp7*$^{-/-}$	Germline	Reduced tumour burden compared to *cis*-*Apc*$^{\Delta 716/+}$*Smad4*$^{-/+}$ *Mmp7*$^{+/+}$ with no effect on invasion, number of stromal fibroblasts or levels of extracellular matrix components in the tumours.		(Kitamura et al., 2009)
Smad4$^{fl/fl}$ *MMTV-Cre*	loxP sites flanked exon 8, deletion in epithelial lineage	No intestinal carcinoma in the GIT[2]	5-16 months	(Kim et al., 2006)
Smad4$^{fl/fl}$ *CD4-Cre* *Smad4*$^{fl/fl}$ *Lck-Cre*	loxP sites flanked exon 8, deletion in T-cell	Epithelial lesion, adenomas and invasive carcinoma in 94% - 100% of the mice	9-16 months	(Kim et al., 2006)
Apc$^{\Delta 1638N/+}$*Smad4*$^{fl/fl}$ *K19-CreERT2*	loxP sites flanked exon 8 and 9 of Smad4, deletion in GIT stem cells	Increased tumour burden in the small and large intestine	5 weeks	(Freeman et al., 2012)

1: juvenile polyposis syndrome (JPS), 2: gastrointestinal tract (GIT).

3.1.1.3 PI3K, RAS-MAPK Igf2/Igf2r pathway

PI3K and RAS-MAPK pathways are reported to be upregulated in CRC due to mutations in *PIK3CA*, *PIK3R1*, *PTEN*, *KRAS*, *NRAS*, *BRAF* (Network et al., 2012; Seshagiri et al., 2012). Also, 22% of CRC patients have shown an overexpression of insulin like growth factor 2 (*IGF2*) gene either through loss of imprinting, or 11p15.5 amplification resulting in CRC promotion (Network et al., 2012; Seshagiri et al., 2012). Moreover, the poly(G)8 tract mutations spanning nucleotides 4089-4096 of insulin-like growth factor 2 receptor *IGF2R* coding sequence have been reported in intestinal tumours (Souza et al., 1996). The insertion or deletion of 2 base pairs in the microsatellite region results in frame shift mutations and premature stop codons, similar to TGFβR-II in MSI and HNPCC. *IGF2R* mutations confer growth advantages to the tumours (Souza et al., 1996).

The cation independent mannose 6-phosphate/ IGF2R binds to IGF2 at the cell surface and internalizes it for lysosomal degradation, thus preventing the accumulation of IGF2. IGF2R consists of 15 extra-cellular domains (Ghosh et al., 2003) and domain 11 binds to IGF2 with high specificity and affinity (Prince et al., 2007), this binding does not lead to signal transduction. The function of IGF2 is mediated via the IGF1 receptor and insulin receptor isoform A, and activates RAS-MAPK, PI3K-Akt which is important for cell growth, proliferation and survival (Hassan, 2003; Ghosh et al., 2003; Donovan and Kummar, 2008). Moreover, IGF2R also promotes the activation of the latent precursor of TGF-β1 (Ghosh et al., 2003). Consequently, IGF2R regulates cell proliferation and apoptosis and is classified as a tumour suppressor (Ghosh et al., 2003; Pollak, 2008). In support of that, over expression of IGF2R decreases the organomegaly induced by excess IGF2 (Zaina and Squire, 1998) and in human cancers, loss of IGF2R function is associated with tumour progression (Hassan, 2003; Ghosh et al., 2003). Overexpression of Igf2 enhanced tumour burden in the $Apc^{Min/+}$, a phenotype can be rescued by high-affinity soluble Igf2r (Harper et al., 2006).

Igf2r is imprinted on the paternally inherited allele and expressed on the maternal allele

in mice. Loss of function of the maternal allele of Igf2r results in perinatal lethality mainly because of Igf2 dependent overgrowth of the embryonic heart, and placenta (Wang et al., 1994; Wylie et al., 2003; Hughes et al., 2013). The perinatal lethality was rescued by breeding *Igf2* knockout mice with *Igf2r* knockout mice (Ludwig et al., 1996). Conditional alleles of Igf2 have been generated, but to date the functional consequences of Igf2 loss of function has not been totally tested. *Igf2r*^{I1565A} is the first *in vivo* model for domain specific loss of function of Igf2r. It results in mutations of domain 11, leading to increased Igf2 levels. Using this mouse model, the question I set out to address was whether loss of function of domain 11 of Igf2r has an effect on the progression of intestinal adenomas in the context of active Wnt signalling in the Lgr5 stem cell compartment.

3.2 Rationale for study

The *Lgr5-CreERT2* mouse model (Barker et al., 2009) when crossed with *Apc*$^{fl/fl}$ (Shibata et al., 1997) drives adenoma formation in the mouse small intestine within 3-5 weeks following tamoxifen induced Cre-activation. Using these mouse models, the aims of this chapter are:

1. To investigate the phenotypic effect of *Smad4* mutation on *Apc*$^{fl/fl}$adenoma

2. To investigate the phenotypic effect of upregulation of Igf2 on PI3K and RAS-MAPK pathways due to domain 11 loss of function in the maternal allele of *Igf2r* on adenoma progression

3.3 Materials and methods

3.3.1 Mouse models

Mouse models used in this chapter were listed in Table 2.1 with the exception of *Villin-CreERT2* mouse model.

3.3.2 Mouse breeding

The breeding strategy and the generated genotypes was described in section 2.1.3.1 and 2.1.3.2.

3.3.3 Genotyping

Mice were identified by genotyping as described in section 2.2. PM samples were taken from experimental mice for further confirmation of the genotype.

3.3.4 Tamoxifen injection and mouse dissection

Experimental mice were injected with tamoxifen, monitored and humane endpoint was performed as described in Methods section 2.1.4 and 2.1.5.

3.3.5 Intestinal tissue collection, adenoma count and histology

Tissues were collected as described in section 2.1.5.1. Adenoma count and scoring was described in section 2.3. Tissue processing for histology was detailed in section 2.4.

3.4 Results

3.4.1 *In vivo Apc$^{fl/fl}$Smad4$^{fl/fl}$Lgr5-CreERT2* adenoma model

The data presented in this chapter is my work except 3.4.1.1 where the data were mainly from a former student in the lab (Dr. Julia Matheson). The survival curve includes my data. My contribution for this section was helping in the breeding, injection, monitoring, and dissection of some of the animals. Figure 3.3 was from Dr. Matheson's work.

3.4.1.1 Improved survival, development of large caecal tumour and reduced small intestinal adenoma burden in $Apc^{fl/fl}Smad4^{fl/fl}$ mice

Survival of $Apc^{fl/fl}Smad4^{+/+}$, $Apc^{fl/fl}Smad4^{fl/+}$, and $Apc^{fl/fl}Smad4^{fl/fl}$ mice following Cre-mediated activation by tamoxifen injection were compared with log-rank test. The $Apc^{fl/fl}Smad4^{fl/fl}$ mice lived significantly longer than the $Apc^{fl/fl}Smad4^{+/+}$ ($p=0.011$) (Figure3.2A). Median survival was 35 days and 44 days for $Apc^{fl/fl}Smad4^{+/+}$, $Apc^{fl/fl}Smad4^{fl/fl}$, respectively. No significant difference in survival between $Apc^{fl/fl}Smad4^{+/+}$ and $Apc^{fl/fl}Smad4^{fl/+}$ was observed. Upon dissection, the $Apc^{fl/fl}Smad4^{fl/fl}$ animals possessed large caecal tumours. 85% of them had tumours greater than 0.5 grams, which was significantly different from the $Apc^{fl/fl}Smad4^{+/+}$ and $Apc^{fl/fl}Smad4^{fl/+}$ ($p<0.001$) control mice. Such a large caecal tumour was not seen with $Apc^{fl/fl}Smad4^{+/+}$ and rarely seen in $Apc^{fl/fl}Smad4^{fl/+}$ (17%) (Figure 3.2B, C) control mice. $Apc^{fl/fl}Smad4^{fl/fl}$ mice have also significantly fewer numbers of small intestinal adenomas compared to $Apc^{fl/fl}Smad4^{+/+}$ and $Apc^{fl/fl}Smad4^{fl/+}$ control mice ($p<0.001$). Mean adenoma count was 42 and 55 for $Apc^{fl/fl}Smad4^{+/+}$ and $Apc^{fl/fl}Smad4^{fl/+}$ mice, respectively compared with 8 for $Apc^{fl/fl}Smad4^{fl/fl}$ mice ($p<0.001$). There was no difference in distal colonic adenoma burden between the different genotypes (Figure 3.2D). There was no significant difference in adenoma size between the different genotypes (Figure 3.2E). $Apc^{fl/fl}Smad4^{fl/fl}$ mice had a significantly decreased proportion of adenomas in the proximal intestine compared to $Apc^{fl/fl}Smad4^{+/+}$ and $Apc^{fl/fl}Smad4^{fl/+}$ mice ($p<0.0278$) (Figure 3.2F).

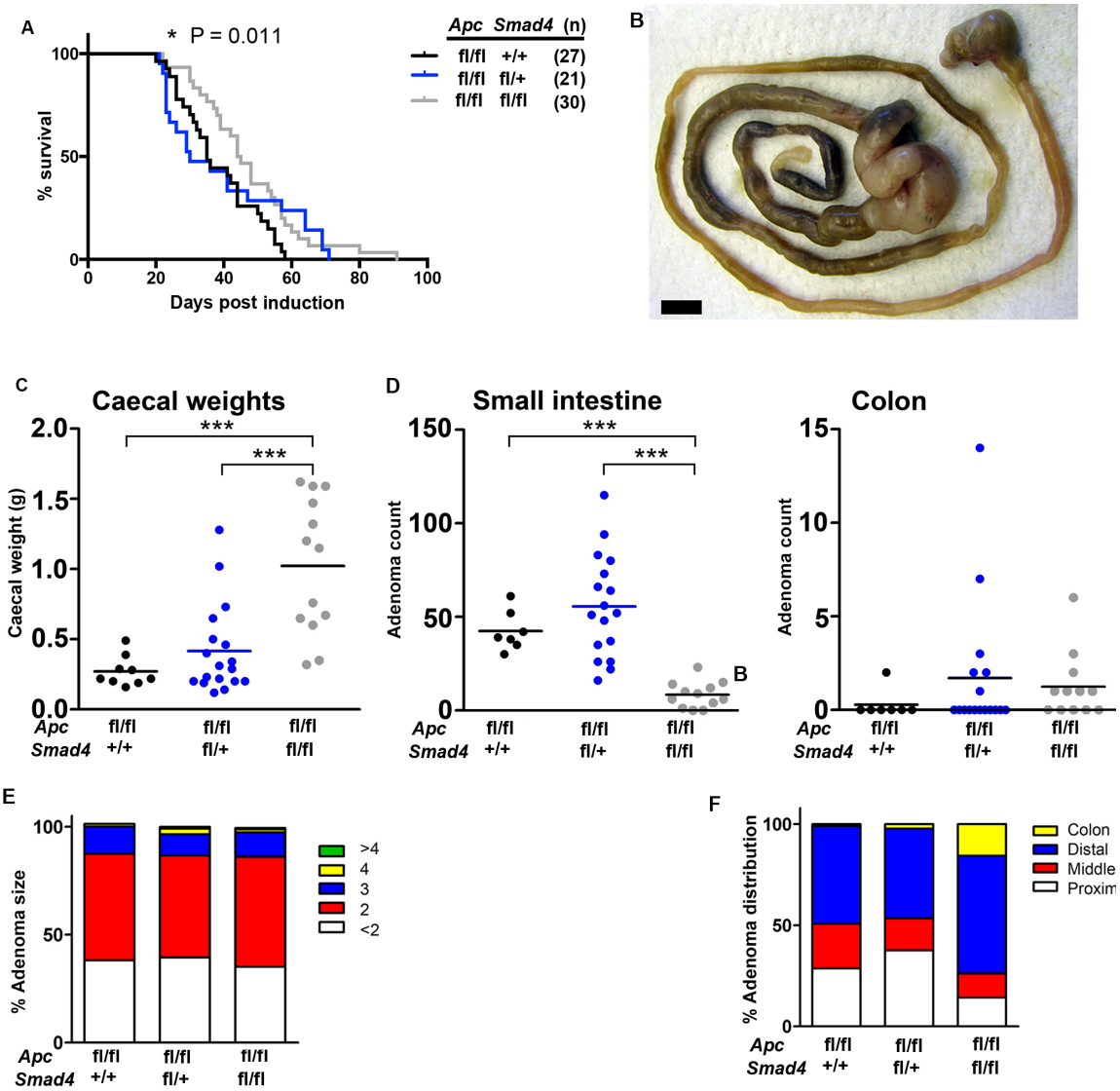

Figure 3.2: ***Apc*$^{fl/fl}$*Smad4*$^{fl/fl}$ mice had better survival with large caecal tumour and reduced small intestinal adenoma burden.** (A) Kaplan-Meier survival curve showing survival of *Apc*$^{fl/fl}$*Smad4*$^{+/+}$, *Apc*$^{fl/fl}$*Smad4*$^{fl/+}$ and *Apc*$^{fl/fl}$*Smad4*$^{fl/fl}$ post tamoxifen induction. Comparison between genotypes was performed by the Log-rank test. *p=0.011. (B) Representative image for a caecal tumour from an *Apc*$^{fl/fl}$*Smad4*$^{fl/fl}$ animal. Scale bar 1cm. (C) Caecal weights for *Apc*$^{fl/fl}$*Smad4*$^{+/+}$ (n=10), *Apc*$^{fl/fl}$*Smad4*$^{fl/+}$ (n=18) and *Apc*$^{fl/fl}$*Smad4*$^{fl/fl}$ (n=13) animals. Statistical analysis was performed using one-way ANOVA with Bonferroni's multiple comparison test. (D-F) Count, size and distribution of adenoma from the small intestine and colon of *Apc*$^{fl/fl}$*Smad4*$^{+/+}$ (n=9), *Apc*$^{fl/fl}$*Smad4*$^{fl/+}$ (n=17) and *Apc*$^{fl/fl}$*Smad4*$^{fl/fl}$ (n=13) animals. Horizontal bars represent the mean and each dot represents an individual animal. Statistical analysis was performed using one-way ANOVA with Bonferroni's multiple comparison test for adenoma counts. Two-way ANOVA for adenoma size and distribution. ***p<0.001. Note: (A) Combined data from Julia's work and my work. (B-F) Julia's data and analysis.

3.4.1.2 *Apc*$^{fl/fl}$*Smad4*$^{fl/fl}$ tumours lack Smad4 protein

The efficiency of the Cre-mediated deletion of Smad4 in this experiment was confirmed by IHC (Matheson, 2012). As shown in Figure 3.3, in *Apc*$^{fl/fl}$*Smad4*$^{+/+}$ mice, Smad4 protein was labelled in tumours and adjacent tissue. However, Smad4 tumours from *Apc*$^{fl/fl}$*Smad4*$^{fl/fl}$ were not labelled for Smad4 protein and tissues adjacent to the tumour were labelled with Smad4 protein.

3.4.1.3 Histopathology of *Apc*$^{fl/fl}$*Smad4*$^{fl/fl}$ tumours

H&E sections were initially assessed by Professor Hans Morreau (Leiden University). *Apc*$^{fl/fl}$*Smad4*$^{+/+}$ mice had sessile adenomatosis. *Apc*$^{fl/fl}$*Smad4*$^{fl/fl}$ mice had tubular adenomas. In all genotypes, small intestinal adenomas were low grade (Figure 3.4). However, histology of the caecal tumours ranged from low grade dysplasia to carcinoma *in situ*. No invasion was reported in these mice (Matheson, 2012). The appearance of the tumour in the caecum raised the question of whether inflammatory infiltrate triggers adenoma formation. For that, the H&E sections were examined for signs of inflammation. Crypt abscesses were seen in sections from all genotypes (Figure 3.5).

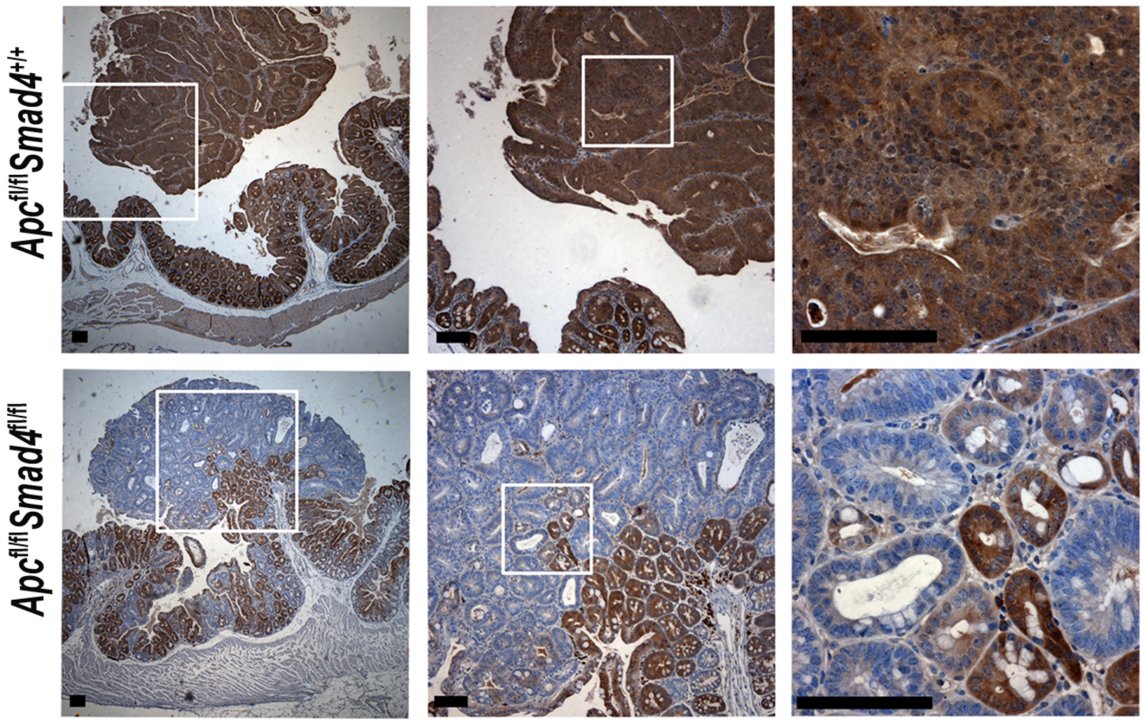

Figure 3.3: **Absence of Smad4 protein from caecal tumours of *Smad4*$^{fl/fl}$ mice .** Representative DAB stain for Smad4 protein in caecal tumours. Tumours with part of the adjacent normal tissue is shown. The panels to the left represent sections of each genotype. Magnification of areas marked with white boxes are shown to the right. Scale bar 100µm. (Matheson, 2012).

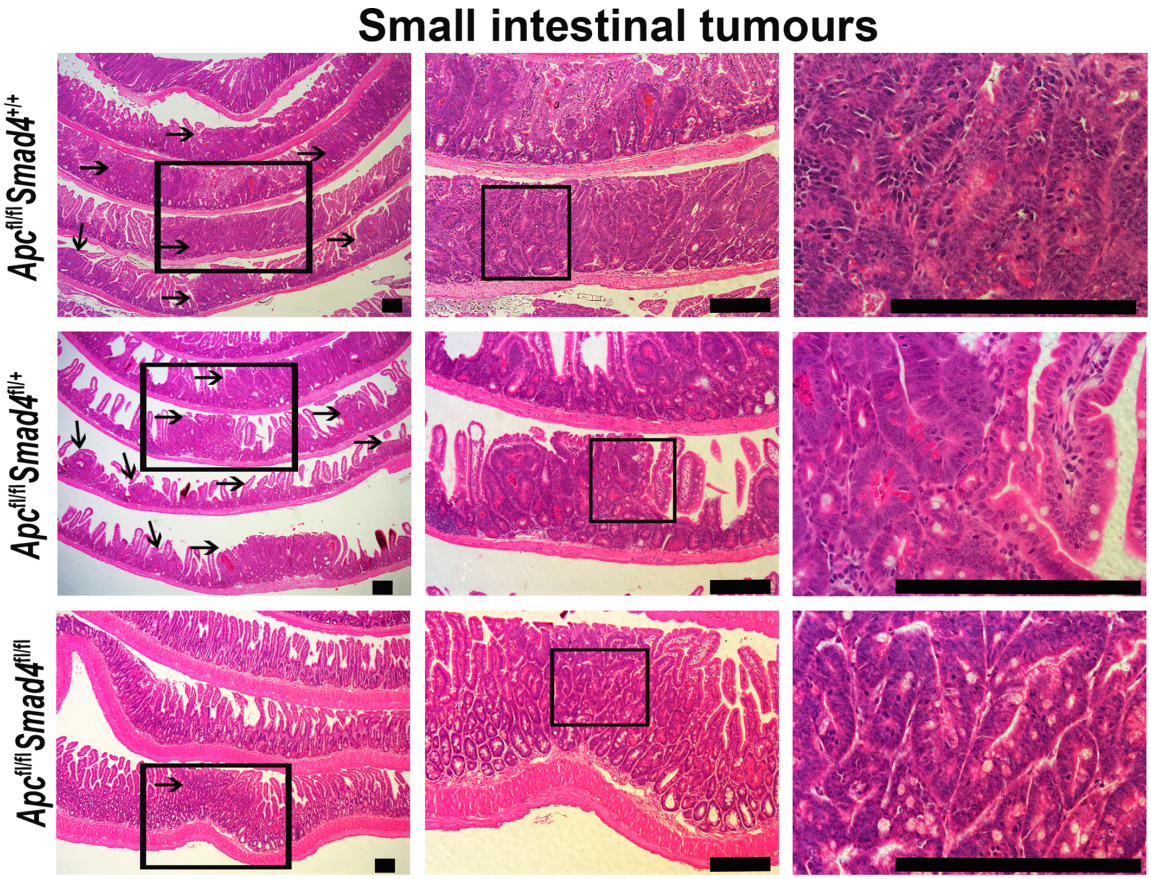

Figure 3.4: ***Apc Smad4 Lgr5-CreERT2* small intestinal histology.** Representative H&E sections of small intestinal histology. The panels to the left represent sections of each genotype. Magnification of areas marked with black boxes are shown to the right, respectively. Sections show adenomas with less differentiation in *Apc*$^{fl/fl}$*Smad4*$^{+/+}$. Arrows show adenomas of different sizes in the small intestine. Scale bar 200µm.

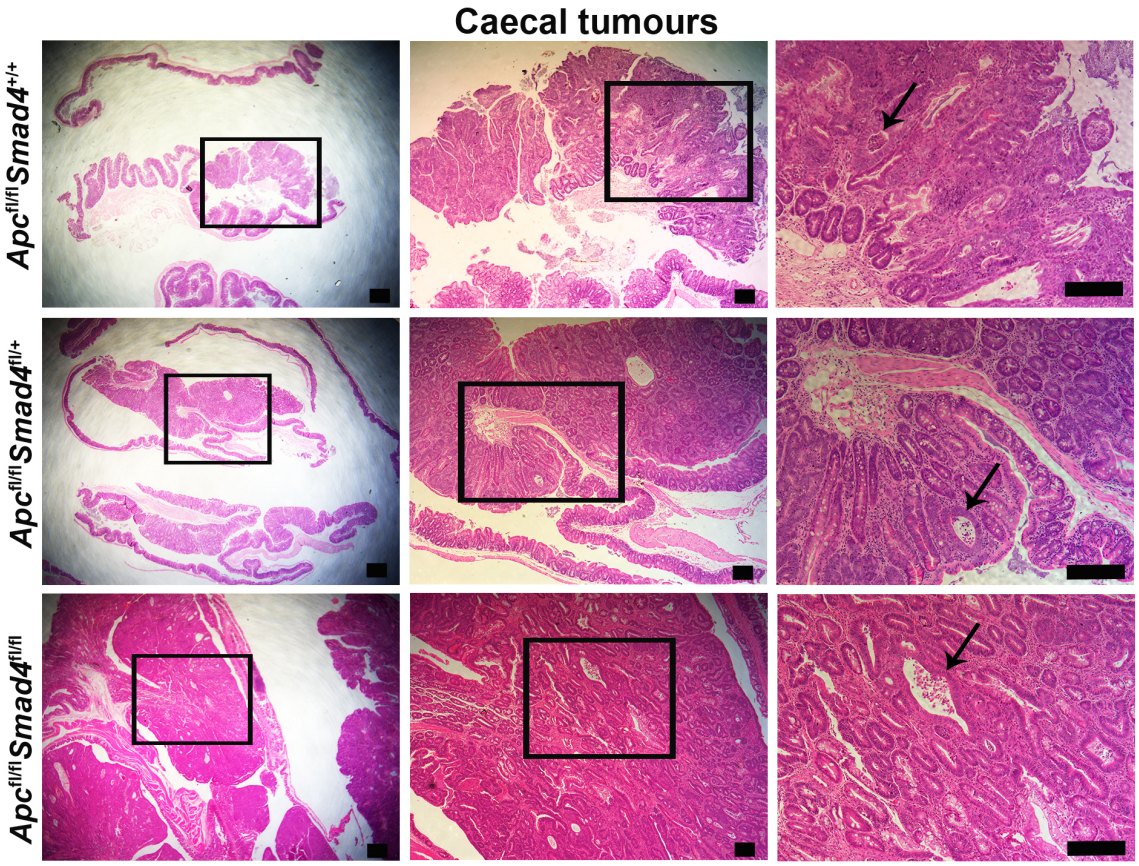

Figure 3.5: ***Apc Smad4 Lgr5-CreERT2* caecal histology with crypt abscesses**. (A) Representative H&E sections of caecal histology. The panels to the left represent sections of each genotype. Magnification of areas marked with black boxes are shown to the right respectively. *Apc*$^{fl/fl}$*Smad4*$^{+/+}$ tumour is undifferentiated with carcinoma *in situ*. *Apc*$^{fl/fl}$*Smad4*$^{fl/fl}$ tumour is low grade, well differentiated with dysplasia. Arrows show examples of crypt abscesses. Scale bars; left panel 600µm; middle and right panels 200µm. Tissue sections from at least 5 mice per genoptype were examined with similar results.

3.4.1.4 Does inflammation trigger adenoma formation?

To further evaluate the hypothesis that inflammation in these tumours drives the formation of caecal tumours, immunolabelling for inflammatory infiltrates was performed. F4/80 and CD11b were used as macrophage markers in mouse, and CD3 as a T-cell marker.

The stroma of mice from both genotypes showed the presence of F4/80^{+} and CD11b^{+} cells, suggesting presence of tumour associated macrophages (TAMs). The mean of F4/80^{+} cells per high power field was 72$\pm$10.8 (SD) for *Smad4*$^{+/+}$ and 70$\pm$18.4 (SD) for *Smad4*$^{fl/fl}$. Lower numbers of CD11b^{+} cells were infiltrating the stroma with no significant difference between genotypes. The mean of CD11b^{+} cells was 12$\pm$6.3 (SD) for *Smad4*$^{+/+}$ and 11$\pm$6.5 (SD) in *Smad4*$^{fl/fl}$ (Figure 3.6). CD3^{+} cells were significantly different between the genotypes with a mean of 48$\pm$5.5 (SD) for *Smad4*$^{+/+}$ and 28$\pm$10.1 (SD) for *Smad4*$^{fl/fl}$ (p=0.0109). However, there were positive areas of CD3 marker that were not easy to quantify meaning the significant difference may not be representative (Figure 3.7). CD3 labelling was performed also by IF, and similar positive areas were obtained.

The presence of active TGF-β signalling in the inflammatory process was reflected by labelling with p-Smad2. Positive DAB detection of p-Smad2 was observed in tumours and the stroma of both genotypes with nuclear localisation in sections from *Smad4*$^{fl/fl}$ mice (Figure 3.8).

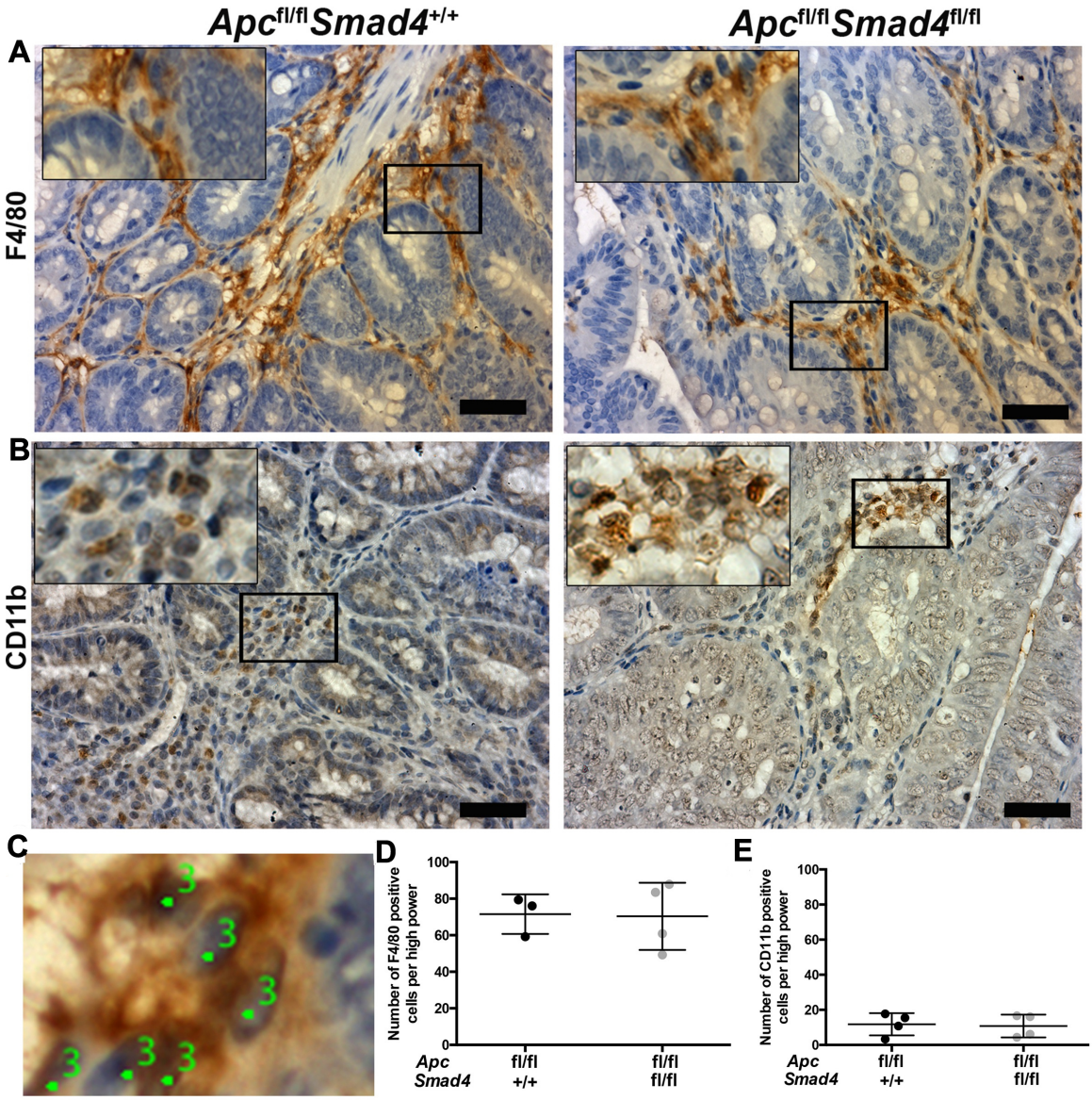

Figure 3.6: **F4/80$^+$ and CD11b$^+$ cells in the stroma.** Infiltration of macrophages was assessed by F4/80 and CD11b labelling. (A, B) Representative DAB stain for F4/80, and CD11b in the stroma of both genotypes (brown). Fields at the left hand side represent magnification of the marked box, scale bar 50µm. Quantification of DAB positive cells was performed using the cell counter from ImageJ plugins. (C) Representative magnified image shows the positive cells being quantified, number 3 is just the colour of the used cell counter. (D, E) Graphs represent the number of positive cells per field. For both markers at least 6 fields at high power per mouse were taken for quantification. Quantification was done on the same day using the same criteria. Dots represent the average number of positive cells per field per mouse. Error bars represent ±SD. Statistical analysis was performed using student's t-test.

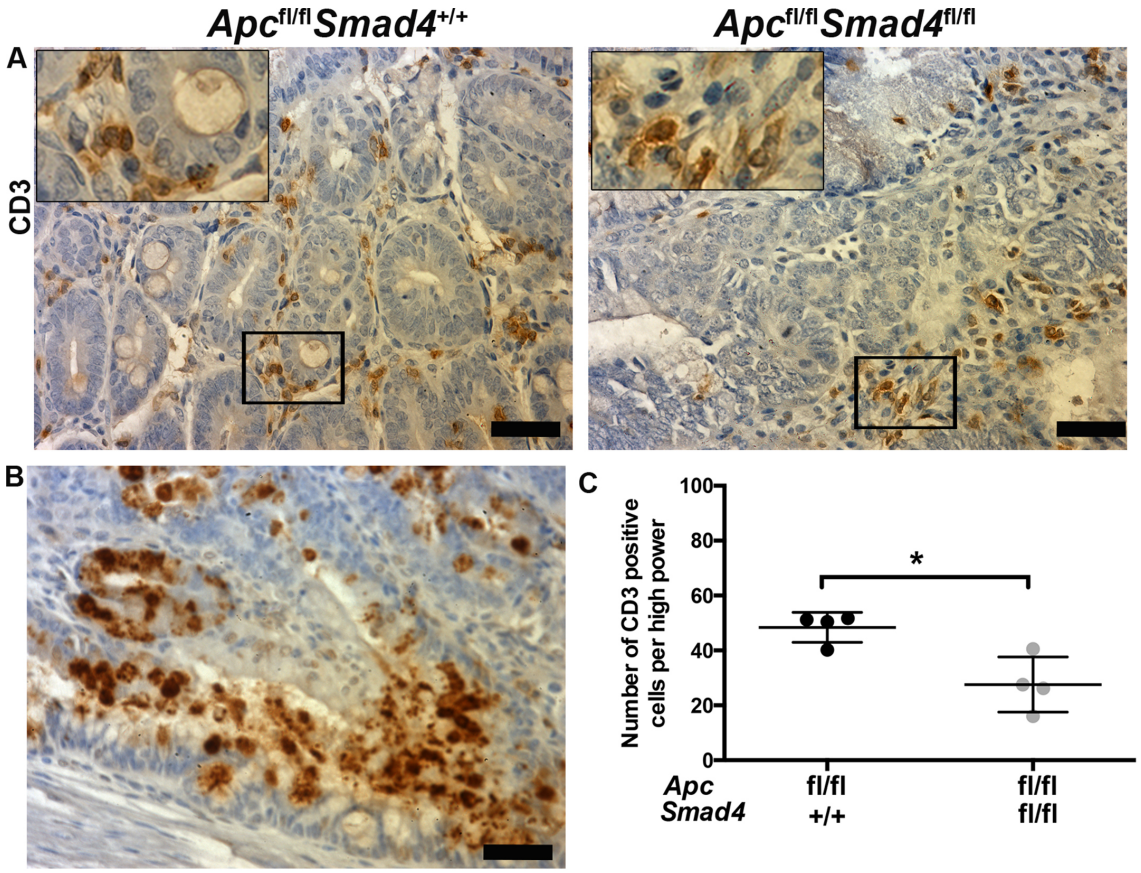

Figure 3.7: **CD3 infiltrate**. Infiltration of T-cells was assessed by CD3 labelling. (A) Representative DAB stain for typical CD3 labelling in the stroma of both genotypes (brown). Fields at the left hand side represent magnification of the marked boxes. Quantification of DAB positive cells was performed using the cell counter from ImageJ plugins. Scale bars 50µm. (B) Representative image shows the presence of CD3 DAB positive labelling. These areas have not been counted as they do not show typical $CD3^+$ cells. Such positive labelling was mainly in *Smad4*$^{fl/fl}$, scale bar 50µm. (C) Quantification of typical $CD3^+$ cells as counted using ImageJ. At least 6 fields per mouse were taken for quantification. Quantification done on the same day using the same criteria. Dots represent the average of positive cells per field per mouse. Error bars represent $\pm$SD. Statistical analysis was performed using student's t-test,*p=0.0109.

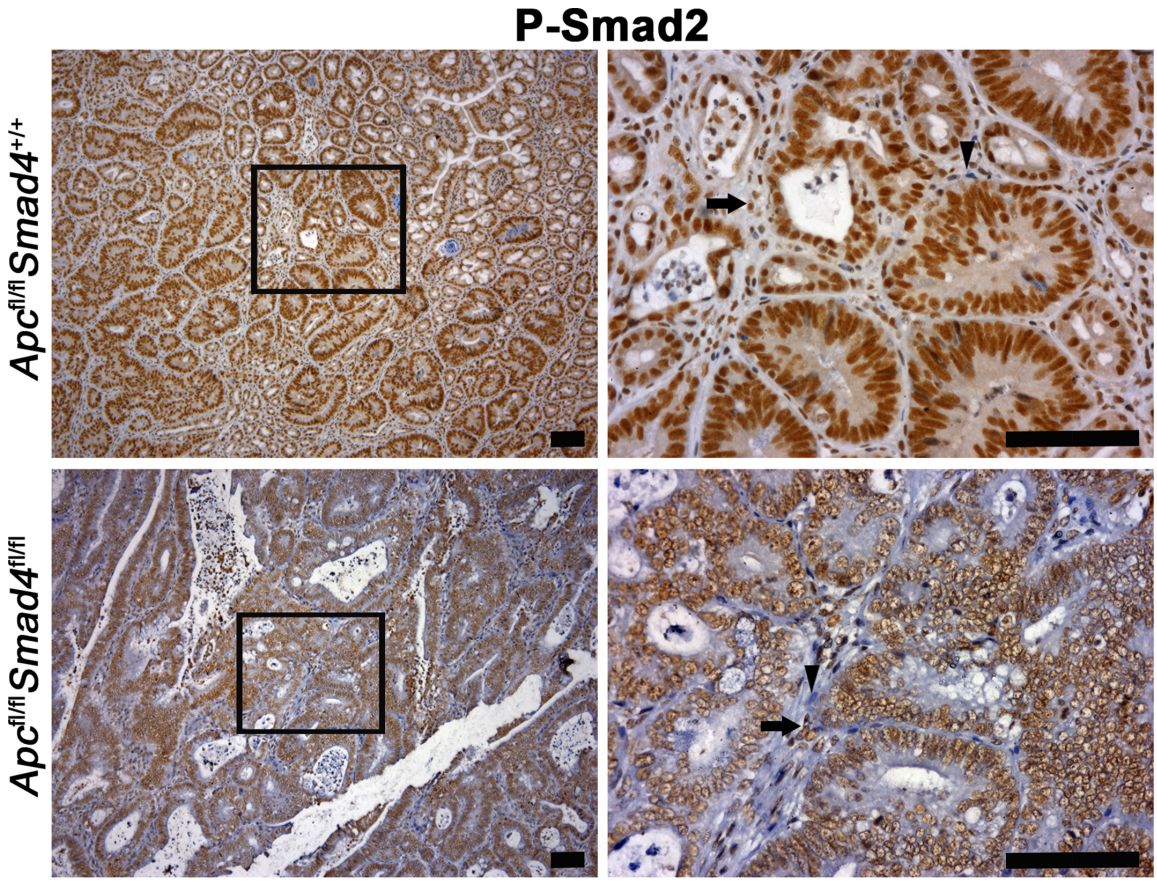

Figure 3.8: **Active TGF-β pathway in the epithelium and stroma in tissue sections from *Smad4*$^{fl/fl}$ mice .** Representative DAB stain shows p-Smad2 labelling in the stroma and epithelium from sections in both genotypes with nuclear localisation in *Smad4*$^{fl/fl}$ tissue sections . Magnification of the marked boxes are shown to the right. Arrows point to cells positively labelled for p-Smad2 in the stroma, and arrowheads point to cells negatively labelled for p-Smad2 in the stroma. Scale bars 100µm.

3.4.2 *In vivo* $Apc^{fl/fl}$ $Igf2r^{I1565Am/+p}$ *Lgr5-CreERT2* adenoma model

3.4.2.1 Deviation from Mendelian ratio in progeny of $Igf2r^{I1565Am/+p}$ mating

To address the functional consequences of Igf2 in the context of impaired binding of Igf2r, I utilised a new knock-in mouse where domain 11 of Igf2r is disrupted with a loss of function mutation where isoleucine was substituted with alanine at position 1565 (I1565A). Breeding for this adenoma model was described in chapter 2 (Figure 2.2). Breeding was performed through two phases. The first phase was to generate females heterozygous for $Igf2r^{I1565A}$ through paternal transmission ($Igf2r^{I1565Ap/+m}$). This step was related to the lower percentage of viable pups with the mutation if it was maternally transmitted. Moreover, females having the mutation through maternal transmission ($Igf2r^{I1565Am/+p}$) are infertile as they have vaginal atresia (unpublished data). Ear notches were performed between postnatal days 8-12 where survival was also evaluated. The segregation of $Igf2r^{I1565Ap/+m}$ was in agreement with Mendelian ratios (χ^2 0.231, p=0.6307 for $Igf2r^{I1565A}$ segregation and χ^2 0.103, p=0.7487 for sex-specific segregation) (Table 3.2). The second phase for breeding was through maternal transmission to generate experimental mice. There was a deviation from Mendelian ratios (χ^2 15.940, P<0.0001 and χ^2 5.526, p=0.0187 for $Igf2r^{I1565A}$ segregation and sex-specific segregation, respectively) (Table 3.2). Only 25% of the pups had the mutation (expected 50%) and most of them were females (23/29) compared to males (6/29). Data presented in the table were from 13 litters (mean litter size 6$\pm$2.2 (SD), range 2-10) and 20 litters (mean litter size 6$\pm$1.8 (SD), range 2-10) for paternal and maternal transmission, respectively. Animal sex was determined by ear-clipping and confirmed after weaning. Segregation of *Apc* and *Lgr5-CreERT2* was normal in all experiments done in the Hassan lab, and has hence not been analysed.

Table 3.2: Mendelian segregation of progeny from *Igf2r*^{l1565A} mating

		Observed	Expected	χ^2	Transmission
	Genotype				Paternal
Igf2r$^{l1565Ap/+m}$ segregation	*Igf2r*$^{+m/+p}$	**37**	39		
	Igf2r$^{l1565Ap/+m}$	**41**	39		
	Total	**78**		0.231	
	Sex				Paternal
Igf2r$^{l1565Ap/+m}$ segregation	Male	**16**	20		
	Female	**25**	20		
	Total	**41**		0.103	
	Genotype				Maternal
Igf2r$^{l1565Am/+p}$ segregation	*Igf2r*$^{+m/+p}$	**88**	59		
	Igf2r$^{l1565Am/+p}$	**29****	59		
	Total	**117**		15.940	
	Sex				Maternal
Igf2r$^{l1565Am/+p}$ segregation	Male	**6***	15		
	Female	**23**	15		
	Total	**29**		5.560	

****p<0.0001, *p=0.0187, Chi-square test.

3.4.2.2 Decreased survival of *Apc*$^{fl/fl}$*Igf2r*$^{l1565Am/+p}$ animals following tamoxifen injection

Igf2r$^{l1565Am/+p}$ mice had a decreased survival following Cre-mediated activation by tamoxifen as determined by log-rank test (p=0.0468) (Figure3.9A). Median survival was 25 and 33 days for *Igf2r*$^{l1565Am/+p}$ and *Igf2r*$^{+m/+p}$, respectively. Animals from both genotypes developed adenomas in the small intestine as well as the colon (95% in the caecum). Median small intestinal adenoma/cm^2 was 1.770 for *Igf2r*$^{+m/+p}$ animals and 2.095 for *Igf2r*$^{l1565Am/+p}$ animals, this was not statistically significant (Mann-Whitney test, p=0.3127). Colonic adenoma count also was not statistically significant as determined by Mann-Whitney test (p=0.2354) with median adenoma/cm^2 of 0.6400 and 1.159 for *Igf2r*$^{+m/+p}$ and *Igf2r*$^{l1565Am/+p}$ animals, respectively (Figure 3.9B). Although adenomas developed in *Igf2r*$^{l1565Am/+p}$ animals were slightly bigger than adenomas developed in the *Igf2r*$^{+m/+p}$ animals, the size was not statistically significant. Only one mouse out of eight developed very big proximal polyps (3) >6mm in diameter. The distribution of adenomas throughout the small intestine and the colon was similar in both genotypes (Figure 3.9 C, D).

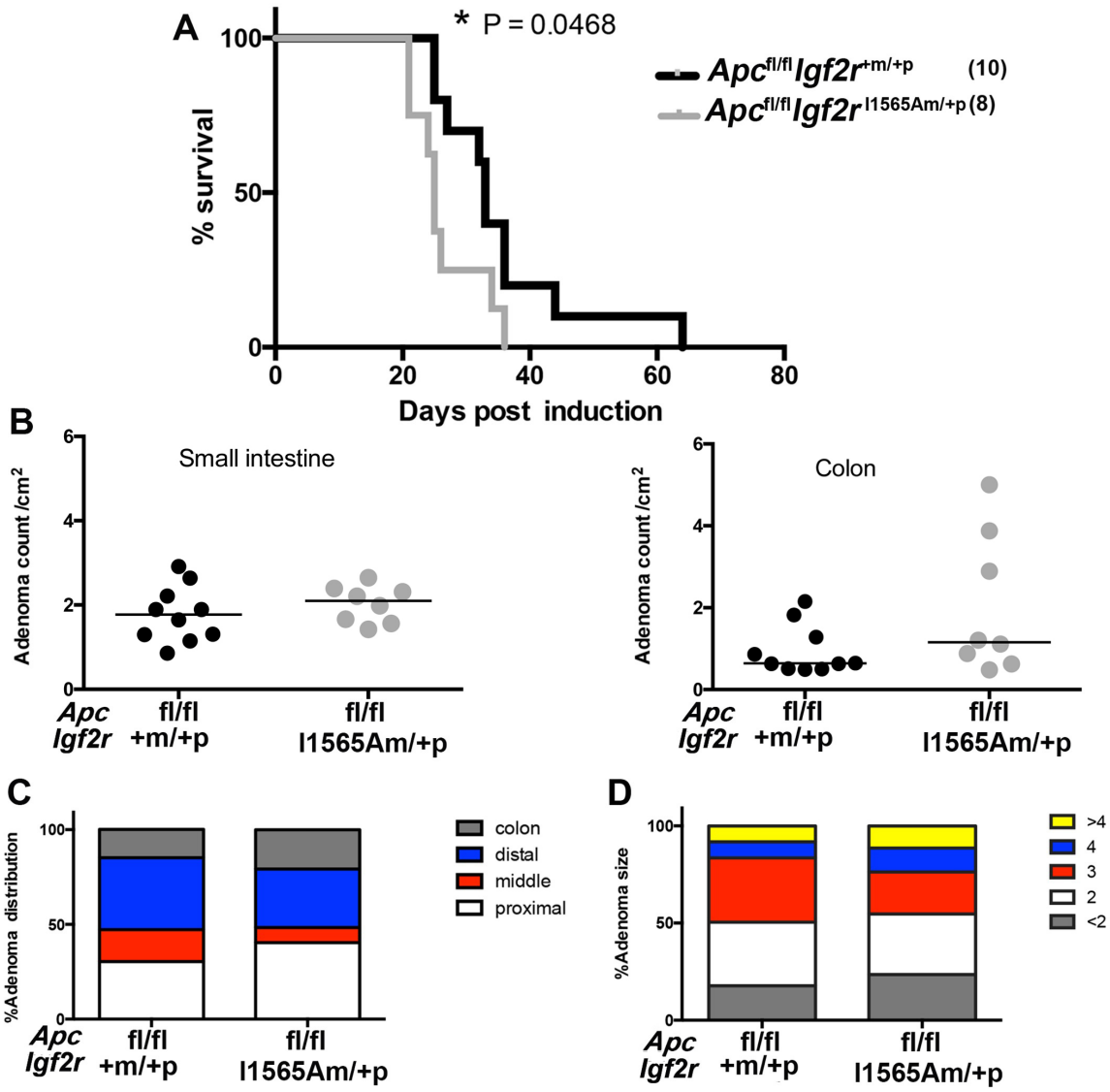

Figure 3.9: **Survival, adenoma count and distribution for the *Apc*$^{fl/fl}$*Igf2r*^{I1565A}*Lgr5-CreERT2* adenoma model.** (A) Kaplan-Meier survival curve showing survival of *Apc*$^{fl/fl}$*Igf2r*$^{+m/+p}$, and *Apc*$^{fl/fl}$*Igf2r*$^{I1565Am/+p}$ post tamoxifen induction. Comparison between genotypes was performed by the Log-rank test, *p=0.0468. (B) Adenoma count per cm^2 in the small intestine and the colon from *Apc*$^{fl/fl}$*Igf2r*$^{+m/+p}$ (n=10) and *Apc*$^{fl/fl}$*Igf2r*$^{I1565Am/+p}$ (n=8) animals. Each dot represents an individual animal. Statistical analysis was performed using Mann-Whitney test with median shown in the graphs. (C, D) Adenoma and size distribution of *Apc*$^{fl/fl}$ *Igf2r*$^{+m/+p}$ (n=10) and *Apc*$^{fl/fl}$ *Igf2r*$^{I1565Am/+p}$ (n=8). Statistical analysis was performed using one-way ANOVA with Sidak's multiple comparison test.

3.4.2.3 *Apc*$^{fl/fl}$*Igf2r*$^{I1565Am/+p}$*Lgr5-CreERT2* histology

Analysis of H&E sections from the small intestine of *Igf2r*$^{I1565Am/+p}$ mice show less differentiated and hyperproliferative epithelial cells (hyperchromatic nuclei) compared to sections from the small intestine of *Igf2r*$^{+m/+p}$ mice (Figure 3.10A). Similar degree of dysplasia in the caecum of both genotypes was seen ranging from from low grade dysplasia to carcinoma *in situ*. No invasion was reported in *Igf2r*$^{I1565Am/+p}$ mice (Figure 3.10B).

In future work, tissue sections will be evaluated for the effect of the mutation on β-catenin, apoptosis and proliferation.

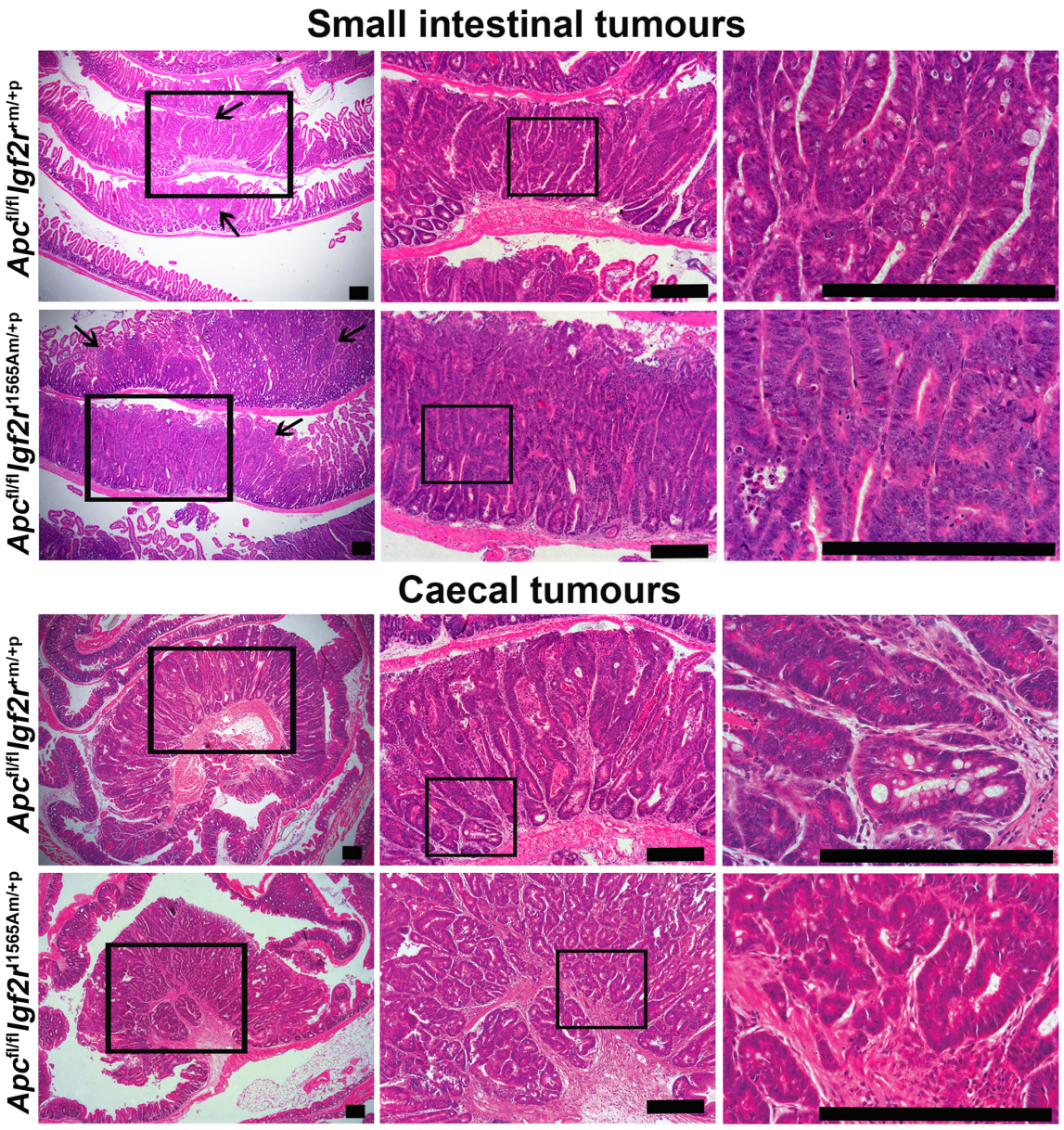

Figure 3.10: ***Apc***$^{fl/fl}$ ***Igf2r***$^{I1565Am/+p}$ ***Lgr5-CreERT2*** **histology.** Representative H&E sections of the small intestinal (A) and caecal (B) tumours from both *Igf2r*$^{+m/+p}$ *Igf2r*$^{I1565Am/+p}$ animals. Arrows point to adenomas in the small intestine. Panels to the left represent sections of each genotype. Magnification of areas marked with black boxes are shown to the right. Scale bars 200µm.

3.5 Discussion

3.5.1 *Apc*$^{fl/fl}$*Smad4*$^{fl/fl}$ adenoma model

The results of the conditional deletion of *Smad4* from the *Apc*$^{fl/fl}$*Lgr5-CreERT2* intestinal adenoma model show a significant decrease in the number of small intestinal adenomas with enhanced survival. *Smad4*$^{fl/fl}$ mice developed large caecal tumours. Histology showed dysplastic tumours. Signs of inflammation were observed at the tumour area including the presence of crypt abscesses and infiltration of macrophages and T-cells in the stroma, with presence of active TGF-β signalling manifest by the presence of p-Smad2 positive cell labelling (Figure 3.2-3.8).

The decreased small intestinal adenoma burden and the appearance of caecal tumours in our model might be the cause of better survival in these animals. The formation of colonic microadenomas in *Apc*$^{fl/fl}$*Lgr5* animals is slower than microadenoma formation in the small intestine and could be related to slower tissue renewal kinetics in the colon (Rizk and Barker, 2012). Takaku *et al.* showed a reduced burden of polyps in the small intestine, with only 82 adenomas formed in *Apc*$^{\Delta 716/+}$*Smad4*$^{+/-}$ when compared with 676 adenomas formed in the *Apc*$^{\Delta 716/+}$*Smad4*$^{+/+}$ mouse model. The cross was on a 129/SV background, when the animals were crossed on a C57BL/6 background, there was no difference in the number of polyps. Regardless of the number, the adenomas in the compound heterozygous mice were bigger and invasive (Takaku et al., 1998). On the other hand, Freeman *et al.* reported an increase in the small intestinal adenoma burden of *Apc*$^{\Delta 1638/+}$*Smad4*$^{fl/fl}$*K19-Cre ERT2* model (Freeman et al., 2012). The appearance of colonic polyps at later stages (14-20 weeks) of *Apc*$^{\Delta 716/+}$*Smad4*$^{-/+}$ animal life has been reported (Takaku et al., 1998). The increase in colonic polyps was also a phenotype in the *Apc*$^{\Delta 1638/+}$*Smad4*$^{fl/fl}$*K19-CreERT2* mouse model (Freeman et al., 2012).

Therefore, similarities and differences in the results could be dependent on the mouse model. Our model is the only one directed toward the *Lgr5* stem cell compartment, the origin of intestinal tumours in the mouse (Barker et al., 2009) and the other models are de-

pendent on germline mutations. In the intestine and at the crypt base, the BMP signalling pathway is downregulated by different inhibitors such as Gremlin and Noggin (He et al., 2004; Wakefield and Hill, 2013). It has been reported that Wnt activity, stem cell numbers and Wnt modulators are variable between different areas of the intestine (Leedham et al., 2012). In the caecal part of the mouse intestine there is high expression of Lgr5 and low expression of Wnt modulators, namely the BMP pathway inhibitors *Grem1*, *Grem2* compared to the small intestine (Leedham et al., 2012).

Polyp formation depends on certain levels of β-catenin that provide the ”just-right" signalling (Albuquerque et al., 2002). Polyps with Smad4 mutations are associated with increased levels of β-catenin (Freeman et al., 2012). Targeted deletion of *Bmpr1a* from the ISC, in a mouse model for JP, showed crypt expansion with increased proliferation, fused villi and polyp formation due to an increase in β-catenin (He et al., 2004). This suggests that in our adenoma model the "just-right" signalling might be affected as both *Smad4* and *Apc* were disrupted at the same time. In the caecum, however, the lower gradient of BMP antagonist means a higher BMP activity. Also there is higher Wnt activity as Lgr5 is a Wnt target gene (Leedham et al., 2012), therefore, the caecum can tolerate the higher β-catenin signal coming from the deletion of the two genes simultaneously. Moreover, as Smad4 is the common mediator for both the BMP and the TGF-β pathways, the "just-right" Wnt activity required for adenoma formation might be achieved due to the presence of active TGF-β pathway as indicated by the presence of nuclear p-Smad2.

The presence of crypt abscesses in the caecal histology with infiltration of more F4/80$^+$ cells than CD11b$^+$ suggests that inflammatory infiltrate may have contributed to colonic adenoma formation. TAMs produce different growth factors for example EGF, VEGF, bFGF, which sustain tumour growth (Galdiero et al., 2013). Our animals are known to be free from *Helicobacter hepaticus*, thus, there is a possibility that commensal microbial population triggers adenoma formation. It has been shown that regions characterised by intense epithelial-microbial interactions, and thus exposed to microbial products, may show an inflammation induced tumour tendency (Elinav et al., 2013). These microbiota may represent

the missing link between inflammatory preconditioning and the risk of tumour development (Elinav et al., 2013). The histology in our model also showed hyperplasia with no invasion. At the invasive front of the tumour the inflammatory infiltrate might change. Kitamura *et al.* showed the presence of a unique population of immature myeloid cells (which express CD34, CD45, CD11b, and CC-chemokine receptor 1 (Ccr1), but not F4/80) which migrate towards CC-chemokine ligand 9 expressed in adenocarcinomas and surrounds the invasive front from *Apc*$^{\Delta 716/+}$*Smad4*$^{-/+}$ tissues. Deletion of *Ccr1* prevents the accumulation of the immature myeloid cells and thus prevents invasion (Kitamura et al., 2007).

The presence of nuclear p-Smad2 labelling in the epithelium and stroma suggested that TGF-β might promote tumour progression. The source of TGF-β based on the staining could be from tumours, the stroma or both. It has been demonstrated that TGF-β promotes tumour initiation in nude mice when injected with tumour cell lines that have mutations in the TGF-β pathway and have been modified to produce TGF-β1 in the first 24h of inoculation (Calon et al., 2012). The source of TGF-β could be either from the tumour cells themselves, macrophages, or cancer associated fibroblasts (Calon et al., 2012).

3.5.2 *Apc*$^{fl/fl}$*Igf2r*$^{I1565Am/+p}$ adenoma model

The results for this mouse model show a decreased survival of pups with *Igf2r*$^{I1565Am/+p}$ genotype. With Cre-mediated recombination of the *Apc* gene, adenomas formed and resulted in decreased survival of *Apc*$^{fl/fl}$*Igf2r*$^{I1565Am/+p}$ animals compared to *Apc*$^{fl/fl}$*Igf2r*$^{+m/+p}$ (Table 3.2, Figure 3.9-3.10).

The decreased survival of the pups when the mutation was maternally transmitted was expected. Perinatal lethality has been reported in different studies evaluating Igf2r in development due to Igf2 dependent overgrowth of the embryonic heart and placenta (Wang et al., 1994; Ludwig et al., 1996; Wylie et al., 2003; Hughes et al., 2013). The survival of maternal Igf2r heterozygous mutants was dependent on the genetic background. For instance, on 129/Sv background the survival was 0%. When the breeding was mixed be-

tween 129/Sv and C57BL/6J the survival was 1.5% (Wang et al., 1994). In a different study when the breeding was between 129/Sv and C57BL/6J the survival was 2.6% (Lau et al., 1994) and increased to 16% when the breeding was between 129/Sv and MF1 genetic background (Ludwig et al., 1996). In this breeding, lower numbers of male pups survived. This effect has not been reported previously although in the Ludwig *el al*. study, 8 Igf2r mutant male mice survived out of 24 (Ludwig et al., 1996). The reason could be because of the heart size might might be bigger in males compared to females with Igf2r$^{I1565Am/+p}$ genotype. It also could be related to the low number of pups being tested in this experiment (29 pups). The differences in the proportion of viable males will be further examined in a different cross with this mouse model.

The presence of different functions for Igf2r suggests that different mechanisms and pathways might be behind the decreased survival and the slightly larger formed adenomas; there will be increase of Igf2 supply and prevention of latent TGF-β1 activation, resulting in increased proliferation and altered growth inhibition (Hébert, 2006; Dynkevich et al., 2013).

In summary, the work presented in this chapter has evaluated alterations in two different pathways involved in intestinal tumorigenesis resulting in interesting phenotypes in both models. The progression seen in the *Apc*$^{fl/fl}$*Igf2r*$^{I1565Am/+p}$ was not expected, but the phenotype of the *Apc*$^{fl/fl}$*Smad4*$^{fl/fl}$ mouse was more apparent. As a result, I decided to pursue the molecular mechanisms underpinning the phenotype of the *Apc*$^{fl/fl}$*Smad4*$^{fl/fl}$ mouse model by using a 3D organoid culture system. The reduced small intestinal tumour burden raised the question of whether the *Apc*$^{fl/fl}$*Smad4*$^{fl/fl}$ adenomas would exhibit the same phenotype *in vitro* as that seen *in vivo*? The aims of the following chapter were to optimise organoid culture (crypt and adenomas) in order to find a suitable model for dissecting Smad4 function in *Apc*$^{fl/fl}$ adenomas.

Chapter 4

Intestinal Organoid Culture

4.1 Introduction

Our understanding of the molecular mechanisms involved in CRC *in vitro* are based mainly on 2D culture systems. The cell lines are derived from human cancers and harbour different mutations and pathway alterations. Understanding the molecular mechanisms that a particular driver mutation contributes to the pathology of disease is challenging. Moreover, 2D culture lacks apparent interactions between tumour cells and their microenvironment, including the heterogeneity found in human tumours *in vivo* (Kim, 2005; Yamada and Cukierman, 2007). There is a need for a 3D culture system in order to address tissue organisation and heterogeneity during the molecular events involved in intestinal tumorigenesis.

Recently, long-term 3D intestinal organoid culture has been developed by Clevers and coworkers (Sato et al., 2009). With the support of a basement membrane matrix and under defined growth conditions, crypts and a single Lgr5 stem cell can be grown into organoids (Sato et al., 2009). Matrigel that is rich mainly in laminin, collagen IV and entactin act as a basement membrane for this culture system (Sato et al., 2009). Although Matrigel is growth factor reduced, it still has 1.7ng ml^{-1} TGF-β in a latent form. Matrigel provides a scaffold for the cells and preserves tissue architecture. The growth requirements for this culture system are optimised based on genetic evidence from intestinal stem cell self-renewal, differentiation, carcinogenesis and the pathways involved in these processes (Sato and Clevers, 2013). Wnt, BMP and EGFR pathways in this culture are regulated by stimulators

and inhibitors. For instance, R-spondin1 is used in crypt culture since it has a potent proliferative effect on intestinal crypt cells *in vivo* by enhancing Wnt pathway (Kim et al., 2005). Recently, R-spondin family members are reported to be ligands for the Lgr family (de Lau et al., 2011). Noggin is a BMP pathway inhibitor. *In vivo*, the crypts are protected by different BMP pathway antagonists such as Noggin, Gremlin 1 and Chordin-like 1 (Wakefield and Hill, 2013). In the context of intestinal homeostasis, the Wnt and the BMP pathways are acting with an opposite gradient. While high Wnt activity at the base of the crypt is required to maintain stemness, high BMP pathway signalling at the villous compartment is required to permit differentiation (Wakefield and Hill, 2013). Overexpression of Noggin in the villous compartment (*in vivo*) results in crypt expansion (Haramis et al., 2004). In adenoma culture, Noggin withdrawal decreases the Lgr5 expression (Sato et al., 2011). EGF stimulates growth in the gastrointestinal tract through the EGFR dependent pathway (Dignass and Sturm, 2001), and is also required for this culture system (Sato et al., 2009). While these are the main growth requirements, other supplements are used on the day of culture. For instance, *N*-acetylcysteine (NAC) an anti-oxidant is used in crypt culture once on the day of culture (Sato et al., 2011) as it reduces the level of reactive oxygen species (ROS) that causes cell death (Spagnuolo et al., 2006; Chaudhari et al., 2007). Y-27632, is a selective inhibitor for p160-Rho-associated coiled-coil kinase (ROCK). It is found to be important for growth and recovery of frozen human embryonic stem cells (hESc) (Heng et al., 2006), and improves the survival and growth of hESC after dissociation (Watanabe et al., 2007). Therefore, Y-27632 is included as a supplement on the day of crypt culture if the extracted cells are FACS sorted before seeding (Sato et al., 2009).

This culture system has been expanded to allow culture of normal human colonic organoids and applied to study intestinal pathology including adenoma and adenocarcinoma by adjusting certain growth factor requirements (Sato et al., 2011). The system can be used to control gene expression by genetic manipulation and genome editing (Koo et al., 2012; Matano et al., 2015; Drost et al., 2015). This culture system might provide different opportunities to understand intestinal development and pathology and replace the need for transgenic mouse models.

4.2 Rationale for study

Organoid culture mimicking *in vivo* tissue organisation is a new technology used to study intestinal biology. The aims of this chapter are:

1. To establish intestinal adenoma culture using *Apc*$^{fl/fl}$ *Rosa26-YFP Lgr5-CreERT2* mouse model
2. To establish intestinal crypt culture
3. Genetically manipulate conditional intestinal crypt culture from *Apc*$^{fl/fl}$ *Rosa26-YFP Villin-CreERT2* mouse model to form adenoma *in vitro*

4.3 Materials and methods

4.3.1 Mouse models

Mouse models used in this chapter were *Apc*$^{fl/fl}$, *Rosa26-YFP*, *Lgr5-EGFP-IRES-CreERT2* and *Villin-CreERT2* listed in Table 2.1.

4.3.2 Mouse breeding

The breeding strategy and the generated genotypes were described in section 2.1.3.1 and 2.1.3.3.

4.3.3 Genotyping

As described in section 2.2, all animals were identified by genotyping postnatally and PM for experimental mice for further confirmation of the genotype. Genotyping was also performed for organoids in culture.

4.3.4 Mouse dissection and tissue collection

Mouse dissection was described in section 2.1.5. Tissue collection for adenoma culture was described in section 2.1.6.1 and crypt culture and *in vitro* manipulation was described in section 2.1.6.2.

4.3.5 Adenoma culture

Adenoma culture was detailed in section 2.5 and summarised in Figure 4.1 and 4.2.

4.3.6 Crypt culture and genetic manipulation

Crypt culture was detailed in section 2.6 and summarised in Figure 4.3 and 4.4.

4.3.7 Immunolabelling

Characterisation of organoids was described in section 2.7.2.

4.3.8 Growth and proliferation assay

Adenoma growth was assessed as described in sections 2.7.4 and 2.8.

4.3.9 Image acquisition

Image acquisition and analysis was described in 2.7.6.

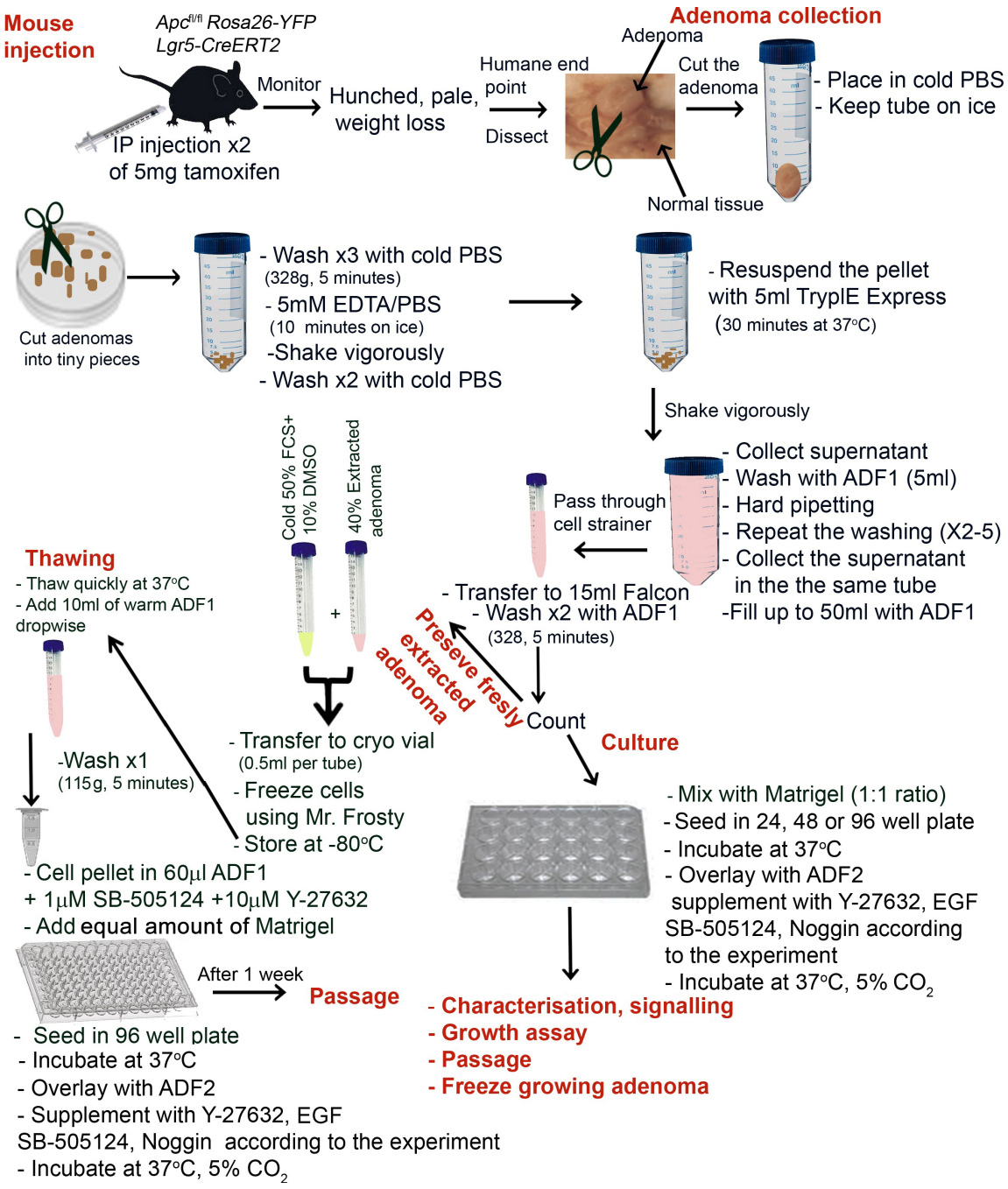

Figure 4.1: **Intestinal adenoma culture flow chart.** Flow chart represents steps required for adenoma culture, freezing and thawing. Adenomas are formed *in vivo* from genetically modified mice following tamoxifen mediated Cre-activation. Extracted adenomas can be used for culture and/or preserved by freezing.

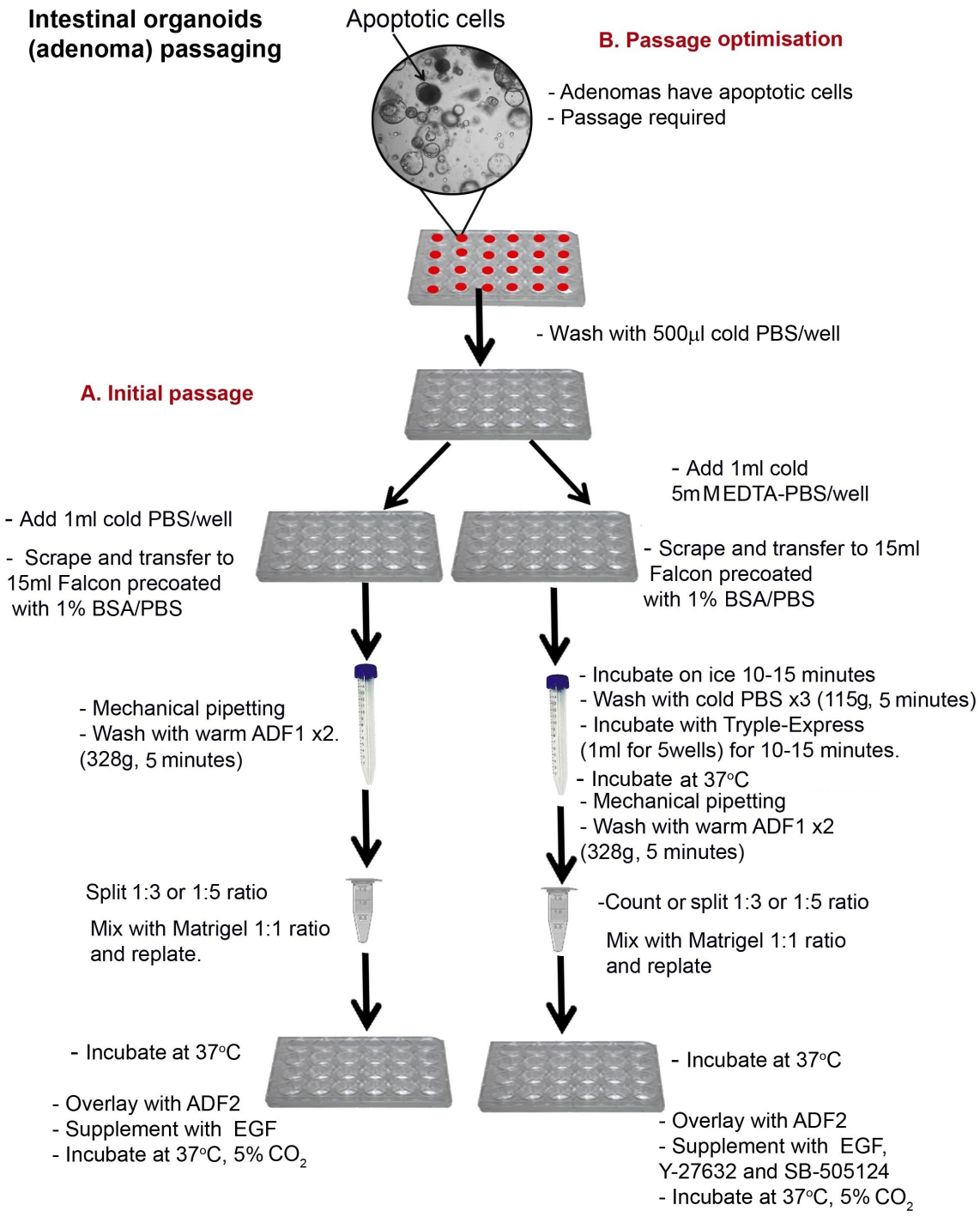

Figure 4.2: **Intestinal adenoma passage flow chart.** Flow chart summarizes two different protocols for adenoma passaging. (A) Initial passage protocol with mechanical dissociation. (B) Optimised protocol in which the Matrigel is first dissolved by cold EDTA-PBS followed by enzymatic dissociation and mechanical dissociation of the adenomas. If adenomas from a few wells are to be passaged, a split ratio for replating is preferable.

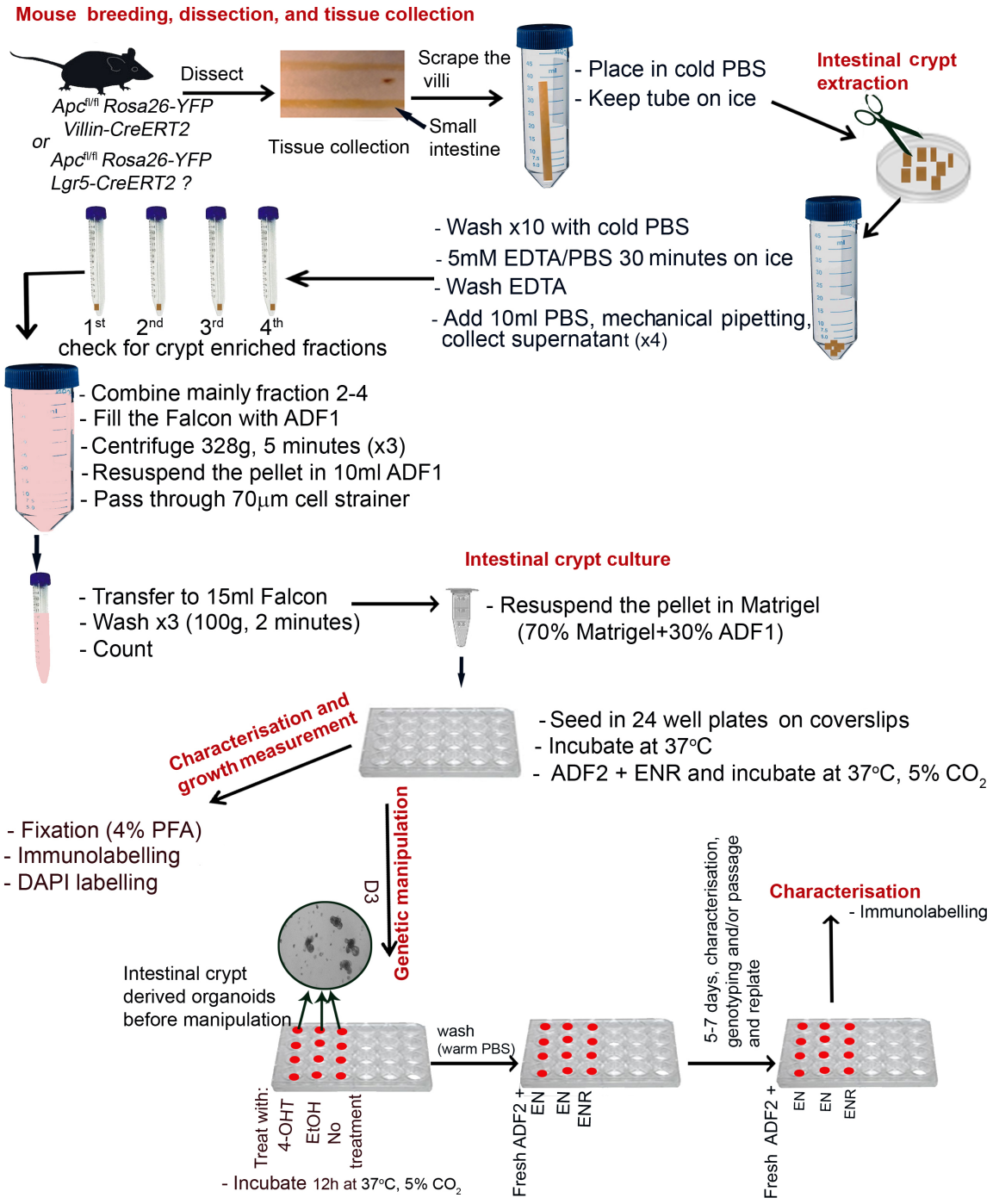

Figure 4.3: **Intestinal crypt culture and genetic manipulation flow chart.** Flow chart represents steps required for crypt culture. Small intestine is taken from genetically modified mouse model, crypts are then extracted, and cultured. Growing intestinal organoids can either be used for characterisation and/or for genetic manipulation.

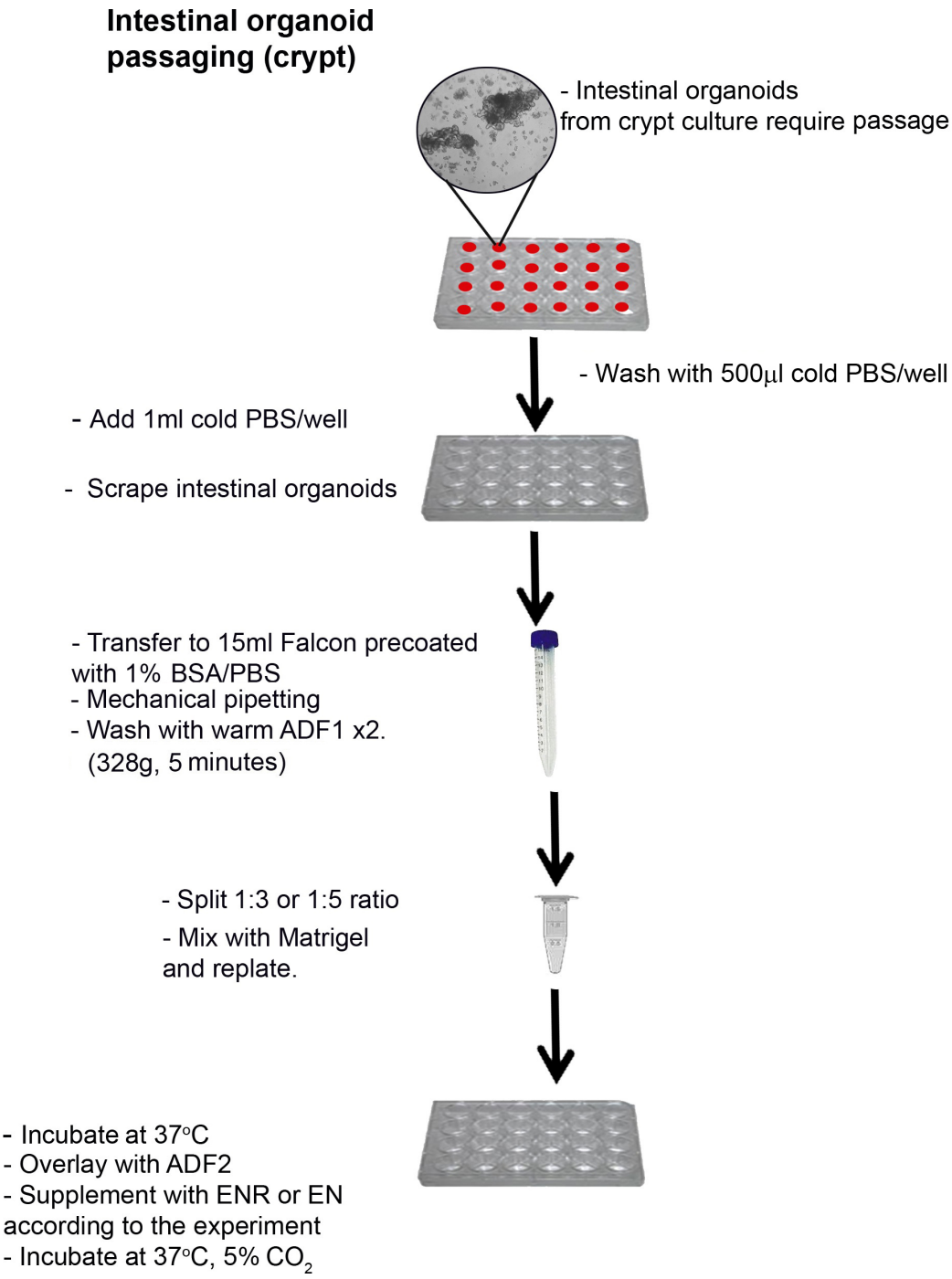

Figure 4.4: **Intestinal crypt derived organoids passaging.** Flow chart represents organoid passaging by mechanical dissociation.

4.4 Results

4.4.1 *Apc*$^{fl/fl}$*Lgr5-CreERT2* adenoma growth is Noggin independent

Establishment of the *in vitro* 3D adenoma culture system used adenomas formed *in vivo* from *Apc*$^{fl/fl}$*Lgr5-CreERT2* animals. Adenoma growth was measured by scoring the size of DAPI labelled adenomas from D2 to D7 (Figure 4.5A-C). Data were normalized to D2 to avoid any differences in adenoma size at seeding. The appearance of apoptotic cells at D7 signalled the need to passage adenomas, so the experiment was terminated here. Area and DAPI fluorescent signal were quantified as they reflect the size and the amount of DNA in an adenoma. However, high fluorescence intensity with small adenoma size was observed occasionally. This may be due to some remaining Matrigel in the labelled adenomas. The ratio of DAPI fluorescence signal to area was also quantified with the R^2 correlation coefficient being 0.888 (Figure 4.5D). Consequently, organoid area alone was used for subsequent measurement of growth. Noggin was used as a supplement in adenoma culture according to the protocol from Professor Owen Sansom (section 2.5). Noggin has normal effect on adenoma growth, and adenomas in culture grew at a similar rate with or without Noggin, as assessed by one-way ANOVA followed by Tukey's multiple comparison test (Figure 4.5E). Noggin independent growth was in agreement with the results from the Clevers' lab (Sato et al., 2011), making it a good control for subsequent optimisation steps.

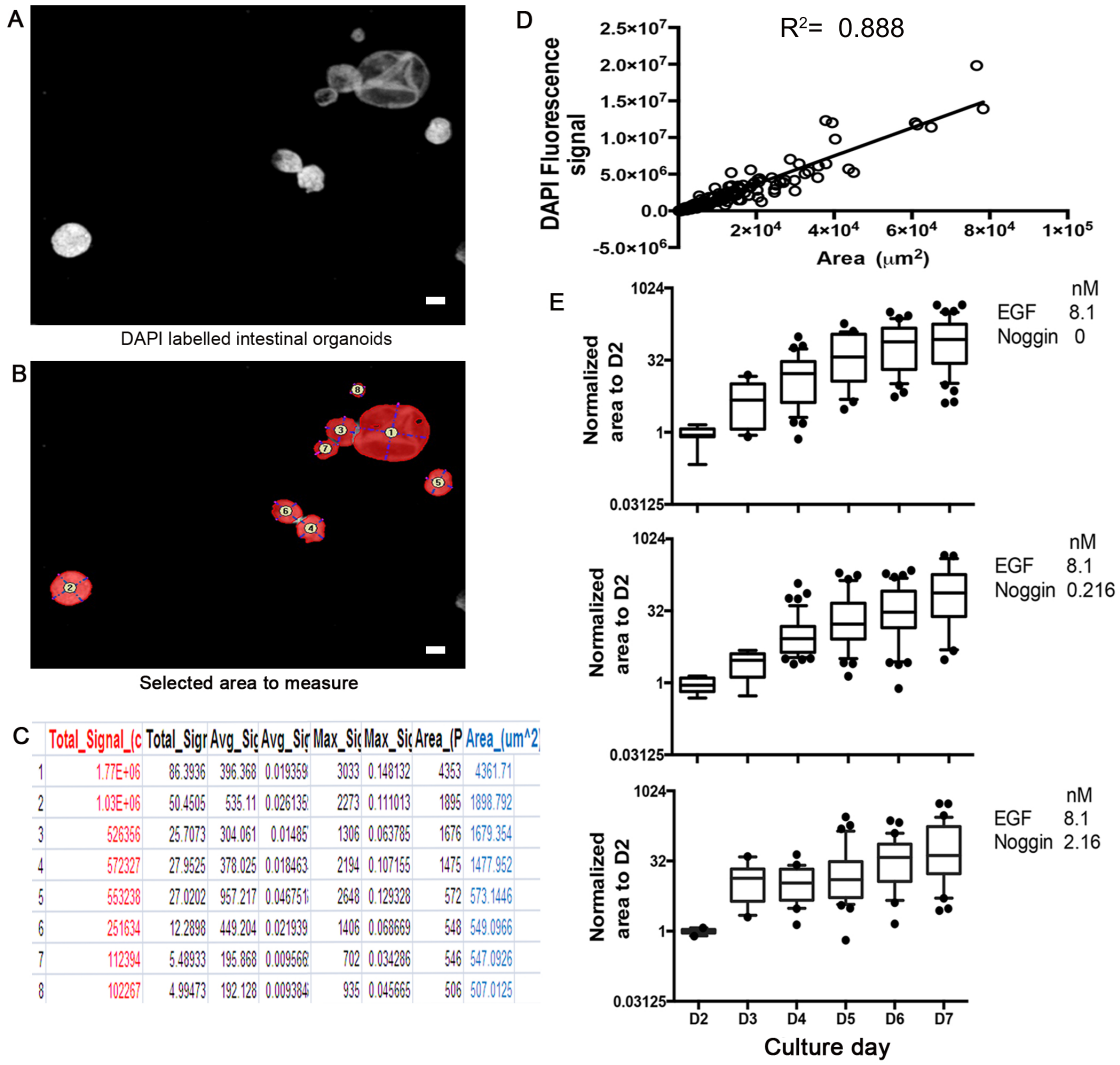

	Total_Signal_(c	Total_Sigr	Avg_Sic	Avg_Sic	Max_Sic	Max_Sic	Area_(P	Area_(um^2
1	1.77E+06	86.3936	396.368	0.019359	3033	0.148132	4363	4361.71
2	1.03E+06	50.4505	535.11	0.026135	2273	0.111013	1895	1898.792
3	526366	25.7073	304.061	0.01485	1306	0.063785	1676	1679.354
4	572327	27.9525	378.025	0.018463	2194	0.107155	1475	1477.952
5	553238	27.0202	957.217	0.046751	2648	0.129328	572	573.1446
6	251634	12.2898	449.204	0.021939	1406	0.068669	548	549.0966
7	112394	5.48933	195.868	0.009568	702	0.034286	546	547.0926
8	102267	4.99473	192.128	0.009384	935	0.045665	506	507.0125

Figure 4.5: ***Apc*$^{fl/fl}$*Lgr5-Cre* in 3D culture**. 6000 single cell adenomas were seeded per well. Adenomas were labelled with DAPI. (A) Representative image showing DAPI labelled adenoma as taken by a fluorescence microscope. (B) Auto-detect to select the area to measure using the CRi-Nuance software. Scale bars 50µm. (C) A representative report by the Nuance software showing the measured parameters. Total signal (red) and area (blue) were used for the subsequent analysis. (D) Scatter plot showing the relationship between DAPI fluorescence signal and area with R^2=0.888 (more than 300 adenomas pooled from different days within the experiment). (E) Adenoma growth measured as ratio of area to D2 with no significant difference in growth based on 10 fold difference in Noggin concentration as analysed by one-way ANOVA followed by Tukey's multiple comparison test. (Scale in y-axis is Log_2, whiskers represent 10-90 percentile).

4.4.2 Crypt culture and mouse intestinal organoid growth is Noggin dependent

Intestinal crypt culture in 3D was also optimised. Small intestine from wild type animals was used for the optimisation step. In two independent experiments, the effect of different combinations of growth factors on crypt growth were examined. The best growth as measured by organoid number and area was obtained when crypts were treated with EGF, Noggin, and R-spondin-1 (ENR) followed by those treated with Noggin, and R-spondin-1 (NR). Crypts deprived of R-spondin1 (R) failed to grow at D2- D3 in culture despite the presence of other growth factors. Results showed Noggin dependency in primary culture (Figure 4.6A-C). In the formed organoids, budding structures appeared on D2-D3. On D7 crypts reached a size where they required passaging. NAC is a potent anti-oxidant used in crypt culture (Sato et al., 2011). Although NAC increased the number of growing organoids (mean organoid number 137 vs 94 when supplemented with ENR in the presence of NAC, respectively), it did not enhance the growth of the organoids without Noggin (Figure 4.6A, n=2, 3 replicates). Organoids without Noggin were low in number (mean 11 and 7 with and without NAC, respectively), and smaller in size but behaved similarly in terms of differentiation. Confocal images showed a single layer of polarized epithelial cells that differentiated into goblet cells (as detected by Muc2), Paneth cells (as marked by lysozyme), enterocytes (as marked by villin) and enteroendocrine cells (as marked with chromogranin A) (Figure 4.6D). Apoptotic cells found in the lumen of the crypts were detected by cleaved caspase-3 (CC3).

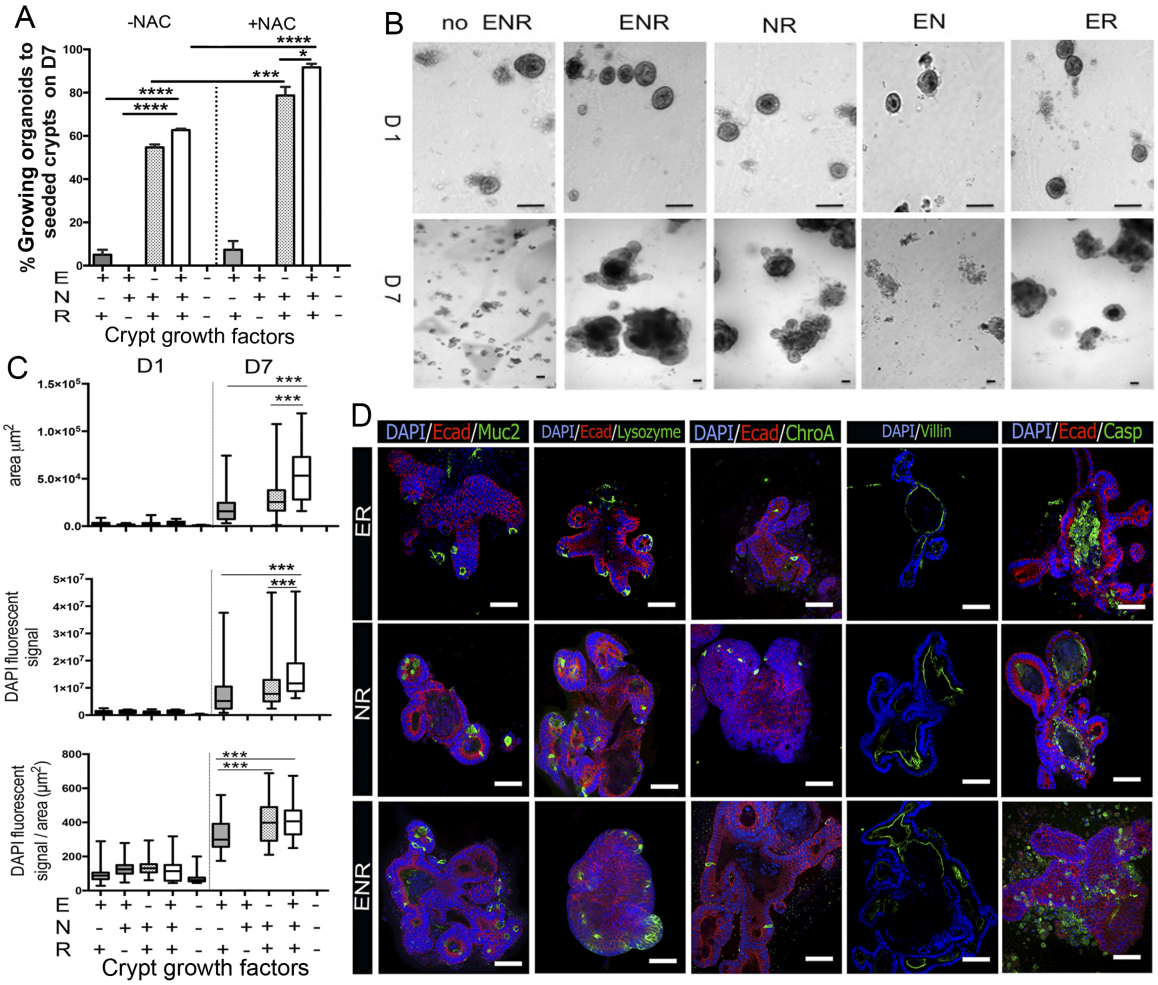

Figure 4.6: **Crypt culture and mouse intestinal organoid growth is Noggin dependent**. (A) 150 crypts were seeded per well, supplemented with different combinations of growth factors with and without NAC. Organoids were counted at D7 by quadrant counting and results represented the percentage of organoids on D7 compared to the seeded crypts. Statistical analysis was performed by one-way ANOVA with Tukey's multiple comparison test *, ***, **** indicates P$\leqslant$0.05, P$\leqslant$0.001 and P$\leqslant$0.0001, respectively. Error bars represent the range (n=2, 3 replicates). (B) Representative bright field images showing the structure of cultured organoids according to different growth factors on D1 and D7, scale bar 50µm. (C) Representative analysis of area, DAPI fluorescent signal and DAPI signal/area for organoids on D1 and D7 as taken by fluorescent microscopy and measured using CRi-Nuance software. Statistical analysis was performed by one-way ANOVA with Tukey's multiple comparison test *** indicates P$\leqslant$0.001 (n=50 for all except ER at D7 when n=13). (D) Representative confocal images for organoids showing in addition to DAPI and E-cadherin (E-cad) their differentiation into goblet cells (Mucin 2 (Muc2)), Paneth cells (lysozyme), enteroendocrine cells (Chromogranin A (ChroA)) enterocytes (Villin). CC3 (Casp) staining show apoptotic cells have been shed out from growing organoids. E (EGF), N (Noggin), R (R-spondin-1). Scale bars 50µm.

4.4.3 Genetic manipulation of conditional crypt culture and adenoma formation *in vitro*

Following the establishment of crypt culture, conditional genetically manipulated crypt culture could commence. Small intestines were taken from healthy animals with *Apc*$^{fl/fl}$ *Villin-CreERT2 Rosa26-YFP* and *Apc*$^{fl/fl}$ *Lgr5-CreERT2 Rosa26-YFP* genotypes. Organoids treated with 4-hydroxy-tamoxifen (4-OHT) (test) and EtOH (control) were deprived of R-spondin1. Organoids receiving 4-OHT remained viable compared to controls. This indicates that the Wnt/β catenin pathway was activated after *Apc* recombination and compensated for R-spondin1 withdrawal (Figure 4.7A). Organoid transformation following 4-OHT administration appeared as rounding at the bottom of the crypts. Transformation and the appearance of the circular structure of adenoma was achieved 2 days after careful passage with limited mechanical pipetting and re-plating in Matrigel (Figure 4.7A). *Apc* recombination was confirmed by the appearance of a 259bp PCR product. This product was absent when the genotype of crypts in the conditional culture was *Apc*$^{fl/fl}$ *Lgr5-CreERT2 Rosa26-YFP*, indicating poor recombination efficiency (Figure 4.7B). *Apc*$^{fl/fl}$ *Villin-CreERT2* transformed organoids formed a circular structure that resembled that of adenoma in culture (formed *in vivo*) (Figure 4.7C). Unlike intestinal organoids, adenomas were highly proliferative as indicated by EdU incorporation at 2h. Proliferative cells in intestinal organoids derived from crypts were restricted to the base of the crypt, while those from adenomas were scattered throughout the adenoma (Figure 4.7D).

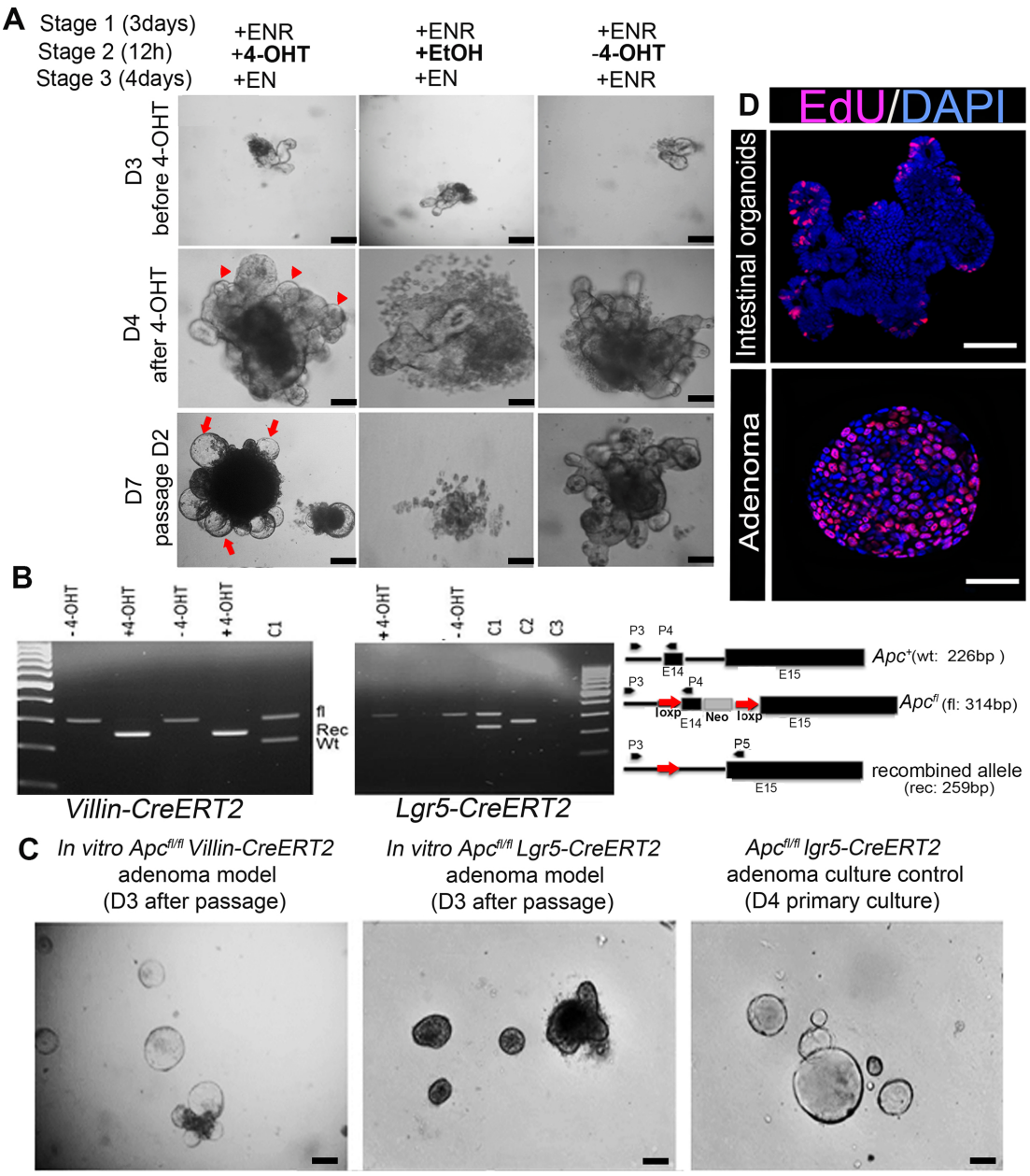

Figure 4.7: **Genetic manipulation of conditional intestinal organoids and adenoma formation in 5 days.** (A) Simple description followed by bright field images for the steps and the controls used in the manipulation of intestinal organoids (intervention in bold). Red arrowheads show expected adenoma within the crypt. Red arrows point to shape change following 4-OHT treatment. (B) Confirmation of *in vitro Apc* gene recombination by PCR. Recombined PCR product of 259bp (middle band) is shown in *Villin-CreERT2* (left) and was absent in *Lgr5-CreERT2* (middle) intestinal organoids. PCR strategy is shown in the diagram on the right. Controls, C1: $Apc^{fl/+}$ mouse ear-clip, C2: recombined $Apc^{fl/fl}$ in culture, C3: No DNA (negative control). P3 is the forward primer and P4, P5 are the reverse primers. (C) Bright field images showing the structure formed after 4-OHT treatment from $Apc^{fl/fl}$ *Villin-CreERT2* and $Apc^{fl/fl}$ *Lgr5-CreERT2* organoids and the shape of cultured adenoma (formed *in vivo*). (D) Confocal images showing EdU incorporation at 2h in both intestinal organoids (crypt culture) and from the cultured adenoma. Scale bars 50µm.

4.4.3.1 Expression of *Rosa26-YFP* and upregulation of Wnt/β-catenin following intestinal organoid manipulation

Further confirmation of efficient *Apc* recombination was the Rosa26-YFP reporter expression and the upregulation of β-catenin as detected by antibodies. Rosa26-YFP was expressed only in *Apc*$^{fl/fl}$ *Villin-CreERT2*$^{+}$ organoids treated with 4-OHT. No expression of Rosa26-YFP was detected in *Apc*$^{fl/fl}$ *Villin-CreERT2*$^{-}$ intestinal organoids, as no Cre was available to mediate the *Apc* gene recombination with 4-OHT. Rosa26-YFP expression was detected in passaged adenomas from *Apc*$^{fl/fl}$ *Villin-CreERT2*$^{+}$ intestinal organoids confirming that these adenomas have originated from genetically manipulated crypts (Figure 4.8). Further confirmation of *Apc* recombination was the localisation of nuclear β-catenin in the formed adenomas indicating upregulation of the Wnt/β-catenin pathway. β-catenin in normal crypts was membrane bound and localised with E-cadherin (Figure 4.9). Adenomas from *Apc*$^{fl/fl}$ *Villin-CreERT2* also had a similar pattern for CD44, Axin2, c-Myc and β-catenin (Wnt/β-catenin regulated genes) when compared to *Apc*$^{fl/fl}$ *Lgr5-CreERT2* (Figure A.1).

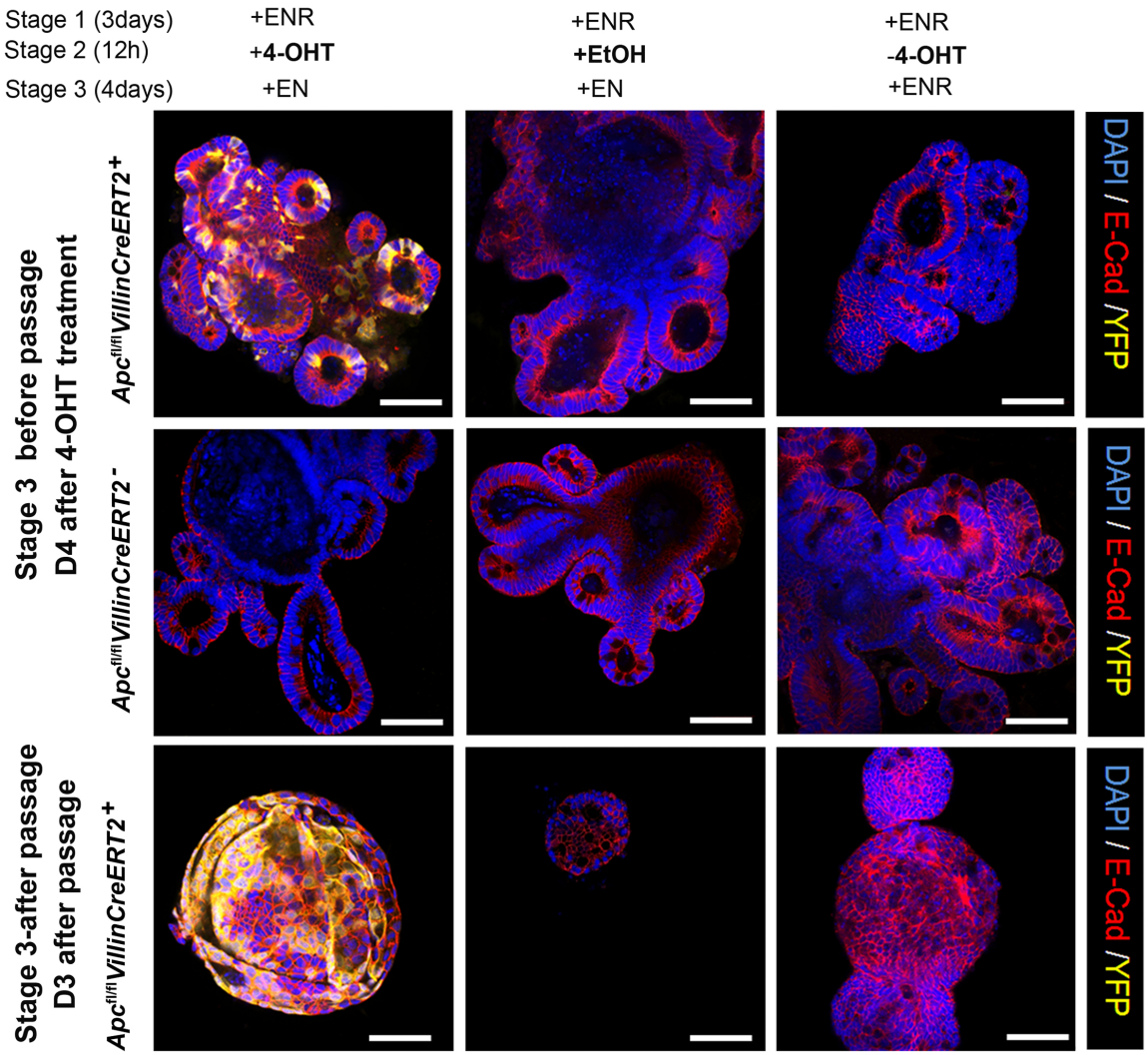

Figure 4.8: **Expression of *Rosa26-YFP* following intestinal organoid manipulation.** *Apc*$^{fl/fl}$ *Villin-CreERT2*$^{+}$ *Rosa26-YFP*$^{fl/fl}$ and *Apc*$^{fl/fl}$ *Villin-CreERT2*$^{-}$ *Rosa26-YFP*$^{fl/fl}$ intestinal organoids were immunolabelled with anti-GFP antibody to detect *Rosa26-YFP* expression. Rosa26-YFP expression was detected only in *Apc*$^{fl/fl}$ *Villin-CreERT2*$^{+}$ organoids treated with 4-OHT (upper panel). No expression of Rosa26-YFP was detected in *Apc*$^{fl/fl}$ *Villin-CreERT2*$^{-}$ intestinal organoids (middle panel). Rosa26-YFP expression was detected in passaged adenomas from *Apc*$^{fl/fl}$ *Villin-CreERT2*$^{+}$ intestinal organoids (lower panel). Scale bars 50µm.

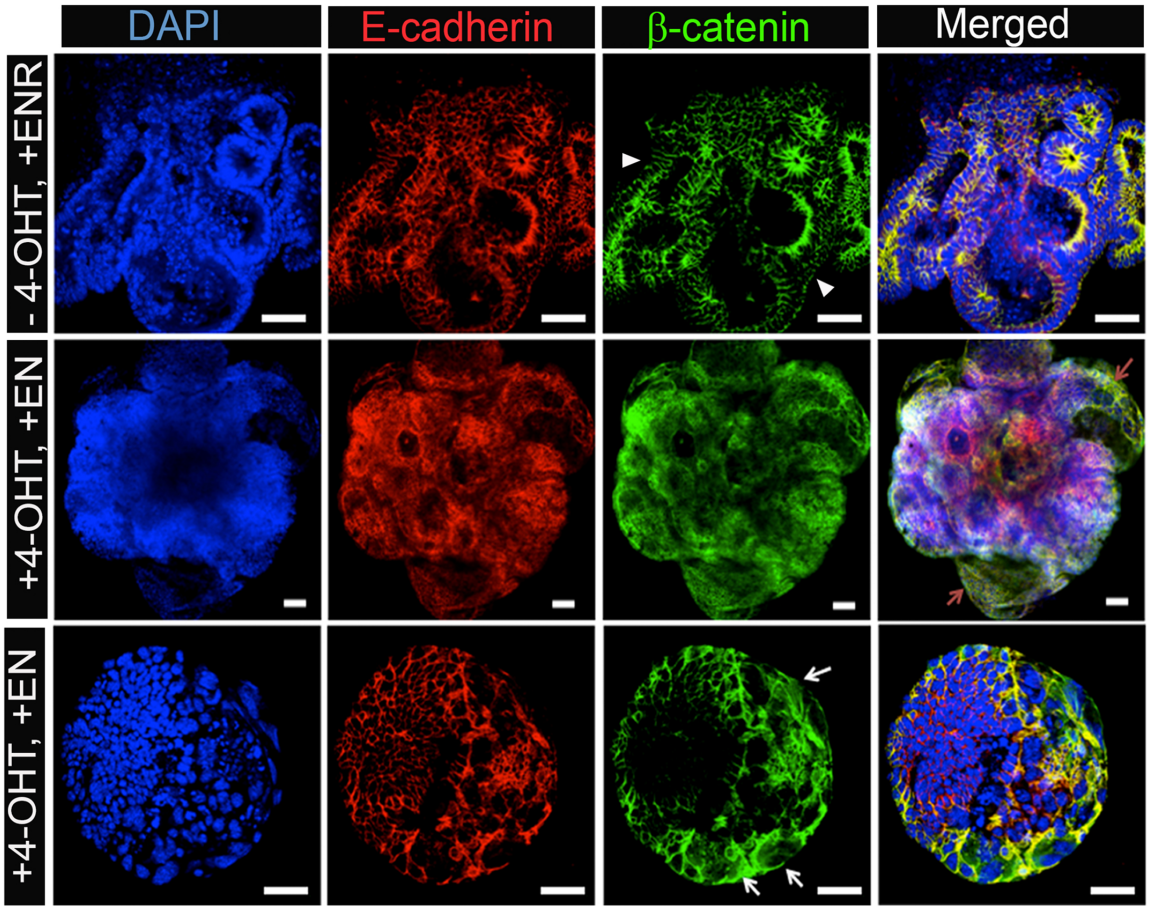

Figure 4.9: **Cytoplasmic β-catenin in *Apc*$^{fl/fl}$ *Villin-CreERT2* adenomas.** Representative confocal images showing cytoplasmic and some nuclear β-catenin (white arrows) in the formed adenoma compared to membrane bound localisation of β-catenin with E-cadherin in the normal organoids (arrowhead). Red arrows show the budding of adenoma. Scale bars 50µm.

4.4.4 Adenoma culture optimisation

4.4.4.1 TryplE Express is better for adenoma extraction

Adenomas were initially extracted using Trypsin, according to the protocol from Professor Owen Samson's lab. Trypsin was replaced by TryplE Express enzyme as the latter enhanced the growth of the extracted adenomas. Adenomas extracted using TryplE Express started to grow as early as D1 (Figure 4.10A). Adenomas extracted by both methods required 8.1nM EGF for their growth. However, there was a significant difference in adenoma number between Trypsin and TryplE extraction enzymes (****$p \leqslant 0.0001$) when counted on D3. The difference in number was reflected by a significant difference in adenoma viability as measured by the percentage of AB reduction with ****$p \leqslant 0.0001$. A similar result for the effect of TryplE was obtained when a colleague kindly repeated the experiment.

4.4.4.2 Viability assay to measure adenoma growth

DAPI area was used to measure adenoma growth. The main disadvantage of this is that it is time consuming. Hence, a high throughput method was required. AlamarBlue (AB) quantitatively measure cell viability. This requires cells to be in the exponential growth phase with optimised cell density and length of incubation. These conditions were met after some optimisation to find that seeding at cell density of 5000 cells per well ($\log_e$=3.70) and adding AB on D3 for 12h was the best for primary *Apc*$^{fl/fl}$ adenoma culture. However, due to other factors (explained in the next chapter) AB reduction was measured after 24h instead of 12h, at this point the relationship between cell density and AB reduction was still high (R^2=0.858) (Figure A.2).

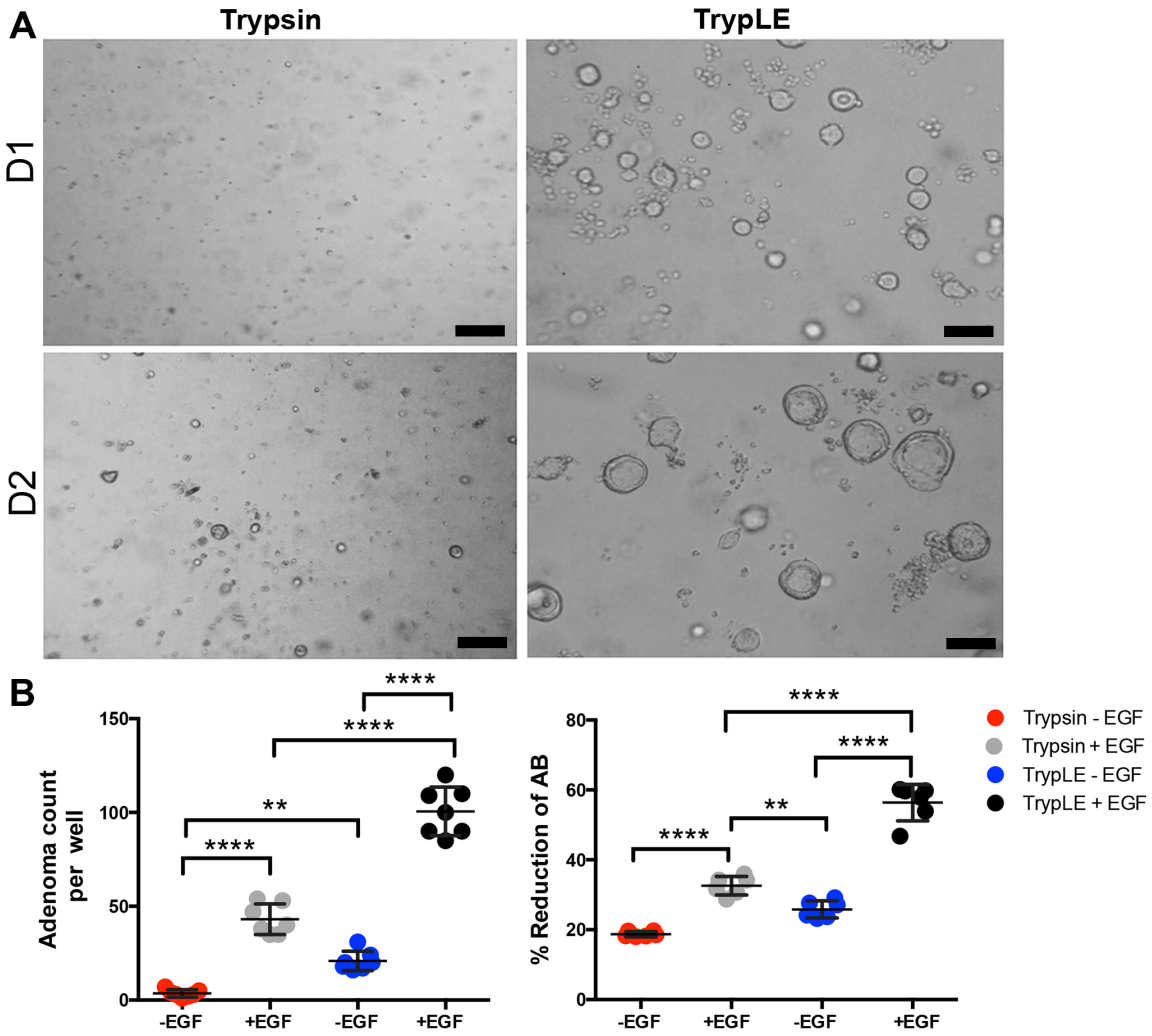

Figure 4.10: **Effect of different extraction enzymes on adenoma growth**. Adenomas taken from mice were extracted using Trypsin and TryplE Express, and seeded at a cell density of 5000 cells/well in a 96 well plate. (A) Representative bright field images show *Apc*$^{fl/fl}$ adenoma on D1 and D2 (D1 represents the day following extraction). (B) Quantification of the growing adenomas on D3 by quadrant counting (left) and viability (right) as measured by percentage reduction of AB. Statistical comparisons were performed by one-way ANOVA with Tukey's multiple comparison test **, **** indicates $P \leqslant 0.01$, $P \leqslant 0.0001$, respectively. Error bars represent $\pm$SD (n=2 independent experiments with 3-4 replicates per condition each represented by dots). Scale bars 100µm.

4.4.4.3 Storage and passage of growing adenoma

Growing adenomas can be stored either in commercial freezing medium or that prepared in the lab. However, the recovery of the adenoma in terms of number after freezing-thawing was significantly improved in the commercial freezing-medium than freezing medium prepared in the lab (10% DMSO-90% ADF2) (mean was 126 and 105 adenoma/well for commercial media and that prepared in the lab, respectively) (*P=0.008), with no significant difference in growth measured by DAPI area (mean 10612 and 10203 μm^2 for commercial media and that prepared in the lab, respectively) (Figure 4.11A). Adenomas can be frozen and thawed several times with no difference in their growth as measured by area between different thawing cycles (Figure 4.11B). Adenomas can be passaged (mechanically) for several cycles as well. The growth of these adenomas was similar as measured by area (Figure 4.11C). Thus, growing adenomas can effectively be stored and passaged. However, the main problems with passaging growing adenomas by this method were dead cells (detected by trypan blue) and Matrigel from the previous cycle and starting the culture from cell aggregates rather than single cells. The challenge was therefore freezing the adenoma directly after extraction from the tumour formed *in vivo*. Having passaged organoids in single cell form without any remaining Matrigel and dead cells from previous culture was another challenge.

4.4.4.4 Freshly extracted adenomas can be frozen directly and recovery of cryopreserved adenomas can be enhanced with TGF-β inhibitor and Rock inhibitor

Recovery of freshly extracted adenomas frozen in Gibco Freezing-Medium (commercial) or (20% FCS, 30% ADF2 and 20% DMSO (prepared in the lab)) was found to be similar in terms of number and growth as measured by area (Figure 4.12). The mean number of adenomas formed was 47 and 45 after being frozen in commercial medium and that prepared in the lab respectively. The mean size of the formed adenomas was 4471 and 6804 μm^2 for those being frozen in the commercial medium and that prepared in the lab respectively. The lab made recipe was used subsequently, however, the recovery was not successful every time. The percentage of viable cells after thawing was very low (mean=33%) compared

to freshly isolated adenomas (mean=89%). The viability of thawed adenomas increased to 54% when 10% DMSO was used in the lab made recipe (Figure 4.13). SB-505124 inhibitor had a significant improvement on adenoma recovery. Moreover, incubating thawed adenomas with SB-505124 inhibitor before seeding enhanced the recovery of thawed adenomas significantly (Figure 4.14A). Y-27632 also had a significant effect on the recovery of cryopreserved adenomas when added before and after seeding. SB-505124 and Y-27632 together, enhanced the recovery of thawed adenoma. The main effect was from Y-27632, however, it was not significant (one-way ANOVA). The mean of normalized AB reduction in descending order was 2.04, 1.85 and 1.69 for Y-27632 alone, Y-27632 and SB-505124 together and SB-505124 alone when added before and after seeding (Figure 4.14B-D). Thus, frozen adenomas require SB-505124 and Y-27632 for their recovery.

4.4.4.5 Enhanced growth of passaged adenomas by Rock inhibitor and TGF-β inhibitor

Adenomas enzymatically passaged to single cells required Y-27632 and SB-505124 supplements post seeding. Mean percentage of AB reduction was 26.8, 35.2, 48.1 and 48.2 for EGF alone, EGF with SB-205124, EGF with Y-27632 and EGF with SB-505124 and Y-27632, respectively. Y-27632 and both inhibitors together enhanced the growth significantly when compared to SB-505124 ($P \leqslant 0.05$) and to EGF alone ($P \leqslant 0.001$). SB-505124 significantly enhanced the growth of passaged adenomas ($P \leqslant 0.01$) compared to EGF alone (Figure 4.15).

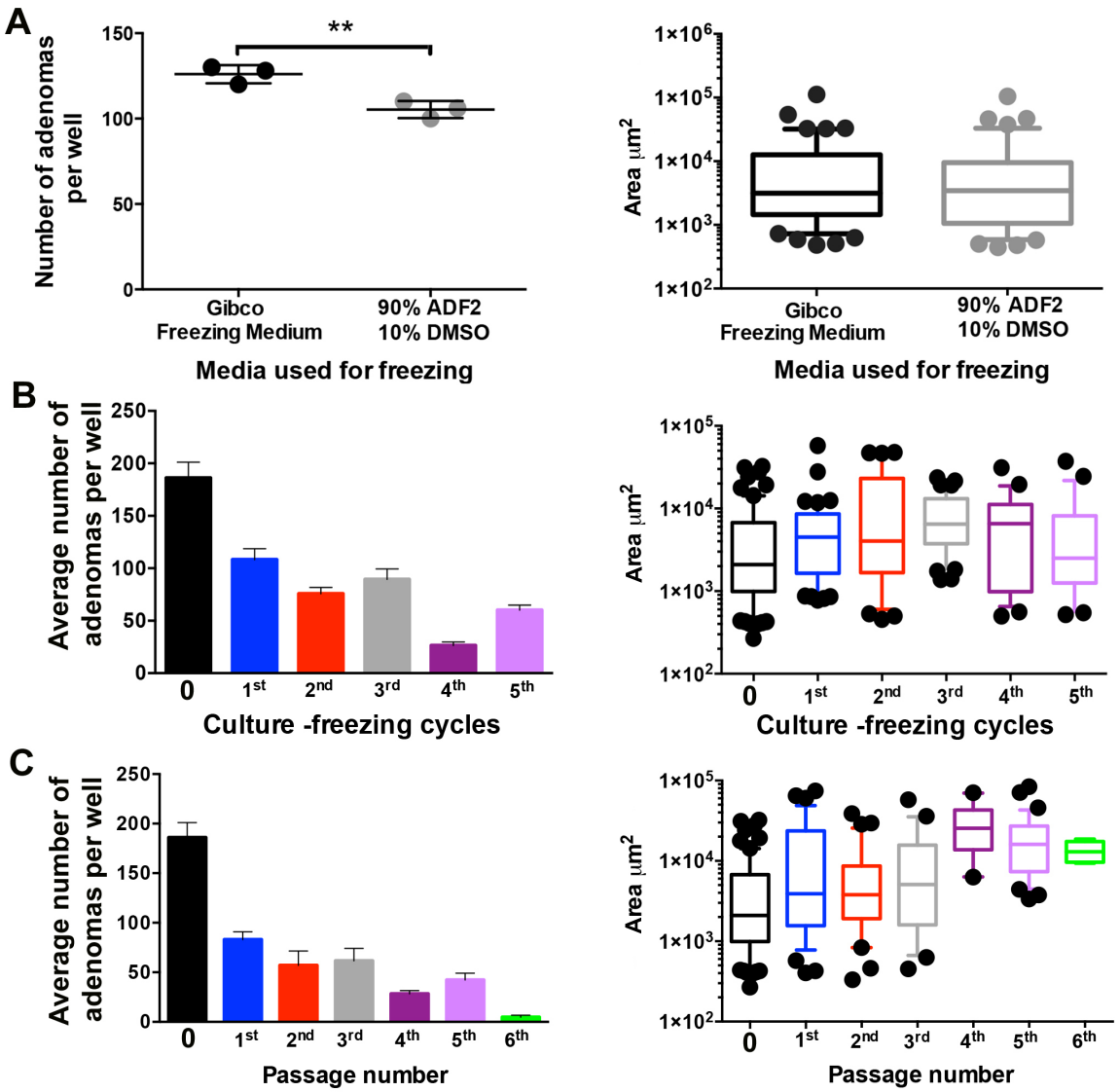

Figure 4.11: **Growing adenomas can be passaged and frozen**. Adenomas from primary culture were subject to freezing and passage cycles. (A) Number of recovered adenomas per well on day 5 after being frozen in different media (left) and adenoma growth as measured by DAPI area (right). ** indicates P=0.008. Statistical comparison was done by unpaired student's t-test (3 replicates represented by dots). (B) Freezing-thawing cycles of growing adenomas. (C) Adenoma passage cycles. The graphs (B, C) represent the average number of adenomas per well (left) and their growth as measured by DAPI area (right). Error bars represent ±SD, whiskers represent 10-90 percentile for count and DAPI area, respectively. Scale in y-axis for area graphs is Log_{10}. In both experiments, fresh extracted adenomas from *Apc*$^{fl/fl}$ mouse were growing in 3 different wells, counted on D5 by quadrant counting. One well was either frozen or passaged and the other 2 wells were used for DAPI labelling. The frozen adenomas were thawed and seeded for another cycle and treated as above. The same applied for passaged adenoma cycles.

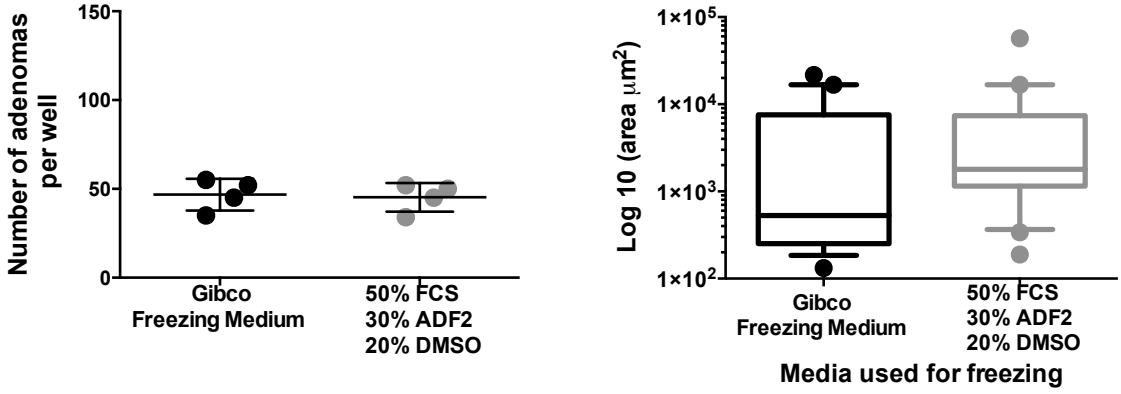

Figure 4.12: **Recovery of fresh frozen adenomas.** Extracted adenomas were frozen in different media, thawed and seeded in Matrigel. The graphs represent the number of recovered adenomas per well on day 7 after being frozen in different media (left) and their growth as measured by DAPI area (right). No statistical difference in the recovery from freezing in both conditions. Statistical analysis was determined by unpaired student's t-test. Error bars represent ±SD and whiskers represent 10-90 percentile for count and DAPI area, respectively. n=1, adenoma count from 4 replicates and DAPI area from 2 replicates.

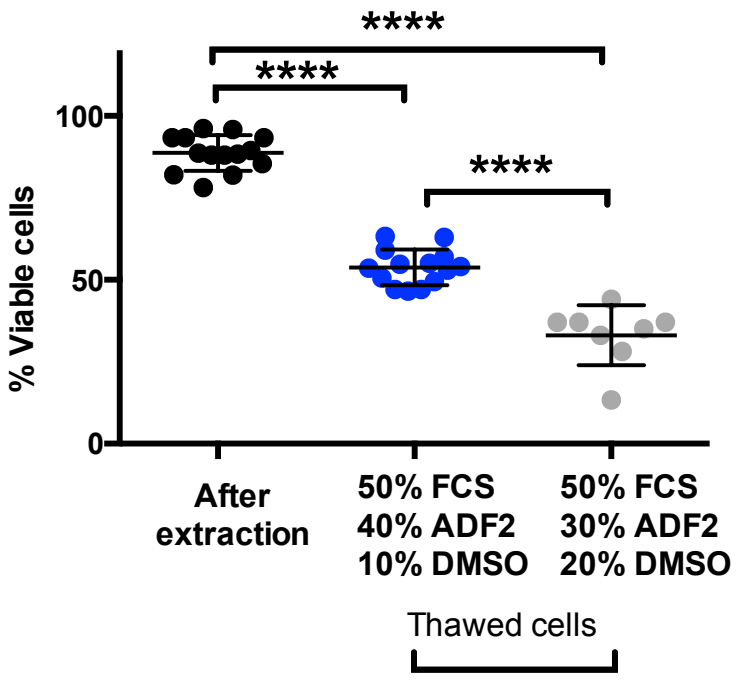

Figure 4.13: **10% DMSO enhanced the viability of frozen adenoma.** Percent of viable thawed cells frozen in different concentration of DMSO compared to the percent of viable cells counted following adenoma extraction as determined by cell counter. **** indicates $P \leqslant 0.0001$. Statistical comparisons were performed by one-way ANOVA with Tukey's multiple comparison. Error bars represent ±SD.

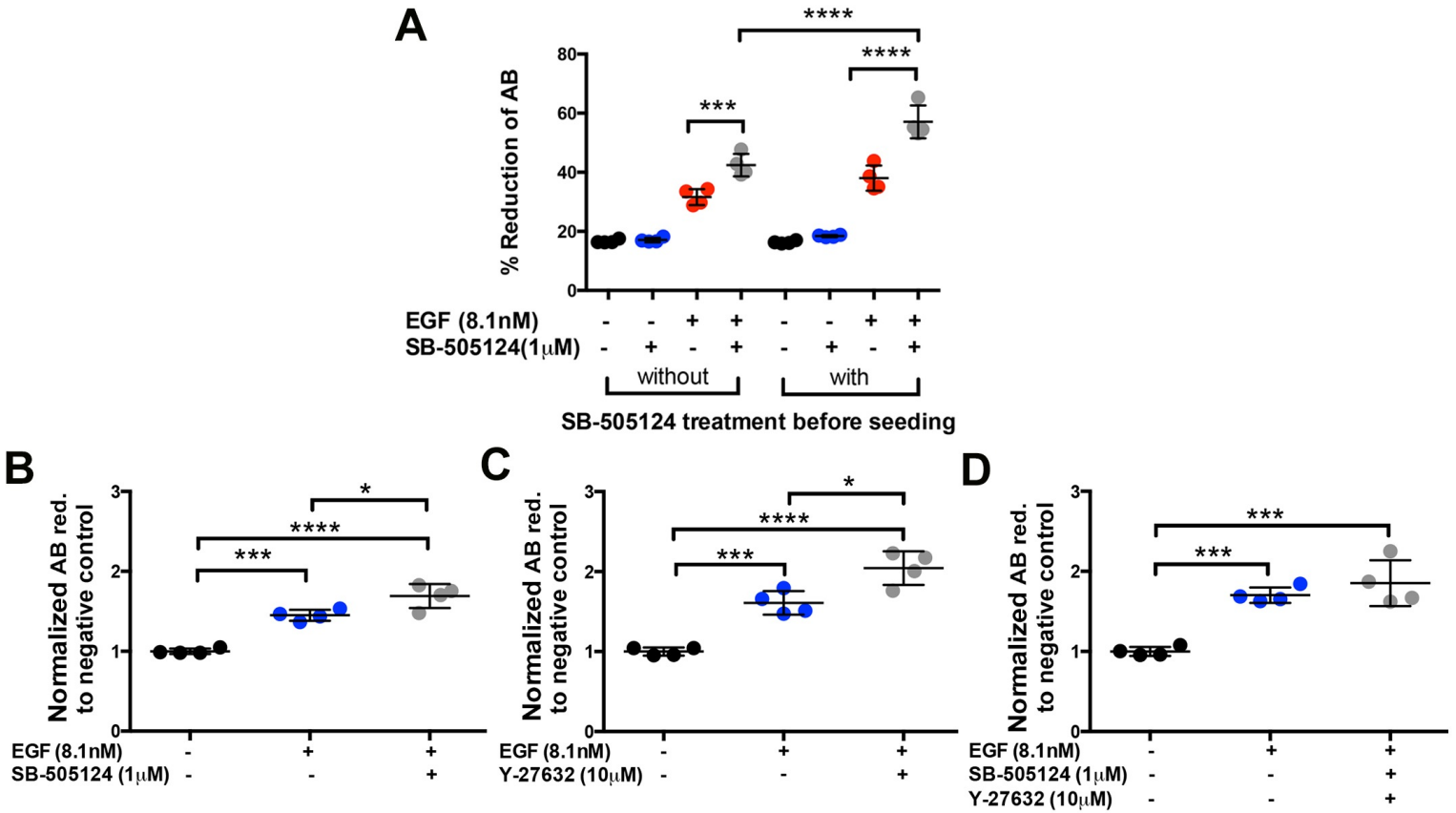

Figure 4.14: **TGF-β inhibitor and Rock inhibitor enhanced the recovery of frozen adenoma.** *Apc*$^{fl/fl}$ adenoma thawed, seeded at a density of 5000 cells/well treated with different inhibitors. AB was added on D4 to measure adenoma growth. (A) SB-505124 (TGF-β inhibitor) treatment before seeding enhanced the growth of adenoma. (B-D) Adenomas treated with SB-505124 (B), Y-27632 (Rock inhibitor) (C), or both (D) before seeding. After seeding adenomas were either supplemented with EGF alone or with EGF and the inhibitor. *, ***, **** indicates $P \leqslant 0.05$, $P \leqslant 0.001$ and $P \leqslant 0.0001$, respectively. Statistical comparisons were done by one-way ANOVA with Tukey's multiple comparison test. Error bars represent ±SD, 4 replicates per condition represented by dots, same sample was used in the experiment. AB red: AB reduction.

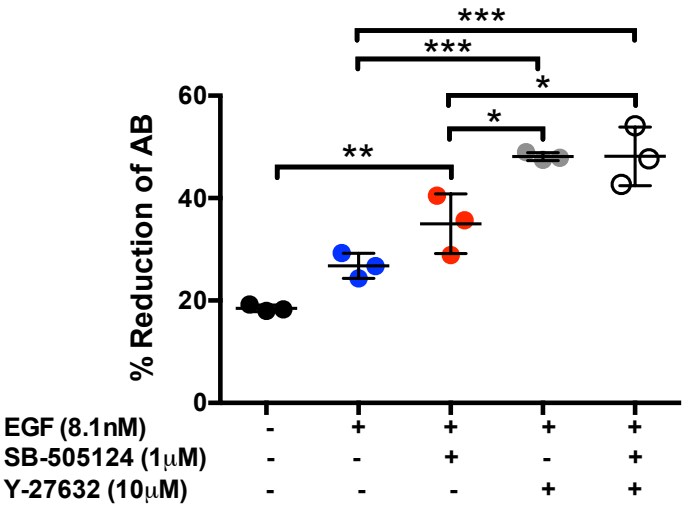

Figure 4.15: **Passage of *Apc*$^{fl/fl}$ adenoma.** *Apc*$^{fl/fl}$ passaged adenoma growth as measured by AB reduction. *, **, *** indicates P$\leqslant$0.05, P$\leqslant$0.01 and P$\leqslant$0.001, respectively. Statistical comparison was done by one-way ANOVA with Tukey's multiple comparison test (3 replicates per condition represnted by dots). Error bars represent $\pm$SD.

4.5 Discussion

A 3D organoid culture system to study intestinal biology was developed by (Sato et al., 2009, 2011). An updated protocol from Professor Owen Sansom, allowed the establishment and expansion of this culture method.

4.5.1 Organoid culture optimisation shows different Noggin requirements

The results from organoid culture -adenoma and crypt- clearly show different requirements for Noggin in primary culture (Figure 4.5 and Figure 4.6 for adenoma and crypt culture, respectively). NAC enhances the number of growing organoids in crypt culture by 1.45 fold. Moreover, while Noggin has an effect on the number and size of growing organoids from crypts, it has no effect on differentiation (Figure 4.6C).

Adenoma culture from *Apc*$^{fl/fl}$*Lgr5-CreERT2* mouse model shows that Noggin is not required for culture. This result was in agreement with Hans Clevers' lab (Sato et al., 2011). They showed that Noggin is not a requirement for adenoma culture from both mouse and human tissue. On the other hand, Noggin is required for primary crypt culture and at passage. This result was not in agreement with the first protocol describing crypt culture, where Noggin was reported to be required at passage but not in the primary culture (Sato et al., 2009). Work presented by the same lab (Sato et al., 2011) reported that ENR is important for murine small intestinal crypt culture along with NAC. NAC, a potent antioxidant, inhibits ROS induced cellular damage and apoptosis (Spagnuolo et al., 2006; Chaudhari et al., 2007). The addition of NAC to the primary crypt culture increased the number of growing organoids but did not change Noggin requirement. The difference in Noggin requirement for crypt culture might be Matrigel batch dependent. It is possible that the second report by the Clevers lab (Sato et al., 2011) was an updated version of the first one (Sato et al., 2009). Moreover, different groups used Noggin in primary crypt culture (Davis et al., 2014) and it is recommended from the Sansom lab's protocol as well.

The formed intestinal organoids from crypts show differentiation into goblet cells, enteroendocrine cells, enterocyte cells and Paneth cells. Crypts deprived of Noggin differentiated normally. Organoid differentiation was in agreement with the first protocol describing the 3D culture system (Sato et al., 2009). Noggin has no effect on differentiation. One possible explanation could be that Noggin is important for crypt expansion. It has been shown *in vivo* that overexpression of Noggin in the villous compartment results in crypt expansion (Haramis et al., 2004). However, in adenoma culture, Noggin withdrawal decreases the Lgr5 expression (Sato et al., 2011), without an effect on growth. Moreover, single cells with high Lgr5-GFP expression were able to grow into organoids (Sato et al., 2009). This might indicate high Wnt/β-catenin signalling as *Lgr5* is a Wnt/β-catenin target gene (Barker et al., 2007). Accordingly, crypts that remain alive when Noggin is not supplemented might be high in Lgr5 and can thus grow and differentiate.

4.5.2 Adenoma formation *in vitro* from conditional crypt culture

Genetic manipulation of conditional intestinal organoids with 4-OHT treatment shows adenoma formation in less than 5 days. Cre-mediated recombination of the *Apc* gene activates the Wnt/β-catenin pathway and provides a survival advantage over the control when deprived of R-spondin1. Adenoma formed from *Apc*$^{fl/fl}$ *Villin-CreERT2* derived crypts but not from the *Apc*$^{fl/fl}$ *Lgr5-CreERT2* crypts. Rosa26-YFP expression in the transformed crypts further confirms the efficiency of recombination (Figure 4.7- 4.9, Figure A.1).

Adenoma formation by genetic manipulation becomes independent of R-spondin1 because the effect of R-spondin1 has been replaced by constitutive activation of the Wnt pathway. Mutation in the *Apc* gene following Cre-mediated recombination results in β-catenin activation. This effect was expected. R-spondin1 is required for crypt culture because it has a potent proliferative effect on intestinal crypt cells *in vivo* (Kim et al., 2005) and enhances the Wnt pathway (De Lau et al., 2012). Mutations in the *Apc* gene also activate the Wnt pathway and allow the formation of benign adenoma *in vivo* (Shibata et al., 1997; Fodde et al., 2001) as mutated Apc protein cannot bind β-catenin for degradation. This allows its

stabilisation and accumulation in the nucleus forming constitutive complexes with Lef/Tcf-4 (Korinek et al., 1997) and upregulating genes involved in tumorigenesis such as c-Myc (Sansom et al., 2004).

Apc gene recombination was detected from D2 onwards in genetically manipulated crypts. However, no recombination of *Apc*$^{fl/fl}$ was detected in the *Lgr5-CreERT2* intestinal crypts. The low percentage of Lgr5 positive cells within the crypts might be the cause of inefficient recombination. *In vivo* studies show that low recombination frequency (<6%) occurs in the Lgr5 compartment and adenoma formed between 3-5 weeks (Barker et al., 2009). High frequency recombination occurs in the *Villin* compartment (Andreu et al., 2005), and mice reached the humane point within 4 days. At that time, mice developed crypt expansion associated with intense proliferation. Moreover, *Villin-CreERT2* organoid were used for intestinal organoids manipulation (Koo et al., 2012; Li et al., 2014). Recently, adenoma formation *in vitro* by genetic manipulation was reported from both *Lgr5-CreERT2* and *Villin-CreERT2* derived organoids (Wiener et al., 2014). One reason for adenoma formation from the *Apc*$^{fl/fl}$*Lgr5-CreERT2* model could be related to the long incubation time with 4-OHT (48h) reported in the study compared to 12h used in my experiments. Consequently, adenoma formed *in vitro* by genetic manipulation within five days post 4-OHT treatment reduces the time needed for these adenoma to be formed *in vivo*. For instance, adenoma formation from the Apc$^{fl/fl}$*lgr5-CreERT2* model takes 3-5 weeks (Barker et al., 2009) (an effect also reported in our *in vivo* adenoma model) and from *Apc*^{Min} model takes at least 150 days (Moser et al., 1993). Moreover, there is no restriction on mice age and weight as for tamoxifen injection in conditional mouse models.

Adenomas with excessive proliferation compared to those restricted to crypt base in the normal intestinal organoids is more evidence of an active Wnt pathway. This excessive proliferation was also reported for adenomas *in vivo* (Sansom et al., 2004; Andreu et al., 2005) and *in vitro* (Sato et al., 2011).

4.5.3 *Apc*$^{fl/fl}$*Lgr5-CreERT2 in vitro* adenoma model optimisation

The results from adenoma culture optimisation show that AB can be used for evaluating adenoma growth (Figure A.2). The results also show an optimisation for freezing adenomas directly after extraction and effectively recovering them after thawing with Y-27632 and SB-505124 inhibitors. Moreover, the optimisation of the passage protocol allows adenomas to re-grow from a single cell (Figure 4.11- 4.15).

4.5.3.1 AlamarBlue: a cell viability assay to measure adenoma growth

DAPI labelling was used to evaluate adenoma growth. This is a simple method. However, it has several disadvantages. In addition to occasional disproportional fluorescence intensity to area, the DAPI method is time consuming, it is expensive and more adenomas are lost during sample preparation. Fluorescence intensity disproportional to adenoma size is solved by taking area for assessment of adenoma growth. However, the loss of adenomas during preparation might hide important differences in adenoma growth. Evaluating adenoma growth is crucial to the project, and the time consuming nature of the method will restrict experiments. Thus, there was need for a high throughput method with a simple, less expensive protocol. AB was a good alternative and has several advantages. For instance, it is a simple to implement, high throughput method that allows different replicates with several conditions to be examined within the same experiment. Moreover, it is water soluble and non-toxic (Rampersad, 2012). It can be used for time-course experiments (Rampersad, 2012), which is important to determine the best time for measurement from the same experiment when dealing with such a difficult culture system. The AB method is relatively inexpensive as the amount of Matrigel used was a quarter of that used in the DAPI method. Application of AB in adenoma culture allowed several optimisations to take place.

4.5.3.2 Adenoma storage and passage

Although the work presented by Clevers and co-workers for the 3D culture system was clearly presented and the results show it is reproducible (Figure 4.11), optimisation was needed. The results show improvement in freezing after extraction and passaging to re-plate the adenomas from a single cell (Figure 4.14, 4.15).

Growing adenomas can be stored effectively according to (Sato et al., 2011). The disadvantages of preserving growing adenomas were related to the need for adenoma growth before storage. Furthermore, lots of adenomas were needed for recovery in order to perform an experiment. Preserving adenomas according to the protocol presented in this chapter using 50% FCS, 40% ADF2, and 10% DMSO has several advantages. First, there is no need to grow the adenomas before storage making it cost effective. Second, extracted adenomas can be frozen in multiple aliquots, consequently decreasing the number of experimental mice and saving time.

The recovery of the freshly obtained cryopreserved samples was very difficult. However, successful and reproducible recovery was shown from other cultures in the lab. The idea of using SB-505124 for the recovery of cryopreserved adenomas came from my work with TGF-β1 and its effect on adenoma growth (more details in chapter 5). In brief, adenomas were not able to grow if supplemented with TGF-β1 on the day of culture. TGF-β1 has an IC50 of 2.7pM when added to adenomas on D1 and 24.0pM when added to D2 adenomas. Latent TGF-β is a component of growth factor reduced Matrigel (1.7ng ml^{-1}). It could be activated via different activator, for example, after binding of the cells to the extracellular matrix, integrin binding, ROS, proteases or low pH (Annes et al., 2003; Hyytiäinen et al., 2004). Within half an hour of TGF-β stimulation, Smad4 and p-Smad2, 3 accumulate in the nucleus (Pierreux et al., 2000). Cell cycle arrest genes and apoptotic genes are among the earliest upregulated genes in response to TGF-β (Levy and Hill, 2005). These steps in adenoma culture take more than half an hour from seeding to polymerisation of Matrigel. Therefore, cell cycle arrest genes might be upregulated and adenoma might be dying be-

fore overlaying with ADF2.

Another correlation was the viability of thawed adenomas. Less viable cells were recovered after freezing when compared to fresh adenomas. This suggests that the difficulty in recovering adenomas after thawing might be related to decrease in viability and increase in apoptosis. For that, a Rock inhibitor, Y-27632, was added. Y-27632 enhances recovery even more if cells are incubated with it directly after thawing. Y-27632 is reported to be important for growth and recovery of frozen human hESc (Heng et al., 2006). Apoptosis is reported to be the mechanism of cell death of cryopreserved hESc cells during freeze-thaw cycles (Heng et al., 2006). Rock inhibitors including Y-27632 have an anti-apoptotic effect and enhance cell recovery after thawing of hESc (Claassen et al., 2009; Martin-Ibanez et al., 2008). Furthermore, Y-27632 enhanced the survival and growth of hESc following dissociation (Watanabe et al., 2007). In intestinal organoid culture, Y-27632 is used following cell sorting to prevent cell death (Sato et al., 2009, 2011). Y-27632 enhanced recovery of the cryopreserved adenoma could be because of the inhibition of apoptosis. Thus, it is crucial to incubate the cryopreserved adenomas with Y-27632 and SB-505124 directly after washing and before seeding.

Passaging organoids is achieved by mechanical pipetting, however, this method has some drawbacks. The presence of some remaining Matrigel along with dead cells from the previous culture interfere with subsequent immunolabelling. Moreover, if *in vitro* manipulation is to be carried out using viruses, the presence of Matrigel may prevent virus delivery to the adenomas. Moreover, mechanical pipetting leaves adenomas in large aggregates. Adenomas dissociated into large aggregates leads to non-uniform culture and thus, not suitable for adenoma growth assessment. The work presented in this chapter allows passaging organoids and re-plating adenomas from single cells, providing pure, uniform culture for growth assays and subsequent functional analysis. Moreover, adenoma manipulation with viruses has been achieved.

The addition of Y-27632 and SB-505124 to passaged adenomas after seeding was enough

for adenoma recovery. While the optimisation work was being completed in our lab, a second group published work that allows the expansion and genetic manipulation of organoid culture (Miyoshi and Stappenbeck, 2013). This work showed some agreement with the optimisation steps presented in this chapter. For instance, similar to our optimisation they used Y-27632 and SB-431542 (another TGF-β inhibitor) in the first 2-3 days of primary culture, after which these inhibitors are no longer required. While I used EDTA-PBS to dissove Matrigel and TryplE Express to dissociate the organoids, they only wash the culture with EDTA-PBS and used trypsin-EDTA to dissociate intestinal organoids. Timing was different, they used 2-5 minutes and I used 10-15 minutes. Our aim from the passage was to have a single cell while they were aiming for cell aggregates. I have used TryplE Express which is recombinant protein and more gentle on the organoids compared to trypsin (after optimising the primary extraction step). Moreover, I used Y-27632 and SB-505124 at passage but they did not. For freezing growing organoids they used 10% DMSO with 80% ADF2 and 10%FCS (Miyoshi and Stappenbeck, 2013), and in my optimisation protocol I used 10% DMSO with 90% ADF2.

This chapter aimed to optimise organoid (crypt and adenoma) culture and genetically manipulate conditional crypts using *Apc*$^{fl/fl}$*Lgr5-CreERT2* and *Apc*$^{fl/fl}$*Villin-CreERT2*. The results show that intestinal organoids can be genetically manipulated and adenoma can be formed within 5 days. Adenomas can also be stored and passaged. Given the aim of the culture is to dissect the molecular consequences of Smad4 loss of function in intestinal adenomas, the questions to be answered in the following chapter are: can we genetically manipulate *Apc*$^{fl/fl}$*Smad4*$^{fl/fl}$*Villin-CreERT2* intestinal crypt culture? Can we culture *Apc*$^{fl/fl}$*Smad4*$^{fl/fl}$*Lgr5-CreERT2* adenomas? What is the effect of TGF-β1 on Smad4 disrupted adenomas?

Chapter 5

TGF-β/Smad4 signalling

5.1 Introduction

TGF-β acts as a tumour suppressor and in a context dependent manner it acts as tumour promoter (Inman, 2011; Massagué, 2012). TGF-β has a tumour suppressor effect on pre-malignant lesions and triggers apoptosis (Massagué, 2012). In the context of intestinal tumorigenesis and pancreatic cancer, when tumour cells incur mutations in the TGF-β pathway such as mutations in *SMAD4*, TGF-βR1 or TGF-βR2, they become resistant to the tumour suppressor effect of TGF-β. These tumour cells escape the cytostatic and apoptotic effects of TGF-β, escape immune surveillance, and acquire an epithelial-mesenchymal (EMT) phenotype. Howerever, in the context of breast cancer, glioma and melanoma, in the presence of different driver mutations in *c-MYC* and *CDNK1A* with functional TGF-β pathway, the tumour cells respond to increased TGF-β production (either from tumour cells and/or microenvironment) and promote metastasis (Massagué, 2012). Disruption of Smad4 was previously thought to completely abolish TGF-β responses (Zhou et al., 1998). Afterwards, different studies showed that the response to TGF-β may be both Smad4 dependent or Smad4 independent (Sirard et al., 2000; Kretschmer et al., 2003; Levy and Hill, 2005; Deckers et al., 2006; Zhao et al., 2008; Zhang et al., 2010).

The effect of Smad4 mutations on TGF-β function is variable among different studies. The role of Smad4 and whether it is required for the switch from TGF-β tumour suppressor to tumour promoter remains poorly understood. The discrepancies could be because the studies were carried out in different contexts with different cell lines such as fibroblasts,

HaCaT cells, pancreatic or CRC cells being investigated. The role of Smad4 was studied either by knockdown or overexpression experiments in 2D culture systems. The question is: what are the molecular consequences of Smad4 loss of function in a purely genetic model and in the setting of active Wnt signalling when a culture system that mimics *in vivo* tissue architecture is used? Understanding this and how the switch from TGF-β tumour suppressor function to tumour promoter and the contribution of Smad4 to this process is critical for therapeutic manipulation.

5.1.1 TGF-β tumour suppressor effect

TGF-β cytostatic effect and inhibition of the cell cycle at G1 phase is dependent on repression of c-Myc and the mobiliztation of cyclin-dependent kinase (CDK) (Massagué, 2008). The repression of *c-Myc* by TGF-β is an early response and occurs within 1h of TGF-β1 stimulation. It is mediated by the binding of E2F4/5-Smad3-Smad4 complex with the retinoblastoma (RB) family member, p107, in MO-91 human AML cells (Chen et al., 2002) and with the transcription factor C/EBP in HaCaT cells (Gomis et al., 2006) to the proximal promoters of c-Myc. c-Myc represses the expression of cell cycle inhibitors, $p15^{INK4b}$ and $p21^{CIP1}$ (Heldin and Moustakas, 2012). In response to TGF-β1, Smads repress *c-Myc* first, consequently, the cell cycle inhibitors can be overexpressed and then further induced in a sustained manner by Smad signalling (Heldin and Moustakas, 2012). For example, $p15^{INK4b}$, is induced by a FoxO-Smad3/Smad4 complex and the transcription factor C/EBP in HaCaT cells (Gomis et al., 2006) and FoxO-Smad3/Smad4 induces expression of $p21^{CIP1}$ in U87MG glioblastoma cells (Seoane et al., 2004). $p57^{KIP2}$ is induced in acute myelogenous leukemia (AML) -MO-91- derived cells (Scandura et al., 2004) and $p27^{KIP1}$ in prostate epithelial cells (Ling et al., 2002) in response to TGF-β1.

The role of Smad4 in growth arrest induced by TGF-β1 in epithelial cells was contradictory between different studies. Growth inhibition was Smad4 independent when Smad4 was knocked down using the stable RNA interference (RNAi) method in the pancreatic cancer cell line, PANC (Jazag et al., 2005). Smad4 independent growth inhibition was reported in

NIH3T3 Smad4 deficient fibroblasts, both Smad4 null cells and their control have similar IC50 (Sirard et al., 2000). However, growth inhibition was Smad4 dependent in HaCaT and Colo-375 pancreatic cancer cell lines after siRNA knockdown of Smad4 (Levy and Hill, 2005). The effect was expected to be related to the downregulation of *Gadd45b* and *Akap12* in Smad4 null cells (Levy and Hill, 2005). A partial effect of Smad4 on growth inhibition has been reported in HaCaT cells when Smad4 was knocked down using GeneBlocs antisense molecules, and might be related to the partial reduction of $p15^{INK4B}$ expression (Kretschmer et al., 2003). Smad3 was the predominant mediator of growth arrest in these cells since its knockdown reduced TGF-β1 induced expression of $p21^{CIP1}$ and completely reversed RB dephosphorylation (Kretschmer et al., 2003).

Growth arrest in epithelial cells by TGF-β1 is also mediated by the suppression of the inhibitor of DNA binding family members- ID1, ID2, and ID3. Repression of ID1 is associated with upregulation of $p27^{KIP1}$ and $p21^{CIP1}$ and occurs within 72h of treatment in prostate epithelial cells (Ling et al., 2002). It is well known that ID1 is an early response gene induced in response to BMP pathway activation (Hollnagel et al., 1999), a process dependent on Smad4-Smad1-Smad5 since the human epithelial cells -MDA-MB468 (Smad4 deficient) were not able to induce *ID1* in response to BMP6. Co-expression of Smad4 in this cell line restored the BMP6 activation of Id1-Luc reporter (Korchynskyi and ten Dijke, 2002). It has been reported that ID1 is also an early TGF-β1 response gene mediated by Smad3-Smad4 complexes. It is overexpressed within 1-1.5h TGF-β1 treatment in MCF10A, HaCaT and HeLa cells, however, the overexpression is transient and reaches below the basal level within 4h of stimulation either by degradation or repression (Liang et al., 2009). ID1 repression is secondary to the upregulation of activating transcription factor 3 (ATF3) (Lasorella et al., 2014) or secondary to the upregulation of $p27^{KIP1}$ and $p21^{CIP1}$ (Ling et al., 2002). Similar to ID1, ID2 and ID3 are early transient responsive TGF-β genes involved in growth inhibition (Kowanetz et al., 2004). Their downregulation is secondary to the early response effect of TGF-β1 (Massagué et al., 2005).

TGF-β apoptotic effect is mediated by changes in the expression of pro-apoptotic and

anti-apoptotic proteins and caspase activation (Siegel and Massagué, 2003). The ROS produced after TGF-β1 stimulation helps in the induction of apoptosis (Ramjaun et al., 2007). TGF-β1 upregulates the pro-apoptotic genes -*Bmf* and *Bim*-, *Tnfrsf5*, *Trib3*, *Polb*, *Hsp70-1* and *Ddit3* (Ramjaun et al., 2007). Suppression of Suvivin -in response to TGF-β1 in NRP-154 prostate cancer cells has been reported to be mediated through Smad3/2 recruitment of RB/E2F4 to the *Survivin* promoter (Yang et al., 2008). Silencing of Smad2 or Smad3 using short-hairpins leaving an intact Smad4 has a partial effect on the suppression and total inhibition was achieved when both genes were silenced together (Yang et al., 2008). In intestinal organoids TGF-β1 induced apoptosis is mediated by the upregulation of *Bim* and suppression of *Survivin* by upregulation of the p38 MAP kinase pathway (Wiener et al., 2014). The stress and cytokine inducible proteins *Gadd45b* and *Gadd45a* inhibit cell growth and induce apoptosis in response to TGF-β1 (Yoo et al., 2003; Li et al., 2015).

5.1.2 TGF-β tumour promoter effect

While inducing growth arrest and promoting apoptosis are TGF-β tumour suppressor effects, TGF-β can also promote tumorigenesis. TGF-β stimulates tumorigenesis by induction of EMT (Massagué, 2012; Heldin et al., 2012). TGF-β also affects the microenvironment in order to promote tumorigenesis. These effects include suppression of immune surveillance, angiogenesis and recruitment of inflammatory cells which secrete several cytokines that act on the tumour cells (Heldin et al., 2012).

EMT is a process where by epithelial cells lose their tight junctions and apical-basal polarity, reorganise their cytoskeleton become motile with spindle-shaped morphology in order to invade. During EMT cells acquire stem cell properties and become resistant to apoptosis (Thiery et al., 2009; Lamouille et al., 2014). In EMT there is downregulation of epithelial markers such as E-cadherin, and upregulation of mesenchymal components such as fibronectin, α-smooth muscle actin and vimentin (Klymkowsky and Savagner, 2009; Ikushima and Miyazono, 2010; Lamouille et al., 2014). Neural cadherin (N-cadherin) is another mesenchymal marker that balances E-cadherin loss in a process known as cadherin

switch (Wheelock et al., 2008). This switch allows tumour cells to gain the ability to activate growth factor receptor pathways to enhance cell growth, motility and invasion (De Wever et al., 2004; Wheelock et al., 2008).

A necessary step for invasion, but not sufficient for EMT, is loss of E-cadherin function and an increase in nuclear β-catenin levels (Fodde et al., 2001; Chiang and Massagué, 2008; Sleeman and Thiery, 2011). E-cadherin is considered a tumour suppressor gene (Larue and Bellacosa, 2005). Loss of E-cadherin function during tumour progression is thought to be the result of transcriptional repression (Peinado et al., 2007), promoter hypermethylation or production of defective protein (Larue and Bellacosa, 2005). Several EMT regulators repress transcription of E-cadherin and lead to anoikis suppression, both of which contribute to metastasis (Huber et al., 2005; Smit et al., 2009). TGF-β/ Smad pathway induces the expression of the *high mobility group A2 (Hmga2)* gene that induces the expression of the zinc-finger transcription factor Snail family (Snail and Slug), and the basic helix-loop-helix (bHLH) factor Twist (Thuault et al., 2006; Peinado et al., 2007). ZEB family, zinc finger TF, also regulates EMT (Peinado et al., 2007). In addition to TGFβ in the tumour microenvironment, hypoxia could participate in the expression and function of these repressor proteins (Peinado et al., 2007). Snail family binds to the E-box of E-cadherin promoter and suppresses its transcription (Nieto, 2002). Snail is stimulated via different pathway such as TGF-β (Nieto, 2002; Thuault et al., 2006), Wnt/β-catenin (Heuberger and Birchmeier, 2010), BMP and FGF signaling (Nieto, 2002). In colon carcinoma cells, Snail is stimulated via integrin-linked kinase (ILK)-dependent pathway (Nieto, 2002) which is activated by the Akt pathway (Larue and Bellacosa, 2005). Snail is an EMT regulator associated with poor cancer prognosis, it represses anoikis and represses epithelial markers such as E-cadherin and claudins (Stemmer et al., 2008; Smit et al., 2009). It has been reported that Snail1 when combined with SMAD3/4, acts as co-repressors for the promoter of the tight junction cell adhesion molecules Coxsackie- and adenovirus receptor (CAR), occludin, claudin-3 and E-cadherin (Vincent et al., 2009). This complex enhances EMT *in vitro* in different cell lines and *in vivo* in a mouse model for breast cancer (Vincent et al., 2009). Snail can protect tumour cells from cell death, as it acts as a survival factor in response to tumour

necrosis factor-α (Tnf-α) as seen in neural crest cells (Peinado et al., 2007). ZEB, Slug and Twist also downregulate E-cadherin expression. The expression of ZEB1 TF was seen in colorectal tumours, it represses E-cadherin in the absence of SNAIL1 (Peinado et al., 2007).

The requirement for Smad4 in TGF-β1 induced EMT was variable between different studies. EMT is Smad4 dependent in keratinocytes and NMnMG cells (Deckers et al., 2006; Valcourt et al., 2005). EMT is Smad4 independent in different pancreatic cells and HaCaT (Zhao et al., 2008; Levy and Hill, 2005). Motility and migration are another feature of EMT. Whether Smad4 is required for them or not is also controversial. Smad4 expression in SW480 and SW620 CRC cells and HaCaT cells prevent TGF-β1 induced motility (Pohl et al., 2010; Zhang et al., 2010; Kretschmer et al., 2003). Motility is inhibited in Colo-375 and HaCaT cells with Smad4 knockdown. Such inhibition is related to the repression of the TGF-β target gene *PAL-1* (Levy and Hill, 2005).

5.2 Rationale for the study

The *in vivo* phenotype result with better survival and reduced small intestinal tumour burden together with a large caecal tumour in the *Apc*$^{fl/fl}$*Smad4*$^{fl/fl}$ mouse model was exciting. The aims of this chapter are:

1. To understand the molecular mechanisms underpinning this phenotype after finding the suitable *in vitro* culture method

2. To evaluate the effect of TGF-β1 on early stages of adenoma formation and at late stages when the TGF-β pathway is downregulated due to Smad4 knockout

5.3 Materials and methods

5.3.1 Mouse models

Mouse models used in this chapter were listed in Table 2.1 with the exception of *Igf2r*^{I1565A} mouse model.

5.3.2 Mouse breeding

The breeding strategy and the generated genotypes was described in section 2.1.3.1 and 2.1.3.3.

5.3.3 Genotyping

As described in section 2.2, all animals were identified by genotyping postnatally and PM for experimental mice for further confirmation of the genotype. Genotyping was also performed for organoids in culture.

5.3.4 Mouse dissection and tissue collection

Mouse dissection was described in section 2.1.5. Tissue collection for adenoma and crypt culture was described in section 2.1.6.1 and 2.1.6.2.

5.3.5 Adenoma culture

Adenoma culture was detailed in section 2.5 and summarised in Figure 4.1 and 4.2.

5.3.6 Crypt culture and genetic manipulation

Crypt culture was detailed in section 2.6 and summarised in Figure 4.3.

5.3.7 Immunolabelling

Characterisation of organoids was described in section 2.7.2.

5.3.8 Growth and proliferation assay

Adenoma growth was assessed as described in section 2.7.4 and in section 2.8.

5.3.9 Image acquisition

Image acquisition and analysis was described in 2.7.6.

5.4 Results

5.4.1 Cultured adenoma and genetically manipulated intestinal organoids lack *Smad4*

Once both culture systems (intestinal adenoma and crypt) were established with the *Apc*$^{fl/fl}$ model, the question arose as to which was the most suitable to proceed with in order to better understand the molecular consequences of *Smad4* disruption on intestinal tumorigenesis. Recombination of *Smad4* was achieved in both culture systems as shown by PCR in Figure 5.1A, B. Recombination of *Smad4* with a PCR product of 512bp was obtained in both the *Lgr5-CreERT2* (Figure 5.1A, lower gel, lane 9-14) and *Villin-CreERT2* (Figure 5.1B, lower gel, lane 8, 11) models. Whilst there was no recombination of *Smad4* in the *Smad4*$^{+/+}$ adenomas (Figure 5.1A, lower gel, lane 4-8) compared to the recombination in *Smad4*$^{fl/fl}$ adenomas (Figure 5.1A, lower gel, lane 9-15), *Apc*$^{fl/fl}$ was recombined in all adenomas (Figure 5.1A, upper gel, lane 4-15). Similarly, *Apc*$^{fl/fl}$ was recombined in both manipulated organoids with the *Villin-CreERT2* model (Figure 5.1B, both gels, lane 2, 5) when treated with 4-OHT, and *Smad4* was recombined only in *Smad4*$^{fl/fl}$ manipulated organoids with 4-OHT (Figure 5.1B, lower gel, lane 8, 11). Both the *Apc*$^{fl/fl}$ gene and *Smad4*$^{fl/fl}$ gene were recombined at the same time and were detected as early as D2 post treatment. Recombination of *Smad4*$^{fl/fl}$ was further confirmed by DNA-sequencing. Intact

Smad4$^{fl/fl}$ allele has 2 loxP sites flanking exon 2, with one loxP site on recombination (Figure 5.1C, lower diagram). One loxP site was detected by DNA-sequencing in the *Smad4*$^{fl/fl}$ adenomas and no loxP sites were detected in *Smad4*$^{+/+}$ (Figure 5.1D, DNA was from *Lgr5-CreERT2* adenoma model). This indicates that *Smad4*$^{fl/fl}$ adenomas had the recombined gene. Rosa26-YFP was expressed in *Apc*$^{fl/fl}$*Smad4*$^{fl/fl}$*Villin-CreERT2* manipulated intestinal organoids, and the expression was maintained in the passaged organoids indicating that formed adenomas originated from the manipulated crypts (Figure 5.1E).

5.4.1.1 *Lgr5-CreERT2* and *Villin-CreERT2* adenoma characterisation

Characterisation of the adenoma from both *Lgr5-CreERT2* and *Villin-CreERT2* by immunofluorescence showed membrane bound E-cadherin. Most of the adenomas were undifferentiated. Some adenomas had cells labelled with Muc2. The proportion of these adenomas varied significantly between *Apc*$^{fl/fl}$*Smad4*$^{fl/fl}$*Lgr5-CreERT2* adenomas compared to *Apc*$^{fl/fl}$*Smad4*$^{+/+}$*Lgr5-CreERT2* adenomas (p=0.0015) (Figure 5.2B-E) (the exact percentage of positive cells within the adenomas was not calculated). Some cells within the adenomas were positive for lysozyme labelling (Paneth cell marker) with no difference between different genotypes. Enteroendocrine cells were very rare in all the adenomas (Chromogranin A labelling) (Figure 5.2). Adenomas incorporated EdU in similar proportions after 2h in the different genotypes and in the different models. Around half the cells within an adenoma were in S phase (Figure 5.3).

Results up to this point showed that *Apc*$^{fl/fl}$*Smad4*$^{fl/fl}$*Lgr5-CreERT2* can be cultured and *Smad4* knockout achieved by *in vitro* genetic manipulation of conditional intestinal organoids. Adenomas with *Smad4* knockout were similar in terms of morphology, proliferation, and differentiation in both models. Given the aim of this chapter was to find a suitable model to understand the molecular consequences of *Smad4* knockout in adenomas, with the preference to work with cells that match the *in vivo* phenotype (section 3.4.1.1), I continued with *Apc*$^{fl/fl}$*Smad4*$^{fl/fl}$*Lgr5-CreERT2* adenoma culture.

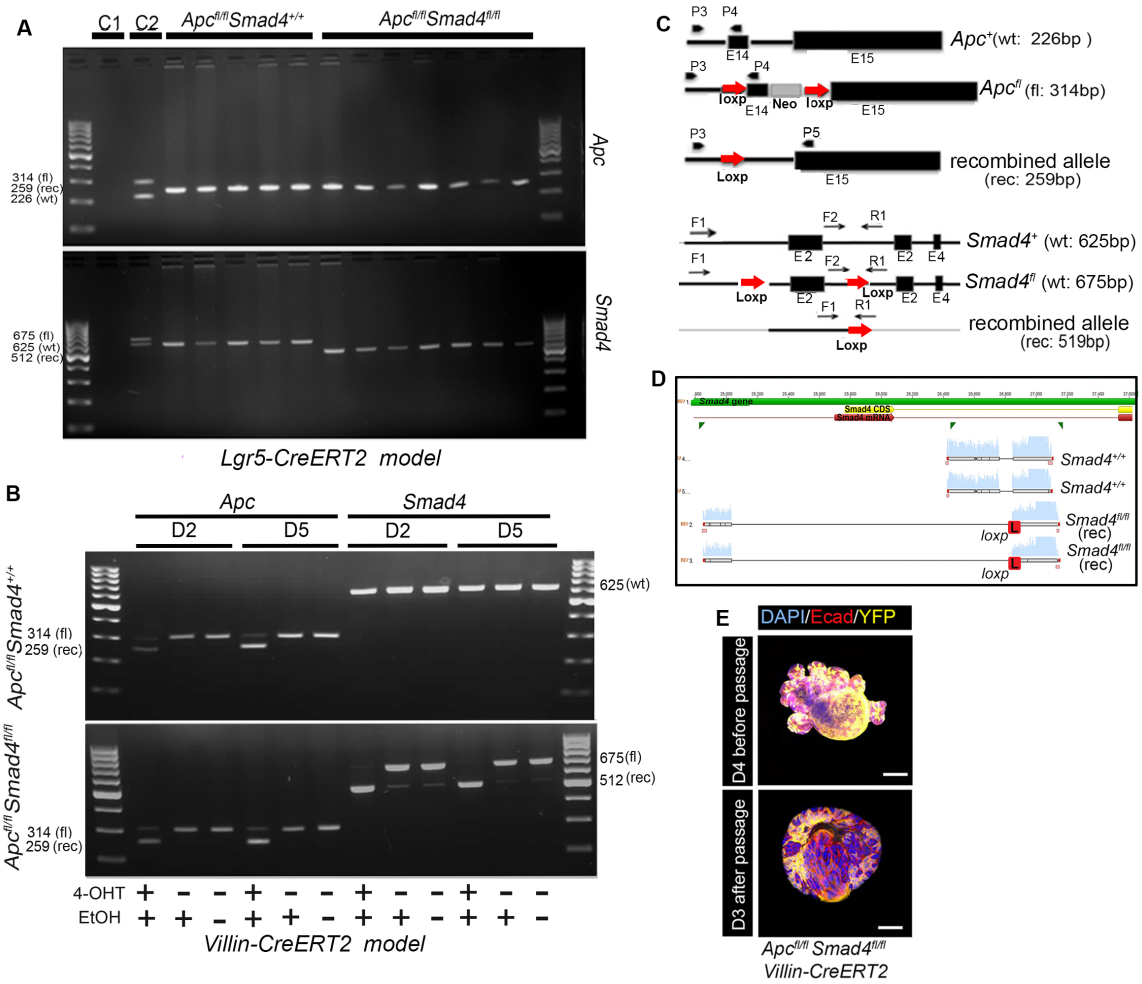

Figure 5.1: **Cultured adenoma and genetically manipulated intestinal organoids lack *Smad4*.** (A) *Apc* (upper gel) and *Smad4* (Lower gel) PCR show recombination of *Apc* and *Smad4* in adenoma culture from *Apc Smad4 Lgr5-Cre* adenoma model (*in vivo* formed). Controls, C1: Negative control (no DNA), C2: $Apc^{fl/+}$ mouse ear-clip (upper gel) and $Smad4^{fl/+}$ mouse ear-clip (lower gel). (B) PCR products show recombination of *Apc* (left side of both gels, lane 2, 5) and *Smad4* (right side lower gel, lane 8, 11) in *Apc Smad4 Villin-CreERT2* adenoma model (genetically manipulated *in vitro* formed) on D2 and D5 post 4-OHT treatment (n=2 with similar results). (C) Diagram showing the recombination of the *Apc* and *Smad4* genes and the PCR strategy. P3: *Apc* forward primer. P4, P5: *Apc* reverse primers. F1, F2: *Smad4* forward primers. R1: *Smad4* reverse primer. (D) Confirmation of *Smad4* recombination by DNA sequence. (E) Confocal images showing the expression of Rosa26-YFP post 4-OHT treatment in the $Apc^{fl/fl}$ $Smad4^{fl/fl}$ *Villin-CreERT2* manipulated organoids. Scale bars 50µm.

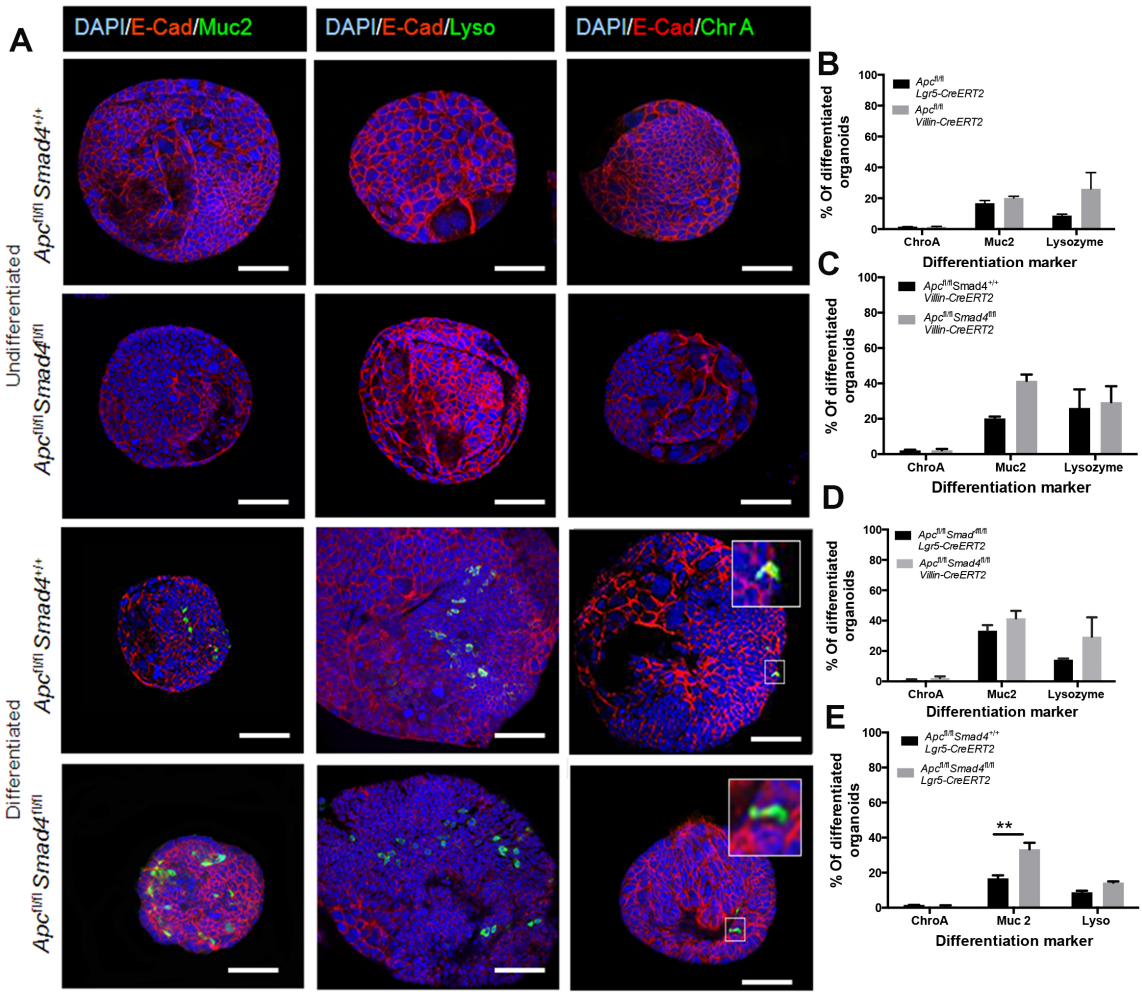

Figure 5.2: **Upregulation of Muc2 in *Apc*$^{fl/fl}$*Smad4*$^{fl/fl}$*Lgr5-CreERT2* adenomas**. (A) Representative confocal images showing undifferentiated (upper two panels) and differentiated (lower two panels) adenomas. Small white box in the adenoma is magnified at the top corner of the marked adenoma. Scale bars 50µm. (B) Adenomas were labelled with Muc2, Chromogranin A (Chro A) and Lysozyme. Cells labelled positively with these markers were counted with a fluorescent microscope from 3 replicates per genotype and presented as percentage of organoids having differentiation markers to the total organoids in the labelled slide (**p=0.0015). Statistical analysis was determined using two-way ANOVA followed by Sidak's multiple comparison test.

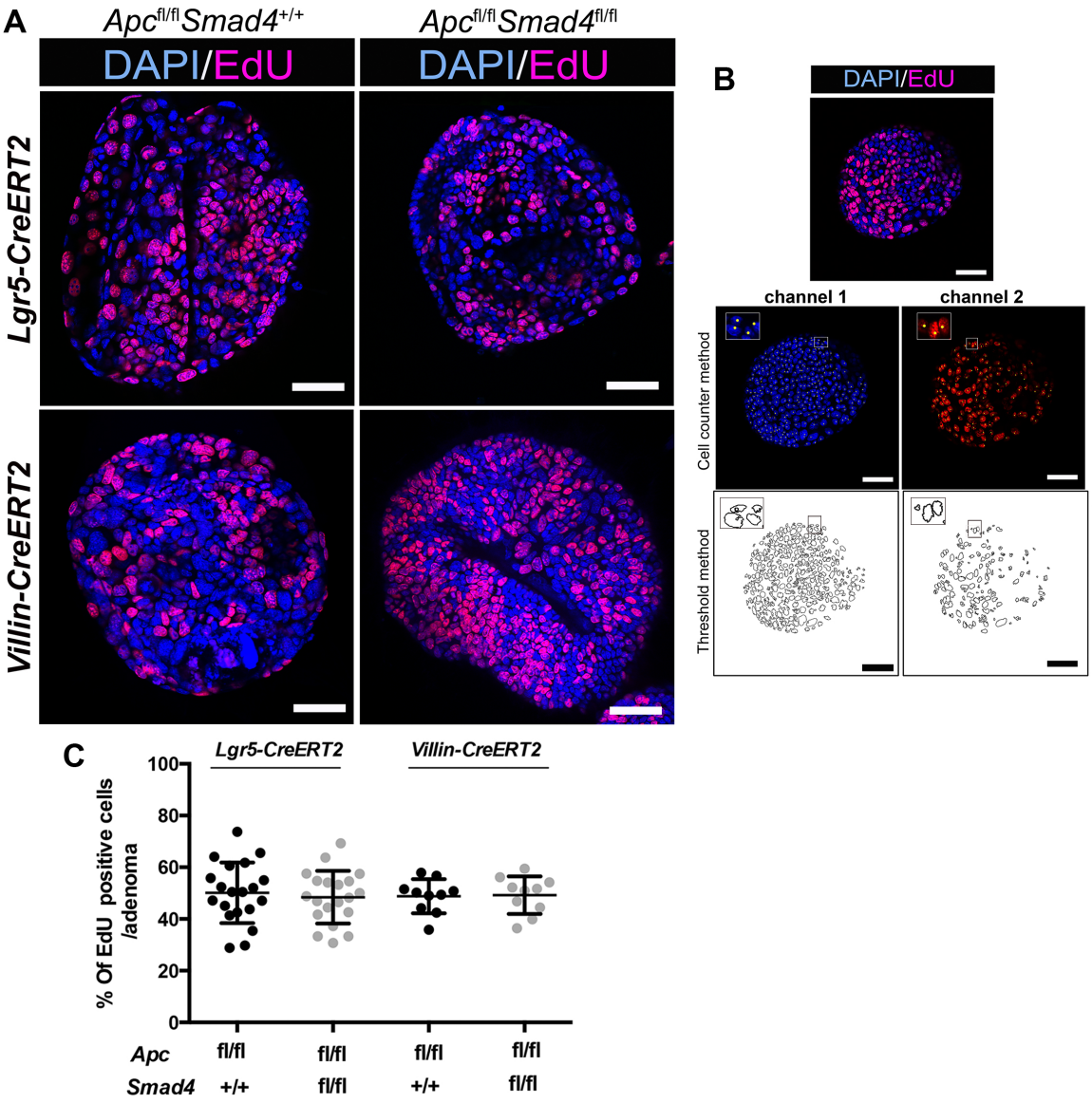

Figure 5.3: **Similar proportion of EdU incorporation in the different adenoma models.** Adenomas on D5 were incubated with EdU for 2h. (A) Representative confocal images show EdU incorporation in *Apc*$^{fl/fl}$*Smad4*$^{+/+}$ and *Apc*$^{fl/fl}$*Smad4*$^{fl/fl}$ in both the *Lgr5-CreERT2* and the *Villin-CreERT2* adenoma models. Scale bars 50µm. (B) Confocal images were analysed and quantified by ImageJ after the split into channels. Upper panel represents the outcome of cell counting using the cell counter plugins in ImageJ. Similar values were achieved using threshold adjustment (lower panel) which was applied subsequently. The boxes are magnified at the top left corner of each individual image. Scale bars 50µm. (C) No significant difference in EdU incorporation between the adenomas. Each dot represents the count of EdU positive cells in one adenoma. Error bars represent ±SD. Statistical analysis was performed with one-way ANOVA followed by Tukey's multiple comparison test.

5.4.2 Slow growth of *Apc*$^{fl/fl}$*Smad4*$^{fl/fl}$ adenomas

With the reduced small intestinal tumour burden and better survival of the *Apc*$^{fl/fl}$*Smad4*$^{fl/fl}$ (*Smad4*$^{fl/fl}$) mouse model, one could hypothesise that their growth *in vitro* might differ from the control. Accordingly, the first question to be addressed by adenoma culture was that of growth. 3D *in vitro* culture showed that *Smad4*$^{fl/fl}$ adenomas had slow growth compared to *Apc*$^{fl/fl}$*Smad4*$^{+/+}$ (*Smad4*$^{+/+}$) adenomas as measured by adenoma area from D2-D7. As shown in the previous chapter, Noggin was required for crypt culture. Smad4 -a central component of the BMP pathway- is mutated in these adenomas, so there was a possibility that the growth is Noggin dependent. To test this hypothesis, the effect of Noggin (with 10 fold difference) on adenoma growth was performed. Noggin had no effect on adenoma growth as measured by area (Figure 5.4A). One step in adenoma culture optimisation (chapter 4, Figure 4.10) was the enzymes used for adenoma extraction. As the growth up to this point was evaluated from trypsin extracted adenomas, it was logical to evaluate adenoma growth when extracted with TryplE Express. This enzyme is a recombinant protein that replaces trypsin and protects the cell's surface proteins. TryplE Express used in extraction did not improve the slow growth of *Smad4*$^{fl/fl}$ adenoma, moreover, the growth was also Noggin independent (Figure 5.4B). The mean of viable adenoma cells after extraction was 89.3% and 90.2% for *Smad4*$^{+/+}$ (n=15) and *Smad4*$^{fl/fl}$ (n=10), respectively. In terms of adenoma appearance in 3D culture, both adenomas appeared similar in Matrigel (Figure 5.4C). Taken together, *Smad4*$^{fl/fl}$ adenomas tend to have a slow growth as verified by adenoma area and AB reduction. The slow growth was neither Noggin dependent nor related to the extraction enzyme.

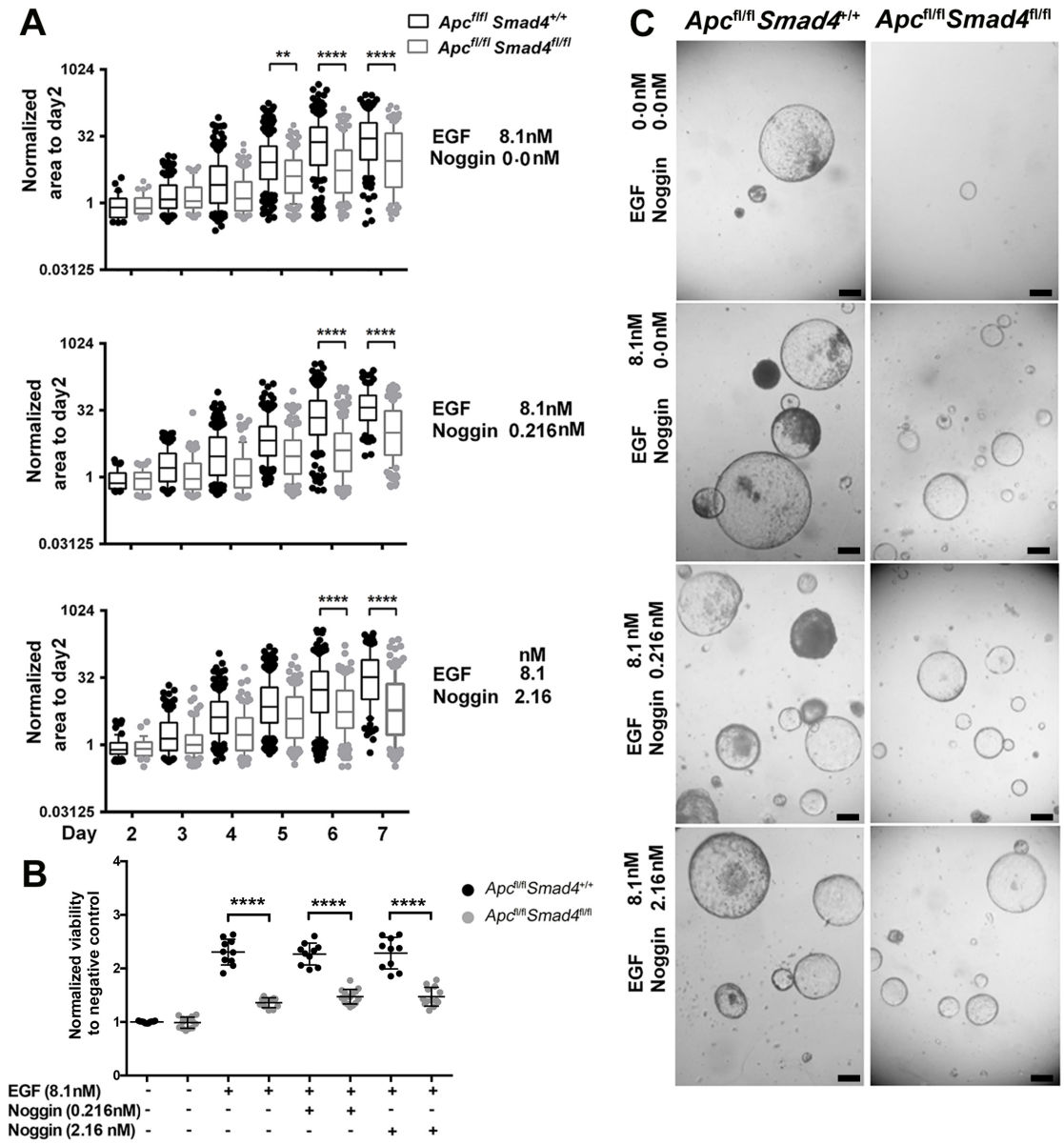

Figure 5.4: **Slow growth of *Apc*$^{fl/fl}$*Smad4*$^{fl/fl}$ adenoma that is Noggin independent**. *Apc*$^{fl/fl}$*Smad4*$^{+/+}$ and *Apc*$^{fl/fl}$*Smad4*$^{fl/fl}$ adenoma growth was examined using 10 fold difference in Noggin concentration (0.216-2.16nM). (A) Growth rate as measured by area normalized to D2. Adenomas in these experiments were extracted by Trypsin (n=3 mice/group, 50 adenoma each. Scale in the y-axis is Log_2, whiskers represent 10-90 percentile). Statistical comparison was done using one-way ANOVA followed by Sidak's multiple comparison test. **, **** indicates $P \leqslant 0.01$ and $P \leqslant 0.0001$, respectively. (B) Adenoma growth as measured by AB reduction and normalized to the negative control. Adenomas were extracted by TrypIE Express. (n=2 mice with *Apc*$^{fl/fl}$*Smad4*$^{+/+}$ and n=3 mice with *Apc*$^{fl/fl}$*Smad4*$^{fl/fl}$ genotype, 4-5 replicates in each experiment represented by the dots). Statistical analysis was performed using one way-ANOVA with Tukey's multiple comparison test, **** indicates $P \leqslant 0.0001$. (C) Bright field images showing adenomas from both genotypes on D7. Scale bars 100µm.

5.4.3 Y-27632 rescued the slow growth of *Apc*$^{fl/fl}$*Smad4*$^{fl/fl}$ adenomas

In an attempt to understand the mechanisms of the slow growth rate for *Smad4*$^{fl/fl}$ adenomas, the effect of SB-505124 and Y-27632 on adenoma growth was tested. While SB-505124 had a minor effect on *Smad4*$^{+/+}$ adenoma (*P$\leqslant$0.05), it had no effect on *Smad4*$^{fl/fl}$ adenoma growth. The fold difference of 1µM SB-505124 on adenoma growth was 1.08 and 1.02, for *Smad4*$^{+/+}$ and *Smad4*$^{fl/fl}$ adenomas respectively when compared to their growth with EGF alone (Figure 5.5A). However, there was a dramatic change in the growth of *Smad4*$^{fl/fl}$ adenomas when treated with Y-27632. In a dose dependent manner, Y-27632 improved the slow growth of the *Smad4*$^{fl/fl}$ adenomas. *Smad4*$^{fl/fl}$ adenomas stared to grow at a similar rate to that of the *Smad4*$^{+/+}$ adenomas. Y-27632 enhanced the growth of the *Smad4*$^{+/+}$ adenomas as well. The fold difference compared to EGF alone was only 1.15 in *Smad4*$^{+/+}$ compared to 2.19 in *Smad4*$^{fl/fl}$ adenomas. Moreover, the response of adenomas to Y-27632 in *Smad4*$^{+/+}$ was different compared to that of *Smad4*$^{fl/fl}$. There was a significant increase in the growth of the latter with 0.1µM Y-27632 (****P$\leqslant$0.0001) but the same concentration had no effect on the growth of the *Smad4*$^{+/+}$ adenomas. The significant effect started with 1µM Y-27632 (*P$\leqslant$0.05) and 10µM Y-27632 (****P$\leqslant$0.0001) in the *Smad4*$^{+/+}$ adenomas (Figure 5.5B). The effect of Y-27632 on the rescue was noticed from D1. If new medium without Y-27632 supplement was used at D2, the *Smad4*$^{fl/fl}$ adenoma in culture was not affected indicating that the effect was transient.

The effect of Y-27632 on *Smad4*$^{fl/fl}$ adenomas also led to question of whether a high dose of EGF was required for *Smad4*$^{fl/fl}$ adenoma growth. The effect of different concentrations of EGF (0.81, 8.1, 81.0nM) has been tested on passaged adenomas. Although the *Smad4*$^{+/+}$ adenomas responded differently to different concentrations of EGF, the *Smad4*$^{fl/fl}$ adenomas had a similar response to the different concentrations. The growth of *Smad4*$^{+/+}$ adenomas decreased with the highest concentration of EGF (81.0nM). This concentration might be toxic to cells as no overgrowth leading to cell-cell contact inhibition was reported in the culture (Figure 5.5C).

Based on these results, the effect of Y-27632 on adenoma growth was further investigated. *Smad4*$^{fl/fl}$ adenomas reached a similar growth to *Smad4*$^{+/+}$ adenomas treated with 8.1nM EGF when treated with 10µM Y-27632 alone (Figure 5.6A, B). Therefore, the slow growth of *Smad4*$^{fl/fl}$ adenomas was rescued by Y-27632 and the growth was not entirely dependent on EGF (Figure 5.6A).

5.4.4 Effect of passage and freezing on *Apc*$^{fl/fl}$*Smad4*$^{fl/fl}$ growth

In addition to *Smad4*$^{fl/fl}$ adenoma growth assessment after adenoma harvesting, the growth of the cryopreserved as well as passaged adenomas was determined. Cryopreserved adenomas (stored directly after harvesting) had a similar pattern of growth to those seeded directly after harvesting. They had a slow growth rate which was rescued by Y-27632. However, this rescue did not allow them to grow at the same level of *Smad4*$^{+/+}$ as observed after harvesting directly from mouse (Figure 5.7A, B). On the other hand, adenomas from both genotypes showed a similar growth when passaged except a slightly significant better growth of *Smad4*$^{fl/fl}$ when treated with Y-27632 (*P$\leqslant$0.05) (Figure 5.7C). When adenomas were treated with both SB-505124 and Y-27632, no additive effect on growth was seen compared to that of Y-27632 alone (Figure 5.7A-C), indicating that both inhibitors were acting on the same pathway and not on two different ones.

The effect of SB-505124 and Y-27632 on the growth of *Smad4*$^{+/+}$ was variable between different experiments . In some experiments there was a significant difference and in others there was not. This could be due to differences in the composition of different batches of Matrigel. Two different batches of Matrigel were tested on the same cryopreserved adenoma from both genotypes. Although there were significant differences in the growth of the *Smad4*$^{+/+}$ adenomas with Y-27632, they had a similar response pattern. *Smad4*$^{fl/fl}$ cryopreserved adenomas had a similar pattern with different batches as well (Figure A.3). Thus, to avoid these differences, the same batch of Matrigel was reserved to continue the project.

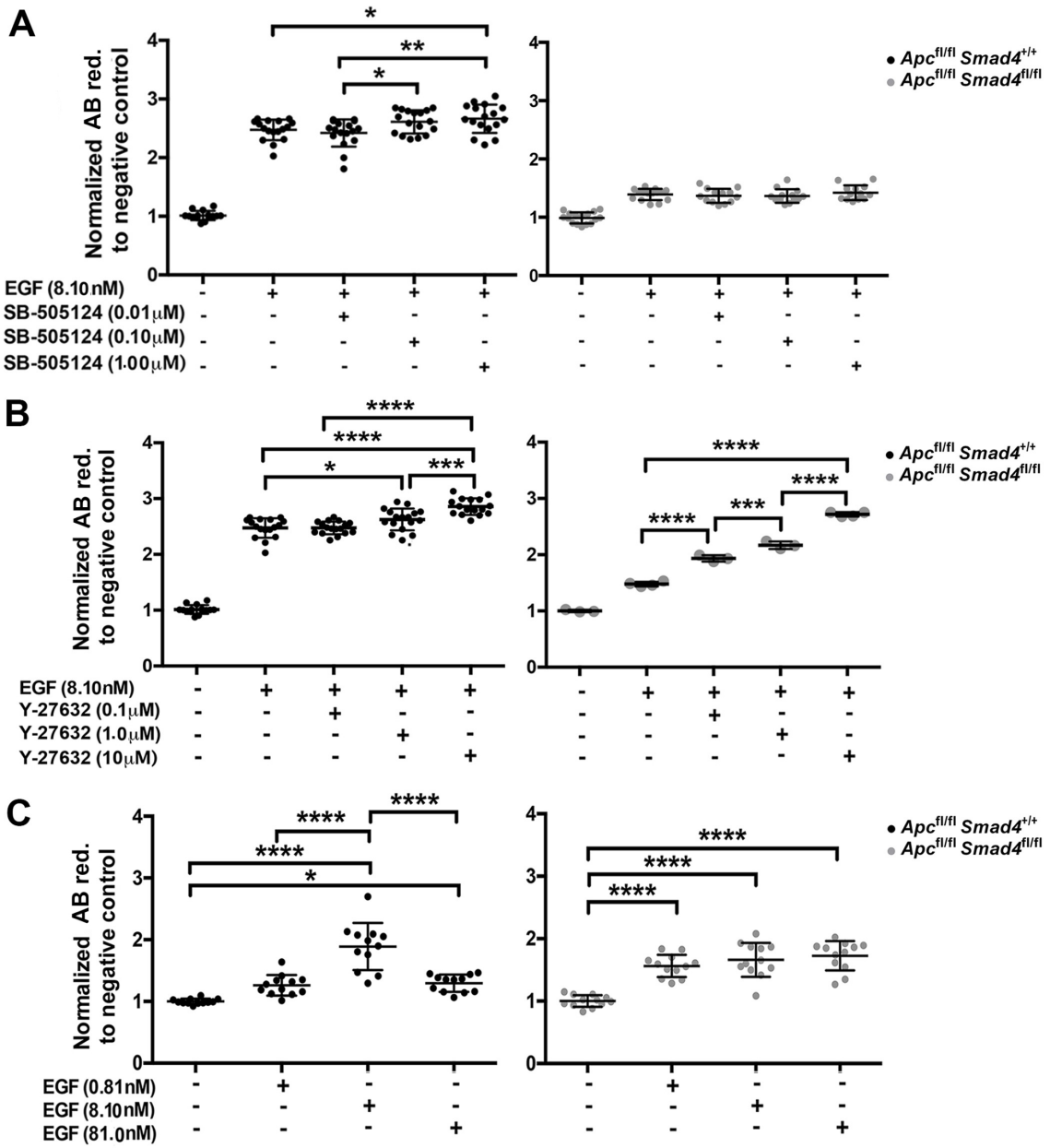

Figure 5.5: **Y-27632 rescued the slow growth of *Apc*$^{fl/fl}$*Smad4*$^{fl/fl}$ adenoma growth.** Adenomas seeded at cell density of 5000 cells/well and adenoma growth measured by AB reduction normalized to negative control after 24h (cells in Matrigel only) after harvesting (A, B) and from passaged adenomas (C). (A) 10 fold difference in SB-505124 (0.01-1.0μM) with 8.1nM EGF (n=3 animals/group, 4-6 replicates each). (B) 10 fold difference in Y-27632 (0.1-10.0μM) with 8.1nM EGF (n=4 *Smad4*$^{+/+}$animals, n=1 in *Smad4*$^{fl/fl}$, 4-6 replicates each). (C) 10 fold difference in EGF (0.81-81.0nM) (n=4, 3-4 replicates each). Replicates are represented by dots (A-C). Statistical analysis was performed using one-way ANOVA with Tukey's multiple comparison test *, **, ***, **** $P \leqslant 0.05$, $P \leqslant 0.01$, $P \leqslant 0.001$, $P \leqslant 0.0001$.

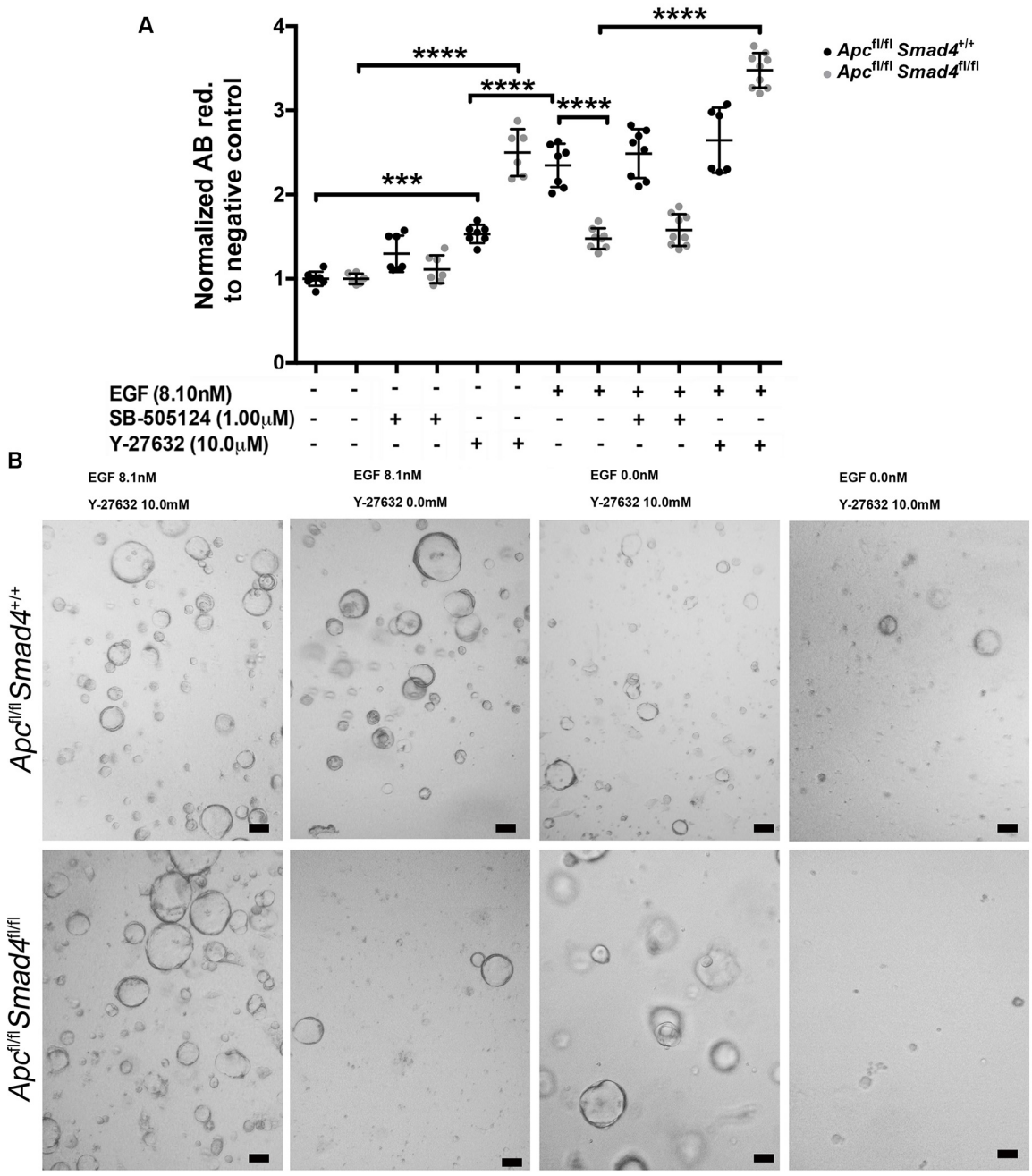

Figure 5.6: **Significant effect of Y-27632 on the recovery of *Smad4*$^{fl/fl}$ growth without EGF.** (A) Adenomas from primary culture were supplemented with or without EGF, SB-505124 and Y-27632. Growth measured by AB reduction after 24h. The fold difference in *Smad4*$^{+/+}$ adenomas compared to the negative control was 1.29, 1.53, 2.35, 2.49 and 2.67 when supplemented with SB-505124, Y-27632, EGF, EGF with SB-505124 and EGF with Y-27632, respectively. However, the fold difference was 1.11, 2.50, 1.48, 1.58 and 3.48 when *Smad4*$^{fl/fl}$ adenomas treated with SB-505124, Y-27632, EGF, EGF with SB-505124 and EGF with Y-27632, respectively. Statistical analysis was performed by one-way ANOVA with Tukey's multiple comparison test ***, ****P$\leqslant$0.001, P$\leqslant$0.0001, (n=2 with 3-5 replicates each, represented by dots). (B) Representative bright field images for adenomas on D3 showing their growth with or without Y-27632. Scale bars 50µm.

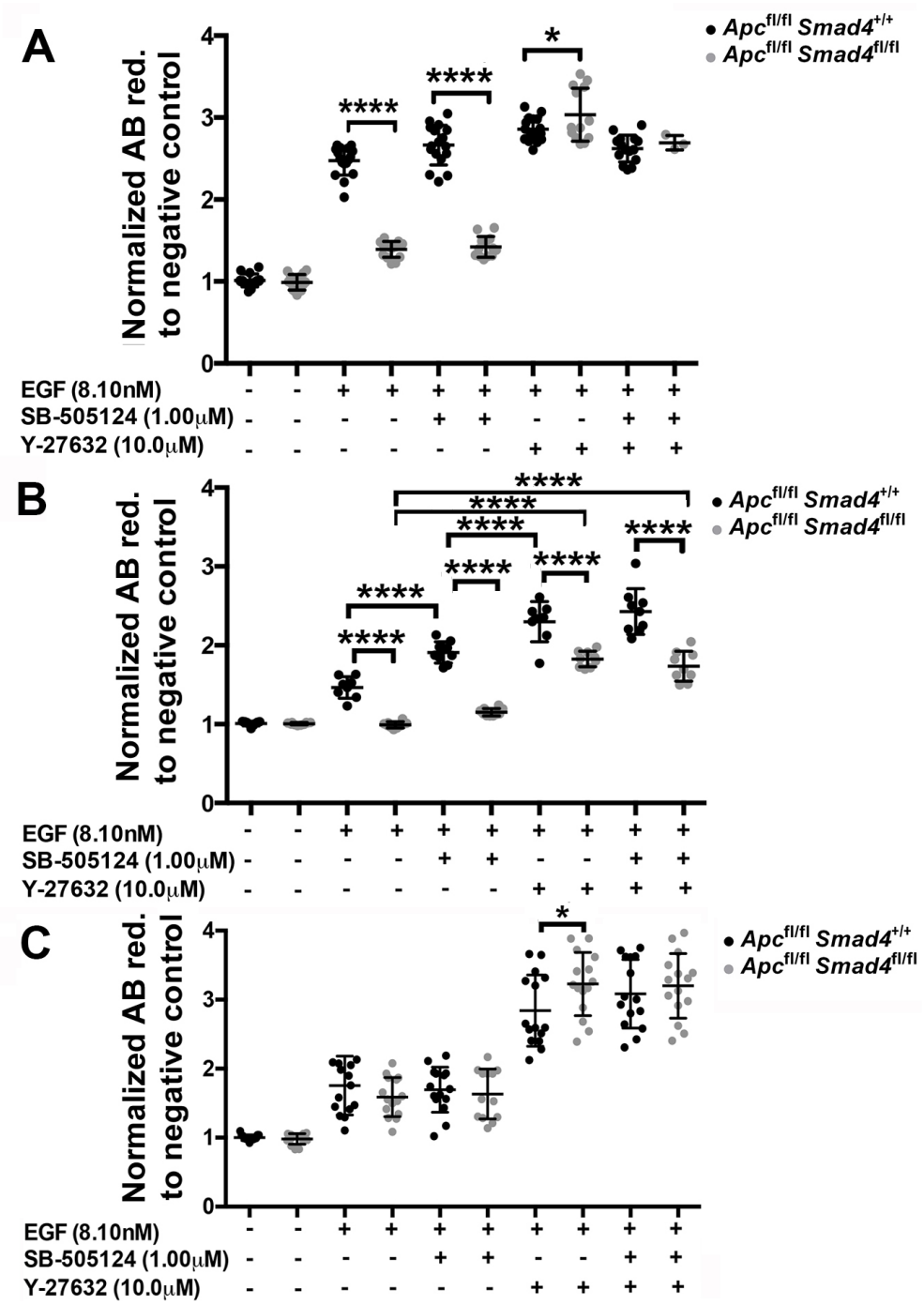

Figure 5.7: **Effect of freezing and passaging on *Smad4*$^{fl/fl}$ adenoma growth.** The growth of *Smad4*$^{fl/fl}$ compared to *Smad4*$^{+/+}$ was compared with SB-505124, Y-27632 and SB-505124, Y-27632 in addition to EGF under different conditions. (A) Growth of adenomas after harvesting directly from mouse (primary culture) (n=4 in all except n=3 with Y-27632 in *Smad4*$^{fl/fl}$). (B) Growth of adenomas post thawing (adenomas cryopreserved directly after harvesting) (n=2). (C) Growth of adenomas at passage (n=4). Dots represent replicates in the experiments (4-6 replicates each experiment). Statistical analysis was performed using one-way ANOVA with Sidak's multiple comparison test *, ****$P \leqslant 0.05$, $P \leqslant 0.0001$, respectively.

5.4.5 Characterisation of Wnt signalling in *Apc*$^{fl/fl}$*Smad4*$^{fl/fl}$ adenoma

The initiating event in adenoma formation is activation of the Wnt/β-catenin pathway, and is manifested in this model by inactivation of the *Apc* gene. Initial screening and characterisation of the adenomas by IF showed a similar pattern for CD44, Axin2, c-Myc, and β-catenin protein labelling. Adenomas had cytoplasmic CD44, nuclear and cytoplasmic Axin2, nuclear c-Myc and some cytoplasmic β-catenin. Adenomas of both genotypes had membrane bound E-cadherin that co-localised with β-catenin (Figure A.4).

5.4.6 MH1 deletion in *Apc*$^{fl/fl}$*Smad4*$^{fl/fl}$ following Cre-mediated recombination

Data previously showed the recombination of Smad4 gene by PCR and DNA sequencing (Figure 5.1). Western blots showed an expression of Smad4 full length protein of 61 kDa in both *Smad4*$^{+/+}$ and *Smad4*$^{fl/+}$ adenomas. Another band of 43 KDa was detected in protein extracts from *Smad4*$^{fl/+}$, *Smad4*$^{fl/fl}$ adenomas using a monoclonal Smad4 antibody (Santa Cruz), indicating that there was truncated protein following recombination (Figure 5.8A). The full length protein in *Smad4*$^{+/+}$ showed a nuclear localisation following 390pM TGF-β1 stimulation for 2h. Under the same conditions no nuclear localisation of Smad4 was detected in *Smad4*$^{fl/fl}$ adenomas (Figure 5.8B). *In silico* analysis was performed to verify the truncated protein. This showed an open reading frame on exon 5 of Smad4 gene, mapping this with ExPASy showed that exon 2 deletion results in a truncated protein with Smad4 MH1 domain deletion. The predicted size of the truncated protein is 43kDa comprising the linker and Smad4 MH2 domain (Figure 5.8C, D). RNA-seq experiments were performed latter in this work (Chapter 6). Two different isoforms of *Smad4* were detected. The first was from *Smad4*$^{+/+}$ adenomas and the second was from *Smad4*$^{fl/fl}$ adenomas. *Smad4* gene tracing by Cuffdiff revealed that the first transcript came from the intact *Smad4* gene and the second transcript came from *Smad4* gene with excised exon 2 (Figure 5.8E, F). Taken together, Cre-mediated recombination of *Smad4* gene resulted in a truncated protein. This truncated protein did not show nuclear localisation following TGF-β1 stimulation. This raised the question of whether it is functional or not?

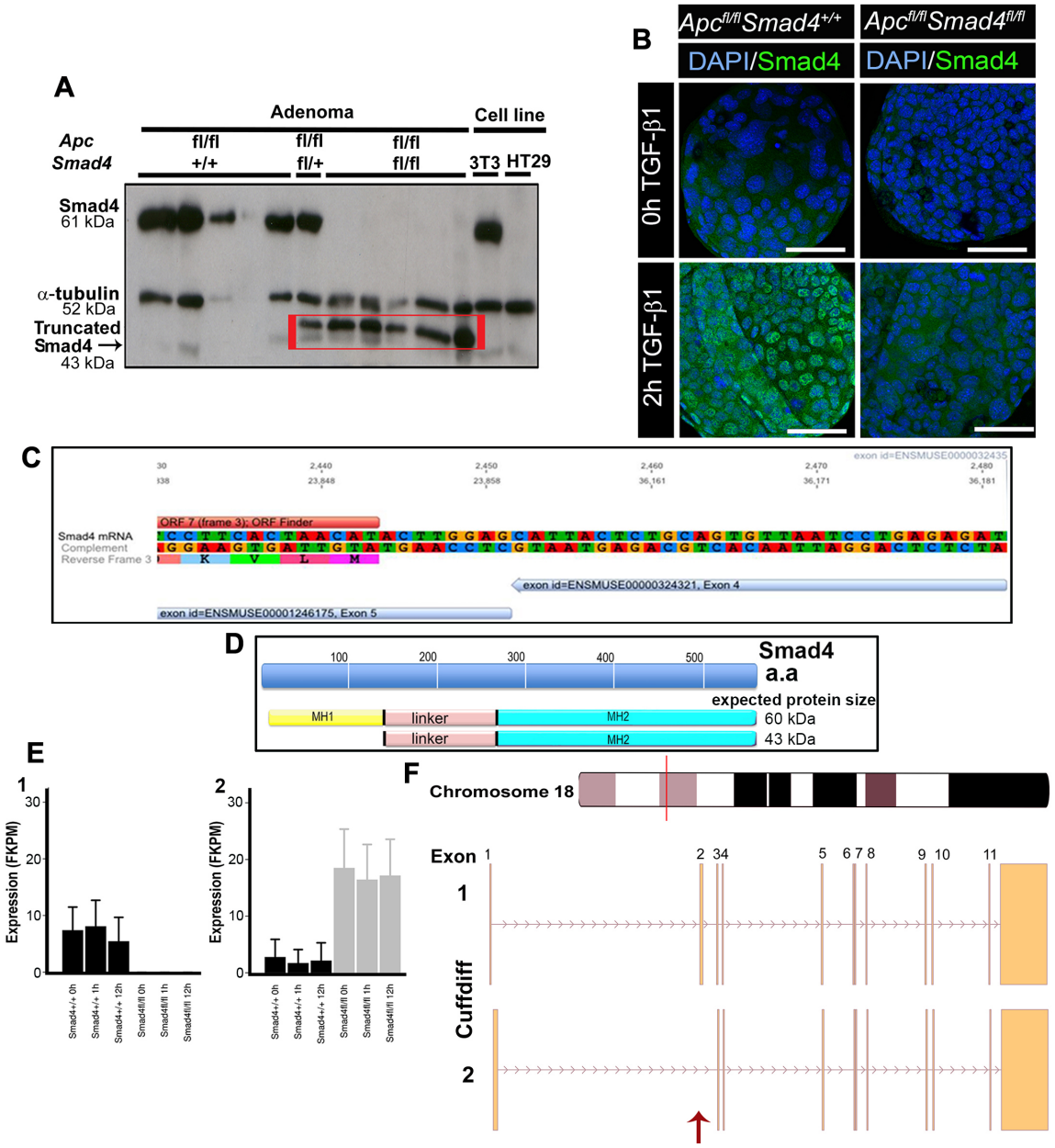

Figure 5.8: **MH1 deletion in *Smad4*$^{fl/fl}$ following Cre-mediated recombination.** (A) Western blots showing Smad4 protein of 61 kDa from *Smad4*$^{+/+}$ and *Smad4*$^{fl/+}$ adenomas, and a truncated Smad4 protein of 43 kDa in the *Smad4*$^{fl/+}$ and *Smad4*$^{fl/fl}$. Controls: 3T3 with intact *Smad4* (positive). HT29 CRC cells has Smad4 mutation (C931 C>T) in the MH2 domain and was used as negative control. (B) Representative confocal images for Smad4 nuclear localisation following 2h of 390pM TGF-β1 treatment (n=4). Scale bars 50µm. (C) *In silico* analysis by Geneious software shows an open reading frame in exon 5 of *Smad4*. (D) Simplified cartoon representing mapping with ExPASy shows deletion of the MH1 domain leaving an intact linker and MH2 domain of Smad4. The predicted size of truncated Smad4 is 43 kDa. (D) Quantitative expression of different isoforms of *Smad4* in FPKM as showed by RNA-seq experiment. (FPKM: Fragments per kilobase per million reads mapped). (F) Isoform tracking by Cuffdiff. Upper allele represents Smad4 full length, and the lower represents Smad4 allele without exon 2 (red arrow).

5.4.7 Nuclear localisation of R-Smads with TGF-β1 treatment in *Apc*$^{fl/fl}$ *Smad4*$^{fl/fl}$ adenomas

TGF-β1 signalling in adenomas was determined by R-Smads phosphorylation in response to TGF-β1 stimulation and/or the inhibitors (SB-505124 and Y-27632). TGF-β1 stimulation resulted in phosphorylation of p-Smad2 and p-Smad3 in both the *Smad4*$^{+/+}$ and the *Smad4*$^{fl/fl}$ adenomas. The level of phosphorylation was decreased if the adenoma was preincubated with TGFβR1 inhibitor, SB-505124. Total R-Smads was also examined. Total Smad2 was the same in both adenomas. The ratio of Smad2 to β-actin was 0.81±0.02 (SD) and 0.83±0.02 (SD) for *Smad4*$^{+/+}$ and *Smad4*$^{fl/fl}$, respectively. On the other hand, Smad3 detection by western blot was not easy with the *Smad4*$^{+/+}$ adenomas. The detection was enhanced with high percentage acrylamide gel (15%) providing a smaller pore size to trap Smad3. Densitometric analysis of the gel showed a slightly higher level of Smad3 in *Smad4*$^{fl/fl}$ but this was not significant. The ratio of Smad3 to β-actin was 0.12±0.01 (SD) and 0.19±0.07 (SD) for *Smad4*$^{+/+}$ and *Smad4*$^{fl/fl}$, respectively (Figure 5.9A, B). The response to TGF-β1 stimulation was similar in both adenomas. There was a rapid gradual accumulation of p-Smad2 following TGF-β1 stimulation that reached high levels after 1-2h and was maintained for around 6h after which there was a gradual decrease in level of p-Smad2 (Figure 5.9C). The next question was whether the p-R-Smads localise in the nucleus in response to TGF-β1 stimulation. Both adenomas respond to TGF-β1 stimulation by nuclear localisation of p-Smads. The nuclear localisation was also inhibited when the adenomas were pre-incubated with SB-505124 (Figure 5.10).

The level of p-Smad2 in adenomas of both genotypes when pre-incubated with Y-27632 was close to its level in adenomas stimulated with TGF-β1 alone. The main inhibition of p-Smad2 was when the adenomas were treated with SB-505124 (Figure 5.11 A, B, C).

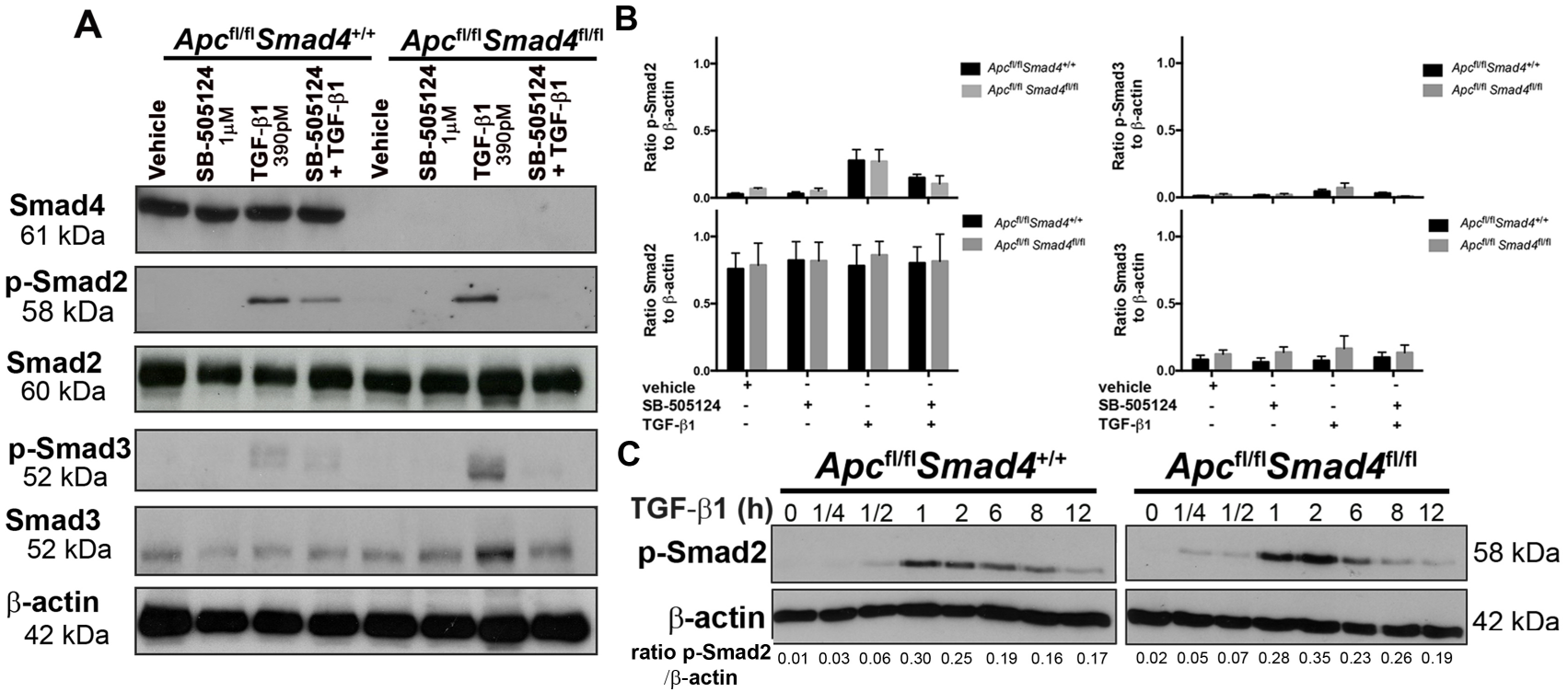

Figure 5.9: **TGF-β1 signalling in *Apc*$^{fl/fl}$*Smad4*$^{fl/fl}$ adenomas**. (A) Representative western blots of Smad4, total R-Smads, and p-R-Smads in *Apc*$^{fl/fl}$*Smad4*$^{+/+}$ and *Apc*$^{fl/fl}$*Smad4*$^{fl/fl}$ adenomas show phosphorylation of R-Smads following TGF-β1 treatment. R-Smad phosphorylation decreased when the adenomas were pre-incubated with SB-505124 for 2h. (B) Ratio of p-Smad2 (upper left), p-Smad3 (upper right), total Smad2 (lower left) and total Smad3 (lower right) to β-actin as determined by densitometric analysis of western blots (n=3 independent experiments). Statistical analysis was performed using nonparametric one-way ANOVA with Dunn's multiple comparison test. (C) Western blots showing p-Smad2 at different time points following 390pM TGF-β1 stimulation. Ratio of p-Smad2 to β-actin is represented below following densitometric analysis of the blots (n=1). Similar level of p-Smad2 at 12h obtained in a different experiment.

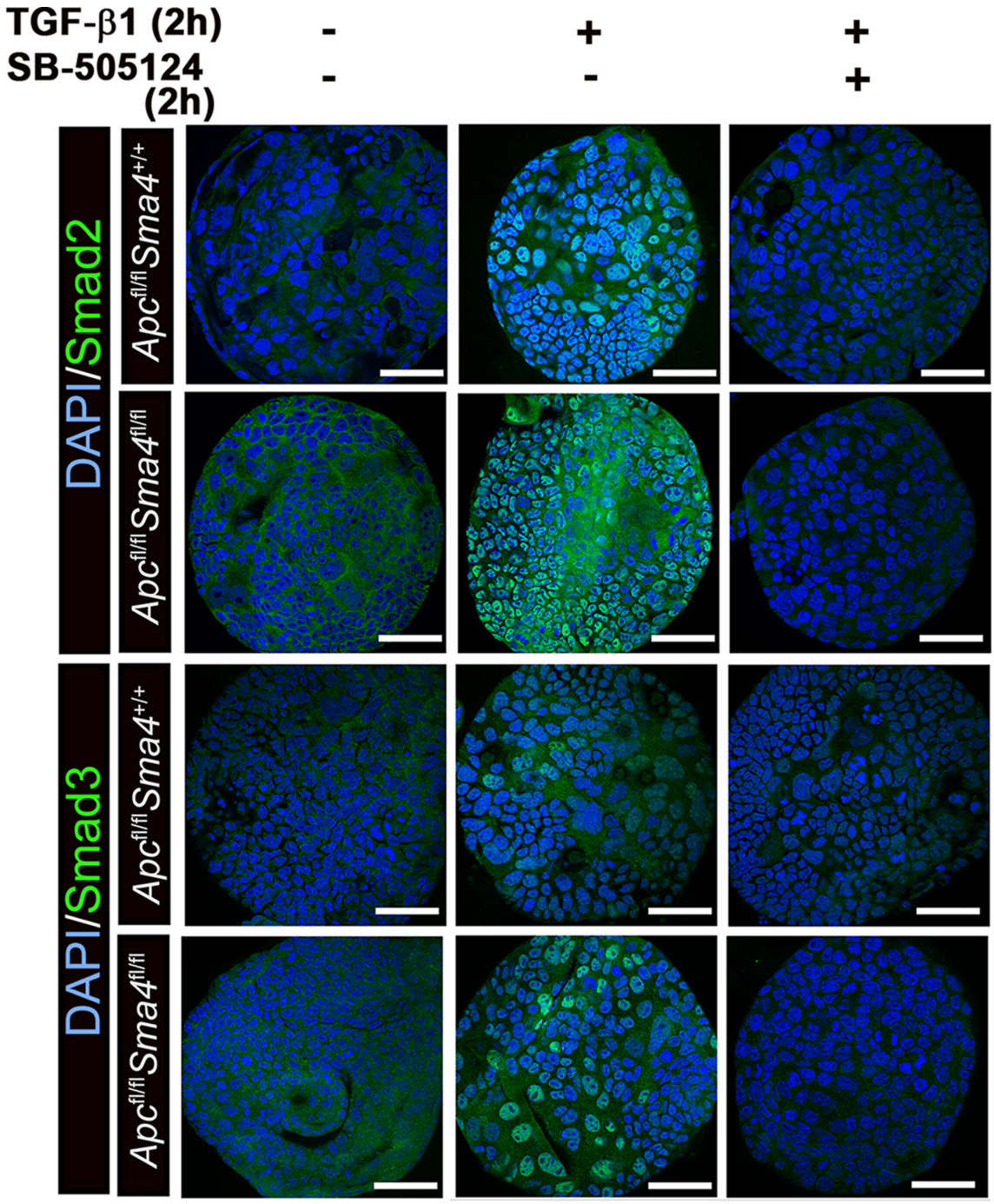

Figure 5.10: **Nuclear localisation of R-Smads with TGF-β1 stimulation.** Confocal images showing nuclear localisation of R-Smads following TGF-β1 treatment. Scale bar 50μm.

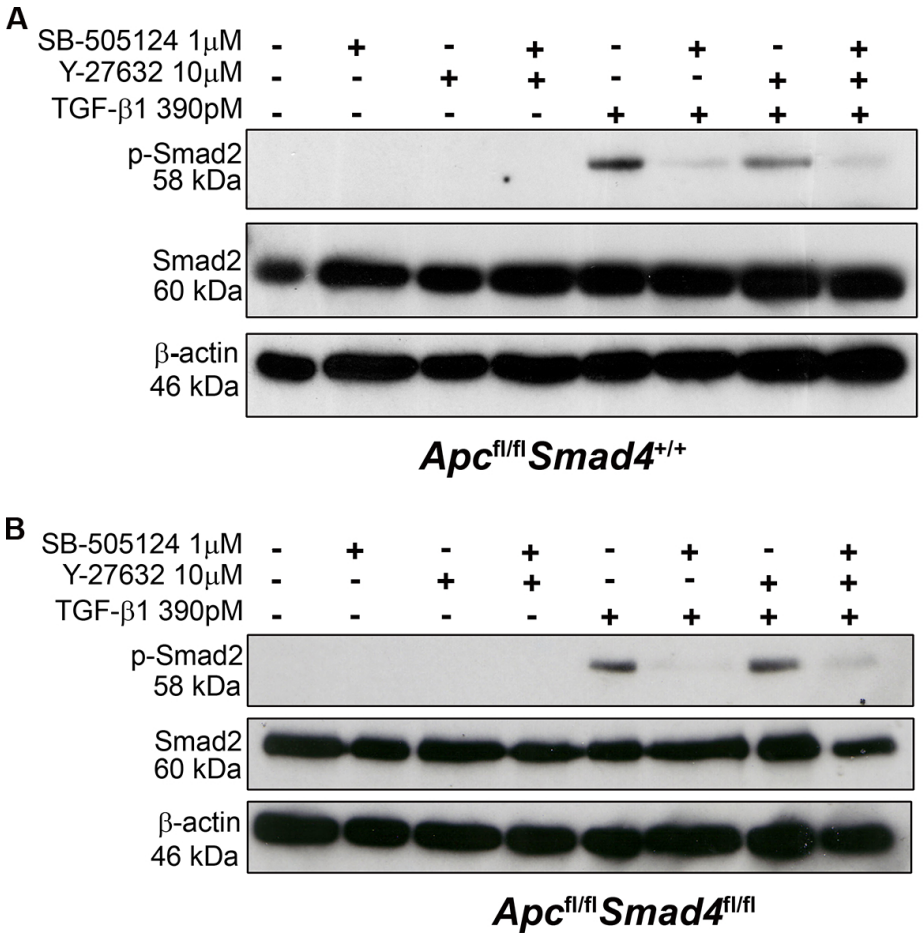

C

	Ratio to β-actin			
	$Apc^{fl/fl}Smad4^{+/+}$	$Apc^{fl/fl}Smad4^{+/+}$	$Apc^{fl/fl}Smad4^{fl/fl}$	$Apc^{fl/fl}Smad4^{fl/fl}$
	p-Smad2	Smad2	p-Smad2	Smad2
Vehicle	0.03	1.03	0.03	0.88
SB-505124 (1μM)	0.01	1.07	0.03	0.89
Y-27632 (10μM)	0.03	1.10	0.02	0.98
SB-505124 (1μM) Y-27632 (10μM)	0.01	1.06	0.02	0.85
TGF-β1 (390pM)	0.26	1.05	0.22	0.83
SB-505124 (1μM) TGF-β1 (390pM)	0.05	1.14	0.03	0.87
Y-27632 (10μM) TGF-β1 (390pM)	0.16	0.95	0.19	0.96
SB-505124 (1μM) Y-27632 (10μM) TGF-β1 (390pM)	0.06	0.90	0.08	0.90

Figure 5.11: **Y-27632 did not block p-R-Smad in response to TGF-β1.** (A, B) Adenomas treated with Y-26732 and SB-505124 before TGF-β1 for 2h. Small effect with Y-27632 on p-Smad2 inhibition compared to the effect of SB-505124. (C) Table shows the ratio of Smad2 and p-Smad2 in the different adenomas in different conditions after densitometric analysis.

5.4.8 TGF-β1 induced growth inhibition of the adenomas

After characterising Smad4 MH1 deletion and the signalling pathway, the effect of TGF-β1 on adenoma growth was assessed. TGF-β1 induced growth inhibition of both the *Smad4*$^{+/+}$ and the *Smad4*$^{fl/fl}$ adenomas was observed. While the decrease in viability as detected by AB started at 0.39pM TGF-β1 for the *Smad4*$^{+/+}$, the decrease in viability started at 39pM TGF-β1 and was very clear at 390pM TGF-β1 in the *Smad4*$^{fl/fl}$. Thus, 390pM TGF-β1 was used for the subsequent analysis. The IC50 of TGF-β1 on *Smad4*$^{+/+}$ was 24.0pM, 22 fold less than that of the *Smad4*$^{fl/fl}$ adenomas. The decrease in viability was rescued when the adenomas were pre-incubated with freshly prepared 1μM SB-505124 for 2h before treatment with TGF-β1 (Figure 5.12). The decrease in viability was accompanied by a shape change in adenomas from both genotypes. Dead cells covered the surface of the adenomas along with the appearance of a new layer of cells underneath the adenomas. Within 24h, around 98% of the *Smad4*$^{+/+}$ adenomas had changed shape, however, it was 72h before all the *Smad4*$^{fl/fl}$ adenomas showed shape change (Figure 5.13 A,B). Confocal images showed migration of the newly formed cells in *Smad4*$^{fl/fl}$ adenomas that was not obvious in *Smad4*$^{+/+}$ adenomas (Figure 5.13 C).

The decrease in viability and shape change was accompanied by a decrease in proliferation and increased apoptosis. Both *Smad4*$^{+/+}$ and *Smad4*$^{fl/fl}$ adenomas showed significant decrease in EdU incorporation compared to the control. EdU incorporation was significantly different between *Smad4*$^{+/+}$ and *Smad4*$^{fl/fl}$ treated adenomas (mean=4% vs 18% for *Smad4*$^{+/+}$ and *Smad4*$^{fl/fl}$, respectively) (Figure 5.14A,B). After 72h, Ki67 positive cells were observed rarely in the *Smad4*$^{+/+}$ compared to *Smad4*$^{fl/fl}$ adenomas as detected by confocal images (not quantified) (Figure 5.14C).

Adenomas of both genotypes had positive cleaved caspase 3 (CC3) in response to TGF-β1 after 24h (pilot labelling experiment with Smad4 wild type adenomas did not show positive caspase labelling before 12h of treatment). While apoptotic cells covered the whole *Smad4*$^{+/+}$ adenomas, they were restricted to certain parts of the *Smad4*$^{fl/fl}$ adenomas -at

the location of the original adenomas- but they were not detected at the migratory phase (Figure 5.15). Lineage tracing showed that both transformed and normal adenomas expressed Rosa26-YFP (Figure 5.16). Taken together, Smad4 knockout had an effect on the cytostatic and apoptotic effect of TGF-β1 by decreasing proliferation and upregulating apoptosis. The effect could be partially Smad4 independent as a more rapid decrease in proliferation, viability, and more apoptosis were observed in the presence of Smad4. Migration is enhanced when Smad4 was knocked out.

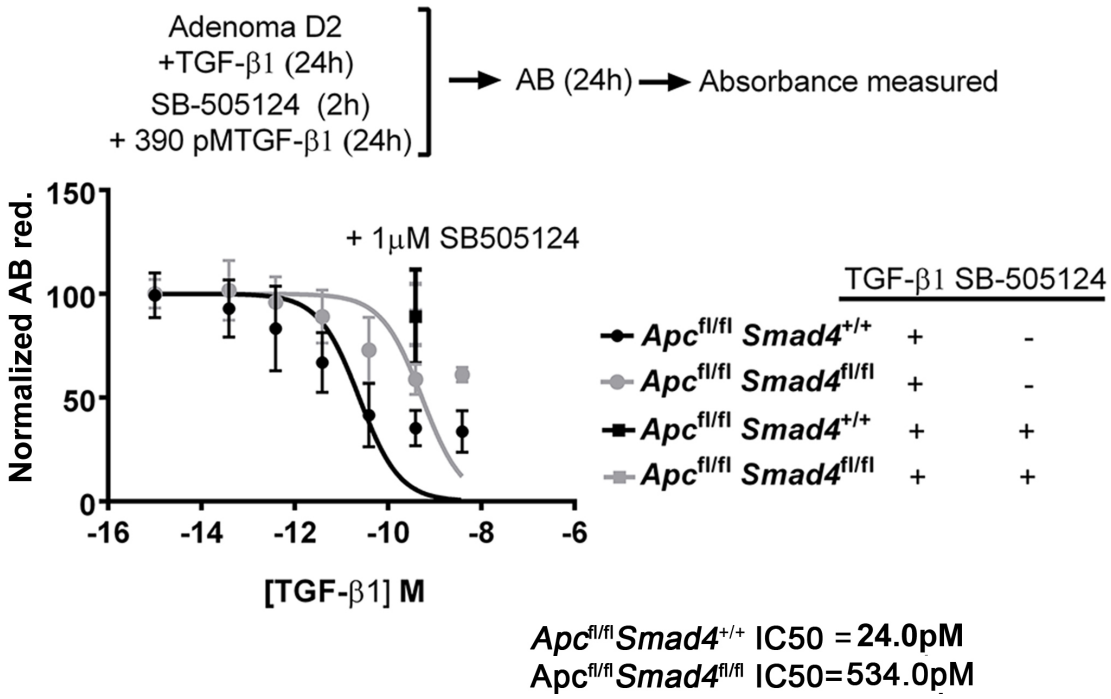

Figure 5.12: **TGF-β1 induced growth inhibition of the adenomas that can be rescued with SB-505124**. Adenomas on D2 were incubated with different concentrations of TGF-β1 (range: 0.039-3900pM, 10 fold serial dilution). AB was added on D3 and measured after 24h. Data were normalized to the untreated control 100% and 0% Matrigel only. (n=4, with 4-6 replicates each. Error bars ±SD). For the rescue adenomas were pre-incubated with SB-505124 for 2h before 390pM TGF-β1 was added. When TGF-β1 was added on D1 a lower IC50 was obtained (2.7pM).

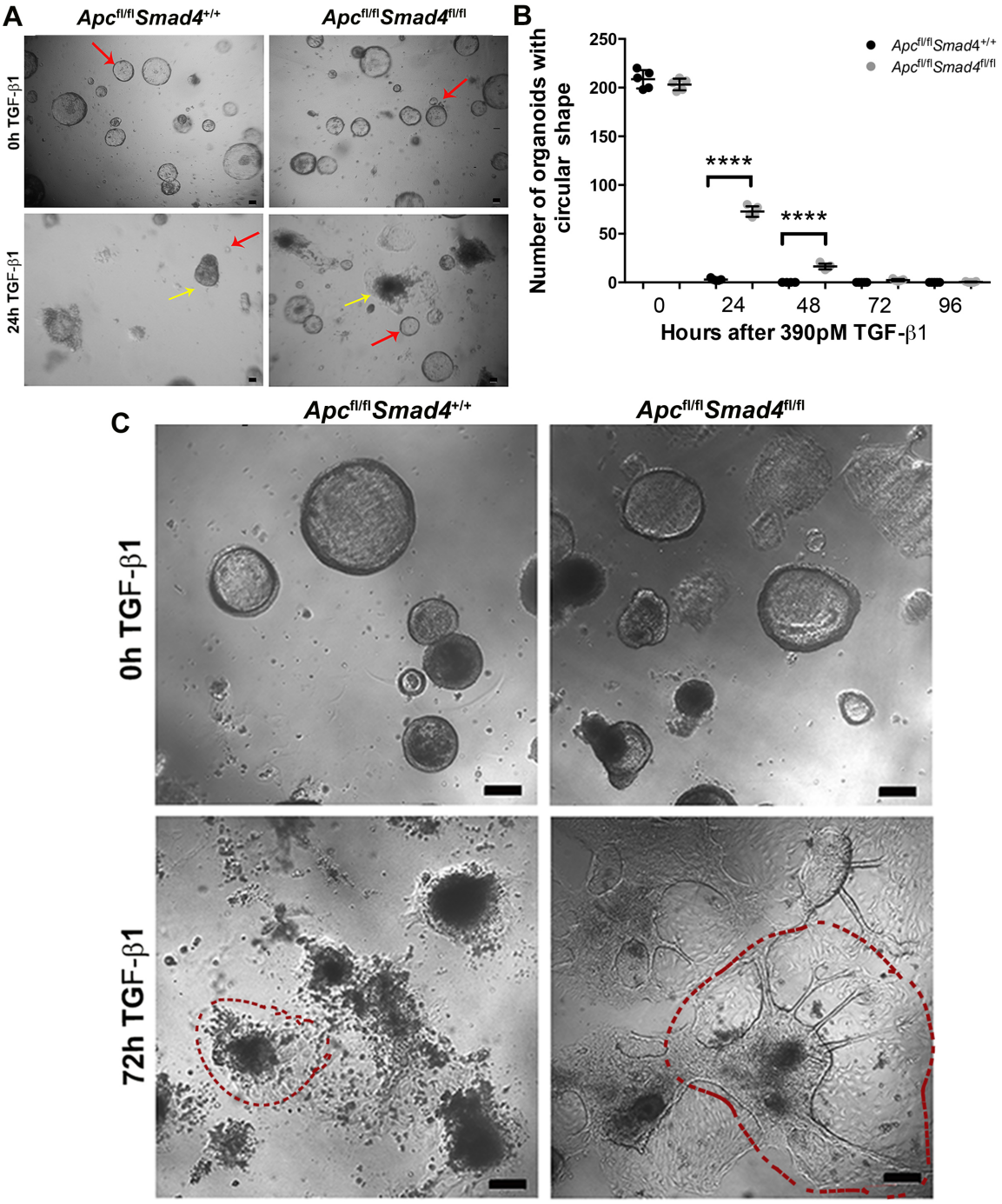

Figure 5.13: **Morphological changes of adenoma following TGF-β1 treatment**.(A) Bright field images show adenomas treated with TGF-β1 for 24h and their controls. (B) Adenomas with a circular shape were counted before treatment and every 24h for 4 days. Yellow arrows point to adenomas with shape change and red arrows point to adenomas with circular shape. (n=3, with 3 replicates each represented by dots). Statistical analysis was performed using one-way ANOVA with Sidak's multiple comparison test ****P$\leqslant$0.0001. (C) Bright field confocal images show adenomas 72h following TGF-β1 addition. Red dots mark the area with shape change around the transformed adenomas. Similar results were obtained every time the experiment was repeated. Scale bars 50µm. TGF-β1 concentration 390pM.

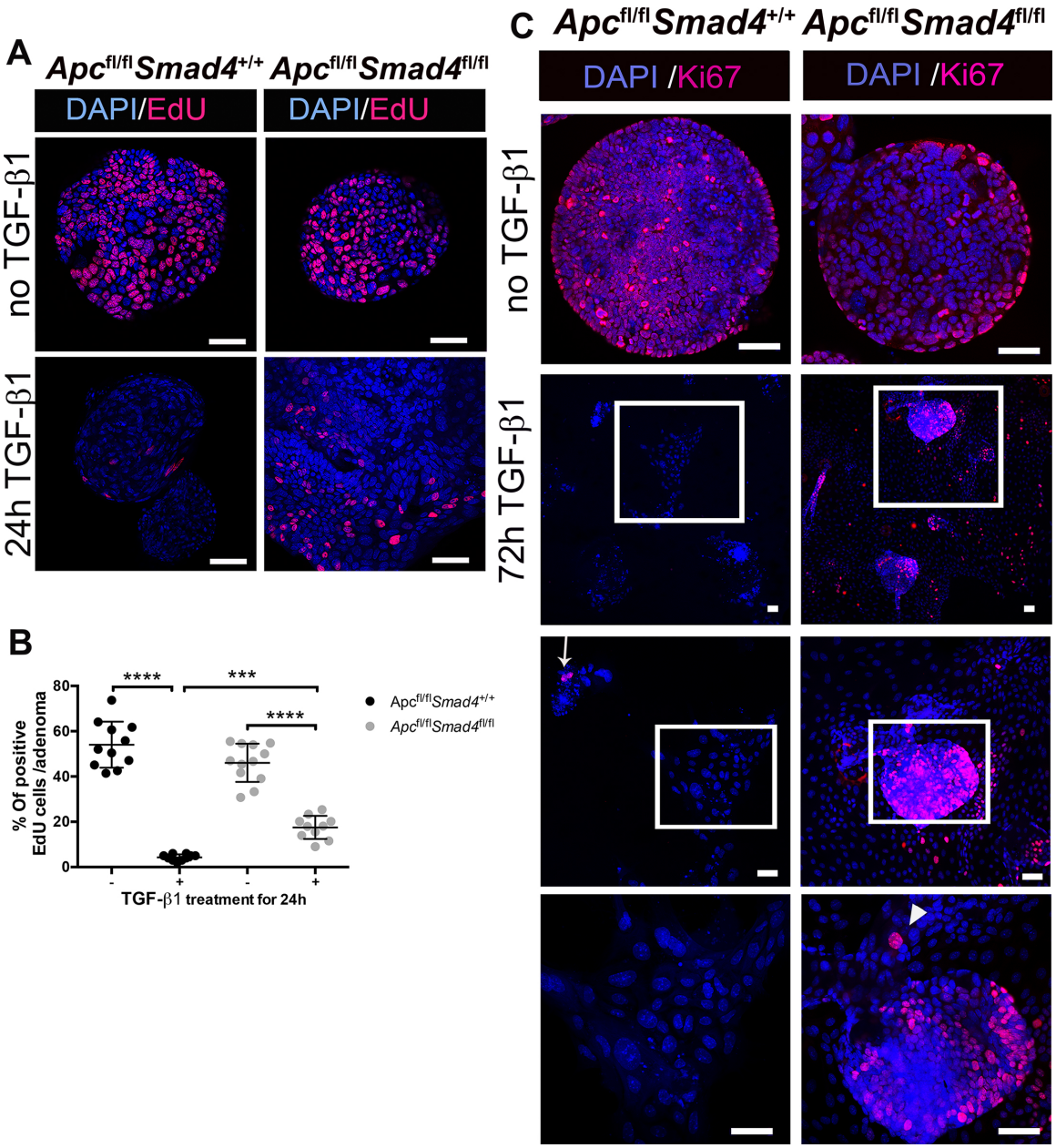

Figure 5.14: **Decrease in adenoma proliferation with TGF-β1.** Proliferation assessed by EdU and Ki67 labelling. (A) 24h post TGF-β1 treatment, adenomas incubated with EdU for 2h. Confocal images showed EdU incorporation in treated and untreated adenomas of both *Smad4*$^{+/+}$ and *Smad4*$^{fl/fl}$ genotypes. (B) Quantification of EdU positive cells by ImageJ (n=10 adenomas). Statistical analysis was performed with one-way ANOVA with Sidak's multiple comparison test ***, ****, $P \leqslant 0.001$ and $P \leqslant 0.0001$, respectively. (C) Confocal images show Ki67 labelling for the adenomas 72h of TGF-β1 addition. Arrowhead points to a positive Ki67 cells with the newly formed layer of cells. Arrow points to a positive Ki67 (rare) in the wild type adenoma. Scale bars 50µm. TGF-β1 concentration 390pM.

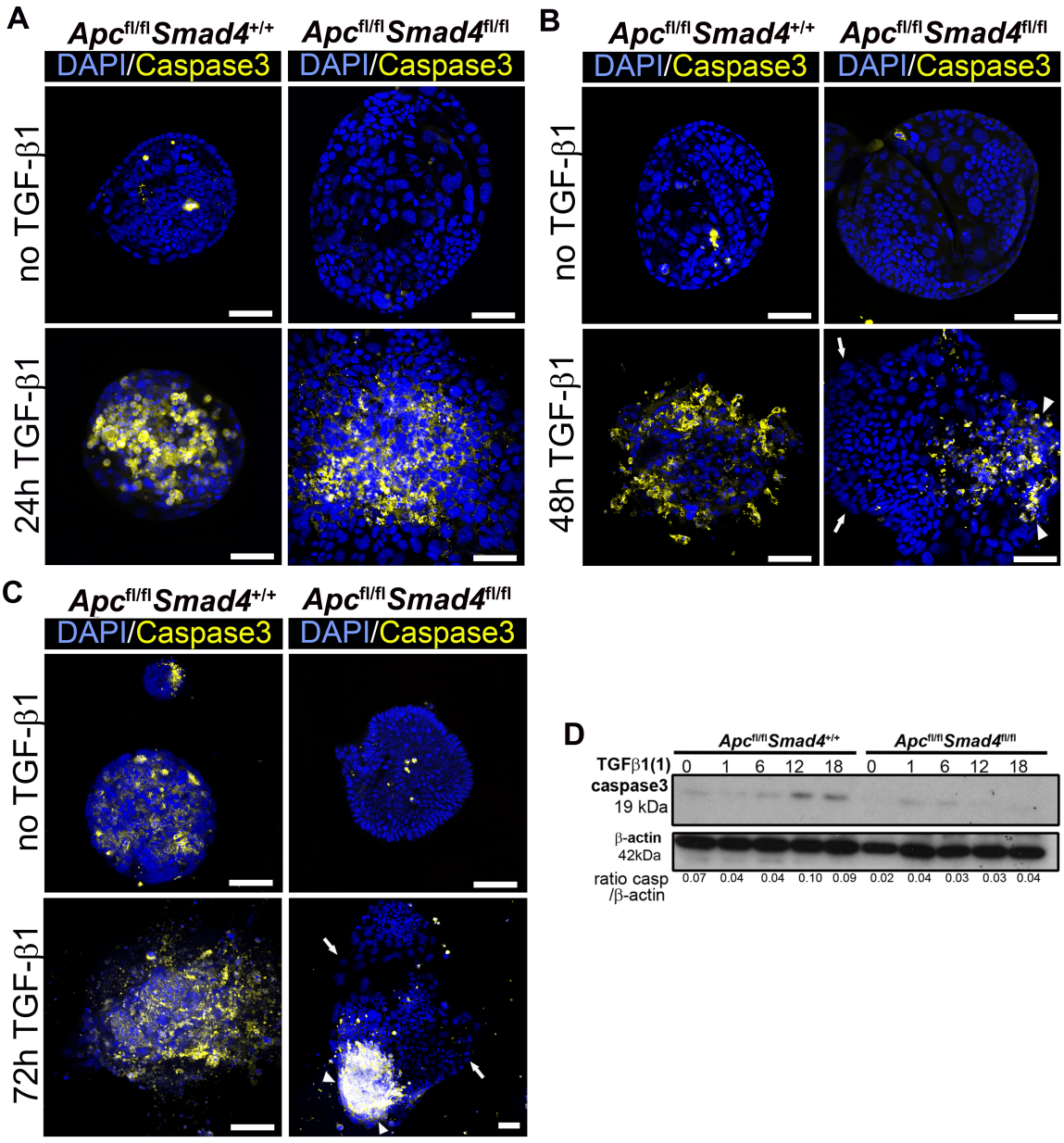

Figure 5.15: **Positive cleaved caspase-3 labelling in *Smad4*$^{+/+}$ and *Smad4*$^{fl/fl}$ adenomas with TGF-β1**. Confocal images show positive CC3 labelling with TGF-β1 after 24h (A), 48h (B) and 72h (C). CC3 was covering the whole area of *Smad4*$^{+/+}$ adenomas compared to certain areas in *Smad4*$^{fl/fl}$ treated adenomas. Arrows point to the newly formed cells, and arrowheads point to the original adenomas. Scale bars 50µm. (D) Western blots show slight upregulation of CC3 12h TGF-β1 treatment. TGF-β1 concentration 390pM. Cleaved caspase 3 (CC3).

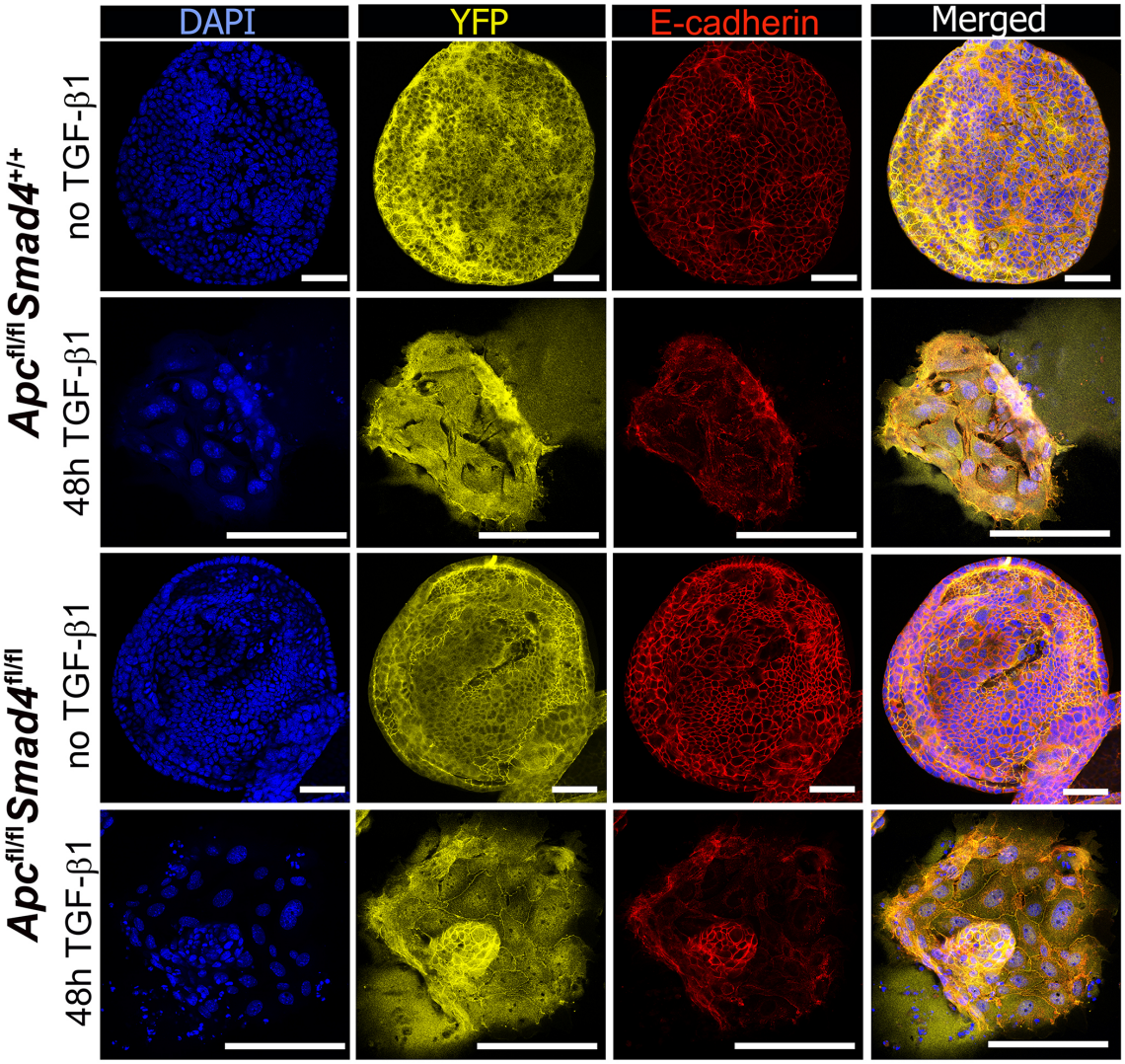

Figure 5.16: **Transformed adenomas expressed Rosa26-YFP**. Confocal images show Rosa26-YFP expression in both normal and transformed adenomas of *Smad4*$^{+/+}$ and *Smad4*$^{fl/fl}$ genotypes. Scale bars 50µm.

5.4.9 Smad4 is not required for EMT

As TGF-β1 is known to induce EMT in different tissues and by this promote tumour progression, the newly formed layer was characterised for EMT markers by western blot and confocal images. The availability of protein for western blotting restricted the assay to between 12h and 18h. Fibronectin was upregulated within 12h of TGF-β1 exposure in adenomas of both genotypes (Figure 5.17A). A minor change in N-cadherin at that time point was seen in *Smad4*$^{+/+}$ but it was not significant. The ratio of N-cadherin to β-actin was 0.91±0.15 (SD) at 0h and 1.04±0.25 (SD) at 18h of TGF-β addition (Figure 5.17C). Vimentin expression was examined using 2 different antibodies . No bands were detected with the Abcam antibody. However, with Proteintech antibodies 2 bands were detected (54 KDa expected and an unexpected band at 44 kDa), but no change in vimentin at these time points in both adenomas was detected (Figure 5.17D). Thus, further characterisation of the EMT was performed by IF. To determine the best time point, adenomas (normal and treated) from both genotypes were labelled with fibronectin for fours days (24h-96h post TGF-β1 addition). Positive fibronectin labelling was detected after 24h TGF-β1 treatment with a persistent expression for the entire experiment. Within the first 24h almost all of the *Smad4*$^{+/+}$ and most of the *Smad4*$^{fl/fl}$ changed in shape. *Smad4*$^{fl/fl}$ adenomas showed the beginnings of migration (Figure 5.18). Migration was very clear at 48h in *Smad4*$^{fl/fl}$ transformed adenomas, with no migration detected in the *Smad4*$^{+/+}$ (Figure 5.19). Migration was persistent at the 72h and 96h time points. The controls (untreated adenomas) from both genotypes started to die at 72h and 96h (Figure 5.20 and 5.21), for that, the characterisation with different EMT markers continued at 48h.

EMT also was evaluated for cadherin switch. Adenomas exposed to TGF-β1 from both genotypes showed a switch from E-cadherin to N-cadherin (Figure 5.22). Vimentin labelling was mainly nuclear with some cytoplasmic (similar labelling pattern was at 72h) in the transformed adenomas. Nuclear vimentin was also detected in the untreated adenomas. F-actin labelled by phalloidin is another evidence of disrupted adherens junction and rearrangement of the cytoskeleton in both adenomas as a result of TGF-β1 treatment.

There was peripheral F-actin in the untreated adenomas (Figure 5.23). Consequently, TGF-β1 treatment resulted in phenotypic changes characteristic of EMT in both *Smad4*$^{+/+}$ and *Smad4*$^{fl/fl}$ adenomas. However, migration was only detected in the *Smad4*$^{fl/fl}$ adenomas.

5.4.10 Effect of TGF-β1 on Wnt/β-catenin pathway

Both genotypes showed multiple bands of β-catenin by western blot below the expected band at 92 KDa. Bands were more clear in the extract from the *Smad4*$^{+/+}$ adenomas (Figure 5.24A). Adenomas exposed to TGF-β1 showed degradation of E-cadherin after 12h of TGF-β1 treatment (Figure 5.24B). c-Myc was downregulated in *Smad4*$^{+/+}$ adenomas after 18h and upregulated in the *Smad4*$^{fl/fl}$ adenomas (Figure 5.24C). Western blot showed that Axin2 was upregulated in the *Smad4*$^{+/+}$ adenomas after 12h (band at 94 kDa) only. The antibody can also detect Axin2 at 75 KDa, this band was detected in both adenomas at different time points (Figure 5.24 D). CD44 was not detectable by western blot. In untreated adenomas of both genotypes, E-cadherin and β-catenin were localised at the adherens junction. With TGF-β1 treatment, the adherens junction was disintegrated due to E-cadherin and β-catenin loss. This is further evidence of EMT. In the transformed part of the adenomas there was nuclear and cytoplasmic β-catenin. Nuclear β-catenin was very clear in the *Smad4*$^{fl/fl}$ adenomas (Figure 5.25). Taken together, TGF-β1 treatment affects the Wnt/β-catenin pathway by upregulating and downregulating important genes in tumorigenesis such as β-catenin, E-cadherin and c-Myc.

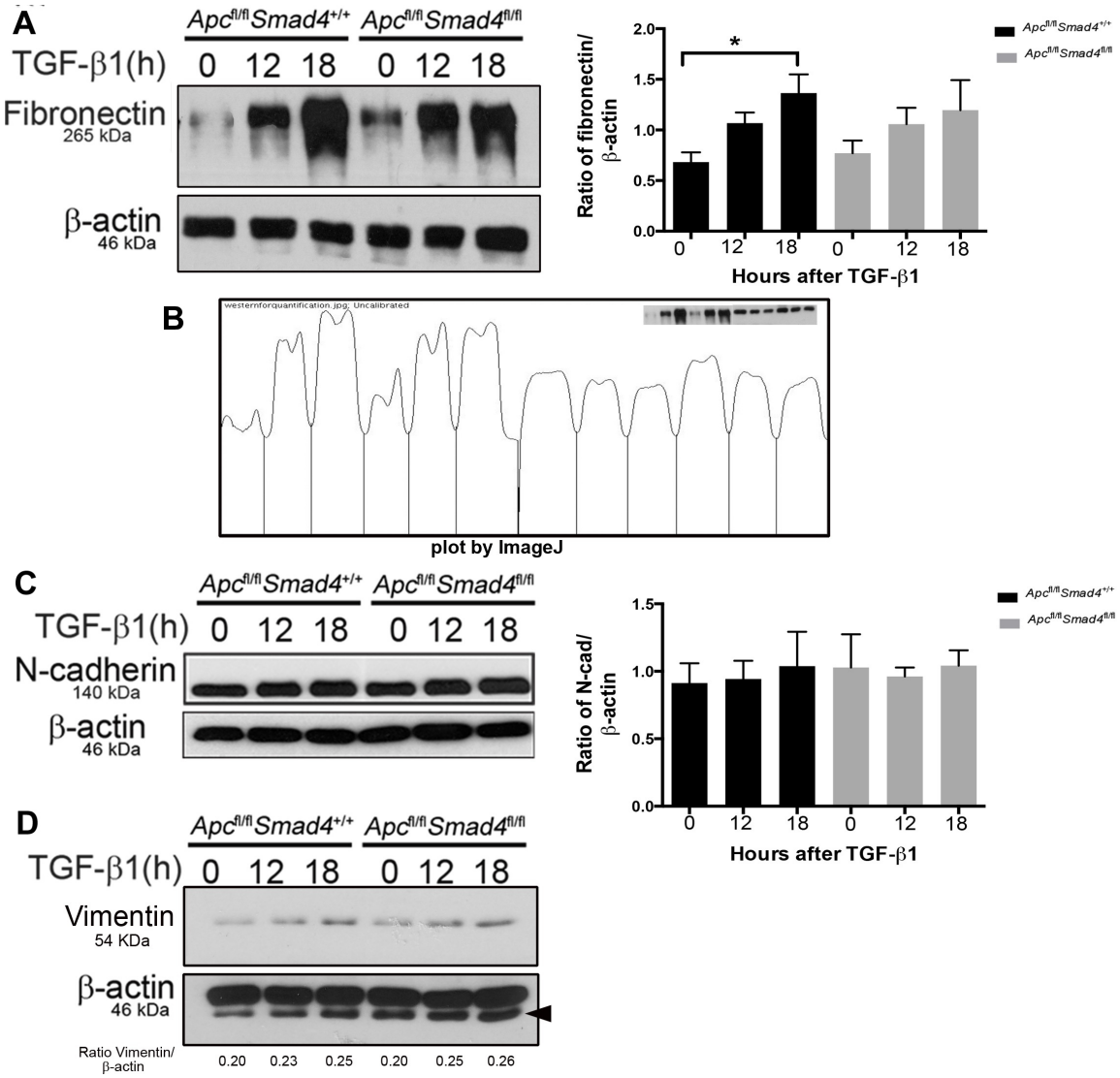

Figure 5.17: **TGF-β1 upregulated fibronectin within 12h.** Western blots for fibronectin, N-cadherin and vimentin after 12h and 18h TGF-β1 treatment. (A) Representative western blot for fibronectin (left) and the ratio of it to β-actin as analysed using ImageJ (right) (n=3). *P=0.0429. (B) Representative densitometric analysis for western blot by ImageJ. The graph represents the lanes plotted by ImageJ for the blot at the right side of the graph (aligned using Photoshop first). The area under the curve was measured by ImageJ. (C) Representative western blot for N-cadherin (left) and the ratio of it to β-actin as analysed using ImageJ (right) (n=3). (D) Representative western blot for vimentin and the ratio to β-actin is below the blot. The expected band size is 54 KDa. An extra band under the loading control appeared (arrowhead) (n=2 with similar results). Statistical analysis was performed using nonparametric one-way ANOVA with Dunn's multiple comparison test. Error bars±SD. TGF-β1 concentration 390pM

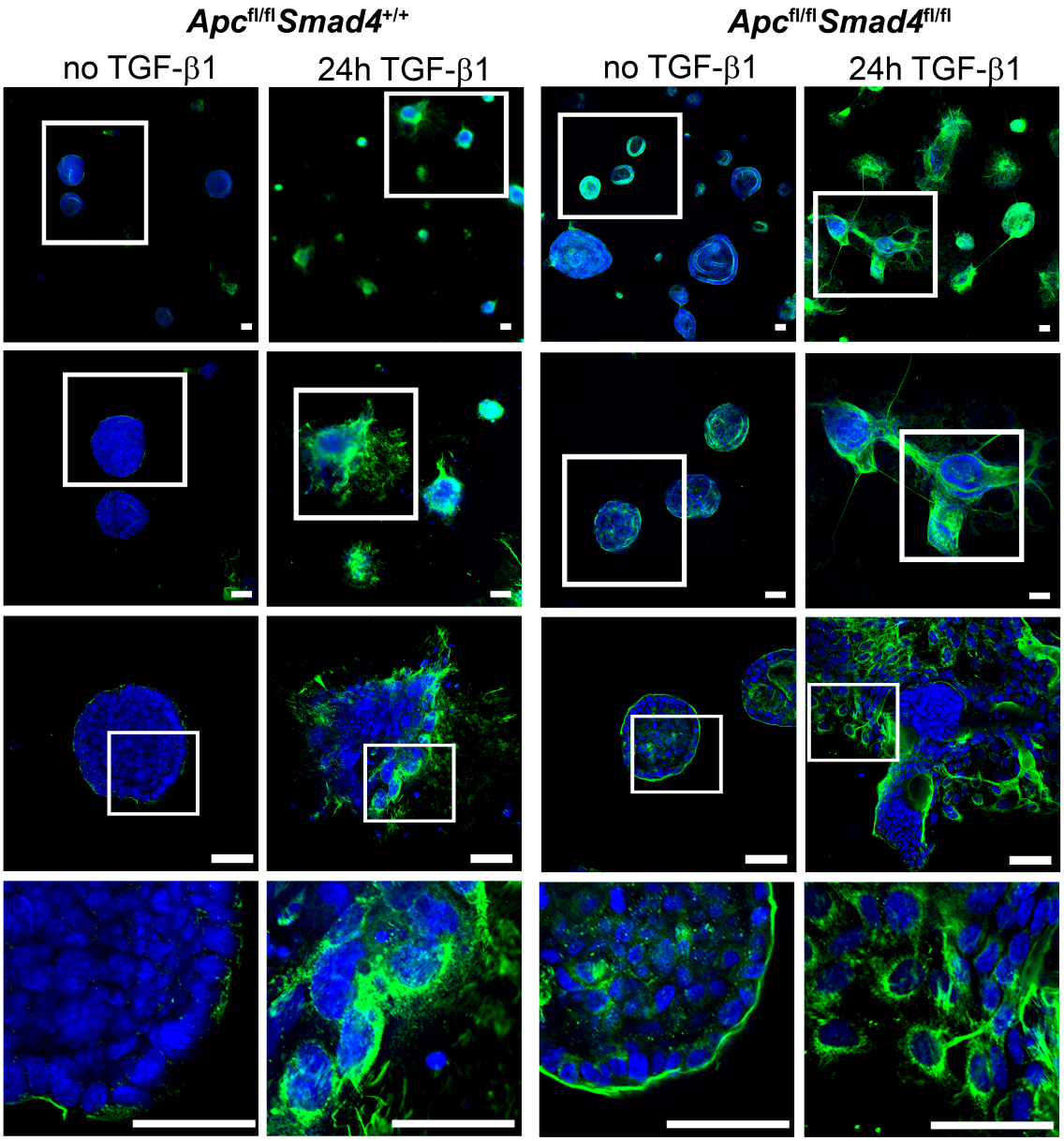

Figure 5.18: **Morphological changes after 24h TGF-β1**. Representative confocal images showing adenomas with morphological changes 24h post 390pM TGF-β1 treatment. Fibronectin is shown in green and nuclei are in blue. White boxes are magnified below each one. Scale bars 50µm.

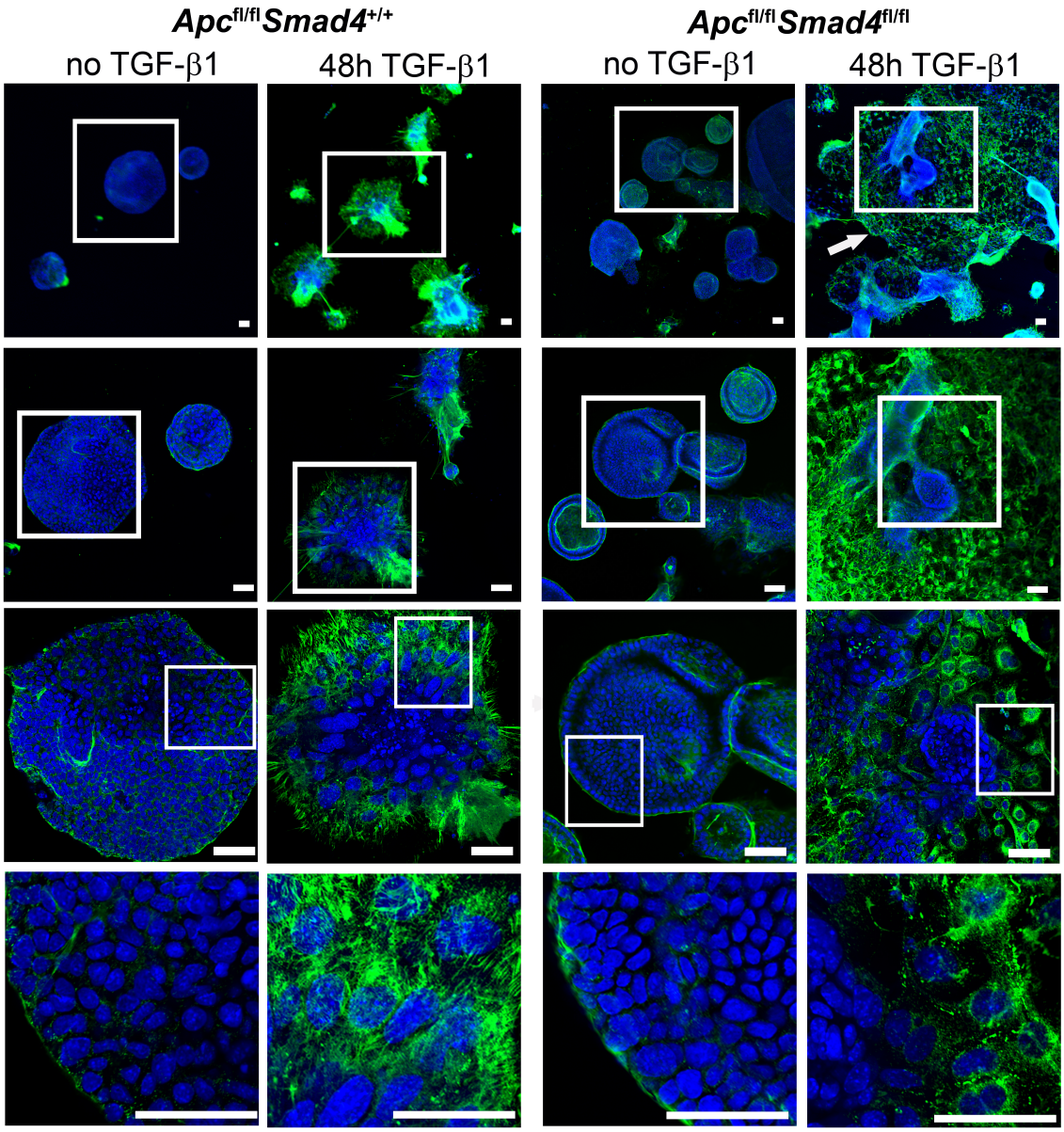

Figure 5.19: **Morphological changes after 48h TGF-β1**. Representative confocal images showing adenomas with morphological changes 48h post 390pM TGF-β1 treatment. Fibronectin is shown in green and nuclei are in blue. White boxes are magnified below each one. Arrow points to migration. Scale bars 50µm.

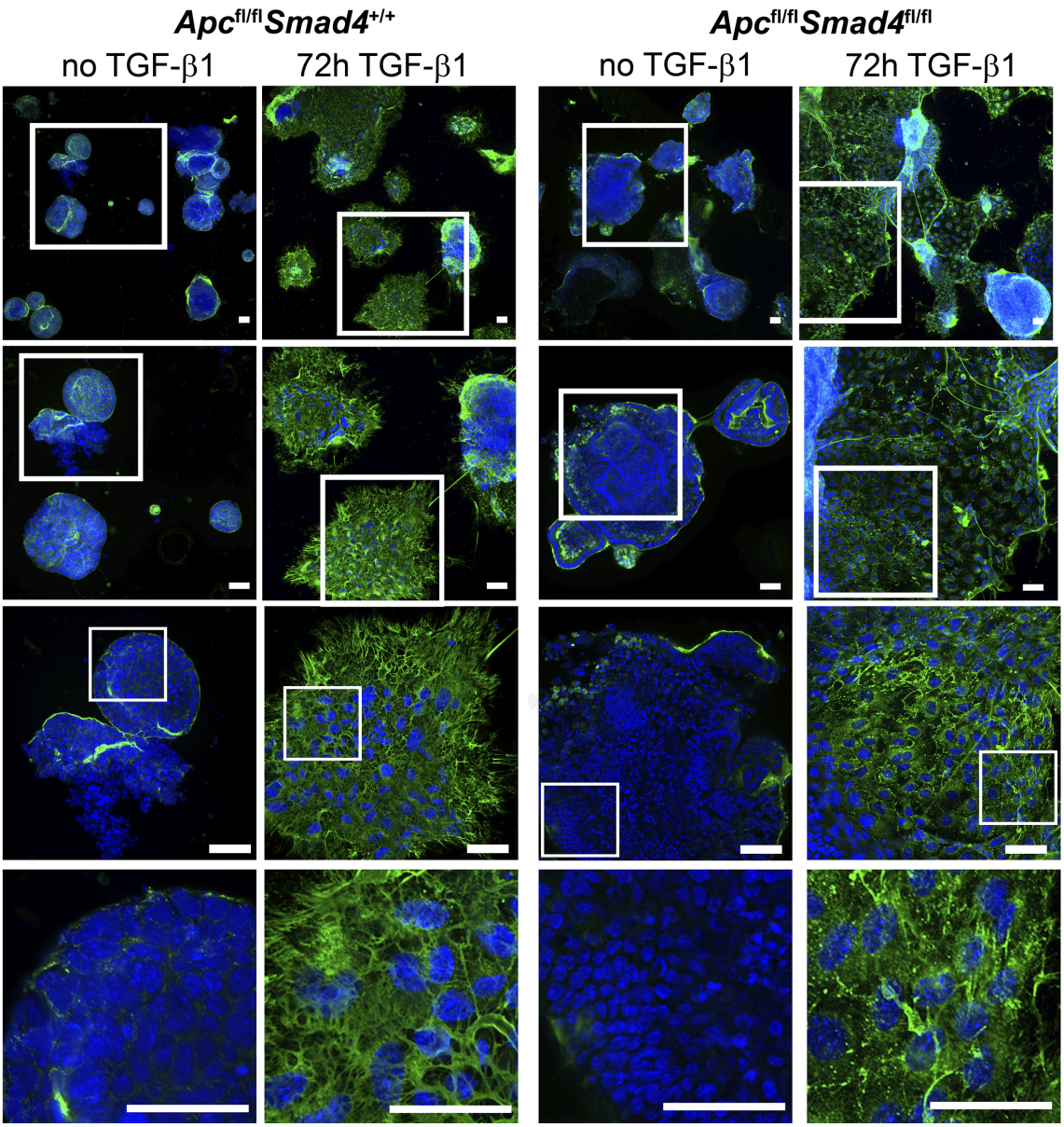

Figure 5.20: **Morphological changes after 72h TGF-β1**. Representative confocal images showing adenomas with morphological changes 72h post TGF-β1 treatment. Fibronectin is shown in green and nuclei are in blue. White boxes are magnified below each one. Scale bars 50µm. TGF-β1 concentration 390pM.

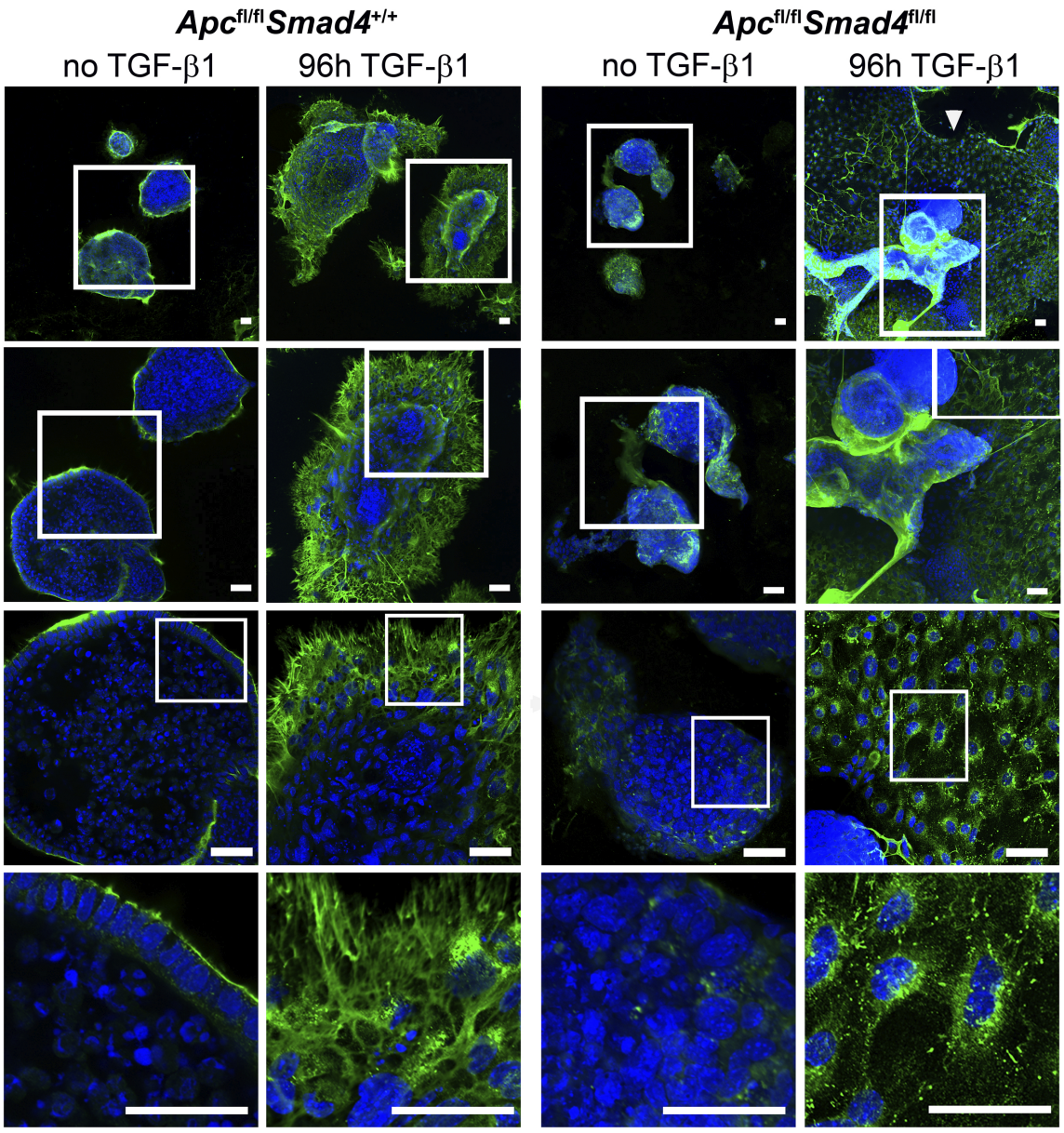

Figure 5.21: **Morphological changes after 96h TGF-β1**. Representative confocal images showing adenomas with morphological changes 98h post TGF-β1 treatment. Fibronectin is shown in green and nuclei are in blue. White boxes are magnified below each one. Arrowhead points to migration. Scale bars 50µm. TGF-β1 concentration 390pM.

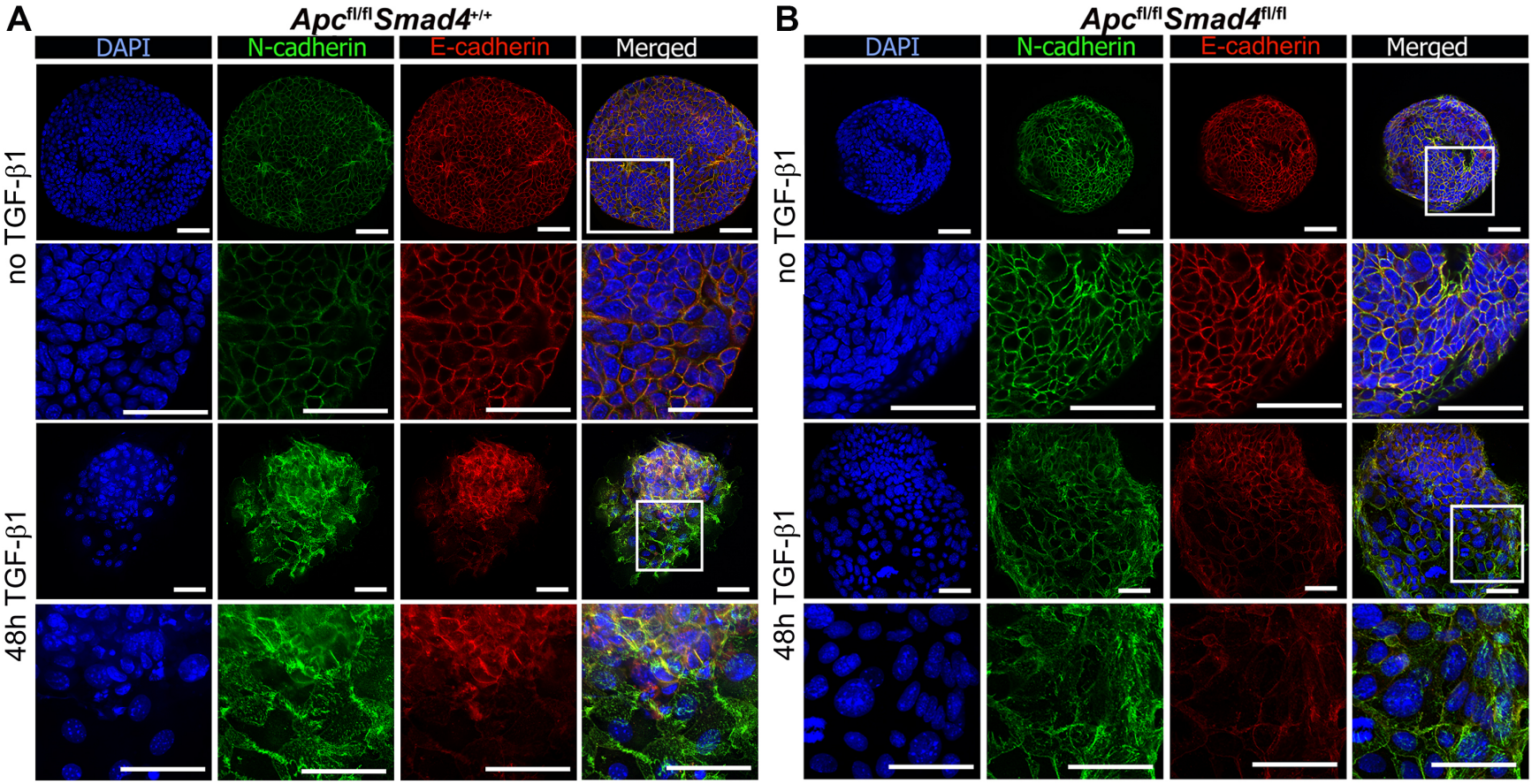

Figure 5.22: **Cadherin switch with TGF-β1.** Representative confocal images showing downregulation of E-cadherin and upregulation of N-cadherin 48h post 390pM TGF-β1 treatment. Magnification of areas marked with white boxes shown in the panel below. Scale bars 50µm.

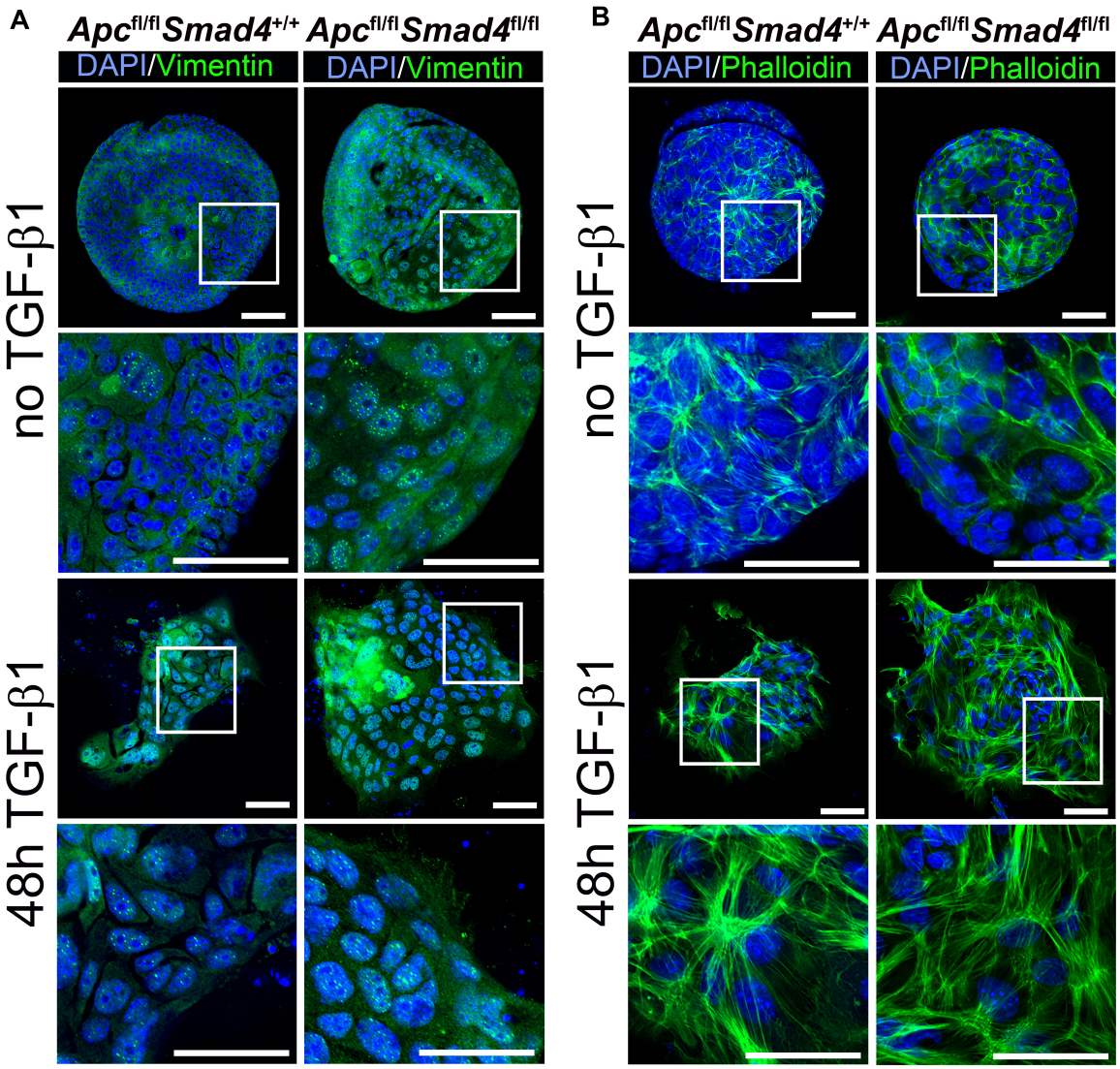

Figure 5.23: **Vimentin and F-actin labelling following TGF-β1 treatment**. (A) Representative confocal images showing vimentin labelling 48hpost 390pM TGF-β1 treatment. (B) F-actin (by phalloidin) labelling 48h post 390pM TGF-β1 treatment. The untreated cells show a peripheral band of actin filaments and polarized epithelial cells, and stress fibers in the treated adenomas. Magnification of areas marked with white boxes shown in the panel below. Scale bars 50µm.

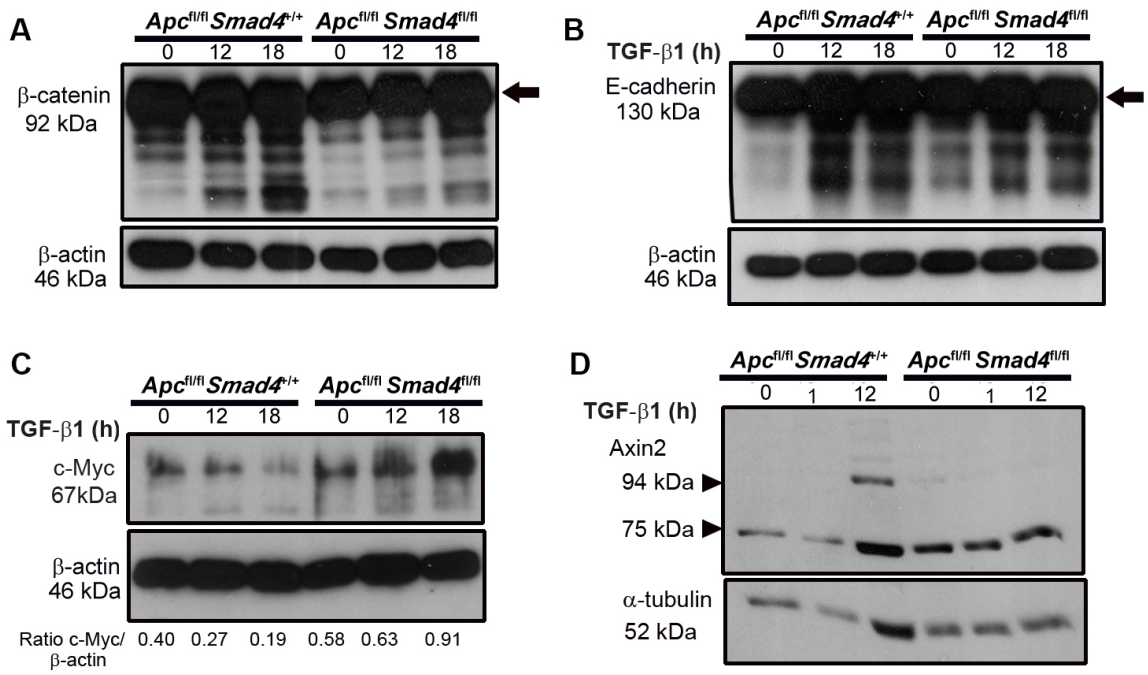

Figure 5.24: **Changes in the expression of Wnt/β-catenin genes by TGF-β1.** Representative western blots showing β-catenin, E-cadherin, c-Myc and Axin2 in both adenomas at different time points following TGF-β1 treatment. (A) β-catenin at 92 kDa (arrow level), multiple bands below (n=3 with similar results). (B) E-cadherin at 130 KDa (arrow level). the bands below are degradation products (n=3 with similar results). (C) c-Myc at 67 KDa. The ratio of c-Myc to β-actin is represented below as determined by densitometric analysis. (n=2, with similar results). (D) Axin2 western blot with 2 bands. The expected bands at 94 KDa and 75 kDa (n=1, exposure time 25 minutes). Loading control: β-actin in A-C, and α-tubulin in D. TGF-β1 concentration 390pM.

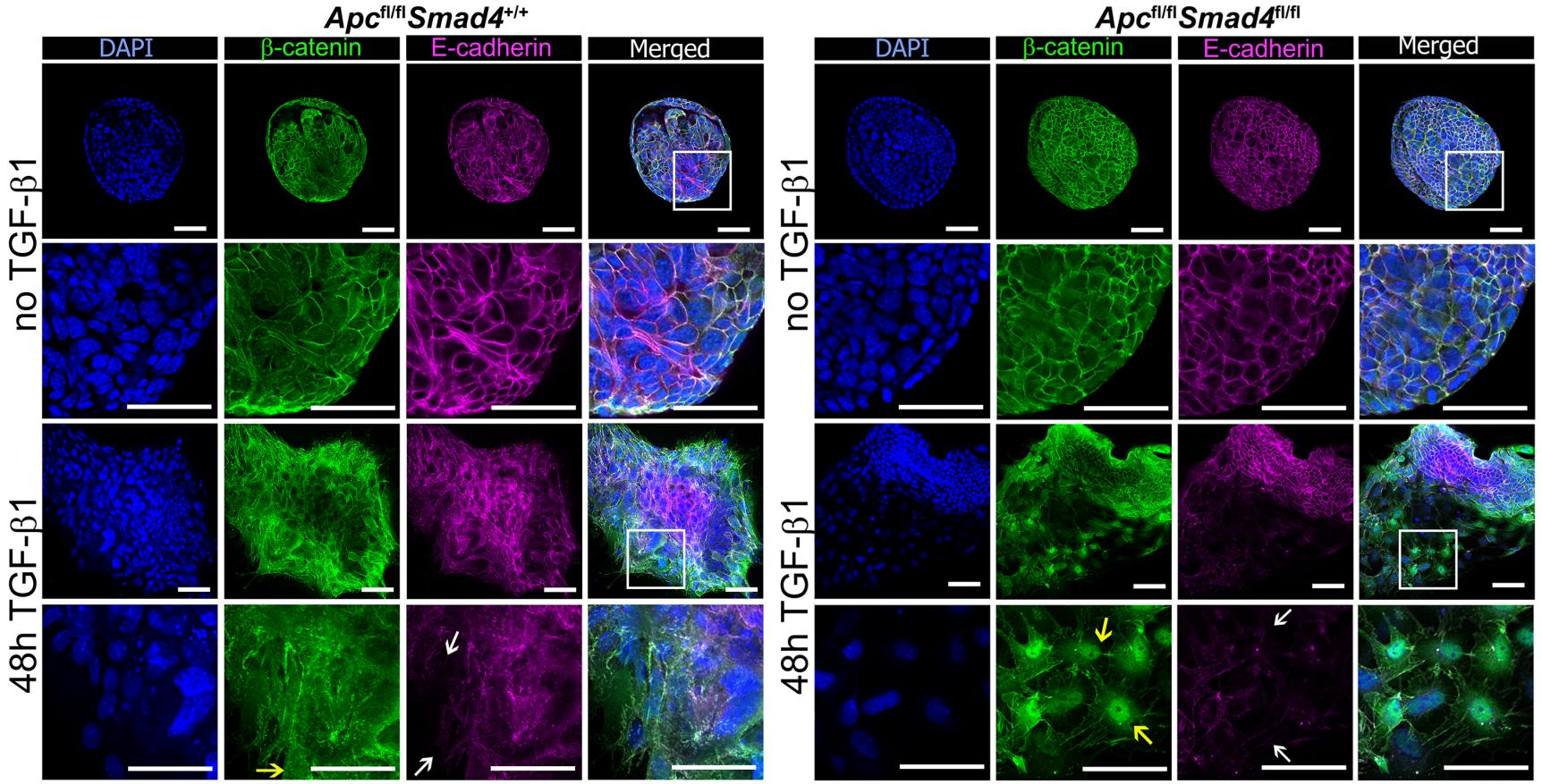

Figure 5.25: **Cytoplasmic and nuclear β-catenin with E-cadherin loss following TGFβ-1 treatment.** Representative confocal images show nuclear and cytoplasmic β-catenin and E-cadherin loss in the transformed adenomas. Yellow arrows point to nuclear β-catenin and white arrows point to E-cadherin loss. Magnification of areas marked with white boxes are shown in the panel below. Scale bars 50µm. TGF-β1 concentration 390pM.

5.5 Discussion

5.5.1 *In vitro* adenomas mimic the *in vivo* adenomas

Data in this chapter shows that Smad4 knockout in culture can be achieved from conditional crypts treated with 4-OHT. Adenomas formed *in vivo* from *Smad4*$^{fl/fl}$ animals can also be cultured (Figure 5.1). Both adenomas are mainly undifferentiated and are highly proliferative. The results also show few differentiated cells (enteroendocrine, goblet and Paneth cells) within the adenomas from both the *Lgr5-CreERT2* or *Villin-CreERT2* models. Muc2 was overexpressed in *Apc*$^{fl/fl}$*Smad4*$^{fl/fl}$*Lgr5-CreERT2* adenomas (Figure 5.2, 5.3).

Adenomas in the 3D culture system behave in a similar way to their *in vivo* counterparts in terms of differentiation and proliferation. A hallmark of Wnt/β-catenin pathway activation is decreased differentiation and increased proliferation. *In vivo* activation of Wnt/β-catenin pathway has been reported to dramatically decrease differentiation into goblet and enteroendocrine cells with commitment toward Paneth cell differentiation with altered position (Sansom et al., 2004; Andreu et al., 2005). Transcription of the Paneth cell markers- lysozymes and cryptdins- is reported to be controlled by β-catenin signalling (Andreu et al., 2005). The presence of few differentiated cells (goblet cells and enteroendocrine cells) within the adenomas was also reported *in vitro* (Sato et al., 2011). More adenomas with Muc2 labelling were seen in *Apc*$^{fl/fl}$*Smad4*$^{fl/fl}$*Lgr5-CreERT2* compared to *Apc*$^{fl/fl}$*Smad4*$^{+/+}$*Lgr5-CreERT2* which could be related to the *Smad4* mutation. Adenomas with mucinous differentiation were reported *in vivo* in *Apc*$^{\Delta 716/+}$*Smad4*$^{+/-}$ mouse model (Takaku et al., 1998).

5.5.2 *Apc*$^{fl/fl}$*Smad4*$^{fl/fl}$ slow growth

The results show that *Apc*$^{fl/fl}$*Smad4*$^{fl/fl}$ adenomas had slow growth. While the slow growth was Noggin independent it was rescued with Y-27632. Moreover, *Smad4*$^{fl/fl}$ adenoma growth was not entirely dependent on EGF. The *Smad4*$^{fl/fl}$ adenoma similar to the *Smad4*$^{+/+}$ adenoma can be cryopreserved after extraction and passaged. The adenomas show a

similar labelling of the Wnt/β catenin genes (Figure 5.4-5.7, A.4).

The slow growth of the *Smad4*$^{fl/fl}$ adenomas could either be a reflection of the reduced burden of the small intestinal tumour *in vivo* or could be related to apoptosis after extraction and seeding. The former is harder to interpret *in vitro* mainly because both the *Smad4*$^{fl/fl}$ adenomas and the *Smad4*$^{+/+}$ adenomas have a similar proliferation as indicated by EdU labelling on D5 (Figure 5.3) and unlike the crypts, growth was Noggin independent (Figure 4.6, 5.4). On the other hand, the slow growth was rescued with Y-27632. The dependency on Y-27632 was transient, suggesting two mechanisms. As discussed in the previous chapter, Y-27632 has an anti-apoptotic effect (Claassen et al., 2009; Martin-Ibanez et al., 2008) and enhances survival and growth of hESCs following dissociation (Watanabe et al., 2007) and cell sorting (Sato et al., 2009, 2011). Moreover, in our lab it enhanced the recovery of cryopreserved adenomas. The possibility that *Smad4*$^{fl/fl}$ adenomas undergo apoptosis after extraction was not obvious before seeding as the percentage of viable cells was 90.1 for *Smad4*$^{fl/fl}$ compared to 89.3 for *Smad4*$^{+/+}$ adenomas. *Smad4*$^{fl/fl}$ adenomas might undergo apoptosis after being seeded in Matrigel. Matrigel is derived from sarcoma tumours meaning that the *Smad4*$^{fl/fl}$ might undergo apoptosis as being seeded in a different microenvironment. As both the *Smad4*$^{+/+}$ and the *Smad4*$^{fl/fl}$ adenomas were from caecal tumours, one would expect that they would behave in a similar way when seeded in Matrigel. The fact that *Smad4*$^{fl/fl}$ adenomas were mucoid (after being excised) and histology showed that they have mucin lakes (results shown in Chapter6, Figure 6.4) might suggest that they were in a different microenvironment even if they are taken from the same anatomical area. Y-27632 enhances the growth of the *Smad4*$^{fl/fl}$ adenomas even without EGF. In the primary culture, EGF was not the major required growth factor for *Smad4*$^{fl/fl}$ growth. This might suggest that the growth of the adenomas is through different pathways. Rho pathway can be activated by cytokine receptors and growth-factor receptors or adhesion to extracellular matrix (McKinsey and Kass, 2007; Buchsbaum, 2007). In human endothelial cells inhibition of Rho-Kinase activates PI3K/Akt pathway (Wolfrum et al., 2004). Moreover, Rho is capable of stimulating PTEN in human embryonic kidney cells and leukocytes (Li et al., 2005). Recently, it has been demonstrated that RhoA inhibition

results in the nuclear accumulation of β-catenin and further activation of the Wnt signalling in SW480/ ADH, SW837 and HCT8/S11 colon cancer cells lines (Rodrigues et al., 2014). Moreover, inactivation of RhoA in the intestine of *Apc*$^{Min/+}$*Vil-CreRhoA*$^{DN/-}$ resulted in reduced survival and increased tumour burden (Rodrigues et al., 2014).

While, Y-27632 is used to enhance the survival of hESCs (Watanabe et al., 2007), one could hypothesise that it might also enhance the survival of the cancer stem cells. There is a possibility that starting culture has less stem cells in Smad4$^{fl/fl}$ compared to Smad4$^{+/+}$ although both cultures started with a similar number of viable cells. Whether the growth of Smad4$^{fl/fl}$ and the number of growing organoids could be similar to that of Smad4$^{+/+}$ adenomas if equal number of stem cells being cultured requires further investigation.

On the other hand, EGF requirement in organoid culture is variable. While mouse adenomas require EGF, most of the human colonic adenomas do not (Sato et al., 2011). In our culture, *Smad4*$^{+/+}$ adenomas require EGF for their growth but EGF has a marginal effect on the growth of the *Smad4*$^{fl/fl}$ adenomas. This suggests that EGF requirement might be variable in the mouse adenoma culture too, mainly if the adenomas have different mutations.

5.5.3 MH1 deletion in Smad4 protein after Cre-mediated recombination

The results show that the mouse model used in this study is directed towards evaluating the effect of Smad4 MH1 domain deletion. The truncated protein was not able to bind the DNA following TGF-β1 stimulation (Figure 5.8).

The mouse model in this study has loxP sites flanking exon 2. While it has been reported that the Smad4 is deleted following Cre-mediated recombination (Chu et al., 2004), the results show that there are different isoforms of *Smad4*, and there is a truncated protein that has a deletion in the MH1 domain with an intact linker and MH2 domain. This truncation prevents Smad4 from DNA binding on TGF-β1 treatment as the MH1 domain is

important for DNA binding (Massagué et al., 2005; Heldin and Moustakas, 2012). Smad4 in these adenomas, as a result of the truncation, also lacks the DNA binding ability as well as NLS. The NLS is important for Smad4 nucleoshuttling (Pierreux et al., 2000). *In silico* analysis showed that the mouse *Smad4* gene has an open reading frame at exon 5 that allows the formation of a truncated Smad4. Such an open reading frame is missing in the human *SMAD4*. The truncated Smad4 protein is stable as it can be detected by western blots in both *Smad4*$^{fl/+}$ and the *Smad4*$^{fl/fl}$ adenomas. However, mutated human SMAD4 in the MH1 domain is phosphorylated by JNK or p38 kinase and then rapidly degraded by Skp1-Cμl-F-box (SCF) E3 complex (Liang et al., 2004). The MH2 domain is required for phosphorylated R-Smad-Smad4 interaction and is the site for binding of many different transcriptional activators or repressors (Massagué, 2012; Gaarenstroom and Hill, 2014). With this mutant many questions arose. What is the signalling pathway in these adenomas in response to TGF-β1 stimulation? What is the effect of TGF-β1 on these adenomas? Is the truncated form of Smad4 functional, can it bind to activated R-Smads?

5.5.4 Nuclear localisation of R-Smad in *Apc*$^{fl/fl}$*Smad4*$^{fl/fl}$ adenomas with TGF-β1 treatment

The results show that TGF-β1 activates Smad2, 3 in both adenomas and that activation can be reduced with TGF-β inhibitors. Smad4 is unnecessary for p-Smad2, 3 nuclear accumulation. In a time dependent manner, a similar response to TGF-β1 in both adenomas is observed. While Y-27632 rescues the slow growth of *Smad4*$^{fl/fl}$, it cannot inhibit TGF-β activation of R-Smad (Figure 5.9-5.11).

Adenomas of both genotypes respond similarly to TGF-β1 stimulation. The gradual accumulation of p-Smad2 in response to ligand stimulation was similar to what has been reported (Pierreux et al., 2000) indicating that the upstream component in the TGF-β pathway is not attenuated in these adenomas either due to *Smad4* or *Apc* mutations and it functions normally in both adenomas. Attenuation in the TGF-β pathway due to rapid fading of p-Smad2 (after 2h) has been reported in PT45 and PANC-1 pancreatic cancer cell

lines due to abnormal type 1 receptor (Nicolas and Hill, 2003). The nuclear localisation of p-Smad2, p-Smad3 in response to TGF-β1 was independent of Smad4 and could be explained by the presence of NLS and NEP in these proteins. It has been reported that Smad3 has NLS that is essential for nuclear localisation in response to TGF-β1 stimulation (Xiao et al., 2000). R-Smad are translocated to the nucleus with importin7, 8 (Xu et al., 2007). Moreover, TAZ has been demonstrated to be important for the nuclear localisation of the complexes and for their stabilisation (Varelas et al., 2008). Nuclear localisation of p-SMAD2, 3 has been reported in different cell lines lacking SMAD4, such as the CRC cell lines VACO-9M and SW480.7, the breast cancer cell line MDA-MB-468, and the pancreatic cell lines BxPC3, Hs766T (Liu et al., 1997; Fink et al., 2003), in SMAD4 knockout cell lines, HaCaT and Colo-375, (Levy and Hill, 2005) and in human lens cell line FHL 124 (Dawes et al., 2009).

Small molecule inhibitors are used widely to study signalling pathways. SB-505124 treatment decreases the level of p-Smads. Y-27632 is not a TGF-β1 inhibitor, it is a RocK inhibitor. It has been used in this study as it enhances growth of the Smad4$^{fl/fl}$ adenomas. Y-27632 has a marginal effect on the level of p-Smad2 indicating that Y-27632 cannot inhibit the canonical TGF-β1 pathway.

5.5.5 The effect of TGF-β1 on *Smad4*$^{+/+}$ and *Smad4*$^{fl/fl}$ adenomas

The results show that in response to TGF-β1 the *Smad4*$^{+/+}$ and *Smad4*$^{fl/fl}$ adenomas undergo apoptosis, decrease in viability, decrease in proliferation as well as upregulation of important EMT markers as assessed by the upregulation of mesenchymal markers fibronectin, vimentin, cadherin switch and cytoskeleton reorganisation and downregulation of adherens junctions. These responses are similar in both adenomas except that *Smad4*$^{+/+}$ adenoma is more sensitive. The cells that acquired an EMT phenotype are caspase negative. The proliferation and migration in Matrigel (indicative of motility) of these cells are variable. The newly formed layer with *Smad4*$^{fl/fl}$ has few proliferative cells and show migration in Matrigel. However, in the *Smad4*$^{+/+}$ transformed adenomas it is very

rare to have proliferative cells, and no migration is observed (Figures 5.12-5.25).

5.5.5.1 TGF-β1 induced growth inhibition in adenomas

In epithelial cells TGF-β1 induces growth inhibition, however, the role of Smad4 was variable between different studies. Moreover, in the context of intestinal tumorigenesis, a pre-malignant lesion exposed to TGF-β1, will undergo apoptosis (Massagué, 2012).

In our adenoma model, where the Smad4 deletion has been verified by RNA-seq and western blots, growth inhibition is in both adenomas as measured by reduced viability (AB reduction), decrease in the percent of proliferative cells and increase in apoptosis as detected by CC3. However, these events occur faster in *Smad4*$^{+/+}$ adenomas indicating that they are more sensitive to TGF-β1. The *Smad4*$^{+/+}$ has a 24.0pM IC50 when TGF-β1 was added on adenoma D2 and 2.7pM when added on D1. IC50 of 2.7pM has also been reported for human mammary epithelial cell line MCF10A (Massagué et al., 1997). The increase in IC50 on D2 is related to differences in cell density (Zi et al., 2012). Moreover, the presence of few EdU and Ki67 positive cells following the treatment might suggest the growth inhibition is partially dependent on Smad4. In agreement with this result, Kretschemer *et al.* showed a partial effect of Smad4 on growth inhibition in HaCaT cells when Smad4 was knocked down (Kretschmer et al., 2003). Growth inhibition was Smad4 independent when Smad4 was knocked down in PANC cells and NIH 3T3 fibroblasts (Jazag et al., 2005; Sirard et al., 2000). However, growth inhibition was Smad4 dependent in HaCaT and Colo-375 and NMuMG breast cancer cells (Levy and Hill, 2005; Deckers et al., 2006). Growth inhibition that is independent of Smad4 might be Smad3 dependent (Kurokawa et al., 1998; Kretschmer et al., 2003). Smad3 induces cell cycle arrest by the expression of different cell cycle inhibitors, for example, p21^{Cip1} (Ijichi et al., 2004), p16^{Ink4a} and p19^{Arf} in response to TGF-β1 (Vijayachandra et al., 2009).

Recently, a similar work using intestinal organoid culture reported that intestinal organoids harbouring mutations in the *Apc* gene undergo apoptosis in response to TGF-β1 by acti-

vating the p38 and Smad signalling pathways that leads to up regulation of Bim expression (Wiener et al., 2014). The effect of Smad4 has not been evaluated in this study but KRas mutation has been. Organoids having Apc-Kras mutations partially inhibit apoptosis in response to low doses or completely by high doses or long duration of TGF-β1 by activating the ERK1/2 pathway and by preventing Bim expression (Wiener et al., 2014).

Thus, the variation could be related either to the method used, to context and/or the presence of other mutations in the used cell lines. However, in our adenoma model although the effect was partial, there is a possibility that it could be related to the concentration used and such effect might not be seen with lower concentrations (Figure 5.12). The partial effect and the presence of few Ki67 positive cells after 72h of TGF-β1 (Figure 5.14) in this study could be also related to culture method. The adenomas are growing as organoids with heterogeneous cells, within these cell, cancer stem cells reside. Thus, one could hypothesise that these cancer stem cells are resistance to the cytostatic and apoptotic effect of TGF-β1. The persistence of these cells might be necessary for fuelling more cells that are resistance to TGF-β1 and are important for the tumour promoter effect of TGF-β.

5.5.5.2 Smad4 is not required for EMT

The requirement of Smad4 in EMT is also variable among different studies. In our adenoma model, EMT was not dependent on Smad4 although it was faster with Smad4. Smad4 knockdown in BxPC3 and Capan-2 cells results in EMT that was enhanced in the presence of Smad4, a process related to ERK activation (Zhao et al., 2008). Also, Smad4 was not required for EMT in HaCaT and Colo-375 (Levy and Hill, 2005). Moreover, the induction of fibronectin in mouse fibroblasts was Smad4 independent (Sirard et al., 2000). Fibronectin expression in response to TGF-β is one of the early known effects (Ignotz and Massague, 1986). Induction of fibronectin in response to TGF-β1 in the human fibrosarcoma HT1080-derived cell line requires activation of JNK- a member of the MAPK kinase family- which modulates the activity of c-Jun and ATF-2 in a Smad4-independent manner (Hocevar et al., 1999). In ductal adenocarcinoma, TGF-β1 induced EMT was Smad4 inde-

pendent, and Smad3 knockdown suppressed EMT (Yamazaki et al., 2014). In a study that included different epithelial cells such as mammary, lung epithelial cells and keratinocytes, EMT was dependent on Smad4 in response to all TGF-β isoforms (Valcourt et al., 2005) together with Smad4 dependent EMT in NMuMG cells (Deckers et al., 2006).

An important step as a consequence of EMT is invasion, migration and motility. In our adenoma model, as the cells were growing in Matrigel, this phenomena was very clear (Figure 5.13, 5.19-5.21) suggesting that invasion and motility is inhibited in the presence of Smad4. The dependency of migration on Smad4 was also variable among different studies. Consistent with the role of Smad4 in inhibiting migration, Smad4 re-expression in SW480 (Pohl et al., 2010) and SW620 (Zhang et al., 2010) inhibited invasion. A mechanism related to ERK activation in response to TGF-β1 which inhibit Stat-3 phosphorylation at Tyr705 (Zhao et al., 2008). Motility was inhibited in HaCaT cells expressing Smad4 (Kretschmer et al., 2003). Moreover, and in the context of BMP pathway, migration, invasion, and formation of invadopodia in HCT116, HT-29, SW480 cells was related to Smad4 mutations due to the activation of Rho/Rock signalling pathway (Voorneveld et al., 2014). On the other hand, Smad4 dependent migration has been reported in HaCaT and Colo-375 cells (Levy and Hill, 2005) and in PANC cancer cell line (Jazag et al., 2005). Taken together, the variable requirements of Smad4 for EMT could be context dependent and might be regulated by different pathways. In addition the variable outcome of the studies might be related to different mutations in the cell line under investigation in addition to the efficiency of Smad4 knockdown.

5.5.5.3 Effect of TGF-β/Smad4 on the Wnt/β-catenin pathway

The results show loss of the adherens junction in both of the adenomas that is independent of Smad4. Moreover, cytoplasmic and nuclear β-catenin are present. TGF-β1 treatment has different effects on c-Myc and Axin2 (Figure 5.22, 5.25- 5.24).

Loss of the adherens junction is one of the EMT markers (Lamouille et al., 2014). It is

characterised in these adenomas by degradation, loss of E-cadherin and cadherin switch. In addition, β-catenin is cytoplasmic and nuclear in the transformed adenomas. The multiple bands in β-catenin western blots might indicate a degradation of β-catenin from the adherens junction or they might be a reflection of the cytoplasmic and nuclear β-catenin that are involved in upregulating Wnt/β-catenin signalling. This is related to the fact that β-catenin has two distinct functions; it is part of the cell-cell adhesion complexes and is therefore localised to the plasma membrane; it is an effector for the Wnt/β-catenin signalling pathway (Orsulic and Peifer, 1996). On the other hand, loss of E-cadherin prevents sequestration and binding of β-catenin, leading it to degrade or allowing it to feed into the nucleus and activate Wnt signalling (Thiery and Sleeman, 2006; Lamouille et al., 2014). This mechanism might be supported by a recent report about Wnt pathway activation. When Wnt is active, the degradation of β-catenin is inhibited since all the intact degradation complex binds to phosphorylated LRP and is still capable of binding and phosphorylating β-catenin until saturation after which β-catenin cannot bind. Newly synthesised β-catenin accumulates in the nucleus (Li et al., 2012; Clevers and Nusse, 2012). Therefore, it might be the dissolution of β-catenin released from the adherens junction feeding into the Wnt pathway. c-Myc might be differentially regulated by Smad4. Downregulation of c-Myc in the *Smad4*$^{+/+}$ is a further confirmation of decrease in viability and proliferation. The downregulation of c-Myc by TGF-β is mediated by the Smad3/4 pathway (Massagué, 2008). With organoid culture a definite answer about the effect of TGF-β/Smad4 on the Wnt pathway is not easy to achieve using Luciferase reporter assays. The use of a CRC cell line that has mutations in *Smad4* similar to our model was considered.

In summary, the work presented in this chapter using organoid culture more closely related to the *in vivo* situation, showed a slow growth with variable growth requirements in the different genotypes. In addition, it showed that growth inhibition was partially dependent on Smad4. EMT in response to TGF-β1 are Smad4 independent although the presence of Smad4 might accelerate the process. It also shows an effect on the Wnt pathway mainly by downregulating c-Myc. As has been discussed earlier, there were some similarities between studies and some differences. Consequently, the role of Smad4 in the context of

intestinal tumorigenesis and the switch from the tumour suppressor effect of TGF-β to a tumour promoter is still unclear. The switch could be related to TGF-β/non-canonical branch of the pathway or could be related to TGF-β/Smad2,3 pathway or cross talk between them. With the aim of understanding the dogma of TGF-β and to interrogate the transcriptome using this genetically pure system with no additional mutations apart from the initiation step, the *Apc* mutation, and *Smad4*, RNA-seq and microRNA-seq were performed and will be presented in the following chapter. In addition to that, a complementation study using Colo205 CRC cell line was considered and the initial steps will be presented.

Chapter 6

RNA-seq and microRNA-seq

6.1 Introduction

Functional analysis described in the previous chapter showed that *Smad4*$^{fl/fl}$ adenomas grow more slowly than *Smad4*$^{+/+}$, and the slow growth can be rescued with the Rock inhibitor, Y-27632. Partial inhibition of cell growth was induced with TGF-β1 when Smad4 was deleted. Smad4 is not required for EMT induced by TGF-β1 and migration was observed in *Smad4*$^{fl/fl}$ adenomas growing in culture. As has been discussed earlier, the results obtained in this study were in agreement with some studies in certain phenotypes and not with others. This was not surprising as it is well accepted that TGF-β acts in a context dependent manner (Massagué, 2012) and different studies used different cell lines and approaches to abrogate or induce Smad4 expression.

Smad transcription factor (TF) binds to the promoter of target genes and differentially regulates their transcription in the presence or absence of TGF-β1 (Lim and Hoffmann, 2006; Heldin and Moustakas, 2012). Cross-talk between TGF-β and the Wnt pathway also exists, partly because both can bind to LEF1/TCF TF (Attisano and Wrana, 2013). A unique transcriptional profile for co-stimulation of the two pathways together has been reported (Labbé et al., 2007) (detailed below). Gene expression is also controlled by microRNA (miRNA) and the function of the TGF-β pathway could be modulated by miRNA. How the transcriptome changes according to Smad4 status is still unknown. Understanding the contribution of Smad4 to the pathogenesis of CRC and how this affects the transcriptome is of great importance for targeted therapy. In line with this, the difference in transcriptome profiling

in response to TGF-β1 on intestinal adenomas based on Smad4 status is also important. This chapter is to evaluate whole-transcriptome profiling using RNA-seq and miRNA-seq from a pure genetic model. In this model, the *Apc* and *Smad4* genes are deleted and RNA was extracted from intestinal organoid culture under defined conditions.

6.1.1 Smad DNA-binding and transcription regulation

Smad bind to a DNA motif, CAGAC, known as the SBE (Massagué, 2012). The affinity of Smads to a single SBE *in vivo* is low and cannot support Smad complex binding (Shi et al., 1998). This low affinity can be enhanced *in vitro* by multiple SBEs (Zawel et al., 1998). *In vivo*, the complex is enhanced by binding to different DNA-binding factors as it is rare to have multiple copies of SBE (Seoane et al., 2004; Massagué et al., 2005). FAST1 or FoxH1 was the first identified partner that binds to activated Smad2-Smad4 complexes in the promoter of the *Xenopus laevis Mix2* gene in response to activin-like members of the TGF-β (Chen et al., 1996, 1997). These transcription factors contain a proline-rich Smad interaction motif (SIM) which bind to the MH2 domains of Smad2 and Smad3 (Germain et al., 2000; Randall et al., 2002). In addition to SBE and the cofactors, Smad3 and Smad4 require a CCAG-motif 3' of the SBE for binding (Inman and Hill, 2002). Other partners also exist, for example, activating transcription factor 2 (ATF2), Sp1, Jun and transcription factor E3 (TFE3) (Heldin and Moustakas, 2012). The transcriptional repressor, ATF3, is another partner. It is an early response gene in the TGF-β pathway (Massagué et al., 2005). ATF3 could be induced from JNK and p38 pathways and in response to TNF-α (Massagué et al., 2005). Smad1 and Smad5 bind to GC rich elements in addition to SBE (Korchynskyi and ten Dijke, 2002; Massagué, 2012). Thus binding to DNA is determined by different SBE and different DNA partners (Massagué, 2012). The diversity in partners and cofactors generates a differential Smad transcriptional response that is also context dependent (Gaarenstroom and Hill, 2014).

To regulate gene expression, Smads either help in chromatin remodelling or gain access to loci that are repressed by histone markers (Massagué, 2012). TF binds either to the

promoter or distal elements such as enhancers. Although there is overlap in the binding of Smad2 and Smad3 to the DNA, ChIP-Chip (chromatin immunoprecipitation (ChIP) with DNA microarray (Chip)) showed there are some areas where only Smad4 binds and some areas are for Smad2, 3 binding. Smad4 binding sites were found to be far from the transcription start sites (TSS) where as Smad2,3 binding sites are near the core promoter (Koinuma et al., 2009). Binding of TF to DNA either results in expression or repression of target genes directly by controlling the gene transcription machinery or indirectly through the recruitment of chromatin remodelling enzymes (Fuda et al., 2009; Gaarenstroom and Hill, 2014). To stimulate transcription, Smads recruit the histone HATs p300/CBP to chromatin leading to acetylation of histone H3 on different sites. They can inhibit gene expression by binding to partners such as TGIF1 which recruits the repressor CTBP which in turn binds to histone deacetylases (HDAC1) (Massagué, 2012). In addition Smads recruit the SWI/SNF nucleosome repositioning complex that help in chromatin remodelling (Xi et al., 2008).

6.1.2 Crosstalk between TGF-β and Wnt/β-catenin pathways

The TGF-β/Smad pathway and Wnt/β-catenin pathway can interact and assemble on a common DNA binding partner, Tcf/Lef1 to cooperatively induce expression of genes that control cell fate (Attisano and Wrana, 2013). For instance, Smad4 binds to Tcf/Lef1-binding element (TBE1) on the *c-Myc* promoter and activates its transcription in the absence of TGF-β1 in tumour cells. The binding is decreased with TGF-β1 stimulation due to the binding of E2f4/5 and p107 to the TGF-β inhibitory element (TIE) in the *c-Myc* promoter which results in *c-Myc* repression. Smad4 knockdown reduces *c-Myc* expression in these cells (Lim and Hoffmann, 2006). Recently, it has been reported that T-cell proliferation is dependent on Smad4 activation of c-Myc in the absence of TGF-β1 (Gu et al., 2015).

A study was performed to evaluate the crosstalk effects on gene expression in the two pathways by co-stimulation of epithelial cells with Wnt3a and TGF-β1. It showed that the effect was not simply a sum of the individual responses, however, the ligands both posi-

tively and negatively modified gene responses in these pathways (Labbé et al., 2007). For example an additive effect on gene expression was observed for *Ankrd1, Axin2, Cav1, Ccnd1, Cpe, Ctgf, Cyr61, Dusp1, Edn1, Gpc1, Hs6st2, IL11, Inhba, Mmp14*, and *Tmsb4x*. Some were induced with Wnt3a and suppressed with TGF-β1 such as *Bag1, Ccna2, serpinb*, and *Spp1*. Other were induced with TGF-β1 and repressed with Wnt3a, for example *Ass1, Bmp1, Dok2, Fbln2, Gadd45g, Lamb3, Msn, Pdgfa, Ptgs2*, and *Serpine1*. Genes such as *Ctsc, Hrmt1l2, Nfat5*, and *Thbs1* were shown to be Wnt target genes. Others were induced in response to TGF-β1, for instance, *Anxa8, Bace, Bhlhb2, Cd81, Furin, Igfbp7, Itgb1, Tm4sf2* and *Zyx* (Labbé et al., 2007). This study was based on ligand stimulation and did not show the crosstalk between pathways in the presence of mutations. How the profile is affected when there is mutation in these pathway is still unknown.

6.1.2.1 MicroRNA

MicroRNAs (miRNAs) are small non-coding RNA molecules, 19-25 nucleotides long (Butz et al., 2012). They are involved in post-transcriptional regulation of gene expression by binding to the 3'-UTR or 5'-UTR or the coding sequence of protein-encoding mRNAs (Butz et al., 2012). They can be used as biomarkers for early diagnosis of cancers and other diseases. They can also be targeted with pharmaceutical targets (Kim et al., 2012).

The TGF-β1 target genes are regulated by miRNA at multiple levels and patients with CRC have upregulation of different miRNAs (Butz et al., 2012; Yang et al., 2013). For instance, upregulation of miRNA-106b, miRNA-93 and miRNA-25 result in loss of TGF-β1 induced growth arrest and apoptosis effect by targeting $p21^{CIP1}$ and BIM in gastric cancer. These miRNA also affect the core TGF-β pathway- TGF-βR2, SMAD2, SMAD4-molecules (Butz et al., 2012). With TGF-β3 treatment there is repression of miRNA-145 in murine mesenchymal stem cells leading to differentiation through Sox9 regulation (Yang et al., 2011). Upregulation of miRNA-21 in tubular epithelial cells in response to TGF-β1 in Smad3 dependent way leads to renal fibrosis (Zhong et al., 2011).

CRC patients showed upregulation of miRNA-21 and miRNA-106 in stool samples compared to normal individuals (Yang et al., 2013). miR-483 from colon organoid culture showed to be dominant driver oncogene at the IGF2 11p15.5 CRC amplicon and is associated with tumorigenesis (Li et al., 2014). Whether miRNA is associated with intestinal tumorigenesis when Smad4 deleted is unknown.

6.1.3 RNA-seq

RNA-seq is a recently developed approach for transcription profiling that uses deep sequencing technologies. It is a quantitative method which doesn't have an upper limit for quantification and very low (if any) background signal. It is not restricted to detecting transcripts that correspond to existing genomic sequence (Wang et al., 2009; Tachibana, 2015). Results obtained from RNA-Seq show high levels of reproducibility, for both technical and biological replicates (Wang et al., 2009). These advantages make RNA-seq superior to DNA microarrays which are based on hybridization approaches and lack sensitivity for genes expressed either at very low or high levels and therefore have a much smaller dynamic range (one-hundredfold to a few-hundredfold) (Wang et al., 2009). In addition to gene expression quantification, RNA-seq can be used to detect alternative splicing (Pan et al., 2008), detection of gene fusion (Maher et al., 2009), discovery of novel genes (Denoeud et al., 2008) and can detect isoforms (Trapnell et al., 2012).

RNA-Seq is based on converting ribosomes depleted of RNA into a library of cDNA fragments with adapters attached to one or both ends. Each molecule is then sequenced in a high-throughput manner. Single-end sequencing is obtained for sequencing from one-end, and pair-end reads are obtained for sequencing from both ends. Pair-end sequencing increase mapping accuracy and provide information useful for isoform detection (Wang et al., 2009; Trapnell et al., 2012). Sequence reads are then counted and mapped to a reference genome (section 6.3.3) (Wang et al., 2009).

6.2 Rationale for the study

Understanding and quantifying the transcriptome is of great importance for interpreting the functional elements of the genome and changes in gene expression under certain conditions. Using RNA-seq and miRNA-seq on adenoma samples that differ only in Smad4 status, the aims of this chapter are:

1. To identify differentially expressed genes (DEG) in *Apc*$^{fl/fl}$*Smad4*$^{fl/fl}$ compared to controls at the basal level
2. To detect early and late response genes following TGF-β1 treatment in the *Apc*$^{fl/fl}$*Smad4*$^{+/+}$ and *Apc*$^{fl/fl}$*Smad4*$^{fl/fl}$ adenomas
3. To identify differentially expressed Smad4 target genes in response to TGF-β1
4. To detect the effect of miRNA on *Apc*$^{fl/fl}$*Smad4*$^{fl/fl}$ adenomas compared to controls at the basal level and in response to TGF-β1
5. To validate some of the RNA-seq results

6.3 Materials and methods

6.3.1 Adenoma culture and passage

Adenoma culture was detailed in section 2.5 and summarised in Figure 4.1 and 4.2.

6.3.2 RNA experiment preparation

RNA preparation was detailed in section 2.10. Biological replicates, treatment, controls and sequencing platform used in this experiment are shown in Figure 6.1.

6.3.3 RNA analysis

RNA-seq analysis was all performed by Dr. David Barnes except for gene ontology analysis.

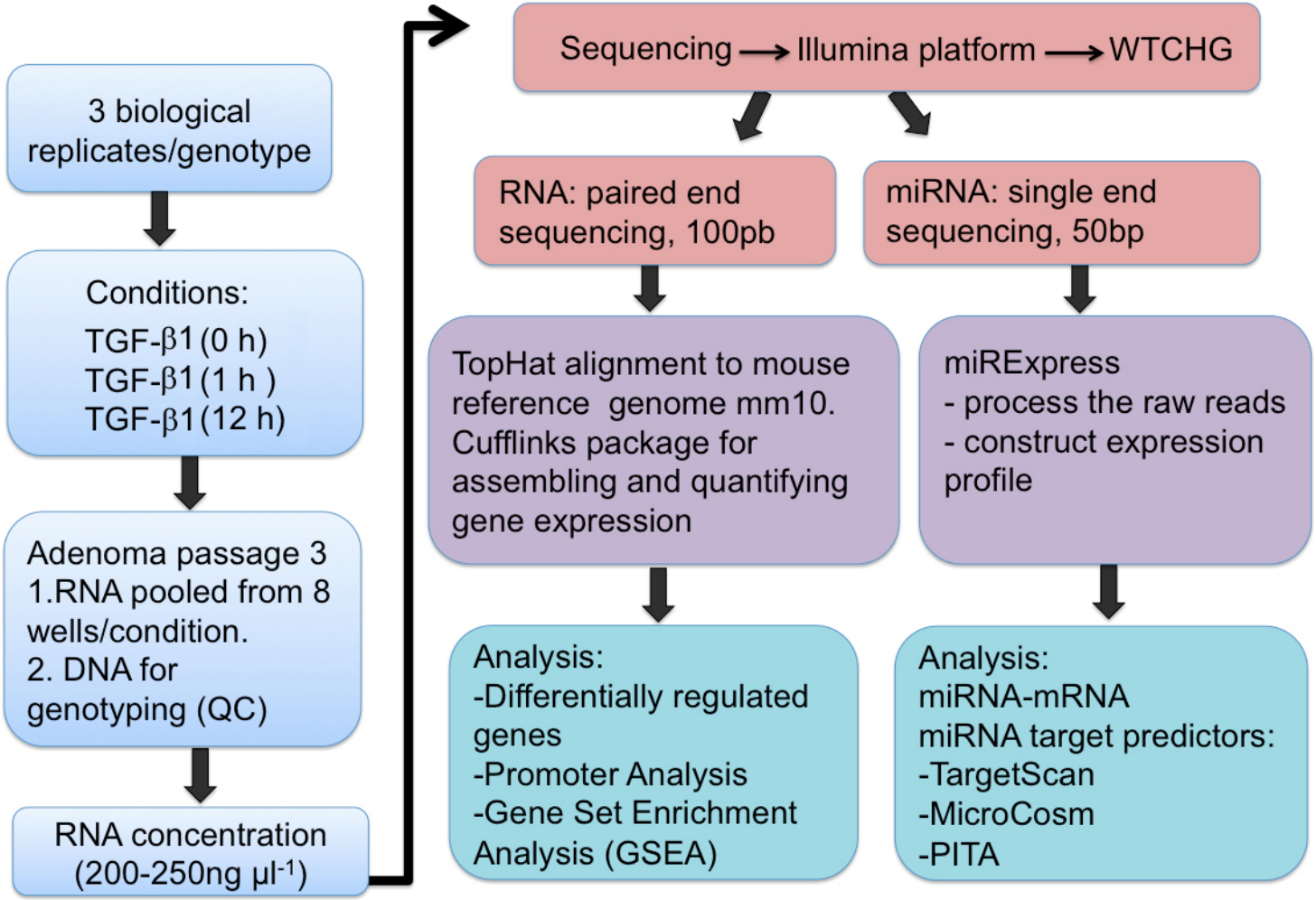

Figure 6.1: **Flow chart summarises the different steps conducted for the RNA-seq and miRNA-seq experiments.** Diagram shows the samples, conditions, sequencing and analysis involved in RNA-seq and miRNA-seq experiments.

Analysis of RNA-seq data was done using the 'Tuxedo' pipeline which consists of the programs: TopHat, Bowtie2, Cufflinks, Cuffmerge, Cuffquant, Cuffdiff and the cummeRbund R package (Trapnell et al., 2012). Raw Fastq reads were aligned to the reference mouse genome (build mm10, made available by Illumina as part of the 'iGenomes' release) using TopHat which, in turn, calls Bowtie2 as the Burrows-Wheeler algorithm aligner. Output from this procedure consists of a bam file for each sample consisting of 'accepted hits', *i.e.* reads which could be successfully aligned with the mm10 genome. In order to quantify abundance of each transcript, the bam files were supplied as input to Cufflinks, which generates a transcript.gtf file for each sample. Cufflinks assigns reads to known transcripts and normalizes expression to transcript length by converting read counts to fragments per kilobase per million mapped read (FPKM) values. To permit comparisons of expression between samples, the individual transcript.gtf files were input to Cuffmerge to generate a single merged gtf file, which was then passed as input to Cuffquant to recalculate expression values using all of the data in the merged file. Statistically significant differences in transcript expression were identified by passing the output of Cuffquant to Cuffdiff, which calculates the Jensen-Shannon distance and a probability, *P*-value, for this statistic, for each pairwise comparison of sample conditions. Cuffdiff performs Benjamini-Hochberg correction for multiple hypothesis testing and annotates transcripts as being significant ('yes') if *P* is greater than the calculated false discovery rate (FDR) for the test statistic. Exploratory data analysis and visualisation was done using the R package, cummeRbund. Heat maps for the 50 most significantly different gene transcripts (criteria was the 50 lowest *P* values) were generated for each pairwise comparison of sample conditions and differential isoform usage was investigated by inspecting isoform expression plots for genes of interest.

6.3.4 Rationale for using Gene Set Enrichment Analysis

Gene Set Enrichment Analysis (GSEA) is a 'knowledge-based' approach for interpreting whole-transcriptome expression data (Subramanian et al., 2005). Prior knowledge, in the form of curated gene sets, is used to inform the analysis. Each gene set contains genes

which are related to each other by a biologically meaningful relationship. These gene sets are maintained in the Molecular Signatures Database v5.0 (MSigDB) at the Broad Institute (www.broadinstitute.org/gsea/msigdb/index.jsp) and are currently organised into 8 collections (H, C1, C2, C3, C4, C5, C6 and C7). Proponents of GSEA argue that it overcomes many of the problems associated with the use of 'classical' statistical tests. Limitations of a purely statistical approach include: (i) there may be only a tiny proportion of genes, or even no genes, which satisfy the criteria for statistical significance after multiple hypothesis testing, (ii) alternatively a long list of genes may be obtained with disparate biological functions and no unifying theme, (iii) there may be failure to identify subtle changes in expression within a pathway which may have greater biological relevance than larger fold-changes in unrelated pathways and (iv) there is often limited reproducibility, or overlap, of statistically significant genes in studies reported by different groups.

6.3.4.1 Gene Set Enrichment Analysis as applied to the RNA-Seq data from this project

In this project, input 'gct' files for GSEA were generated using the FPKM expression values reported by cummeRbund (Trapnell et al., 2012). Genes in the gct file were ranked by the GSEA program according to these expression values and gene sets from MSigDB were assigned enrichment scores that reflect the degree to which each set is overrepresented at the top or bottom extremes of the ranked gene list. Each enrichment score is calculated by 'walking down' the ranked gene list, increasing a running sum when a gene is found in the gene set and decreasing it when genes not in the gene set are encountered. A plot of the running sum for a gene set reveals that it increases to a maximum deviation from zero and then decreases subsequently for the remainder of the genes in the set. The leading-edge subset of genes is formally defined as those genes in a gene set which appear in the ranked list at, or before, the point at which the running sum reaches its maximum deviation from zero. Genes in the leading-edge subsets are those genes which contribute the 'core enrichment' signal. In all analyses in this project, genes annotated by the GSEA program as being leading-edge core enrichment genes for the 20 most significant gene sets (the de-

fault report setting) were extracted for special consideration. Leading-edge set genes were ranked according to the number of gene sets in which they were included in order to identify the most functionally relevant genes. Enrichment scores were normalized for multiple hypothesis testing and a FDR q-value was calculated for each gene set. Gene sets were not excluded if they had high q-values as an FDR as high as 0.25 is still considered significant for GSEA (www.broadinstitute.org/cancer/software/gsea/wiki/index.php/FAQ) and high FDR in the context of this analysis can occur when the biological signals are subtle. Promoters from leading-edge set genes (1 kb 5' to transcription start site) were exported from cummeRbund and were analysed using PScan for transcription factor binding sites (TFBS) that were significantly overrepresented (Zambelli et al., 2009). From the lists of significant TFBS ($P<0.05$), transcriptional network diagrams were generated using Graphviz (www.graphviz.org). When interpreting the data by GSEA, the aim was to use the statistics as a guide for exploring and discovering patterns in the transcriptome data in order to generate hypotheses for further testing.

Leading-edge genes were used to identify the common genes between the different sets with FDR<0.25. Gene ontology (GO) for functional prediction of these genes were identified using GeneMANIA (http://www.genemania.org/). GeneMANIA is open source software and is a Cytoscape app that allows the construction of a network from a gene list (Montojo et al., 2014).

6.3.4.2 MiRNA-seq analysis

Analysis of miRNA expression was done using miRExpress (Wang et al., 2009). Briefly, raw fastq reads output from an Illumina HiSeq 2000 were supplied as input to miRExpress, which trims adapter sequences from the reads before aligning them to known miRNAs in the miRBase database. Expression for each miRNA was then calculated, within miRExpress, from the sum of read counts. The alignment criteria for a valid read were that the read must equal the length of the miRNA and must have 100% alignment to the sequence of the miRNA. Mean miRNA expression was then calculated from the replicate expression

values for each sample.

To identify potential targets of express miRNAs, an integrated analysis was done using the miRNAmRNA R package (van Iterson et al., 2013). Briefly, an FPKM matrix containing expression values for all gene transcripts under all of the sample conditions was exported from cummeRbund and was used as the input in miRNAmRNA for mRNA targets. A matrix was generated from the output of miRExpress, by combining multiple tables for each sample, and was used as the miRNA expression input for miRNAmRNA. Statistically significant miRNAs were identified by miRNAmRNA using the 'global test' (P<0.05) and potential targets for these miRNAs were reported by the program using curated data from three databases (TargetScan, microCosm and PITA). Tables and expression plots were generated using the appropriate output functions in miRNAmRNA.

6.4 Results

6.4.1 Differentially expressed genes at the basal level in *Apc*$^{fl/fl}$*Smad4*$^{fl/fl}$ adenomas

RNA-seq data showed that there were 21514 genes expressed (FPKM>0) and 4960 genes were not expressed (FPKM=0) in both genotypes. 1058 genes were expressed in *Smad4*$^{+/+}$ adenomas but were not expressed in *Smad4*$^{fl/fl}$. 884 genes were expressed in the *Smad4*$^{fl/fl}$ adenomas and not expressed in the *Smad4*$^{+/+}$ adenomas (Figure 6.2A). The first question to be answered was, what are the consequences of *Smad4* knockout on gene expression in the context of active Wnt signalling due to *Apc* mutations? First, we examined the DEG in *Smad4*$^{fl/fl}$ compared to *Smad4*$^{+/+}$ adenomas. Figure 6.2B shows a heat map for the top 50 DEG followed by gene description and fold change in Table 6.1. Among these genes four were not annotated and might be novel genes. *Muc2, Muc4, Sox2, Gata4, Reg3*γ*, Reg3*β, and *Pla2g2a* were among the DEG (Table 6.1). Second, to identify functional gene sets correlated with Smad4 status in the adenomas, GSEA was applied. The enriched gene sets for *Apc*$^{fl/fl}$*Smad4*$^{+/+}$ compared to *Apc*$^{fl/fl}$*Smad4*$^{fl/fl}$ analysis are shown in Table 6.2. Among these sets were enrichment for c-Myc. However, the

FDR values in these sets were $\geq$0.327, indicating that there is no significant enrichment in this comparison. The complementary analysis showed an enrichment for different sets such as Pid_Tgfbr_Pathway, Reactome_Response_To_Elevated_Platelet_Cytosolic_Ca2, Pid_Integrin1_Pathway and Biocarta_P38mapk_Pathway in *Apc*$^{fl/fl}$*Smad4*$^{fl/fl}$ compared to *Apc*$^{fl/fl}$ *Smad4*$^{+/+}$ with FDR <0.25 (Table 6.3).

To identify what is common between these sets, we examined the leading edge subset for each gene set (FDR <0.25) according to the diagram shown in Figure 6.3. Functional analysis for the genes in the list, GO, was then determined by GeneMANIA. Table 6.4 shows the upregulated genes, their description and GO for *Apc*$^{fl/fl}$*Smad4*$^{fl/fl}$ at the basal level. Most of these genes are involved in the TGF-β pathway, for example, *Skil, Fos, Tgfb1* and *Jun*. These genes were predicted to be involved in the regulation of myeloid leukocyte differentiation and cytokine production. *Ctnnb*1 and *Fos* were among the leading edge genes.

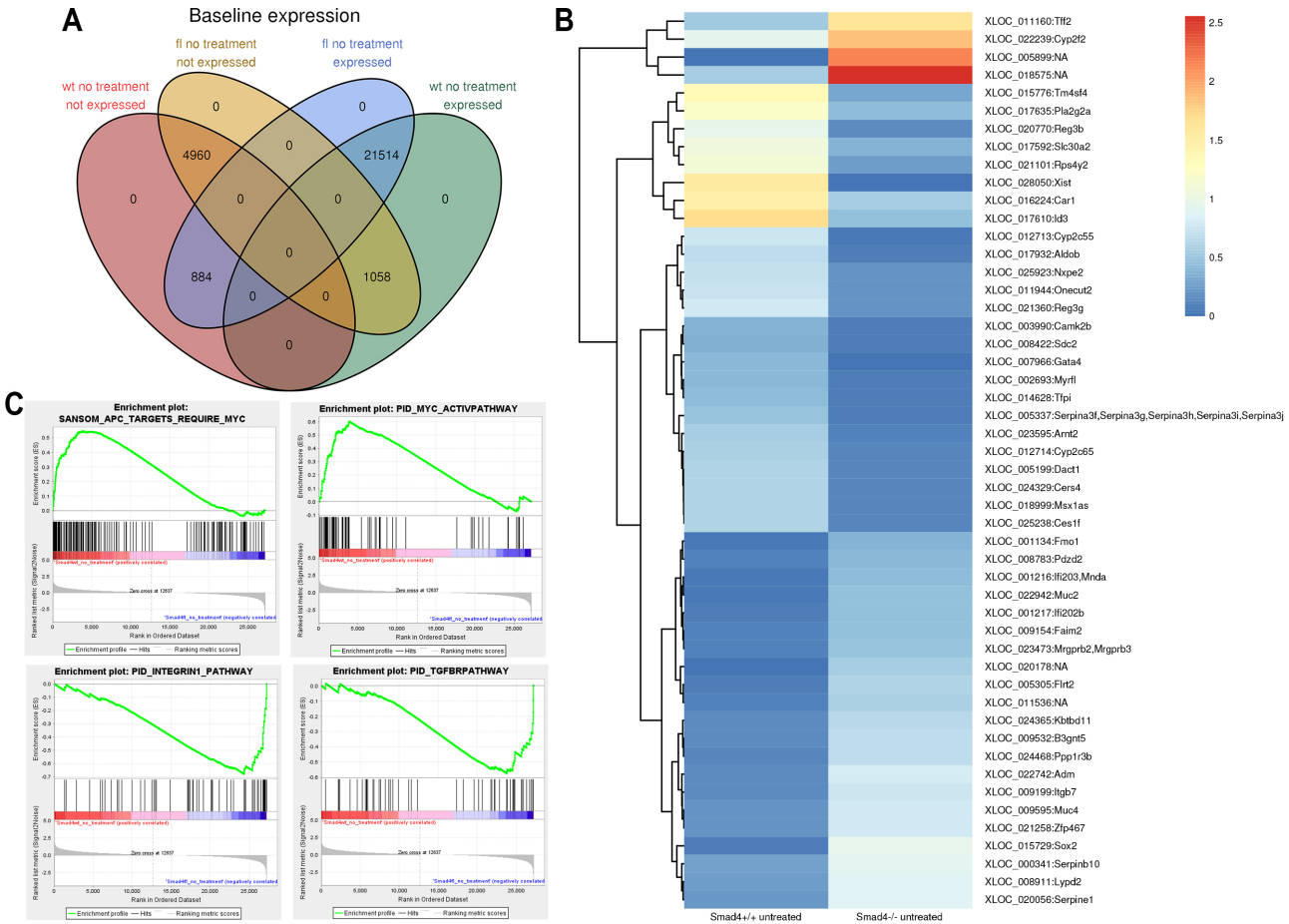

Figure 6.2: **Differentially expressed genes in adenomas from RNA-seq data with fold difference at the basal level.** (A) Venn diagram shows the number of genes expressed at the basal level (no treatment) with overlapping of expressed or not expressed between the different genotypes. Genes with FPKM>0 are considered as expressed and genes with FPKM=0 are considered to be not expressed. FPKM: Fragments per kilobase per million reads mapped. wt: *Smad4*$^{+/+}$, fl: *Smad4*$^{fl/fl}$. (B) Heat map shows the top 50 DEG by comparing the expression from *Smad4*$^{fl/fl}$ with *Smad4*$^{+/+}$ adenomas in Log_{10}FPKM scale. Key: Log_{10}FPKM=0 in blue and Log_{10}FPKM=2.5 in red. (C) Examples of GSEA plots in the *Smad4*$^{+/+}$ (upper panel) and *Smad4*$^{fl/fl}$ (lower panel) adenomas.

Table 6.1: Description of the top 50 DEG in *Apc*$^{fl/fl}$*Smad4*$^{fl/fl}$ adenomas at the basal level compared to *Apc*$^{fl/fl}$*Smad4*$^{+/+}$

XLOC	Symbol	Description	Fold-change
			Upregulated in *Smad4*$^{fl/fl}$
XLOC_005899	***NA***		143.72
XLOC_018575	***NA***		140.28
XLOC_015729	***Sox2***	SRY (sex determining region Y)-box 2	43.86
XLOC_001216	***Ifi203***	interferon activated gene 203	19.37
XLOC_001216	***Mnda***	myeloid cell nuclear differentiation antigen	19.37
XLOC_022942	***Muc2***	mucin 2	18.98
XLOC_011160	***Tff2***	trefoil factor 2 (spasmolytic protein 1)	17.16
XLOC_005305	***Flrt2***	fibronectin leucine rich transmembrane protein 2	16.18
XLOC_022742	***Adm***	adrenomedullin	13.03
XLOC_024468	***Ppp1r3b***	protein phosphatase 1, regulatory (inhibitor) subunit 3B	12.77
XLOC_001134	***Fmo1***	flavin containing monooxygenase 1	12.73
XLOC_011536	***NA***		12.35
XLOC_009199	***Itgb7***	integrin beta 7	11.15
XLOC_009532	***B3gnt5***	UDP-GlcNAc:betaGal beta-1,3-N-acetylglucosaminyltransferase 5	11.07
XLOC_001217	***Ifi202b***	interferon activated gene 202B	10.51
XLOC_020056	***Serpine1***	(or cysteine) peptidase inhibitor, clade E, member 1	10.41
XLOC_024365	***Kbtbd11***	kelch repeat and BTB (POZ) domain containing 11	9.58
XLOC_022239	***Cyp2f2***	cytochrome P450, family 2, subfamily f, polypeptide 2	9.52
XLOC_009595	***Muc4***	mucin 4	9.23
XLOC_008911	***Lypd2***	Ly6/Plaur domain containing 2	9.01
XLOC_000341	***Serpinb10***	serine (or cysteine) peptidase inhibitor, clade B (ovalbumin), member 10	8.84
XLOC_021258	***Zfp467***	zinc finger protein 467	8.72
XLOC_009154	***Faim2***	Fas apoptotic inhibitory molecule 2	8.04
XLOC_023473	***Mrgprb2***	MAS-related GPR, member B2	8.04
XLOC_023473	***Mrgprb3***	MAS-related GPR, member B3	8.04
XLOC_008783	***Pdzd2***	PDZ domain containing 2	7.87
XLOC_020178	***NA***		2.52
			Upregulated in *Smad4*$^{+/+}$
XLOC_028050	***Xist***	inactive X specific transcripts (x-chromosome)	653.78
XLOC_007966	***Gata4***	GATA binding protein 4	51.17
XLOC_012713	***Cyp2c55***	cytochrome P450, family 2, subfamily c, polypeptide 55	36.36
XLOC_017610	***Id3***	inhibitor of DNA binding 3	28.66
XLOC_017932	***Aldob***	aldolase B, fructose-bisphosphate	26.55
XLOC_020770	***Reg3b***	regenerating islet-derived 3 beta	23.16
XLOC_015776	***Tm4sf4***	transmembrane 4 superfamily member 4	22.35
XLOC_021101	***Rps4y2***		15.74
XLOC_005337	***Serpina3j***	serine (or cysteine) peptidase inhibitor, clade A (alpha-1 antiproteinase, antitrypsin), member 3J	11.93
XLOC_005337	***Serpina3i***	serine (or cysteine) peptidase inhibitor, clade A, member 3I	11.93
XLOC_005337	***Serpina3h***	serine (or cysteine) peptidase inhibitor, clade A, member 3H	11.93
XLOC_005337	***Serpina3f***	serine (or cysteine) peptidase inhibitor, clade A, member 3F	11.93
XLOC_005337	***Serpina3g***	serine (or cysteine) peptidase inhibitor, clade A, member 3G	11.93
XLOC_016224	***Car1***	carbonic anhydrase 1	11.12
XLOC_005199	***Dact1***	dapper homolog 1, antagonist of beta-catenin (xenopus)	10.86
XLOC_002693	***Myrfl***	myelin regulatory factor-like	10.54
XLOC_024329	***Cers4***	ceramide synthase 4	10.36
XLOC_023595	***Arnt2***	aryl hydrocarbon receptor nuclear translocator 2	10.29
XLOC_018999	***Msx1as***		9.68
XLOC_025238	***Ces1f***	carboxylesterase 1F	9.30
XLOC_012714	***Cyp2c65***	cytochrome P450, family 2, subfamily c, polypeptide 65	9.28
XLOC_008422	***Sdc2***	syndecan 2	8.99
XLOC_017635	***Pla2g2a***	phospholipase A2, group IIA (platelets, synovial fluid)	8.89
XLOC_021360	***Reg3g***	regenerating islet-derived 3 gamma	8.73
XLOC_014628	***Tfpi***	tissue factor pathway inhibitor	8.51
XLOC_017592	***Slc30a2***	solute carrier family 30 (zinc transporter), member 2	7.74
XLOC_011944	***Onecut2***	one cut domain, family member 2	7.70
XLOC_025923	***Nxpe2***	neurexophilin and PC-esterase domain family, member 2	7.36
XLOC_003990	***Camk2b***	calcium/calmodulin-dependent protein kinase II, beta	7.36

Table 6.2: Gene set enrichment in *Apc*$^{fl/fl}$*Smad4*$^{+/+}$ compared to *Apc*$^{fl/fl}$*Smad4*$^{fl/fl}$ at the basal level

NAME	SIZE[1]	NES[2]	NOM p-val[3]	FDR q-val[4]
KEGG_DRUG_METABOLISM_OTHER_ENZYMES	33	1.79	0.000	0.327
MOROSETTI_FACIOSCAPULOHUMERAL_MUSCULAR_DISTROPHY_UP	18	1.66	0.002	1.000
SANSOM_APC_TARGETS_REQUIRE_MYC	183	1.66	0.000	0.845
FERRANDO_T_ALL_WITH_MLL_ENL_FUSION_DN	83	1.65	0.000	0.716
DIRMEIER_LMP1_RESPONSE_LATE_DN	28	1.65	0.012	0.595
SCHLOSSER_MYC_AND_SERUM_RESPONSE_SYNERGY	31	1.64	0.002	0.544
NIKOLSKY_BREAST_CANCER_5P15_AMPLICON	24	1.64	0.000	0.523
HESS_TARGETS_OF_HOXA9_AND_MEIS1_UP	61	1.62	0.000	0.592
GAZDA_DIAMOND_BLACKFAN_ANEMIA_MYELOID_DN	31	1.61	0.008	0.573
SHIPP_DLBCL_VS_FOLLICULAR_LYMPHOMA_UP	43	1.61	0.002	0.517
RODRIGUES_THYROID_CARCINOMA_UP	15	1.61	0.000	0.482
SCHUHMACHER_MYC_TARGETS_UP	73	1.61	0.004	0.458
PID_MYC_ACTIVPATHWAY	74	1.60	0.002	0.457
GAJATE_RESPONSE_TO_TRABECTEDIN_DN	18	1.60	0.020	0.462
GARCIA_TARGETS_OF_FLI1_AND_DAX1_DN	147	1.59	0.000	0.486
COLLER_MYC_TARGETS_UP	25	1.59	0.010	0.468
REACTOME_SULFUR_AMINO_ACID_METABOLISM	22	1.59	0.000	0.442
ZHAN_MULTIPLE_MYELOMA_MS_DN	36	1.58	0.004	0.448
BURTON_ADIPOGENESIS_5	116	1.58	0.002	0.441
YAO_TEMPORAL_RESPONSE_TO_PROGESTERONE_CLUSTER_8	45	1.58	0.000	0.423

[1]Size: number of genes in the set, [2]NES: Normalized Enrichment Score, [3]NOM: Nominal p- value, [4]FDR: False Discovery Rate (q-value).

Table 6.3: Gene set enrichment in *Apc*$^{fl/fl}$*Smad4*$^{fl/fl}$ compared to *Apc*$^{fl/fl}$*Smad4*$^{+/+}$ at the basal level

NAME	SIZE[1]	NES[2]	NOM p-val[3]	FDR q-val[4]
MISHRA_CARCINOMA_ASSOCIATED_FIBROBLAST_UP	20	-1.90	0.000	0.074
GAVIN_PDE3B_TARGETS	21	-1.87	0.000	0.066
KANG_AR_TARGETS_DN	17	-1.86	0.000	0.050
KEGG_HYPERTROPHIC_CARDIOMYOPATHY_HCM	80	-1.85	0.000	0.046
COLIN_PILOCYTIC_ASTROCYTOMA_VS_GLIOBLASTOMA_DN	27	-1.84	0.000	0.052
UZONYI_RESPONSE_TO_LEUKOTRIENE_AND_THROMBIN	37	-1.83	0.000	0.053
PID_INTEGRIN1_PATHWAY	62	-1.82	0.000	0.049
WIKMAN_ASBESTOS_LUNG_CANCER_UP	16	-1.81	0.000	0.050
PID_IL12_STAT4PATHWAY	32	-1.81	0.000	0.046
KEGG_DILATED_CARDIOMYOPATHY	87	-1.81	0.000	0.042
REACTOME_RESPONSE_TO_ELEVATED_PLATELET_CYTOSOLIC_CA2_	76	-1.81	0.000	0.042
BIOCARTA_P38MAPK_PATHWAY	36	-1.80	0.000	0.040
PID_TGFBRPATHWAY	53	-1.80	0.000	0.037
KEGG_VASOPRESSIN_REGULATED_WATER_REABSORPTION	43	-0.65	0.000	0.042
YANG_BREAST_CANCER_ESR1_BULK_UP	26	-1.78	0.000	0.045
VERNELL_RETINOBLASTOMA_PATHWAY_DN	18	-1.78	0.000	0.044
DOANE_BREAST_CANCER_CLASSES_UP	62	-1.77	0.000	0.046
PID_ATF2_PATHWAY	56	-1.77	0.000	0.043
RICKMAN_HEAD_AND_NECK_CANCER_E	78	-1.77	0.000	0.047
STOSSI_RESPONSE_TO_ESTRADIOL	46	-1.77	0.000	0.044

[1]Size: number of genes in the set, [2]NES: Normalized Enrichment Score, [3]NOM: Nominal p- value, [4]FDR: False Discovery Rate (q-value).

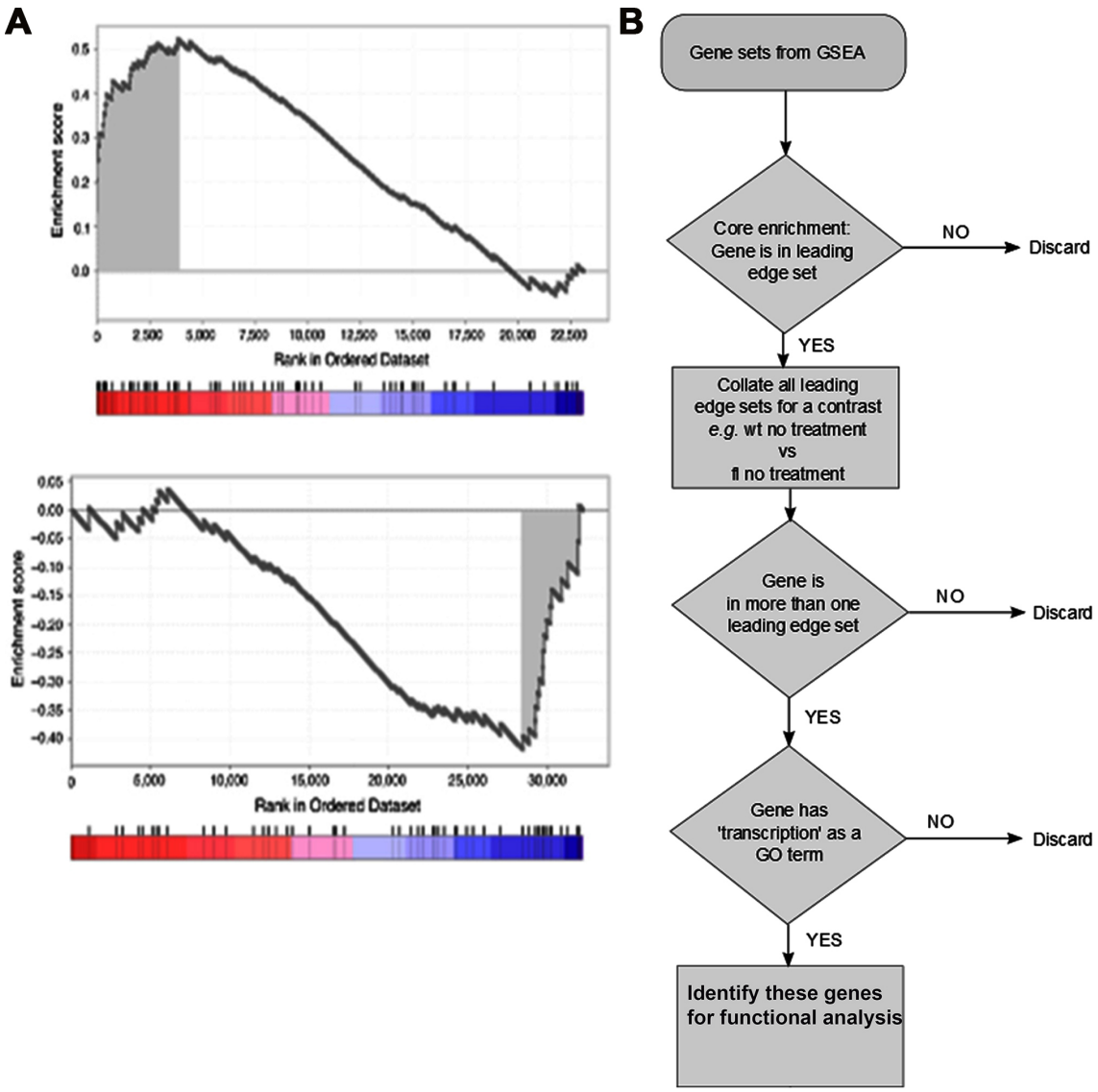

Figure 6.3: **Identification of common genes in different sets.** (A) Example of an enrichment plot showing the leading edge genes in grey. (B) Diagram represents the work flow programming to identify the common genes in the different gene sets. wt: *Smad4*$^{+/+}$, fl: *Smad4*$^{fl/fl}$

Table 6.4: Leading edge genes upregulated in *Apc*$^{fl/fl}$*Smad4*$^{fl/fl}$ at basal level compared to *Apc*$^{fl/fl}$ *Smad4*$^{+/+}$

Symbol	Description	GO annotations[1]
Ddit3	DNA-damage inducible transcript 3 [MGI:109247]	cellular response to abiotic stimulus; intrinsic apoptotic signaling pathway in response to endoplasmic reticulum stress; positive regulation of cytokine production
Egr1	early growth response 1 [MGI:95295]	cellular response to abiotic stimulus; lymphocyte differentiation; RNA polymerase II core promoter proximal region sequence-specific DNA binding transcription factor activity; T cell differentiation; transmembrane receptor protein serine/threonine (Ser/Thr) kinase signaling pathway
Skil	SKI-like [MGI:106203]	cell cycle arrest; cellular response to TGF-β stimulus; extrinsic and intrinsic apoptotic signaling pathway; SMAD binding
Foxa1	forkhead box A1 [MGI:1347472]	epithelial cell development; regulation of EMT; regulation of stem cell differentiation; RNA polymerase II transcription regulatory region sequence-specific DNA binding transcription factor activity involved in positive regulation of transcription
Tnf	tumour necrosis factor [MGI:104798]	cell-cell adhesion; cellular response to biotic stimulus; negative regulation of ion transport; positive regulation of cell adhesion; positive regulation of chemokine and cytokine production; positive regulation of leukocyte differentiation; regulation of reactive oxygen species metabolic process; stress-activated MAPK cascade
Fos	FBJ osteosarcoma oncogene [MGI:95574]	cellular response to external stimulus; cellular response to TGF-β stimulus; double-stranded DNA binding; myeloid leukocyte differentiation; SMAD protein signal transduction
Vegf	vascular endothelial growth factor A [MGI:103178]	cell maturation; cell-cell junction organisation; cell-substrate adhesion; extrinsic apoptotic signaling pathway; positive regulation of cell migration and motility; stem cell proliferation; stress-activated MAPK cascade
Creb1	cAMP responsive element binding protein 1 [MGI:88494]	cellular response to TGF-β stimulus; positive regulation of cytokine production; positive regulation of myeloid leukocyte differentiation; RNA polymerase II distal enhancer sequence-specific DNA binding
Tgfb1	transforming growth factor, beta 1 [MGI:98725]	cell junction organisation; cell-cell adhesion; cellular response to biotic stimulus; epidermal growth factor receptor signaling pathway; positive regulation of EMT; TGF-β receptor signalling pathway
Jun	Jun oncogene [MGI:96646]	cellular response to TGF-β stimulus; positive regulation of myeloid leukocyte differentiation; positive regulation of RNA polymerase II transcription regulatory region sequence-specific DNA binding transcription factor activity involved in positive regulation of transcription; SMAD protein signal transduction
Ctnnb1	catenin (cadherin associated protein), beta 1 [MGI:88276]	cell junction organisation; cell maturation; cell-cell adhesion; cellular response to abiotic stimulus; epithelial cell proliferation; EMT; R-SMAD binding; regulation of cellular response to growth factor stimulus; RNA polymerase II activating transcription factor binding

[1]GO: Gene ontology as described by GeneMANIA.

6.4.1.1 Mucin pools in tissue sections from *Apc*$^{fl/fl}$*Smad4*$^{fl/fl}$ mice

As a validation of mucin overexpression in the RNA-seq data, histochemistry and IF were performed for tissue sections from both genotypes. Histochemistry with Alcain blue-PAS stain was used to detect acidic (stain blue) and neutral mucins (stain magenta). The presence of mucin pools in tissue sections from the *Smad4*$^{fl/fl}$ animals with blue colour indicates the presence of acidic mucins (Figure 6.4 A). Immunolabelling with Muc2 antibodies showed an overexpression of Muc2 in sections from *Smad4*$^{fl/fl}$ animals (*p=0.0153). The area occupied by Muc2 in proportion to tumour area was 2.1$\pm$1.6 (SD) for the *Smad4*$^{+/+}$ sections and 6.3$\pm$2.2 (SD) for the *Smad4*$^{fl/fl}$ sections (p=0.0153). Analysis for Muc2 area was performed by a lab member (Figure 6.4 B).

Muc2, Muc4, Muc20 and *Muc1* were expressed more than 2 fold in *Smad4*$^{fl/fl}$ adenomas. Other mucins were expressed with less than a fold difference in *Smad4*$^{fl/fl}$ when compared to *Smad4*$^{+/+}$, for instance, *Muc13, Muc6* and *Muc5b* (Figure 6.4 C).

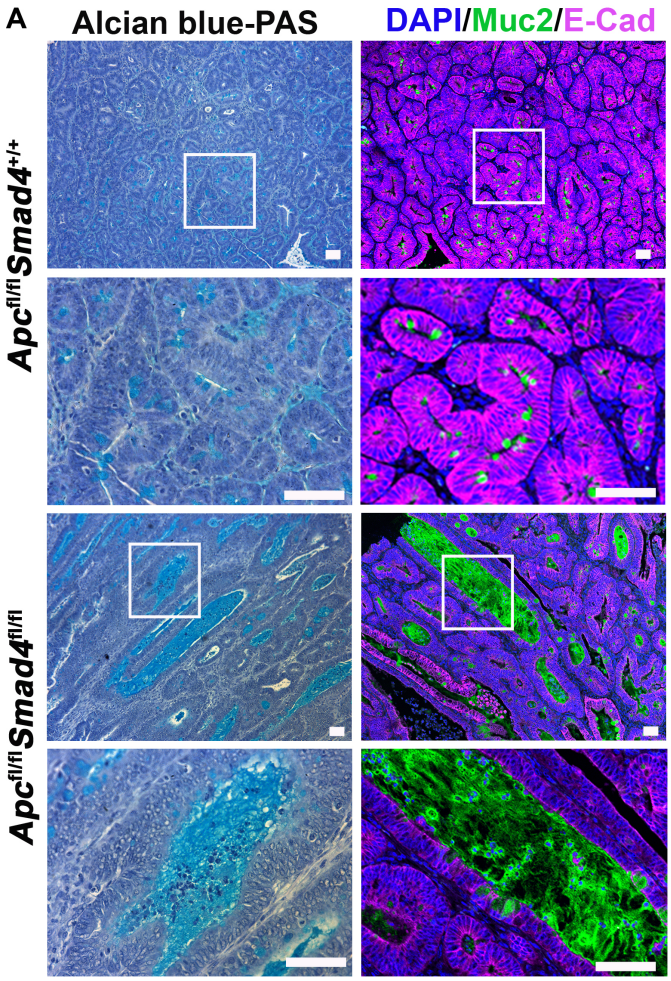

B

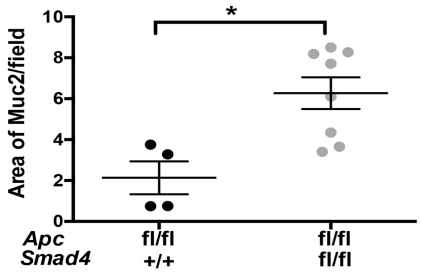

C

XLOC	Symbol	Fold difference
XLOC_022942	Muc2	18.98
XLOC_009595	Muc4	9.23
XLOC_009942	Muc20	3.59
XLOC_015876	Muc1	2.72
XLOC_009606	Muc13	0.78
XLOC_024037	Muc6	0.58
XLOC_022944	Muc5b	0.52
XLOC_008660	Muc19,Smgc	0
XLOC_009221	Mucl1,Spt1	0

Figure 6.4: **Mucins in *Apc*$^{fl/fl}$*Smad4*$^{fl/fl}$.** (A) Representative images for Alcian blue-PAS stain and Muc2 labelling from tissue sections of both genotypes. White boxes are magnified below each one, scale bars 100µm. (B) Quantification of Muc2 area in the sections by ImageJ represented by the percentage of Muc2 positive area to the tumour area. Statistical analysis was performed using student's t-test,*p=0.0153. Error bars±SD. Each dot represents the average of area from 5 fields from sections of the same mouse (n=4 for *Smad4*$^{+/+}$, and n=8 for *Smad4*$^{fl/fl}$). (C) Expression of different mucins from RNA-seq data with the fold difference in their expression (fold difference = FPKM reads from *Smad4*$^{fl/fl}$ divided by the reads from *Smad4*$^{+/+}$ adenomas).

6.4.2 Gene regulation in response to TGF-β1 treatment

6.4.2.1 Transcriptome of *Apc*$^{fl/fl}$*Smad*$^{+/+}$ adenomas

In this work two time points with TGF-β1 treatment were used to detect the early, direct (1h) and late (12h) response genes of TGF-β1. The approach used in the analysis and interpreting the data was similar to that described earlier in section 6.4.1. Briefly, the top 50 DEG, GSEA, Leading edge genes and GO. TGF-β1 target genes were determined by comparing the expression from Smad4$^{+/+}$ adenomas in the presence or absence of TGF-β1.

Among the top 50 differentially regulated genes are the upregulation of the TGF-β1 target gene *Serpine1*, and the upregulation of the TGF-β negative regulatory genes *Smad7*, *Skil* and *Smad6*, and genes that are important for apoptosis and cell cycle regulation such as upregulation of *Gadd45a*, *Gadd45g*, *Ddit4* and downregulation of *c-Myc* with transient upregulation of *Id1* and *Id3* (Figure 6.5, Table 6.5). GSEA showed no significant difference in enrichment between 0h and 1h (FDR$\geq$0.920) (Table 6.6). On the other hand, the complementary analysis showed an enrichment for different sets such as the TGF-β pathway, Pid_Smad2_3 nuclear_Pathway and Gentile_UV_High_Dose_Dn with a significant FDR values ($\leq$0.009) (Table 6.7). Leading edge genes show upregulation of several transcription factors such as *Atf3, Fos, Runx1*. GO for the leading edge genes showed that these genes are involved in the regulation of the TGF-β and BMP pathways. They are also predicted to be involved in the regulation of myeloid and leukocyte differentiation for example *Tgfb1, Jun, junb, Fos, Vega, NF-kbia, Klf10* and *Runx1*. Some genes are involved in intrinsic apoptotic pathways such as *Ddit3, Cav1* and *Skil* (Table 6.8).

Several genes were also differentially regulated after 12h of TGF-β1 treatment (Table 6.9). GSEA showed different functional gene sets to be correlated with TGF-β1 treatment with significant FDR values of $\leq$0.005 when the comparison was between 0h vs 12h and for the complementary analysis (12h vs 0h) (Table 6.10-6.11). GO for the leading edge genes in these sets showed that there is upregulation of genes with different functions. They might

be involved in the regulation of myeloid cell differentiation such as *Tgfb1, Ets1, Bcl6, Fos, Vega, Jag1, Zpf36*, and *Myh9*. Genes such as *Itga6, Tgfb1,Bcl10, Vega, Col1a1* and *Cyr61* are involved in adhesion. *Itga6, Tgfb1, Bcl10, Vega, Col1a1* and *Ecm1* in extracellular matrix binding. *Tgfb1, Vega* and *Jup* are involved in cell-cell organisation. These functions are regulated by different pathways such as TGF-β, BMP, Wnt, ERK1, ERK2 and MAPK pathways (Table 6.12). The complementary analysis showed that there was downregulation of genes involved in cell cycle regulation, cytokinesis and DNA replication such as *Birc5, Aurkb, Plk1 and E2f8* (Table 6.13).

A Venn diagram showed that 4679 genes were induced in response to TGF-β1 stimulation, 1249 genes were early response with 683 having sustained expression at 12h. 4638 genes were downregulated in response to TGF-β1 stimulation, 1382 genes were early repressed genes and 694 genes were still repressed at 12h (Figure 6.5C, D). GSEA were also applied for genes at the intersection. Table 6.14 shows a list of the leading edge genes that have been enriched in $\geq$3 of the sets and their description. GO from GeneMANIA predicts that these genes, such as *Onecut2, Ets1, Tnfrsf11b, Lamc2, Lama3 Itga2, Aplp1, Lgals3,* and *Vegfa* could be involved in epithelial cell migration and cell motility, extracellular matrix organisation and positive regulation of angiogenesis. Leading edge genes following GSEA for the repressed genes at the intersection are shown in Table 6.15. GO for downregulated genes such as *Pold2, Lig1, Cdc20, Pola1, Aspm Pole, Rfc1, Foxm1, Cenpf* predicts as an involvement in DNA replication and regulation of cell division.

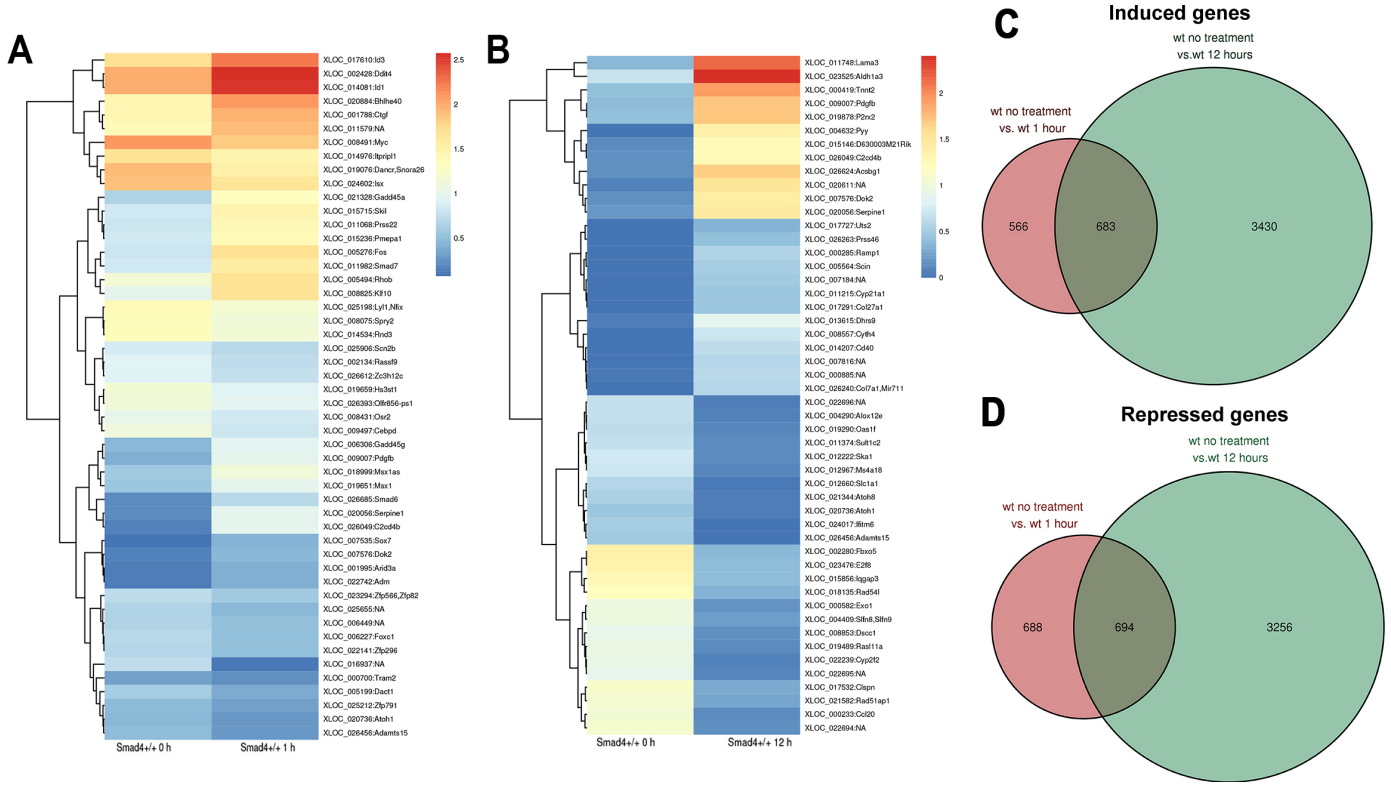

Figure 6.5: **Early and late response genes differentially regulated in *Smad*$^{+/+}$ adenomas with TGF-β1 treatment.** Top 50 differentially regulated early response genes (A) and late response genes (B) are represented by heat maps. Key: Log_{10}FPKM=0 in blue and Log_{10}FPKM=2.5 in red. Venn diagrams showing the numbers of early and late response genes that either induced (C) or repressed (D) in response to TGF-β1.

Table 6.5: Description of the top 50 differentially regulated genes in *Apc*$^{fl/fl}$*Smad4*$^{+/+}$ after 1h TGF-β1 treatment compared to 0h

XLOC	Symbol	Description	Fold-change
			Upregulated 1h
XLOC_026049	***C2cd4b***	C2 calcium-dependent domain containing 4B	20.65
XLOC_020056	***Serpine1***	serine (or cysteine) peptidase inhibitor, clade E, member 1	14.28
XLOC_005276	***Fos***	FBJ osteosarcoma oncogene	9.24
XLOC_007535	***Sox7***	SRY (sex determining region Y)-box 7	9.10
XLOC_026685	***Smad6***	SMAD family member 6	6.21
XLOC_011982	***Smad7***	SMAD family member 7	5.97
XLOC_009007	***Pdgfb***	platelet derived growth factor, B polypeptide	5.73
XLOC_021328	***Gadd45a***	growth arrest and DNA-damage-inducible 45 alpha	5.61
XLOC_008825	***Klf10***	Kruppel-like factor 10	5.35
XLOC_015715	***Skil***	SKI-like	4.99
XLOC_020884	***Bhlhe40***	basic helix-loop-helix family, member e40	4.75
XLOC_001995	***Arid3a***	AT rich interactive domain 3A (BRIGHT-like)	4.58
XLOC_011068	***Prss22***	protease, serine 22	4.46
XLOC_018999	***Msx1as***		4.32
XLOC_006306	***Gadd45g***	growth arrest and DNA-damage-inducible 45 gamma	4.15
XLOC_007576	***Dok2***	docking protein 2	4.14
XLOC_022742	***Adm***	adrenomedullin	3.95
XLOC_015236	***Pmepa1***	prostate transmembrane protein, androgen induced 1	3.94
XLOC_002428	***Ddit4***	DNA-damage-inducible transcript 4	3.85
XLOC_014081	***Id1***	inhibitor of DNA binding 1	3.57
XLOC_005494	***Rhob***	ras homolog gene family, member B	3.53
XLOC_001788	***Ctgf***	connective tissue growth factor	3.44
XLOC_019651	***Msx1***	msh homeobox 1	3.41
XLOC_017610	***Id3***	inhibitor of DNA binding 3	3.41
XLOC_011579	***NA***		3.35
			Upregulated 0h
XLOC_016937	***NA***		14.44
XLOC_019076	***Dancr***	differentiation antagonizing non-protein coding RNA	2.56
XLOC_019076	***Snora26***	small nucleolar RNA, H/ACA box 26	2.56
XLOC_026456	***Adamts15***	a disintegrin-like and metallopeptidase (reprolysin type) with thrombospondin type 1 motif, 15	2.33
XLOC_005199	***Dact1***	dapper homolog 1, antagonist of beta-catenin (xenopus)	2.16
XLOC_009497	***Cebpd***	CCAAT/enhancer binding protein (C/EBP), delta	2.08
XLOC_020736	***Atoh1***	atonal homolog 1 (Drosophila)	1.94
XLOC_025655	***NA***		1.91
XLOC_022141	***Zfp296***	zinc finger protein 296	1.80
XLOC_025212	***Zfp791***	zinc finger protein 791	1.79
XLOC_019659	***Hs3st1***	heparan sulfate (glucosamine) 3-O-sulfotransferase 1	1.78
XLOC_008491	***Myc***	myelocytomatosis oncogene	1.78
XLOC_002134	***Rassf9***	Ras association (RalGDS/AF-6) domain family (N-terminal) member 9	1.77
XLOC_006227	***Foxc1***	forkhead box C1	1.76
XLOC_008075	***Spry2***	sprouty homolog 2 (Drosophila)	1.75
XLOC_024602	***Isx***	intestine specific homeobox	1.72
XLOC_014976	***Itpripl1***	inositol 1,4,5-triphosphate receptor interacting protein-like 1	1.70
XLOC_000700	***Tram2***	translocating chain-associating membrane protein 2	1.63
XLOC_025198	***Lyl1***	lymphoblastomic leukemia 1	1.61
XLOC_025198	***Nfix***	nuclear factor I/X	1.61
XLOC_023294	***Zfp566***	zinc finger protein 566	1.58
XLOC_023294	***Zfp82***	zinc finger protein 82	1.58
XLOC_026393	***Olfr856-ps1***		1.57
XLOC_008431	***Osr2***	odd-skipped related 2	1.57
XLOC_014534	***Rnd3***	Rho family GTPase 3	1.57
XLOC_006449	***NA***		1.55
XLOC_025906	***Scn2b***	sodium channel, voltage-gated, type II, beta	1.54
XLOC_026612	***Zc3h12c***	zinc finger CCCH type containing 12C	1.53
XLOC_008075	***Spry2***	sprouty homolog 2 (Drosophila)	0.57

Table 6.6: Gene set enrichment in *Apc*$^{fl/fl}$*Smad4*$^{+/+}$ at 0h after TGF-β1 treatment compared to 1h

NAME	SIZE[1]	NES[2]	NOM p-val[3]	FDR q-val[4]
NIKOLSKY_BREAST_CANCER_12Q24_AMPLICON	15	1.74	0.006	0.920
SCHAEFFER_PROSTATE_DEVELOPMENT_AND_CANCER_BOX4_DN	29	1.65	0.015	1.000
MITSIADES_RESPONSE_TO_APLIDIN_DN	231	1.65	0.023	1.000
BIOCARTA_RARRXR_PATHWAY	15	1.62	0.002	1.000
CHIN_BREAST_CANCER_COPY_NUMBER_UP	24	1.60	0.023	1.000
ZHENG_RESPONSE_TO_ARSENITE_DN	17	1.60	0.002	1.000
MONNIER_POSTRADIATION_TUMOR_ESCAPE_UP	355	1.58	0.023	1.000
BIOCARTA_CARM_ER_PATHWAY	32	1.56	0.008	1.000
KYNG_RESPONSE_TO_H2O2_VIA_ERCC6_UP	37	1.55	0.042	1.000
REACTOME_TRANSCRIPTIONAL_REGULATION_OF_WHITE_ADIPOCYTE_DIFFERENTIATION	70	1.55	0.002	1.000
BIOCARTA_WNT_PATHWAY	24	1.54	0.014	1.000
KEGG_GLYCOSAMINOGLYCAN_BIOSYNTHESIS_HEPARAN_SULFATE	25	1.52	0.033	1.000
CONRAD_STEM_CELL	38	1.51	0.012	1.000
PID_THROMBIN_PAR4_PATHWAY	15	1.51	0.034	1.000
REACTOME_CTNNB1_PHOSPHORYLATION_CASCADE	15	1.49	0.057	1.000
ACOSTA_PROLIFERATION_INDEPENDENT_MYC_TARGETS_UP	70	1.49	0.017	1.000
VANTVEER_BREAST_CANCER_BRCA1_UP	29	1.49	0.099	1.000
BACOLOD_RESISTANCE_TO_ALKYLATING_AGENTS_DN	51	1.49	0.048	1.000
BIOCARTA_IGF1R_PATHWAY	19	1.48	0.058	1.000
PID_IL2_STAT5PATHWAY	27	1.47	0.050	1.000

[1]Size: number of genes in the set, [2]NES: Normalized Enrichment Score, [3]NOM: Nominal p-value, [4]FDR: False Discovery Rate (q-value).

Table 6.7: Gene set enrichment in *Apc*$^{fl/fl}$*Smad4*$^{+/+}$ at 1h after TGF-β1 treatment compared to 0h

NAME	SIZE[1]	NES[2]	NOM p-val[3]	FDR q-val[4]
PID_ATF2_PATHWAY	56	-2.26	0.000	0.002
PID_SMAD2_3NUCLEARPATHWAY	79	-2.14	0.000	0.002
BIOCARTA_ATM_PATHWAY	19	-2.14	0.000	0.001
GENTILE_UV_HIGH_DOSE_DN	293	-2.13	0.000	0.001
REACTOME_SIGNALING_BY_TGF_BETA_RECEPTOR_COMPLEX	53	-2.01	0.000	0.009
PID_TGFBRPATHWAY	53	-2.00	0.000	0.009
GENTILE_UV_RESPONSE_CLUSTER_D4	54	-1.99	0.000	0.009
THEILGAARD_NEUTROPHIL_AT_SKIN_WOUND_UP	71	-1.99	0.000	0.008
REACTOME_TGF_BETA_RECEPTOR_SIGNALING_ACTIVATES_SMADS	22	-1.99	0.000	0.007
GENTILE_RESPONSE_CLUSTER_D3	56	-1.98	0.000	0.007
KEGG_P53_SIGNALING_PATHWAY	62	-1.98	0.000	0.007
HALMOS_CEBPA_TARGETS_DN	42	-1.98	0.000	0.006
REACTOME_DOWNREGULATION_OF_TGF_BETA_RECEPTOR_SIGNALING	19	-1.97	0.000	0.006
GOTTWEIN_TARGETS_OF_KSHV_MIR_K12_11	58	-1.97	0.000	0.006
COULOUARN_TEMPORAL_TGFB1_SIGNATURE_UP	102	-1.97	0.000	0.005
ADDYA_ERYTHROID_DIFFERENTIATION_BY_HEMIN	64	-1.97	0.000	0.005
HAN_JNK_SINGALING_UP	34	-1.97	0.000	0.005
VARELA_ZMPSTE24_TARGETS_UP	36	-1.96	0.000	0.005
ONO_FOXP3_TARGETS_UP	22	-1.96	0.000	0.006
GROSS_HYPOXIA_VIA_HIF1A_DN	105	-1.95	0.000	0.006

[1]Size: number of genes in the set, [2]NES: Normalized Enrichment Score, [3]NOM: Nominal p-value, [4]FDR: False Discovery Rate (q-value).

Table 6.8: Leading edge genes upregulated in *Apc*$^{fl/fl}$*Smad4*$^{+/+}$ after 1h TGF-β1 treatment compare to 0h

Symbol	Description	GO annotations[1]
Runx1	runt related transcription factor 1 [MGI:99852]	positive regulation of myeloid and leukocyte differentiation; regulation of leukocyte differentiation
Fosl2	fos-like antigen 2 [MGI:102858]	positive regulation of fibroblast proliferation; RNA polymerase II regulatory region DNA binding
Klf10	Kruppel-like factor 10 [MGI:1101353]	positive regulation of myeloid and leukocyte differentiation; myeloid cell differentiation;
Id2	inhibitor of DNA binding 2 [MGI:96397]	negative regulation of cell cycle; myeloid leukocyte differentiation
Atf3	activating transcription factor 3 [MGI:109384]	skeletal muscle cell differentiation
Fos	FBJ osteosarcoma oncogene [MGI:95574]	cellular response to TGF-β stimulus; myeloid leukocyte differentiation; R-SMAD binding; SMAD protein signal transduction
Cyr61	cysteine rich protein 61 [MGI:88613]	BMP signalling pathway; positive regulation of transmembrane receptor protein Ser/Thr kinase signalling pathway
Hes1	hairy and enhancer of split 1 (Drosophila) [MGI:104853]	regulation of BMP signalling pathway; regulation of DNA binding; regulation of transmembrane receptor protein Ser/Thr kinase signalling pathway
Taf11	RNA polymerase II, TATA box binding protein (TBP)-associated factor [MGI:1916026]	transcription factor TFIID complex
Id3	inhibitor of DNA binding 3 [MGI:96398]	muscle cell development; regulation of DNA replication
Junb	Jun-B oncogene [MGI:96647]	myeloid leukocyte differentiation; RNA polymerase II regulatory region DNA binding
Ddit3	DNA-damage inducible transcript 3 [MGI:109247]	mRNA transcription; muscle cell development;response to endoplasmic reticulum stress; response to extracellular stimulus
Smad7	SMAD family member 7 [MGI:1100518]	regulation of BMP signalling pathway; cellular response to TGF-β stimulus; I-SMAD binding;negative regulation of transmembrane receptor protein Ser/Thr kinase signalling pathway
Tgfb1	transforming growth factor, beta 1 [MGI:98725]	extrinsic apoptotic signalling pathway; homeostasis of number of cells; myeloid cell differentiation; pathway-restricted SMAD protein phosphorylation; positive regulation of transmembrane receptor protein Ser/Thr kinase signalling pathway
Zfp36	zinc finger protein 36 [MGI:99180]	negative regulation of myeloid cell differentiation; positive regulation of nuclear-transcribed mRNA poly(A) tail shortening; regulation of mRNA 3'-end processing
Bhlhe40	basic helix-loop-helix family, member e40 [MGI:1097714]	RNA polymerase II activating transcription factor binding; RNA polymerase II core promoter proximal region
Nfkbia	nuclear factor of kappa light polypeptide gene enhancer in B cells inhibitor, alpha [MGI:104741]	negative regulation of myeloid cell differentiation; negative regulation of sequence-specific DNA binding transcription factor activity
Vegfa	vascular endothelial growth factor A [MGI:103178]	erythrocyte homeostasis; extrinsic apoptotic signalling pathway; regulation of p38MAPK cascade
Smad6	SMAD family member 6 [MGI:1336883]	BMP signalling pathway; co-SMAD binding; cytokine receptor binding; I-SMAD binding; negative regulation of transmembrane receptor protein Ser/Thr kinase signalling pathway; regulation of pathway-restricted SMAD protein phosphorylation
Skil	SKI-like [MGI:106203]	cellular response to TGF-β stimulus and negative regulation of TGF-β receptor signalling pathway
Tgif1	TGFB-induced factor homeobox 1 [MGI:1194497]	co-SMAD binding; positive regulation of fibroblast proliferation; transmembrane receptor protein Ser/Thr kinase signalling pathway
Tmsb4x	thymosin, beta 4, X chromosome [MGI:99510]	muscle cell differentiation; regulation of muscle cell differentiation
Jun	Jun oncogene [MGI:96646]	transmembrane receptor protein Ser/Thr kinase signalling pathway; myeloid leukocyte differentiation; R-SMAD binding; regulation of epithelial cell proliferation; RNA polymerase II activating transcription factor binding; SMAD protein import into nucleus

[1]GO: Gene ontology as described by GeneMANIA

Table 6.9: Description of the top 50 differentially regulated genes in *Apc*$^{fl/fl}$*Smad4*$^{+/+}$ after 12h TGF-β1 treatment compared to 0h

XLOC	Symbol	Description	Fold-change
			Upregulated at 12h
XLOC_011215	***Cyp21a1***	cytochrome P450, family 21, subfamily a, polypeptide 1	247.12
XLOC_020611	***NA***		137.96
XLOC_014207	***Cd40***	CD40 antigen	135.39
XLOC_026624	***Acsbg1***	acyl-CoA synthetase bubblegum family member 1	102.11
XLOC_011748	***Lama3***	laminin, alpha 3	99.90
XLOC_008557	***Cyth4***	cytohesin 4	88.40
XLOC_017291	***Col27a1***	collagen, type XXVII, alpha 1	74.75
XLOC_026240	***Col7a1***	collagen, type VII, alpha 1	66.69
XLOC_026240	***Mir711***	microRNA 711	66.69
XLOC_005564	***Scin***	scinderin	65.80
XLOC_023525	***Aldh1a3***	aldehyde dehydrogenase family 1, subfamily A3	65.60
XLOC_007576	***Dok2***	docking protein 2	53.96
XLOC_000285	***Ramp1***	receptor (calcitonin) activity modifying protein 1	51.05
XLOC_000419	***Tnnt2***	troponin T2, cardiac	49.19
XLOC_015146	***D630003M-21Rik***	RIKEN cDNA D630003M21 gene	48.99
XLOC_000885	***NA***		46.10
XLOC_020056	***Serpine1***	serine (or cysteine) peptidase inhibitor, clade E, member 1	45.52
XLOC_007184	***NA***		43.78
XLOC_013615	***Dhrs9***	dehydrogenase/reductase (SDR family) member 9	41.87
XLOC_026049	***C2cd4b***	C2 calcium-dependent domain containing 4B	39.78
XLOC_009007	***Pdgfb***	platelet derived growth factor, B polypeptide	33.02
XLOC_019878	***P2rx2***	purinergic receptor P2X, ligand-gated ion channel, 2	32.37
XLOC_004632	***Pyy***	peptide YY	22.44
XLOC_007816	***NA***		2.95
XLOC_026263	***Prss46***	protease, serine 46	1.63
XLOC_017727	***Uts2***	urotensin 2	1.28
			Upregulated at 0h
XLOC_026456	***Adamts15***	a disintegrin-like and metallopeptidase (reprolysin type) with thrombospondin type 1 motif, 15	40.17
XLOC_022239	***Cyp2f2***	cytochrome P450, family 2, subfamily f, polypeptide 2	30.25
XLOC_000233	***Ccl20***	chemokine (C-C motif) ligand 20	27.10
XLOC_012660	***Slc1a1***	solute carrier family 1 (neuronal/epithelial high affinity glutamate transporter, system Xag), member 1	25.06
XLOC_022694	***NA***		24.76
XLOC_022695	***NA***		23.77
XLOC_019489	***Rasl11a***	RAS-like, family 11, member A	21.83
XLOC_022696	***NA***		21.04
XLOC_021344	***Atoh8***	atonal homolog 8 (Drosophila)	16.74
XLOC_002280	***Fbxo5***	F-box protein 5	16.62
XLOC_004290	***Alox12e***	arachidonate lipoxygenase, epidermal	15.51
XLOC_023476	***E2f8***	E2F transcription factor 8	15.25
XLOC_008853	***Dscc1***	defective in sister chromatid cohesion 1 homolog (S. cerevisiae)	15.06
XLOC_000582	***Exo1***	exonuclease 1	14.74
XLOC_012967	***Ms4a18***	membrane-spanning 4-domains, subfamily A, member 18	14.73
XLOC_020736	***Atoh1***	atonal homolog 1 (Drosophila)	14.09
XLOC_019290	***Oas1f***	2'-5' oligoadenylate synthetase 1F	13.60
XLOC_012222	***Ska1***	spindle and kinetochore associated complex subunit 1	13.02
XLOC_021582	***Rad51ap1***	RAD51 associated protein 1	12.85
XLOC_017532	***Clspn***	claspin	12.61
XLOC_018135	***Rad54l***	RAD54 like (S. cerevisiae)	11.91
XLOC_015856	***Iqgap3***	IQ motif containing GTPase activating protein 3	11.72
XLOC_011374	***Sult1c2***	sulfotransferase family, cytosolic, 1C, member 2	11.42
XLOC_004409	***Slfn8***	schlafen 8	11.34
XLOC_004409	***Slfn9***	schlafen 9	11.34
XLOC_024017	***Ifitm6***	interferon induced transmembrane protein 6	2.35

Table 6.10: Gene set enrichment in *Apc*$^{fl/fl}$*Smad4*$^{+/+}$ at 0h after TGF-β1 treatment compared to 12h

NAME	SIZE[1]	NES[2]	NOM p-val[3]	FDR q-val[4]
WILCOX_PRESPONSE_TO_ROGESTERONE_UP	129	2.08	0.000	0.001
GAL_LEUKEMIC_STEM_CELL_DN	217	2.06	0.000	0.001
SHEPARD_CRUSH_AND_BURN_MUTANT_DN	165	2.01	0.000	0.001
SHEPARD_BMYB_TARGETS	63	1.96	0.000	0.003
TURASHVILI_BREAST_DUCTAL_CARCINOMA_VS_LOBULAR_NORMAL_UP	66	1.96	0.000	0.002
REACTOME_LOSS_OF_NLP_FROM_MITOTIC_CENTROSOMES	48	1.95	0.000	0.002
ZHENG_GLIOBLASTOMA_PLASTICITY_UP	229	1.94	0.000	0.002
CHIARETTI_T_ALL_RELAPSE_PROGNOSIS	19	1.93	0.000	0.003
STEIN_ESR1_TARGETS	80	1.92	0.000	0.003
POOLA_INVASIVE_BREAST_CANCER_UP	244	1.92	0.000	0.003
HADDAD_T_LYMPHOCYTE_AND_NK_PROGENITOR_DN	59	1.90	0.000	0.003
BENPORATH_ES_2	38	1.90	0.000	0.003
SU_TESTIS	67	1.90	0.000	0.003
CROONQUIST_NRAS_VS_STROMAL_STIMULATION_DN	94	1.88	0.000	0.004
SHEPARD_BMYB_MORPHOLINO_DN	183	1.88	0.000	0.004
CHICAS_RB1_TARGETS_GROWING	222	1.88	0.000	0.004
WEST_ADRENOCORTICAL_TUMOR_UP	272	1.88	0.000	0.004
REACTOME_RECRUITMENT_OF_MITOTIC_CENTROSOME_PROTEINS_AND_COMPLEXES	55	1.87	0.000	0.004
MATZUK_SPERMATOCYTE	66	1.87	0.000	0.004
GOLDRATH_ANTIGEN_RESPONSE	315	1.87	0.000	0.004

[1]Size: number of genes in the set, [2]NES: Normalized Enrichment Score, [3]NOM: Nominal p- value, [4]FDR: False Discovery Rate (q-value).

Table 6.11: Gene set enrichment in *Apc*$^{fl/fl}$*Smad4*$^{+/+}$ at 12h after TGF-β1 treatment compared to 0h

NAME	SIZE[1]	NES[2]	NOM p-val[3]	FDR q-val[4]
KANG_AR_TARGETS_DN	17	-2.01	0.000	0.005
KEGG_DILATED_CARDIOMYOPATHY	87	-1.98	0.000	0.006
ZHAN_LATE_DIFFERENTIATION_GENES_UP	31	-1.98	0.000	0.004
KEGG_HYPERTROPHIC_CARDIOMYOPATHY_HCM	80	-1.97	0.000	0.005
MCDOWELL_ACUTE_LUNG_INJURY_UP	42	-1.96	0.000	0.005
MORI_PLASMA_CELL_DN	28	-1.96	0.000	0.004
KEGG_COMPLEMENT_AND_COAGULATION_CASCADES	63	-1.95	0.000	0.005
CAIRO_HEPATOBLASTOMA_CLASSES_DN	189	-1.94	0.000	0.004
MARSON_FOXP3_TARGETS_UP	58	-1.94	0.000	0.004
VERRECCHIA_RESPONSE_TO_TGFB1_C2	24	-1.94	0.000	0.004
GROSS_HYPOXIA_VIA_ELK3_DN	146	-1.94	0.000	0.004
LEE_DOUBLE_POLAR_THYMOCYTE	24	-1.93	0.000	0.004
TOMIDA_METASTASIS_DN	15	-1.93	0.000	0.004
WANG_LSD1_TARGETS_DN	37	-1.93	0.000	0.003
BIOCARTA_NKT_PATHWAY	28	-1.93	0.000	0.003
PID_INTEGRIN1_PATHWAY	62	-1.93	0.000	0.003
SHAFFER_IRF4_TARGETS_IN_PLASMA_CELL_VS_MATURE_B_LYMPHOCYTE	63	-1.92	0.000	0.003
KEGG_ARRHYTHMOGENIC_RIGHT_VENTRICULAR_CARDIOMYOPATHY_ARVC	73	-1.92	0.000	0.003
YAO_TEMPORAL_RESPONSE_TO_PROGESTERONE_CLUSTER_5	27	-1.91	0.000	0.004
AMIT_EGF_RESPONSE_120_HELA	62	-1.91	0.000	0.004

[1]Size: number of genes in the set, [2]NES: Normalized Enrichment Score, [3]NOM: Nominal p-value, [4]FDR: False Discovery Rate (q-value).

Table 6.12: Leading edge genes upregulated in *Smad4*$^{+/+}$ after 12h TGF-β1 treatment compare to 0h

Symbol	Description	GO annotations[1]
Jag1	jagged 1 [MGI:1095416]	regulation of myeloid cell differentiation; regulation of stem cell differentiation
Ets1	E26 avian leukemia oncogene 1, 5' domain [MGI:95455]	extracellular matrix organisation; histone acetyltransferase binding; regulation of myeloid cell differentiation; positive regulation of cell migration and motility
Myh9	myosin, heavy polypeptide 9, non-muscle [MGI:107717]	anchoring junction; cell-cell adherens junction; cell-cell adhesion; epithelial cell migration; myeloid cell differentiation
Fos	FBJ osteosarcoma oncogene [MGI:95574]	cellular response to TGF-β stimulus; R-SMAD binding; R- SMAD protein signal transduction; positive regulation of myeloid and leukocyte cell differentiation
Bcl6	B cell leukemia/lymphoma 6 [MGI:107187]	negative regulation of cell-matrix adhesion; immunoglobulin production; regulation of inflammatory response
Col1a1	collagen, type I, alpha 1 [MGI:88467]	regulation of canonical Wnt signalling pathway; negative regulation of cell adhesion, migration and motility, positive regulation of EMT; regulation of stem cell differentiation
Egr1	early growth response 1 [MGI:95295]	BMP signalling pathway; negative regulation of Wnt signalling pathway; RNA polymerase II core promoter proximal region sequence-specific DNA binding transcription factor activity involved in positive regulation of transcription; transmembrane receptor protein Ser/Thr kinase signalling pathway
Atf3	activating transcription factor 3 [MGI:109384]	carbohydrate biosynthetic process; gluconeogenesis
Cyr61	cysteine rich protein 61 [MGI:88613]	regulation of ERK1 and ERK2 cascade;regulation of transmembrane receptor protein Ser/Thr kinase signalling pathway; BMP signalling pathway; cell-cell adhesion; extracellular matrix binding and organisation; integrin binding; positive regulation of cell adhesion, migration and motility
Ecm1	extracellular matrix protein 1 [MGI:103060]	cytokine-mediated signalling pathway;regulation of epithelial cell proliferation; extracellular matrix binding; growth factor receptor binding; laminin binding; negative regulation of cytokine-mediated signalling pathway
Cav1	caveolin 1, caveolae protein [MGI:102709]	BMP signalling pathway; regulation of canonical Wnt signalling pathway; regulation of transmembrane receptor protein Ser/Thr kinase signalling pathway; ERK1 and ERK2 cascade; extrinsic apoptotic signalling pathway; inactivation of MAPK activity, negative regulation of cytokine-mediated signalling pathway
Basp1	brain abundant, membrane attached signal protein 1 [MGI:1917600]	kidney development
Klf6	Kruppel-like factor 6 [MGI:1346318]	cytokine-mediated signalling pathway; double-stranded DNA binding; structure-specific DNA binding
Tgfb1	transforming growth factor, beta 1 [MGI:98725]	cell-cell junction organisation; cellular response to TGF-β stimulus; cytokine receptor binding; epithelial cell migration; extracellular matrix assembly; regulation of MAP kinase activity; regulation of reactive oxygen species metabolic process; SMAD protein import into nucleus
Jup	junction plakoglobin [MGI:96650]	negative regulation of Wnt signalling pathway; cell-cell adherens junction; regulation of stem cell differentiation
Itga6	integrin alpha 6 [MGI:96605]	cell-cell adherens junction; positive regulation of cell-matrix adhesion; integrin binding; laminin binding; leukocyte migration
Bcl10	B cell leukemia/lymphoma 10 [MGI:1337994]	adaptive immune response; cytokine biosynthetic process; myeloid leukocyte activation; NF-κB binding; positive regulation of apoptotic signalling pathway
Vegfa	vascular endothelial growth factor A [MGI:103178]	regulation of ERK1 and ERK2 cascade; regulation of extrinsic apoptotic signalling pathway; regulation of histone deacetylation; regulation of MAP kinase; endothelial cell migration; blood vessel morphogenesis; cell-cell junction organisation; cell-matrix adhesion
Bhlhe40	basic helix-loop-helix family, member e40 [MGI:1097714]	negative regulation of sequence-specific DNA binding transcription factor activity; RNA polymerase II activating transcription factor binding
Zfp36	zinc finger protein 36 [MGI:99180]	regulation of myeloid cell differentiation; nuclear-transcribed mRNA poly(A) tail shortening; positive regulation of mRNA 3'-end processing; response to extracellular stimulus

[1]GO:Gene ontology as described by GeneMANIA

Table 6.13: Leading edge genes downregulated in *Apc*$^{fl/fl}$*Smad4*$^{+/+}$ after 12h TGF-β1 treatment compare to 0h

Symbol	Description	GO annotations[1]
Cenpf	centromere protein F [MGI:1313302]	cell cycle G2/M phase transition
Chaf1a	chromatin assembly factor 1, subunit A (p150) [MGI:1351331]	chromatin assembly or disassembly
Tmpo	thymopoietin [MGI:106920]	chromatin
Cbx5	chromobox 5 [MGI:109372]	histone deacetylase binding
Dnmt1	DNA methyltransferase (cytosine-5) 1 [MGI:94912]	DNA methylation or demethylation
Top2a	topoisomerase (DNA) II alpha [MGI:98790]	cell cycle checkpoint; DNA-dependent DNA replication; histone deacetylase binding
E2f8	E2F transcription factor 8 [MGI:1922038]	regulation of DNA replication; cytokinesis; positive regulation of cell cycle process
Tacc3	transforming, acidic coiled-coil containing protein 3 [MGI:1341163]	maintenance of location in cell; microtubule cytoskeleton
Plk1	polo-like kinase 1 [MGI:97621]	cell cycle checkpoint; cell cycle G2/M phase transition; microtubule cytoskeleton organisation
Ckap2	cytoskeleton associated protein 2 [MGI:1931797]	negative regulation of microtubule polymerization or depolymerization
Hells	helicase, lymphoid specific [MGI:106209]	chromatin assembly or disassembly; DNA alkylation; DNA methylation or demethylation
Hopx	HOP homeobox [MGI:1916782]	regulation of binding; regulation of protein binding
Mlf1	myeloid leukemia factor 1 [MGI:1341819]	myeloid progenitor cell differentiation; cell cycle arrest
Hmgb2	high mobility group box 2 [MGI:96157]	condensed chromosome; DNA ligation; histone binding
Uhrf1	ubiquitin-like, containing PHD and RING finger domains, 1 [MGI:1338889]	DNA alkylation; DNA methylation; histone binding; methyl-CpG binding
Aurkb	aurora kinase B [MGI:107168]	cellular protein complex disassembly; negative regulation of microtubule depolymerization; spindle organisation
Cdca7l	cell division cycle associated 7 like [MGI:2384982]	
Gmnn	geminin [MGI:1927344]	histone deacetylase binding; regulation of DNA metabolic process; regulation of DNA replication
Asf1b	ASF1 anti-silencing function 1 homolog B (S. cerevisiae) [MGI:1914179]	chromatin assembly or disassembly; DNA packaging; histone binding
Birc5	baculoviral IAP repeat-containing 5 [MGI:1203517]	cell cycle G2/M phase transition; microtubule cytoskeleton organisation; positive regulation of cell cycle process; spindle checkpoint
Ccna2	cyclin A2 [MGI:108069]	pronucleus
Irf8	interferon regulatory factor 8 [MGI:96395]	positive regulation of transcription; defense response to bacterium
Pcna	proliferating cell nuclear antigen [MGI:97503]	nuclear chromosome part; regulation of DNA metabolic process; regulation of nuclease activity; replication fork
Ezh2	enhancer of zeste homolog 2 (Drosophila) [MGI:107940]	negative regulation of cell cycle process; regulation of gene expression, epigenetic

[1]GO: Gene ontology as described by GeneMANIA

Table 6.14: Leading edge genes induced in *Apc*$^{fl/fl}$*Smad4*$^{+/+}$ adenomas after 1h TGF-β1 treatment and maintained expression

Symbol	Description
Slc4a11	solute carrier family 4, sodium bicarbonate transporter-like, member 11 [MGI:2138987]
Ncoa4	nuclear receptor coactivator 4 [MGI:1350932]
Dusp4	dual specificity phosphatase 4 [MGI:2442191]
Trim15	tripartite motif-containing 15 [MGI:1916347]
Onecut2	one cut domain, family member 2 [MGI:1891408]
Cttnbp2nl	CTTNBP2 N-terminal like [MGI:1933137]
Smurf1	SMAD specific E3 ubiquitin protein ligase 1 [MGI:1923038]
Med21	mediator complex subunit 21 [MGI:1347064]
Ets1	E26 avian leukemia oncogene 1, 5' domain [MGI:95455]
Pdlim7	PDZ and LIM domain 7 [MGI:1914649]
Myl12b	myosin, light chain 12B, regulatory [MGI:107494]
Ndufa1	NADH dehydrogenase (ubiquinone) 1 alpha subcomplex, 1 [MGI:1929511]
Tnfrsf11b	tumour necrosis factor receptor superfamily, member 11b (osteoprotegerin) [MGI:109587]
Cox4i1	cytochrome c oxidase subunit IV isoform 1 [MGI:88473]
Eif2ak3	eukaryotic translation initiation factor 2 alpha kinase 3 [MGI:1341830]
Lamc2	laminin, gamma 2 [MGI:99913]
Pim1	proviral integration site 1 [MGI:97584]
Cox7a2l	cytochrome c oxidase subunit VIIa polypeptide 2-like [MGI:106015]
Pgk1	phosphoglycerate kinase 1 [MGI:97555]
Acvr1	activin A receptor, type 1 [MGI:87911]
Gch1	GTP cyclohydrolase 1 [MGI:95675]
Rtn4	reticulon 4 [MGI:1915835]
Itga2	integrin alpha 2 [MGI:96600]
Sphk1	sphingosine kinase 1 [MGI:1316649]
Bag3	BCL2-associated athanogene 3 [MGI:1352493]
Lama3	laminin, alpha 3 [MGI:99909]
Bcap31	B cell receptor associated protein 31 [MGI:1350933]
Krt16	keratin 16 [MGI:96690]
Mal	myelin and lymphocyte protein, T cell differentiation protein [MGI:892970]
Gpr56	G protein-coupled receptor 56 [MGI:1340051]
Cox6a1	cytochrome c oxidase subunit VIa polypeptide 1 [MGI:103099]
Snrk	SNF related kinase [MGI:108104]
Pkp1	plakophilin 1 [MGI:1328359]
Pmp22	peripheral myelin protein 22 [MGI:97631]
Pdcd6	programmed cell death 6 [MGI:109283]
Shfm1	split hand/foot malformation (ectrodactyly) type 1 [MGI:109238]
Anxa2	annexin A2 [MGI:88246]
Sprr1a	small proline-rich protein 1A [MGI:106660]
Aplp1	amyloid beta (A4) precursor-like protein 1 [MGI:88046]
Sfn	stratifin [MGI:1891831]
Prdm1	PR domain containing 1, with ZNF domain [MGI:99655]
Tinagl1	tubulointerstitial nephritis antigen-like 1 [MGI:2137617]
Cd9	CD9 antigen [MGI:88348]
Rhob	ras homolog gene family, member B [MGI:107949]
Lgals3	lectin, galactose binding, soluble 3 [MGI:96778]
Vegfa	vascular endothelial growth factor A [MGI:103178]
Krt6b	keratin 6B [MGI:1333768]
Etfa	electron transferring flavoprotein, alpha

Genes from leading edge genes that are found in 3 or more sets

Table 6.15: Leading edge genes repressed in *Apc*$^{fl/fl}$*Smad4*$^{+/+}$ adenomas after 1h TGF-β1 treatment and maintained repression

Symbol	Description
Kif14	kinesin family member 14 [MGI:1098226]
Pax2	paired box gene 2 [MGI:97486]
Chaf1a	chromatin assembly factor 1, subunit A (p150) [MGI:1351331]
Sgol2	shugoshin-like 2 (S. pombe) [MGI:1098767]
Whsc1	Wolf-Hirschhorn syndrome candidate 1 (human) [MGI:1276574]
Kif18b	kinesin family member 18B [MGI:2446979]
Kif15	kinesin family member 15 [MGI:1098258]
Casc5	cancer susceptibility candidate 5 [MGI:1923714]
Cenpf	centromere protein F [MGI:1313302]
Espl1	extra spindle poles-like 1 (S. cerevisiae) [MGI:2146156]
Tfap4	transcription factor AP4 [MGI:103239]
Foxm1	forkhead box M1 [MGI:1347487]
Mdc1	mediator of DNA damage checkpoint 1 [MGI:3525201]
Nfatc2ip	nuclear factor of activated T cells, cytoplasmic, calcineurin dependent 2 interacting protein [MGI:1329015]
Nr4a2	nuclear receptor subfamily 4, group A, member 2 [MGI:1352456]
Acaca	acetyl-Coenzyme A carboxylase alpha [MGI:108451]
Nfix	nuclear factor I/X [MGI:97311]
Nucks1	nuclear casein kinase and cyclin-dependent kinase substrate 1 [MGI:1934811]
Iqgap3	IQ motif containing GTPase activating protein 3 [MGI:3028642]
Ptch1	patched homolog 1 [MGI:105373]
Nfib	nuclear factor I/B [MGI:103188]
Msh2	mutS homolog 2 (E. coli) [MGI:101816]
Nf2	neurofibromatosis 2 [MGI:97307]
Rfc1	replication factor C (activator 1) 1 [MGI:97891]
Mcm5	minichromosome maintenance deficient 5, cell division cycle 46 (S. cerevisiae) [MGI:103197]
Pole	polymerase (DNA directed), epsilon [MGI:1196391]
Akap1	A kinase (PRKA) anchor protein 1 [MGI:104729]
Myb	myeloblastosis oncogene [MGI:97249]
Stc2	stanniocalcin 2 [MGI:1316731]
Srsf1	serine/arginine-rich splicing factor 1 [MGI:98283]
Dnmt1	DNA methyltransferase (cytosine-5) 1 [MGI:94912]
Nup62	nucleoporin 62 [MGI:1351500]
Kpnb1	karyopherin (importin) beta 1 [MGI:107532]
E2f8	E2F transcription factor 8 [MGI:1922038]
Mki67	antigen identified by monoclonal antibody Ki 67 [MGI:106035]
Pold1	polymerase (DNA directed), delta 1, catalytic subunit [MGI:97741]
Exo1	exonuclease 1 [MGI:1349427]
Mybl2	myeloblastosis oncogene-like 2 [MGI:101785]
Aspm	asp (abnormal spindle)-like, microcephaly associated (Drosophila) [MGI:1334448]
Homer2	homer homolog 2 (Drosophila) [MGI:1347354]
Mcm3	minichromosome maintenance deficient 3 (S. cerevisiae) [MGI:101845]
Ncl	nucleolin [MGI:97286]
Pola1	polymerase (DNA directed), alpha 1 [MGI:99660]
Maz	MYC-associated zinc finger protein (purine-binding transcription factor) [MGI:1338823]
Rrp1b	ribosomal RNA processing 1 homolog B (S. cerevisiae) [MGI:1919712]
Mis18bp1	MIS18 binding protein 1 [MGI:2145099]
Usp1	ubiquitin specific peptidase 1 [MGI:2385198]
Trappc10	trafficking protein particle complex 10 [MGI:1336209]
Lig1	ligase I, DNA, ATP-dependent [MGI:101789]
Tmem97	transmembrane protein 97 [MGI:1916321]
Ak2	adenylate kinase 2 [MGI:87978]
Topbp1	topoisomerase (DNA) II binding protein 1 [MGI:1920018]
Smc2	structural maintenance of chromosomes 2 [MGI:106067]
Cdc20	cell division cycle 20 [MGI:1859866]
Ccnf	cyclin F [MGI:102551]
Mcm2	minichromosome maintenance deficient 2 mitotin (S. cerevisiae) [MGI:105380]
Uhrf1	ubiquitin-like, containing PHD and RING finger domains, 1 [MGI:1338889]
Brca2	breast cancer 2 [MGI:109337]
Phc1	polyhomeotic-like 1 (Drosophila) [MGI:103248]
Mrpl12	mitochondrial ribosomal protein L12 [MGI:1926273]
Ddx21	DEAD (Asp-Glu-Ala-Asp) box polypeptide 21 [MGI:1860494]
Pold2	polymerase (DNA directed), delta 2, regulatory subunit [MGI:1097163]

Genes from leading edge genes that are found in 3 or more sets

6.4.2.2 *Smad4* is a tumour suppressor

To analyse the effect of TGF-β1 on regulating gene expression in *Smad4*$^{fl/fl}$ adenomas, Venn diagrams were created by comparing expression at 1h and 12h with 0h. Venn diagrams showed that there were 1794 genes induced and 1749 genes repressed in Smad4$^{fl/fl}$ at 1h compared to 0h. By this, Smad4 disruption increased the expression of 565 genes and repressed 367 genes if compared to Smad4$^{+/+}$. These genes might be involved in cancer and hence Smad4 is acting as a tumor suppressor (Figure 6.6). To identify *Smad4*$^{fl/fl}$ target genes, the analysis continued as before by comparing the expression for each time point with the expression from *Smad4*$^{+/+}$ adenomas. Heat maps are shown in Figure 6.7 . Table 6.16 showed the top 50 DEG in Smad4$^{fl/fl}$ compared to Smad4$^{+/+}$ adenomas at 1h. Eleven differentially regulated genes were unannotated and might be novel genes. Different gene sets were enriched for Smad4$^{+/+}$ adenomas in comparison with Smad4$^{fl/fl}$ at 1h. Some of these sets have FDR>0.25 and are considered as insignificant enrichment. Those with FDR<0.25 such as Plasari_TGF-β1_Targets_1hr_Up, Reactome_Synthesis_of_DNA and Reactome_G1_Phase are considered to be significant (Table 6.17). The leading edge genes in these sets are shown in Table 6.19. These genes are predicted to be involved in transcription, DNA replication and cell cycle regulation. The complementary analysis in this comparison showed enrichment for different sets, some of which were significant based on the FDR values (Table 6.18). The leading edge genes in these sets and their GO are shown in Table 6.20. These genes are predicted to be involved in cytokine production, cell junction organisation by regulating different pathways such as NF-κB, JUK, MAPK and ERK1/ERK2 pathways.

The top 50 differentially regulated late response genes of TGF-β1 in *Smad4*$^{fl/f}$ adenomas to are shown in Table 6.21. Twenty-two genes were not annotated and could be novel genes. GSEA showed some sets to be significantly enriched (FDR 0.168-0.243) in *Smad4*$^{+/+}$ compared to *Smad4*$^{fl/fl}$ at 12h. Examples of these sets are Reactome_Gap_Junction- Assembly and Plasari_TGF-β1_Targets_10hr_Up (Figure 6.22). The leading edge genes with their GO are shown in Table 6.24. These genes include different genes that are expected

to be involved in the regulation of leukocyte proliferation, cell-cell adhesion, cell-substrate adhesion, extracellular matrix organisation and regulation of cell migration through the regulation of different pathways such as PI3K, NF-κB, JUK, MAPK and ERK1/ERK2 pathways. There was upregulation of the Wnt pathway as indicated by *Ctnnb1, Cdh1* and *Jup* upregulation. The complementary analysis showed a significant enrichment for different sets (FDR<0.001) (Table 6.23). The leading edge genes for these sets with their GO are shown in Table 6.25. GO showed that these genes are involved in cell cycle regulation, DNA replication and epigenetic regulation. Among these genes is the Wnt pathway gene *Birc5* and this has been chosen for validation.

6.4.3 Survivin modulation with TGF-β1 as validation to the RNA-seq data

Gene expression data showed differential regulation of genes involved in the cell cycle and proliferation. Among these genes is *Birc5/Survivin* (Table 6.25). It has been chosen for validation because it is a Wnt target gene and has been shown to be upregulated in CRC (Kim et al., 2003). It is also involved in resistance to cancer chemotherapeutics, such as 5-fluorouracil (5-FU)(Zhang et al., 2014). As shown in Figure 6.8, Survivin has been modulated with TGF-β1. There was 1.6 fold reduction in the expression of *Birc5* after 12h TGF-β1 in *Smad4*$^{fl/fl}$ (34.5 FPKM (12h) vs 55.8 FPKM for (0h)) and 6.5 fold reduction in *Smad4*$^{+/+}$ (12.9 FPKM (12h) vs 89.9 FPKM for (0h)). At the protein level there was a decrease in Survivin level after 12h, becoming hardly detectable after 18h in *Smad4*$^{+/+}$. There was a slight reduction in its level at these time points in *Smad4*$^{fl/fl}$ adenomas (Figure 6.8C, repeated at least 3 times). Confocal images confirm nuclear localisation of Survivin and its persistence in *Smad4*$^{fl/fl}$ adenomas after 48h (Figure 6.8D).

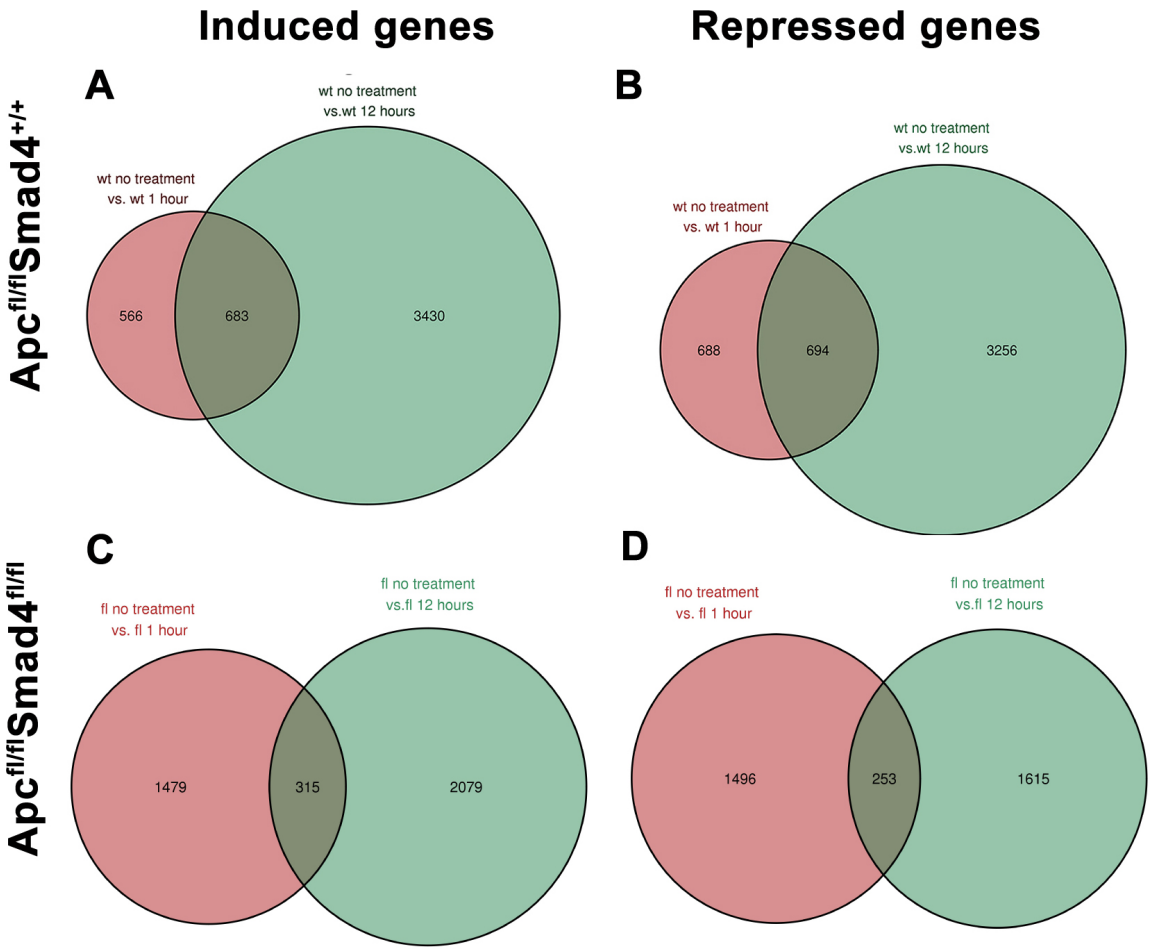

Figure 6.6: **Differential regulation of gene expression represented by Venn diagrams**. Venn diagrams show the number of genes induced or repressed with TGF-β1 treatment at 1h and 12h compared with 0h. The intersection represents the genes that are early response gene with sustained expression or repression. (A, B) Venn diagrams for *Smad4*$^{+/+}$. (C, D) Venn diagrams for *Smad4*$^{fl/fl}$.

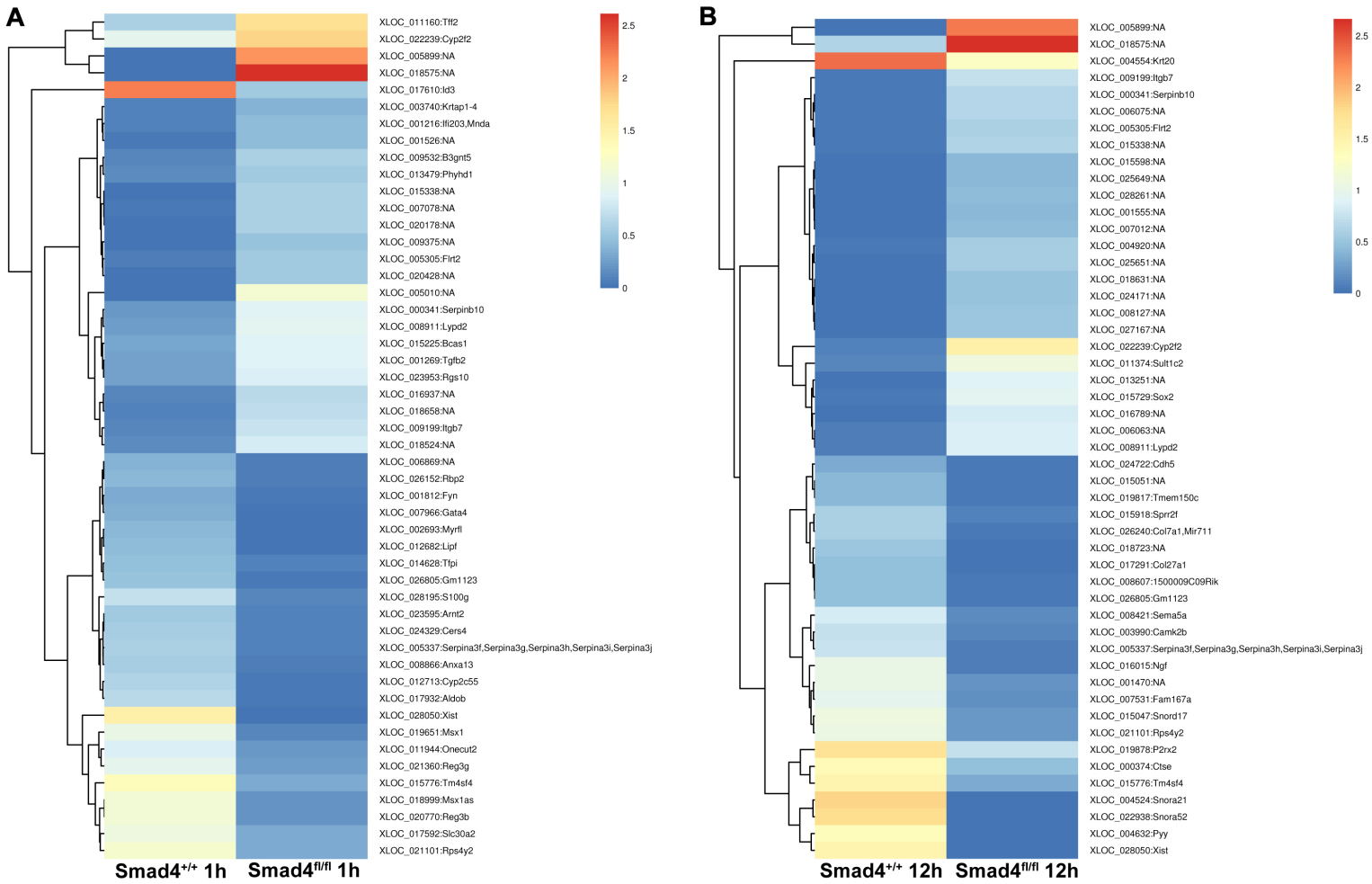

Figure 6.7: **Heat maps of *Smad4*$^{fl/fl}$ compared to *Smad4*$^{+/+}$**. Heat maps show the top 50 differentially regulated genes (A) at 1h , (B) at 12h . Key: Log_{10}FPKM=0 in blue and Log_{10}FPKM=2.5 in red.

Table 6.16: Description of the top 50 differentially regulated genes in *Apc*$^{fl/fl}$*Smad4*$^{fl/fl}$ compared to *Apc*$^{fl/fl}$*Smad4*$^{+/+}$ following 1h TGF-β1 treatment

XLOC	Symbol	Description	Fold-change
			Upregulated in *Smad4*$^{fl/fl}$
XLOC_018575	***NA***		409.76
XLOC_005899	***NA***		132.30
XLOC_005010	***NA***		13.78
XLOC_015338	***NA***		63.18
XLOC_020428	***NA***		53.11
XLOC_020178	***NA***		45.16
XLOC_007078	***NA***		39.11
XLOC_009375	***NA***		34.26
XLOC_001526	***NA***		18.70
XLOC_018658	***NA***		18.14
XLOC_011160	***Tff2***	trefoil factor 2 (spasmolytic protein 1)	16.88
XLOC_018524	***NA***		15.46
XLOC_009199	***Itgb7***	integrin beta 7	14.92
XLOC_005305	***Flrt2***	fibronectin leucine rich transmembrane protein 2	14.49
XLOC_016937	***NA***		12.10
XLOC_008911	***Lypd2***	Ly6/Plaur domain containing 2	10.54
XLOC_000341	***Serpinb10***	serine (or cysteine) peptidase inhibitor, clade B (ovalbumin), member 10	9.85
XLOC_009532	***B3gnt5***	UDP-GlcNAc:betaGal beta-1,3-N-acetylglucosaminyltransferase 5	8.97
XLOC_022239	***Cyp2f2***	cytochrome P450, family 2, subfamily f, polypeptide 2	7.90
XLOC_001216	***Ifi203***	interferon activated gene 203	7.73
XLOC_001216	***Mnda***	myeloid cell nuclear differentiation antigen	7.73
XLOC_023953	***Rgs10***	regulator of G-protein signalling 10	7.09
XLOC_003740	***Krtap1-4***	keratin associated protein 1-4	6.86
XLOC_001269	***Tgfb2***	transforming growth factor, beta 2	6.82
XLOC_013479	***Phyhd1***	phytanoyl-CoA dioxygenase domain containing 1	6.64
XLOC_015225	***Bcas1***	breast carcinoma amplified sequence 1	6.35
			Upregulated in *Smad4*$^{+/+}$
XLOC_028050	***Xist***	inactive X specific transcripts	1015.11
XLOC_017610	***Id3***	inhibitor of DNA binding 3	70.20
XLOC_012713	***Cyp2c55***	cytochrome P450, family 2, subfamily c, polypeptide 55	43.29
XLOC_017932	***Aldob***	aldolase B, fructose-bisphosphate	39.83
XLOC_019651	***Msx1***	msh homeobox 1	25.76
XLOC_007966	***Gata4***	GATA binding protein 4	25.32
XLOC_002693	***Myrfl***	myelin regulatory factor-like	25.13
XLOC_020770	***Reg3b***	regenerating islet-derived 3 beta	22.86
XLOC_018999	***Msx1as***		22.49
XLOC_015776	***Tm4sf4***	transmembrane 4 superfamily member 4	17.60
XLOC_008866	***Anxa13***	annexin A13	17.35
XLOC_026805	***Gm1123***	predicted gene 1123	16.03
XLOC_021101	***Rps4y2***		13.11
XLOC_026152	***Rbp2***	retinol binding protein 2, cellular	11.89
XLOC_028195	***S100g***	S100 calcium binding protein G	11.82
XLOC_005337	***Serpina3j***	serine (or cysteine) peptidase inhibitor, clade A (alpha-1 antiproteinase, antitrypsin), member 3J	10.84
XLOC_005337	***Serpina3i***	serine (or cysteine) peptidase inhibitor, clade A, member 3I	10.84
XLOC_005337	***Serpina3h***	serine (or cysteine) peptidase inhibitor, clade A, member 3H	10.84
XLOC_005337	***Serpina3f***	serine (or cysteine) peptidase inhibitor, clade A, member 3F	10.84
XLOC_005337	***Serpina3g***	serine (or cysteine) peptidase inhibitor, clade A, member 3G	10.84
XLOC_024329	***Cers4***	ceramide synthase 4	9.89
XLOC_021360	***Reg3g***	regenerating islet-derived 3 gamma	9.66
XLOC_001812	***Fyn***	Fyn proto-oncogene	9.55
XLOC_023595	***Arnt2***	aryl hydrocarbon receptor nuclear translocator 2	9.54
XLOC_017592	***Slc30a2***	solute carrier family 30 (zinc transporter), member 2	9.41
XLOC_011944	***Onecut2***	one cut domain, family member 2	9.21
XLOC_006869	***NA***		8.70
XLOC_014628	***Tfpi***	tissue factor pathway inhibitor	8.67
XLOC_012682	***Lipf***	lipase, gastric	1.65

Table 6.17: Gene set enrichment in *Apc*$^{fl/fl}$*Smad4*$^{+/+}$ compared to *Apc*$^{fl/fl}$*Smad4*$^{fl/fl}$ after 1h TGF-β1 treatment

NAME	SIZE[1]	NES[2]	NOM p-val[3]	FDR q-val[4]
REACTOME_CELL_CYCLE_CHECKPOINTS	105	1.77	0.000	0.719
MOROSETTI_FACIOSCAPULOHUMERAL_MUSCULAR_DISTROPHY_UP	18	1.75	0.000	0.488
KEGG_STEROID_HORMONE_BIOSYNTHESIS	37	1.75	0.000	0.334
PEART_HDAC_PROLIFERATION_CLUSTER_UP	49	1.75	0.000	0.264
GARCIA_TARGETS_OF_FLI1_AND_DAX1_DN	147	1.74	0.000	0.235
MOREAUX_MULTIPLE_MYELOMA_BY_TACI_DN	152	1.74	0.000	0.214
KEGG_NITROGEN_METABOLISM	20	1.72	0.000	0.251
REACTOME_MITOCHONDRIAL_TRNA_AMINOACYLATION	19	1.72	0.000	0.221
REACTOME_HIV_LIFE_CYCLE	99	1.72	0.002	0.198
REACTOME_MITOTIC_G1_G1_S_PHASES	121	1.71	0.000	0.192
REACTOME_HIV_INFECTION	174	1.71	0.000	0.180
KEGG_RNA_DEGRADATION	54	1.70	0.000	0.193
REACTOME_LATE_PHASE_OF_HIV_LIFE_CYCLE	86	1.70	0.002	0.183
REACTOME_ORC1_REMOVAL_FROM_CHROMATIN	62	1.70	0.002	0.180
NIKOLSKY_BREAST_CANCER_5P15_AMPLICON	24	1.70	0.000	0.174
PLASARI_TGFB1_TARGETS_1HR_UP	34	1.69	0.000	0.169
BURTON_ADIPOGENESIS_PEAK_AT_24HR	39	1.69	0.002	0.176
REACTOME_SYNTHESIS_OF_DNA	87	1.69	0.004	0.174
REACTOME_G1_PHASE	31	1.68	0.000	0.170
REACTOME_M_G1_TRANSITION	73	1.68	0.002	0.173

[1]Size: number of genes in the set, [2]NES: Normalized Enrichment Score, [3]NOM: Nominal p-value, [4]FDR: False Discovery Rate (q-value).

Table 6.18: Gene set enrichment in *Apc*$^{fl/fl}$*Smad4*$^{fl/fl}$ compared to *Apc*$^{fl/fl}$*Smad4*$^{+/+}$ after 1h TGF-β1 treatment

NAME	SIZE[1]	NES[2]	NOM p-val[3]	FDR q-val[4]
DEBOSSCHER_NFKB_TARGETS_REPRESSED_BY_GLUCOCORTICOIDS	23	-1.90	0.000	0.072
BIOCARTA_P38MAPK_PATHWAY	36	-1.79	0.000	0.268
GAVIN_PDE3B_TARGETS	21	-1.77	0.000	0.245
KEGG_VASOPRESSIN_REGULATED_WATER_REABSORPTION	43	-1.74	0.000	0.282
BIOCARTA_INFLAM_PATHWAY	28	-1.74	0.000	0.238
WANG_IMMORTALIZED_BY_HOXA9_AND_MEIS1_DN	23	-1.73	0.002	0.223
WANG_METASTASIS_OF_BREAST_CANCER_ESR1_DN	24	-1.73	0.002	0.197
HALMOS_CEBPA_TARGETS_UP	50	-1.71	0.000	0.226
SESTO_RESPONSE_TO_UV_C4	20	-1.71	0.000	0.202
WEST_ADRENOCORTICAL_TUMOR_MARKERS_DN	19	-1.71	0.000	0.189
BIOCARTA_CTCF_PATHWAY	23	-1.70	0.000	0.192
BIOCARTA_NKT_PATHWAY	28	-1.70	0.002	0.186
RICKMAN_HEAD_AND_NECK_CANCER_E	78	-1.69	0.000	0.206
DUTERTRE_ESTRADIOL_RESPONSE_6HR_DN	87	-1.69	0.000	0.196
ABBUD_LIF_SIGNALING_1_DN	25	-1.68	0.002	0.196
BUCKANOVICH_T_LYMPHOCYTE_HOMING_ON_TUMOR_UP	19	-1.68	0.000	0.192
ONDER_CDH1_TARGETS_3_DN	50	-1.68	0.000	0.199
YANG_BREAST_CANCER_ESR1_BULK_UP	26	-1.67	0.002	0.220
KEGG_SMALL_CELL_LUNG_CANCER	80	-1.66	0.000	0.214
BIOCARTA_CYTOKINE_PATHWAY	20	-1.65	0.015	0.252

[1]Size: number of genes in the set, [2]NES: Normalized Enrichment Score, [3]NOM: Nominal p-value, [4]FDR: False Discovery Rate (q-value).

Table 6.19: Leading edge genes upregulated in *Apc*$^{fl/fl}$*Smad4*$^{+/+}$ compared to *Apc*$^{fl/fl}$ *Smad4*$^{fl/fl}$ following 1h of TGF-β1 treatment

Symbol	Description	GO annotations[1]
Hmga1-rs1	high mobility group AT-hook I, related sequence 1 [MGI:96161]	carbon-oxygen lyase activity; chromatin; DNA repair; transcription coactivator activity
Taf4b	TAF4B RNA polymerase II, TATA box binding protein (TBP)-associated factor [MGI:2152345]	
Taf4a	TAF4A RNA polymerase II, TATA box binding protein (TBP)-associated factor [MGI:2152346]	DNA-directed RNA polymerase complex; histone acetyltransferase complex; transcription factor TFIID complex
Gtf2h2	general transcription factor II H, polypeptide 2 [MGI:1345669]	ATP catabolic process; DNA-directed RNA polymerase II, holoenzyme
Wdr61	WD repeat domain 61 [MGI:1917493]	regulation of DNA-templated transcription and elongation from RNA polymerase II promoter
Ccnh	cyclin H [MGI:1913921]	ATP catabolic process; holo TFIIH complex; nuclear DNA-directed RNA polymerase complex; RNA polymerase II carboxy-terminal domain kinase activity
Hmga1	high mobility group AT-hook 1 [MGI:96160]	
Gtf2h3	general transcription factor IIH, polypeptide 3 [MGI:1277143]	ATP catabolic process; holo TFIIH complex; nuclear DNA-directed RNA polymerase complex; nuclear transcription factor complex; nucleoside monophosphate catabolic process
E2f2	E2F transcription factor 2 [MGI:1096341]	core promoter binding
Polr2k	polymerase (RNA) II (DNA directed) polypeptide K [MGI:102725]	DNA-directed RNA polymerase activity; RNA polymerase I activity; RNA polymerase III activity
Taf5	TAF5 RNA polymerase II, TATA box binding protein (TBP)-associated factor [MGI:2442144]	acetyltransferase activity; acetyltransferase complex; DNA-directed RNA polymerase complex; DNA-directed RNA polymerase II, holoenzyme; DNA-templated transcription,transcription factor TFIID complex
Polr2j	polymerase (RNA) II (DNA directed) polypeptide J [MGI:109582]	DNA-directed RNA polymerase activity; DNA-directed RNA polymerase II, holoenzyme; nuclear DNA-directed RNA polymerase complex; RNA polymerase activity
Psip1	PC4 and SFRS1 interacting protein 1 [MGI:2142116]	chromatin; structure-specific DNA binding; transcription coactivator activity
Taf12	TAF12 RNA polymerase II, TATA box binding protein (TBP)-associated factor [MGI:1913714]	acetyltransferase activity; DNA-directed RNA polymerase complex;histone acetyltransferase complex; histone H3 acetylation; internal peptidyl-lysine acetylation; internal protein amino acid acetylation; transcription factor TFIID complex
E2f3	E2F transcription factor 3 [MGI:1096340]	core promoter binding
Supt4a	suppressor of Ty 4A [MGI:107416]	positive regulation of DNA-templated transcription, regulation of transcription elongation from RNA polymerase II promoter
Polr2l	polymerase (RNA) II (DNA directed) polypeptide L [MGI:1913741]	DNA-directed RNA polymerase activity
Cdk7	cyclin-dependent kinase 7 [MGI:102956]	ATP catabolic process; cyclin-dependent protein kinase activity; cyclin-dependent protein Ser/Thr kinase activity; DNA-directed RNA polymerase II, holoenzyme; holo TFIIH complex
Taf9	TAF9 RNA polymerase II, TATA box binding protein (TBP)-associated factor [MGI:1888697]	
E2f5	E2F transcription factor 5 [MGI:105091]	cell cycle phase transition; G1/S transition of mitotic cell cycle; mitotic cell cycle phase transition
Mnat1	menage a trois 1 [MGI:106207]	ATP catabolic process; cell cycle phase transition; DNA-directed RNA polymerase complex; G1/S transition of mitotic cell cycle; holo TFIIH complex; mitotic cell cycle phase transition
Polr2c	polymerase (RNA) II (DNA directed) polypeptide C [MGI:109299]	DNA-directed RNA polymerase activity; RNA polymerase complex
Taf11	TAF11 RNA polymerase II, TATA box binding protein (TBP)-associated factor [MGI:1916026]	DNA-directed RNA polymerase complex; DNA-directed RNA polymerase II, transcription factor TFIID complex
Gtf2h1	general transcription factor II H, polypeptide 1 [MGI:1277216]	ATP catabolic process; DNA-dependent ATPase activity; DNA-directed RNA polymerase complex; holo TFIIH complex;
Gtf2f2	general transcription factor IIF, polypeptide 2 [MGI:1915955]	

Continued on following page

Symbol	Description	GO annotations[1]
Polr2f	polymerase (RNA) II (DNA directed) polypeptide F [MGI:1349393]	DNA-directed RNA polymerase activity
Klf10	Kruppel-like factor 10 [MGI:1101353]	myeloid cell differentiation
Tfdp1	transcription factor Dp 1 [MGI:101934]	
Polr2f	polymerase (RNA) II (DNA directed) polypeptide F [MGI:1349393]	DNA-directed RNA polymerase activity
Polr2g	polymerase (RNA) II (DNA directed) polypeptide G [MGI:1914960]	DNA-directed RNA polymerase activity; transcription initiation from RNA polymerase II promoter
Mybl2	myeloblastosis oncogene-like 2 [MGI:101785]	
Tcea1	transcription elongation factor A (SII) 1 [MGI:1196624]	erythrocyte differentiation; myeloid cell differentiation
Tceb1	transcription elongation factor B (SIII), polypeptide 1 [MGI:1915173]	positive regulation of DNA-templated transcription, transcription elongation from RNA polymerase II promoter
Xrcc5	X-ray repair complementing defective repair in Chinese hamster cells 5 [MGI:104517]	carbon-oxygen lyase activity; DNA repair;structure-specific DNA binding
Gtf2a2	general transcription factor II A, 2 [MGI:1933289]	DNA-directed RNA polymerase complex; transcription initiation from RNA polymerase II promoter
Ccnt1	cyclin T1 [MGI:1328363]	transcription elongation factor complex
Rbl1	retinoblastoma-like 1 (p107) [MGI:103300]	regulation of lipid kinase activity
Polr2d	polymerase (RNA) II (DNA directed) polypeptide D [MGI:1916491]	DNA-directed RNA polymerase activity
Id2	inhibitor of DNA binding 2 [MGI:96397]	chromatin; erythrocyte differentiation; G1/S transition of mitotic cell cycle
Polr2e	polymerase (RNA) II (DNA directed) polypeptide E [MGI:1913670]	DNA-directed RNA polymerase activity
Polr2b	polymerase (RNA) II (DNA directed) polypeptide B [MGI:2388280]	DNA-directed RNA polymerase activity
Tceb2	transcription elongation factor B (SIII), polypeptide 2 [MGI:1914923]	transcription elongation factor complex
Id3	inhibitor of DNA binding 3 [MGI:96398]	negative regulation of osteoblast differentiation
Id1	inhibitor of DNA binding 1 [MGI:96396]	negative regulation of osteoblast differentiation; regulation of DNA binding
Polr2i	polymerase (RNA) II (DNA directed) polypeptide I [MGI:1917170]	DNA repair; DNA-directed RNA polymerase activity
Cdk2	cyclin-dependent kinase 2 [MGI:104772]	Ser/Thr kinase activity; G1/S transition of mitotic cell cycle
Taf10	TAF10 RNA polymerase II, TATA box binding protein (TBP)-associated factor [MGI:1346320]	acetyltransferase activity; cell cycle phase transition
Ccna2	cyclin A2 [MGI:108069]	pronucleus
Polr2h	polymerase (RNA) II (DNA directed) polypeptide H [MGI:2384309]	DNA-directed RNA polymerase activity; RNA polymerase activity
Gmnn	geminin [MGI:1927344]	repressing transcription factor binding
Xrcc6	X-ray repair complementing defective repair in Chinese hamster cells 6 [MGI:95606]	carbon-oxygen lyase activity; DNA repair; protein C-terminus binding; structure-specific DNA binding
Rb1	retinoblastoma 1 [MGI:97874]	cell cycle phase transition; G1/S transition of mitotic cell cycle; RNA polymerase II transcription factor binding
Cdk4	cyclin-dependent kinase 4 [MGI:88357]	cell cycle phase transition; chromatin; G1/S transition of mitotic cell cycle
Exosc5	exosome component 5 [MGI:107889]	chromatin
Psma6	proteasome (prosome, macropain) subunit, alpha type 6 [MGI:1347006]	
Ssrp1	structure specific recognition protein 1 [MGI:107912]	
Psmc5	protease (prosome, macropain) 26S subunit, ATPase 5 [MGI:105047]	ATP catabolic process; DNA-directed RNA polymerase complex
Tbp	TATA box binding protein [MGI:101838]	DNA-directed RNA polymerase complex; transcription factor TFIID complex
Pcna	proliferating cell nuclear antigen [MGI:97503]	cyclin-dependent protein kinase holoenzyme complex; DNA repair; structure-specific DNA binding

[1]GO: Gene ontology as described by GeneMANIA. (Continued from previous page).

Table 6.20: Leading edge genes upregulated in *Apc*$^{fl/fl}$*Smad4*$^{fl/fl}$ compared to *Apc*$^{fl/fl}$*Smad4*$^{+/+}$ after 1h TGF-β1 treatment

Symbol	Description	GO annotations[1]
Bmyc	brain expressed myelocytomatosis oncogene [MGI:88184]	
Il1a	interleukin 1 alpha [MGI:96542]	cytokine biosynthetic process; developmental programmed cell death; extrinsic apoptotic signalling pathway; interleukin-2 (IL-2) production; IL-6 positive regulation of cell cycle process; positive regulation of cell migration; positive regulation of ERK1 and ERK2 cascade; positive regulation of I-κB kinase/NF-κB signalling; regulation of angiogenesis
Myc	myelocytomatosis oncogene [MGI:97250]	cellular iron ion homeostasis; cellular response to drug; cellular transition metal ion homeostasis; myeloid leukocyte differentiation; negative regulation of cell cycle; positive regulation of epithelial cell and mesenchymal cell proliferation; regulation of cell division; regulation of stem cell proliferation
Tgfb1	transforming growth factor, beta 1 [MGI:98725]	adaptive immune response; cell cycle arrest; cell junction organisation; cell-cell adhesion; cell-cell junction organisation; cellular response to TGF-β stimulus; collagen biosynthetic process; epithelial cell migration and proliferation; EMT; positive regulation of MAP kinase activity; positive regulation of NF-κB transcription factor activity
Tgfb3	transforming growth factor, beta 3 [MGI:98727]	activation of protein kinase activity; cell junction organisation; cell-cell junction organisation; cellular response to TGF-β stimulus; collagen biosynthetic process; cytokine production involved in immune response; EMT; myeloid leukocyte cytokine production; negative regulation of cytokine production involved in immune response; positive regulation of MAP kinase activity; positive regulation of multicellular organismal metabolic process; positive regulation of pathway-restricted SMAD protein phosphorylation
Foxa1	forkhead box A1 [MGI:1347472]	cell fate commitment; cell fate specification; negative regulation of EMT; positive regulation of cell cycle; RNA polymerase II distal enhancer sequence-specific DNA binding transcription factor activity; stem cell differentiation
Tnf	tumour necrosis factor [MGI:104798]	acute inflammatory response; acute-phase response; adaptive immune response; protein kinase B signalling; protein localisation to nucleus; protein secretion; positive regulation of I-κB kinase/NF-κB signalling; positive regulation of interferon-gamma production; positive regulation of IL-6 production; positive regulation of intracellular protein transport; positive regulation of intracellular transport; positive regulation of JNK cascade; positive regulation of lipid metabolic process; positive regulation of MAP kinase activity

[1]GO:Gene ontology as described by GeneMANIA

Table 6.21: Description of the top 50 differentially regulated genes in *Apc*$^{fl/fl}$*Smad4*$^{fl/fl}$ compared to *Apc*$^{fl/fl}$*Smad4*$^{+/+}$ following 12h TGF-β1 treatment

XLOC	Symbol	Description	Fold-change
			Upregulated in *Smad4*$^{fl/fl}$
XLOC_005899	***NA***		205.99
XLOC_018575	***NA***		146.68
XLOC_022239	***Cyp2f2***	cytochrome P450, family 2, subfamily f, polypeptide 2	134.65
XLOC_015729	***Sox2***	SRY (sex determining region Y)-box 2	69.23
XLOC_009199	***Itgb7***	integrin beta 7	62.01
XLOC_001555	***NA***		56.94
XLOC_025649	***NA***		47.63
XLOC_015338	***NA***		43.61
XLOC_024171	***NA***		43.27
XLOC_028261	***NA***		42.34
XLOC_018631	***NA***		38.06
XLOC_015598	***NA***		36.81
XLOC_011374	***Sult1c2***	sulfotransferase family, cytosolic, 1C, member 2	36.59
XLOC_005305	***Flrt2***	fibronectin leucine rich transmembrane protein 2	35.70
XLOC_004920	***NA***		35.05
XLOC_006063	***NA***		34.81
XLOC_006075	***NA***		34.66
XLOC_008911	***Lypd2***	Ly6/Plaur domain containing 2	31.67
XLOC_000341	***Serpinb10***	serine (or cysteine) peptidase inhibitor, clade B (ovalbumin), member 10	29.98
XLOC_013251	***NA***		7.05
XLOC_016789	***NA***		6.04
XLOC_025651	***NA***		2.64
XLOC_027167	***NA***		2.40
XLOC_008127	***NA***		2.30
XLOC_007012	***NA***		1.71
			Upregulated in *Smad4*$^{+/+}$
XLOC_028050	***Xist***	inactive X specific transcripts	468.10
XLOC_004524	***Snora21***	small nucleolar RNA, H/ACA box 21	67.69
XLOC_016015	***Ngf***	nerve growth factor	64.22
XLOC_022938	***Snora52***	small nucleolar RNA, H/ACA box 52	58.63
XLOC_017291	***Col27a1***	collagen, type XXVII, alpha 1	33.42
XLOC_026805	***Gm1123***	predicted gene 1123	25.97
XLOC_015776	***Tm4sf4***	transmembrane 4 superfamily member 4	24.98
XLOC_005337	***Serpina3j***	serine (or cysteine) peptidase inhibitor, clade A (alpha-1 antiproteinase, antitrypsin), member 3J	24.87
XLOC_005337	***Serpina3i***	serine (or cysteine) peptidase inhibitor, clade A, member 3I	24.87
XLOC_005337	***Serpina3h***	serine (or cysteine) peptidase inhibitor, clade A, member 3H	24.87
XLOC_005337	***Serpina3f***	serine (or cysteine) peptidase inhibitor, clade A, member 3F	24.87
XLOC_005337	***Serpina3g***	serine (or cysteine) peptidase inhibitor, clade A, member 3G	24.87
XLOC_026240	***Col7a1***	collagen, type VII, alpha 1	23.15
XLOC_026240	***Mir711***	microRNA 711	23.15
XLOC_004632	***Pyy***	peptide YY	22.44
XLOC_015051	***NA***		21.98
XLOC_008607	***1500009C09-Rik***	RIKEN cDNA 1500009C09 gene	20.63
XLOC_007531	***Fam167a***	family with sequence similarity 167, member A	17.06
XLOC_015047	***Snord17***	small nucleolar RNA, C/D box 17	16.82
XLOC_019817	***Tmem150c***	transmembrane protein 150C	16.74
XLOC_001470	***NA***		16.65
XLOC_003990	***Camk2b***	calcium/calmodulin-dependent protein kinase II, beta	15.03
XLOC_008421	***Sema5a***	sema domain, seven thrombospondin repeats (type 1 and type 1-like), (semaphorin) 5A	14.88
XLOC_021101	***Rps4y2***		14.25
XLOC_015918	***Sprr2f***	small proline-rich protein 2F	13.54
XLOC_000374	***Ctse***	cathepsin E	12.34
XLOC_004554	***Krt20***	keratin 20	12.09
XLOC_019878	***P2rx2***	purinergic receptor P2X, ligand-gated ion channel, 2	12.05
XLOC_024722	***Cdh5***	cadherin 5	11.95
XLOC_018723	***NA***		2.23

Table 6.22: Gene set enrichment in *Apc*$^{fl/fl}$*Smad4*$^{+/+}$ compared to *Apc*$^{fl/fl}$*Smad4*$^{fl/fl}$ at 12h after TGF-β1 treatment

NAME	SIZE[1]	NES[2]	NOM p-val[3]	FDR q-val[4]
PAL_PRMT5_TARGETS_DN	27	1.80	0.000	0.648
BIOCARTA_DC_PATHWAY	20	1.79	0.000	0.408
REACTOME_PROTEIN_FOLDING	42	1.77	0.000	0.393
LABBE_TGFB1_TARGETS_UP	98	1.74	0.000	0.435
LIEN_BREAST_CARCINOMA_METAPLASTIC	32	1.73	0.000	0.407
REACTOME_CELL_JUNCTION_ORGANIZATION	74	1.73	0.000	0.342
KEGG_GRAFT_VERSUS_HOST_DISEASE	28	1.73	0.004	0.316
XU_CREBBP_TARGETS_DN	40	1.73	0.000	0.282
REACTOME_CELL_CELL_COMMUNICATION	113	1.72	0.002	0.259
KEGG_ALLOGRAFT_REJECTION	30	1.72	0.002	0.243
PID_INTEGRIN3_PATHWAY	43	1.72	0.000	0.222
KEGG_STEROID_HORMONE_BIOSYNTHESIS	37	1.72	0.000	0.221
REACTOME_GAP_JUNCTION_ASSEMBLY	17	1.72	0.000	0.208
KYNG_ENVIRONMENTAL_STRESS_RESPONSE_NOT_BY_UV_IN_OLD	23	1.71	0.000	0.199
HANSON_HRAS_SIGNALING_VIA_NFKB	22	1.71	0.000	0.190
PLASARI_TGFB1_TARGETS_10HR_UP	191	1.71	0.000	0.184
TSUNODA_CISPLATIN_RESISTANCE_DN	42	1.71	0.000	0.179
ALONSO_METASTASIS_NEURAL_UP	17	1.71	0.000	0.176
MARKEY_RB1_CHRONIC_LOF_DN	108	1.70	0.000	0.173
REACTOME_ASSOCIATION_OF_TRIC_CCT_WITH_TARGET_PROTEINS_DURING _BIOSYNTHESIS	25	1.70	0.000	0.168

[1]Size: number of genes in the set, [2]NES: Normalized Enrichment Score, [3]NOM: Nominal p-value, [4]FDR: False Discovery Rate (q-value).

Table 6.23: Gene set enrichment in *Apc*$^{fl/fl}$*Smad4*$^{fl/fl}$ compared to *Apc*$^{fl/fl}$*Smad4*$^{+/+}$ at 12h after TGF-β1 treatment

NAME	SIZE[1]	NES[2]	NOM p-val[3]	FDR q-val[4]
WANG_RECURRENT_LIVER_CANCER_UP	18	-2.16	0.000	0.000
TURASHVILI_BREAST_DUCTAL_CARCINOMA_VS_LOBULAR_NORMAL_UP	66	-2.13	0.000	0.000
REACTOME_KINESINS	22	-2.11	0.000	0.000
MATZUK_SPERMATOCYTE	66	-2.08	0.000	0.000
WILCOX_PRESPONSE_TO_ROGESTERONE_UP	129	-2.02	0.000	0.001
HORIUCHI_WTAP_TARGETS_DN	282	-2.01	0.000	0.001
POOLA_INVASIVE_BREAST_CANCER_UP	244	-1.99	0.000	0.001
WHITFIELD_CELL_CYCLE_G2_M	196	-1.99	0.000	0.001
ZHENG_GLIOBLASTOMA_PLASTICITY_UP	229	-1.99	0.000	0.001
AFFAR_YY1_TARGETS_DN	224	-1.98	0.000	0.001
NAKAYAMA_SOFT_TISSUE_TUMORS_PCA2_UP	84	-1.98	0.000	0.001
VANTVEER_BREAST_CANCER_METASTASIS_DN	107	-1.98	0.000	0.001
MATZUK_MEIOTIC_AND_DNA_REPAIR	35	-1.96	0.000	0.001
SCIBETTA_KDM5B_TARGETS_DN	69	-1.96	0.000	0.001
CHICAS_RB1_TARGETS_GROWING	222	-1.96	0.000	0.001
GOLDRATH_ANTIGEN_RESPONSE	315	-1.95	0.000	0.001
XU_HGF_SIGNALING_NOT_VIA_AKT1_48HR_DN	17	-1.95	0.000	0.001
OLSSON_E2F3_TARGETS_DN	41	-1.95	0.000	0.001
RUIZ_TNC_TARGETS_DN	129	-1.94	0.000	0.001
SHEPARD_CRUSH_AND_BURN_MUTANT_DN	165	-1.94	0.000	0.001

[1]Size: number of genes in the set, [2]NES: Normalized Enrichment Score, [3]NOM: Nominal p-value, [4]FDR: False Discovery Rate (q-value).

Table 6.24: Leading edge genes upregulated in *Apc*$^{fl/fl}$*Smad4*$^{+/+}$ compared to *Apc*$^{fl/fl}$*Smad4*$^{fl/fl}$ after 12h TGF-β1 treatment

Symbol	Description	GO annotations[1]
Jag1	jagged 1 [MGI:1095416]	positive regulation of myeloid cell differentiation; stem cell differentiation
Sox7	SRY-box containing gene 7 [MGI:98369]	regulation of canonical Wnt signalling pathway; positive regulation of cysteine-type endopeptidase activity involved in apoptotic process
Il11	interleukin 11 [MGI:107613]	cytokine receptor binding; growth factor activity; regulation of peptidyl-tyrosine phosphorylation
Cd40	CD40 antigen [MGI:88336]	regulation of adaptive immune response; leukocyte proliferation; positive regulation of MAP kinase and NF-κB transcription Factor activity; positive regulation of protein Ser/Thr kinase activity; positive regulation of Ras GTPase activity; protein kinase C signalling
Pdgfb	platelet derived growth factor, B polypeptide [MGI:97528]	activation of protein kinase B activity; ameboidal cell migration; epithelial cell development and proliferation; leukocyte chemotaxis; leukocyte migration; positive regulation of ERK1 and ERK2 cascade; positive regulation of fibroblast proliferation; positive regulation of MAP kinase activity; positive regulation of phosphatidylinositol 3-kinase activity
H2-Ab1	histocompatibility 2, class II antigen A, beta 1 [MGI:103070]	adaptive immune response; immunoglobulin production; leukocyte mediated immunity; mononuclear cell proliferation; negative regulation of T cell proliferation
Sphk1	sphingosine kinase 1 [MGI:1316649]	cytokine-mediated signalling pathway; fibroblast proliferation; positve regulation of I-κB kinase/NF-κB signalling; IL-1β production; positive regulation of cell cycle; positive regulation of cell growth; positive regulation of cell migration; positive regulation of cell motility
Il1a	interleukin 1 alpha [MGI:96542]	cytokine metabolic process; cytokine-mediated signalling pathway; developmental programmed cell death; granulocyte migration; I-κB kinase/NF-κB signalling; IL-6 production; JNK cascade; leukocyte migration; positive regulation of cytokine production; positive regulation of ERK1 and ERK2 cascade; positive regulation of I-κB kinase/NF-κB signalling; positive regulation of stress-activated MAPK cascade
Fstl3	follistatin-like 3 [MGI:1890391]	BMP signalling pathway; cell-cell adhesion; fibronectin binding; negative regulation of myeloid leukocyte differentiation; positive regulation of cell adhesion; regulation of transmembrane receptor protein Ser/Thr kinase signalling pathway
Ngf	nerve growth factor [MGI:97321]	cytokine receptor binding; positive regulation of growth; positive regulation of stem cell proliferation; protein autophosphorylation; stem cell proliferation; tumor necrosis factor receptor superfamily binding
Fbxw7	F-box and WD-40 domain protein 7 [MGI:1354695]	blood vessel morphogenesis; negative regulation of DNA replication; positive regulation of ERK1 and ERK2 cascade; positive regulation of peptidyl-tyrosine phosphorylation
Cyr61	cysteine rich protein 61 [MGI:88613]	BMP signalling pathwayt; cell-cell adhesion; cell-substrate adhesion; extracellular matrix organisation; regulation of ERK1 and ERK2 cascade; regulation of transmembrane receptor protein Ser/Thr kinase signalling pathway
Tnf	tumour necrosis factor [MGI:104798]	regulation of I-κB kinase/NF-κB signalling; regulation of immunoglobulin mediated immune response; regulation of JNK cascade; regulation of leukocyte differentiation; regulation of MAP kinase activity; ; transcription factor import into nucleus; tumor necrosis factor receptor superfamily binding; tumor necrosis factor-mediated signalling pathway
Junb	Jun-B oncogene [MGI:96647]	cellular response to calcium ion; myeloid leukocyte differentiation; ossification; osteoblast differentiation; response to calcium ion; structure-specific DNA binding; vasculogenesis
Tgfb1	transforming growth factor, beta 1 [MGI:98725]	cellular response to TGF-β stimulus; lymphocyte mediated immunity; mesenchymal cell differentiation; positive regulation of MAP kinase activity; positive regulation of NF-κB transcription factor activity; positive regulation of phosphatidylinositol 3-kinase activity; SMAD protein import into nucleus
Vegfa	vascular endothelial growth factor A [MGI:103178]	adaptive immune response; cytokine receptor binding; developmental cell growth; endothelial cell migration and proliferation; extracellular matrix; positive regulation of leukocyte chemotaxis; positive regulation of MAP kinase and ERK1 and ERK2 activity; positive regulation of mesenchymal cell proliferation; vascular endothelial growth factor signalling pathway
Bhlhe40	basic helix-loop-helix family, member e40 [MGI:1097714]	activating transcription factor binding; RNA polymerase II activating transcription factor binding; RNA polymerase II distal enhancer sequence-specific DNA binding transcription factor activity; RNA polymerase II transcription factor binding
Ilk	integrin linked kinase [MGI:1195267]	BMP signalling pathway; canonical Wnt signalling pathway; cell-cell junction; cell-matrix adhesion; extracellular matrix; extracellular matrix organisation; positive regulation of cell growth; positive regulation of cell migration and motility; positive regulation of cell projection organisation; positive regulation of MAP kinase activity
Jup	junction plakoglobin [MGI:96650]	adherens junction; anchoring junction; apical junction complex; beta-catenin destruction complex; cadherin binding; canonical Wnt signalling pathway;
Ctnnb1	catenin (cadherin associated protein), beta 1 [MGI:88276]	activating transcription factor binding; adherens junction; anchoring junction; apical junction complex; canonical Wnt signalling pathway; leukocyte and lymphocytes proliferation; mesenchymal cell proliferation; positive regulation of epithelial cell proliferation; positive regulation of EMT; positive regulation of I-κB kinase/NF-κB signalling; RNA polymerase II activating transcription factor binding; SMAD binding
Cdh1	cadherin 1 [MGI:88354]	adherens junction; anchoring junction; apical junction complex; canonical Wnt signalling pathway; regulation of canonical Wnt signalling pathway

[1]GO: Gene ontology as described by GeneMANIA

Table 6.25: Leading edge genes upregulated in *Apc*$^{fl/fl}$*Smad4*$^{fl/fl}$ compared to *Apc*$^{fl/fl}$*Smad4*$^{+/+}$ following 12h TGF-β1 treatment

Symbol	Description	GO annotations[1]
Pir	pirin [MGI:1916906]	
Arid5b	AT rich interactive domain 5B (MRF1-like) [MGI:2175912]	
Cenpf	centromere protein F [MGI:1313302]	cell cycle G2/M phase transition; condensed chromosome
Depdc1a	DEP domain containing 1a [MGI:1923381]	
Tmpo	thymopoietin [MGI:106920]	chromatin
Cbx5	chromobox 5 [MGI:109372]	chromatin; histone binding; kinetochore; protein-DNA complex
Mybl1	myeloblastosis oncogene-like 1 [MGI:99925]	
Mybl2	myeloblastosis oncogene-like 2 [MGI:101785]	microtubule cytoskeleton organisation; mitosis; spindle organisation
E2f8	E2F transcription factor 8 [MGI:1922038]	cytokinesis; DNA replication; negative regulation of cell cycle process; positive regulation of cell cycle process
Brca1	breast cancer 1 [MGI:104537]	cell cycle checkpoint; DNA modification; DNA replication; positive regulation of cell cycle process; positive regulation of DNA metabolic process; postreplication repair
Top2a	topoisomerase (DNA) II alpha [MGI:98790]	cell cycle checkpoint; cellular component disassembly; chromosome condensation; regulation of cell cycle phase transition; structure-specific DNA binding
Plk1	polo-like kinase 1 [MGI:97621]	cell cycle checkpoint; cell cycle G2/M phase transition; regulation of protein binding; sister chromatid segregation; spindle checkpoint; spindle microtubule; spindle pole
Psip1	PC4 and SFRS1 interacting protein 1 [MGI:2142116]	heterochromatin; nuclear chromosome part; nuclear heterochromatin; nuclear periphery; structure-specific DNA binding
Tacc3	transforming, acidic coiled-coil containing protein 3 [MGI:1341163]	maintenance of location in cell; microtubule cytoskeleton organisation; organelle localisation
Cav1	caveolin 1, caveolae protein [MGI:102709]	cellular response to abiotic stimulus; maintenance of location in cell; microtubule cytoskeleton organisation; regulation of protein binding
Ckap2	cytoskeleton associated protein 2 [MGI:1931797]	cellular protein complex disassembly; cytokinesis
Hells	helicase, lymphoid specific [MGI:106209]	chromatin; chromosome, centromeric region; DNA alkylation; DNA conformation change; DNA methylation or demethylation
Hmgb2	high mobility group box 2 [MGI:96157]	condensed chromosome; DNA ligation; histone binding; nucleosome binding; regulation of nuclease activity
Uhrf1	ubiquitin-like, containing PHD and RING finger domains, 1 [MGI:1338889]	chromatin; DNA alkylation; DNA methylation or demethylation; DNA modification; heterochromatin; histone binding
Aurkb	aurora kinase B [MGI:107168]	cellular protein complex disassembly; positive regulation of cell division; positive regulation of cytokinesis; ; protein-DNA complex; regulation of binding; regulation of cell division; regulation of cytokinesis; regulation of cytoskeleton organisation
Blm	Bloom syndrome, RecQ helicase-like [MGI:1328362]	cellular response to abiotic stimulus; condensed nuclear chromosome; DNA conformation change; DNA replication
Asf1b	ASF1 anti-silencing function 1 homolog B (S. cerevisiae) [MGI:1914179]	chromatin; DNA conformation change; DNA packaging; histone binding
Ccna2	cyclin A2 [MGI:108069]	pronucleus
Pcna	proliferating cell nuclear antigen [MGI:97503]	nuclear chromosome part; nuclear periphery; positive regulation of DNA metabolic process; postreplication repair; regulation of DNA metabolic process; replication fork; structure-specific DNA binding
Birc5	baculoviral IAP repeat-containing 5 [MGI:1203517]	cell cycle checkpoint; cell cycle G2/M phase transition; microtubule associated complex; mitotic cell cycle phase transition; positive regulation of cell cycle process; protein-DNA complex; spindle checkpoint

[1]GO: Gene ontology as described by GeneMANIA

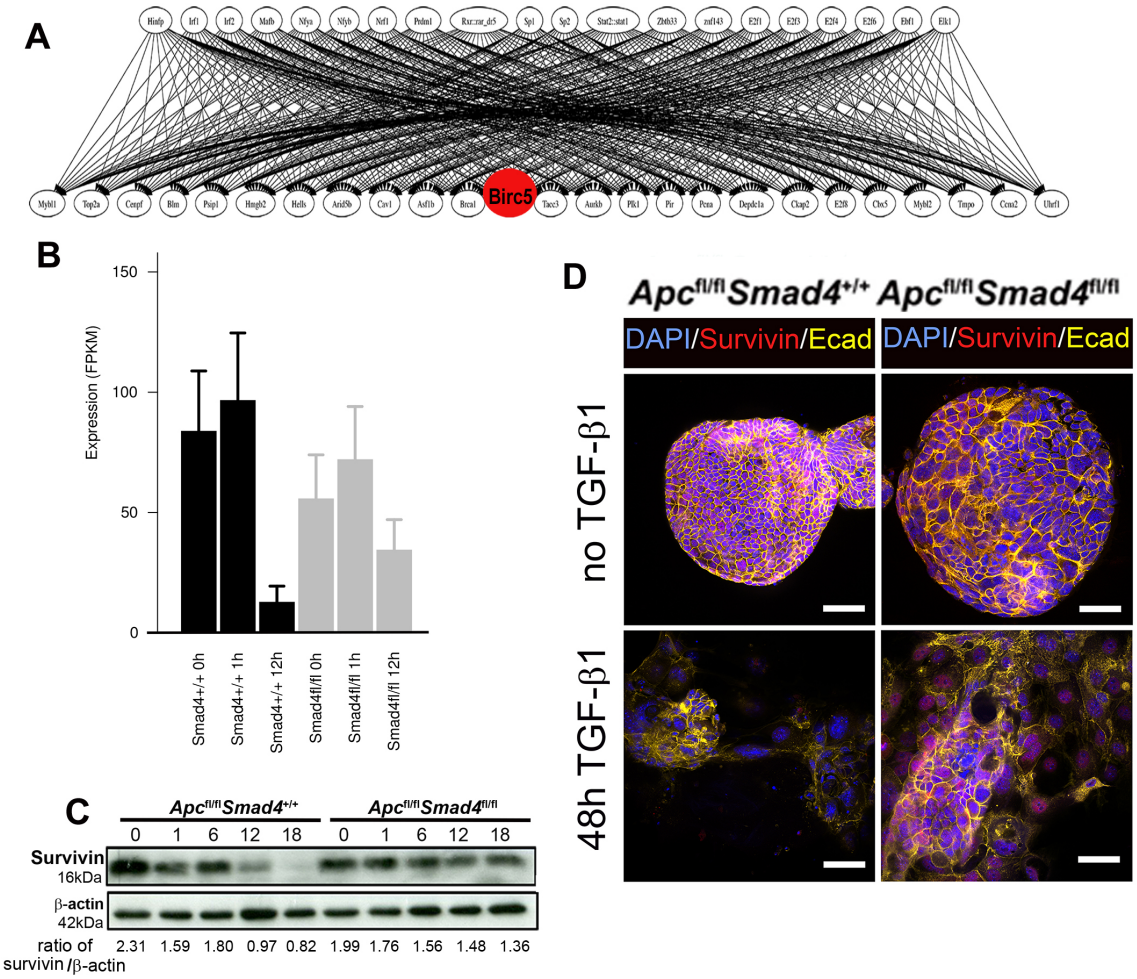

Figure 6.8: **Survivin modulation by TGF-β1 in *Smad4*$^{fl/fl}$ adenomas** (A) Network from promoter analysis shows *Birc5* among the leading edge genes. B. *Birc5* expression in FPKM as shown in the RNA-seq data. (C) Representative western blots showing the down-regulation of survivin within 12h TGF-β1 treatment in *Smad4*$^{+/+}$ adenomas. (D) Confocal images show survivin expression after 48h of TGF-β1 treatment in *Smad4*$^{fl/fl}$ adenomas. Scale bars 50µm.

6.4.4 Promoter analysis for the identification of Smad4 target genes in differentially regulated genes

In order to understand which genes are regulated by Smad4, promoter analysis for leading edge genes was performed according to the strategy shown in figure 6.9. Promoters from 1 kb 5' to TSS were scanned. Unfortunately, Smad4 binding to the promoters of the differentially regulated genes was not successful. Different TFs were shown to be active (data not shown but available upon request). This might be limited to the fact that promoters from 1 kb 5' to TSS were scanned and Smad4 binding sites are at the enhancers. The activated promoters show different TFs that might be Smad4 partners.

6.4.4.1 Smad4 dependent and independent genes

The identification of Smad4 independent genes was carried out according to the diagram shown in Figure 6.10. Briefly, genes that were regulated in both genotypes were ignored and only those regulated in Smad4 knockout adenomas were considered. The comparison was based on early response genes as late response genes might be secondary events to the primary ones.

The leading edge genes were evaluated for functional analysis with GeneMANIA. Table 6.26 showed Smad4 independent genes that were upregulated. Those genes are predicted to regulate different process, for instance, cytokinesis, primary cilium, GTPase activity and regulation of DNA methylation. Likewise, Smad4 independent genes that were downregulated in response to TGF-β1 treatment were also evaluated for functional analysis. Table 6.27 shows genes that are downregulated in response to TGF-β1. These genes are predicted to be be involved in regulation of GTPase signal transduction and cell leading edge.

6.4.4.2 *Serpine1* and Smad4 dependency

Serpine1 known as *Plasminogen activator inhibitor 1*, *PAI-1*, was among the top 50 up-regulated genes on *Smad4*$^{fl/fl}$ adenomas when compared with *Smad4*$^{+/+}$ at the basal level (Table 6.1). It did not show and up or downregulation in the different comparisons done with TGF-β1 treatment in the two genotypes although it was among the top early 50 DEG in *Smad4*$^{+/+}$ in response to TGF-β1 (Table 6.5). This was interesting as *PAI-1* induction in response to TGF-β and Smad4 requirement is controversial. In mouse fibroblasts, *PAI-1* expression was Smad4 independent (Sirard et al., 2000) and in HaCaT and Colo-357 cells the expression was Smad4 dependent (Levy and Hill, 2005). RNA-seq data showed that at the basal level there was 10.41 fold difference (*Smad4*$^{fl/fl}$ divided by *Smad4*$^{+/+}$). With TGF-β1 treatment and *Smad4*$^{+/+}$ adenomas, *Serpine1* expression increased to 14.2 and 45.52 fold at 1h and 12h, respectively, compared to 0h. In *Smad4*$^{fl/fl}$ however, *Serpine1* expression when compared to 0h was similar at 1h with 1.02 fold and showed a slight increase at 12h with 2.75 fold. The overall difference in *Serpine1* expression with Smad4 status was 2.16 (*Smad4*$^{+/+}$ divided by *Smad4*$^{fl/fl}$) and 1.56 at 1h and 12h, respectively. Taken together, this result indicates that the presence of Smad4 accelerates the induction of *Serpine1*.

6.4.5 MiRNA in intestinal adenomas

MiRNA-seq was performed on adenomas with or without TGF-β1 treatment. Analysis for the miRNA-seq was performed by Dr.David Barnes in the Hassan lab. Different miRNA were detected and had mainly similar expression with the exception of miR-125a-5p and miR-125b-5p. These two miRNA were upregulated in the *Smad4*$^{fl/fl}$ adenomas at 0h. These miRNA were also differentially regulated with TGF-β1 (Figure 6.11).

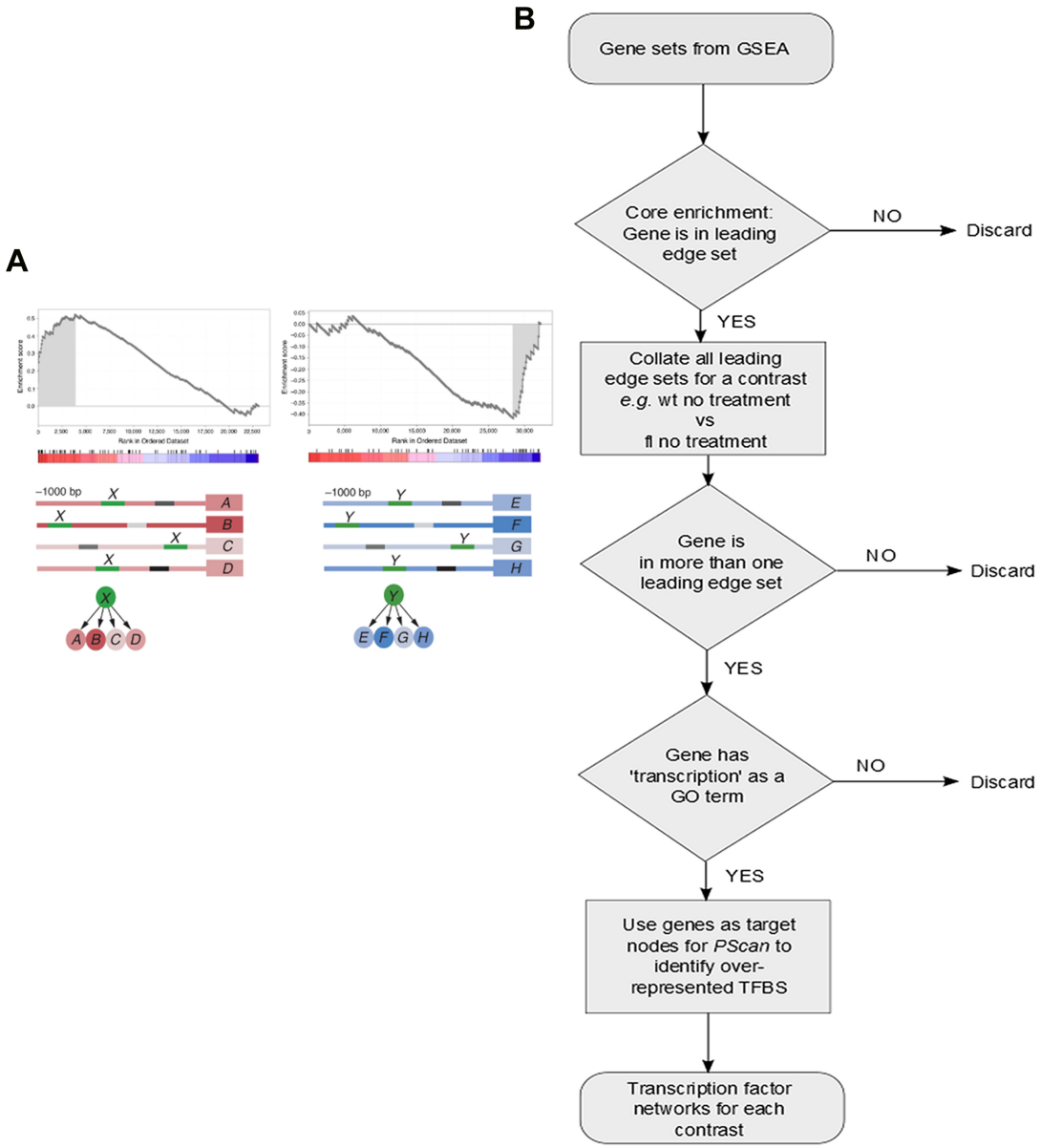

Figure 6.9: **Core enriched genes promoter analysis**. (A) GSE graphs show the leading edge genes used for analysis in grey. (B) Flow chart shows the steps used in promoter analysis for the identification of transcription factors involved in gene regulation.

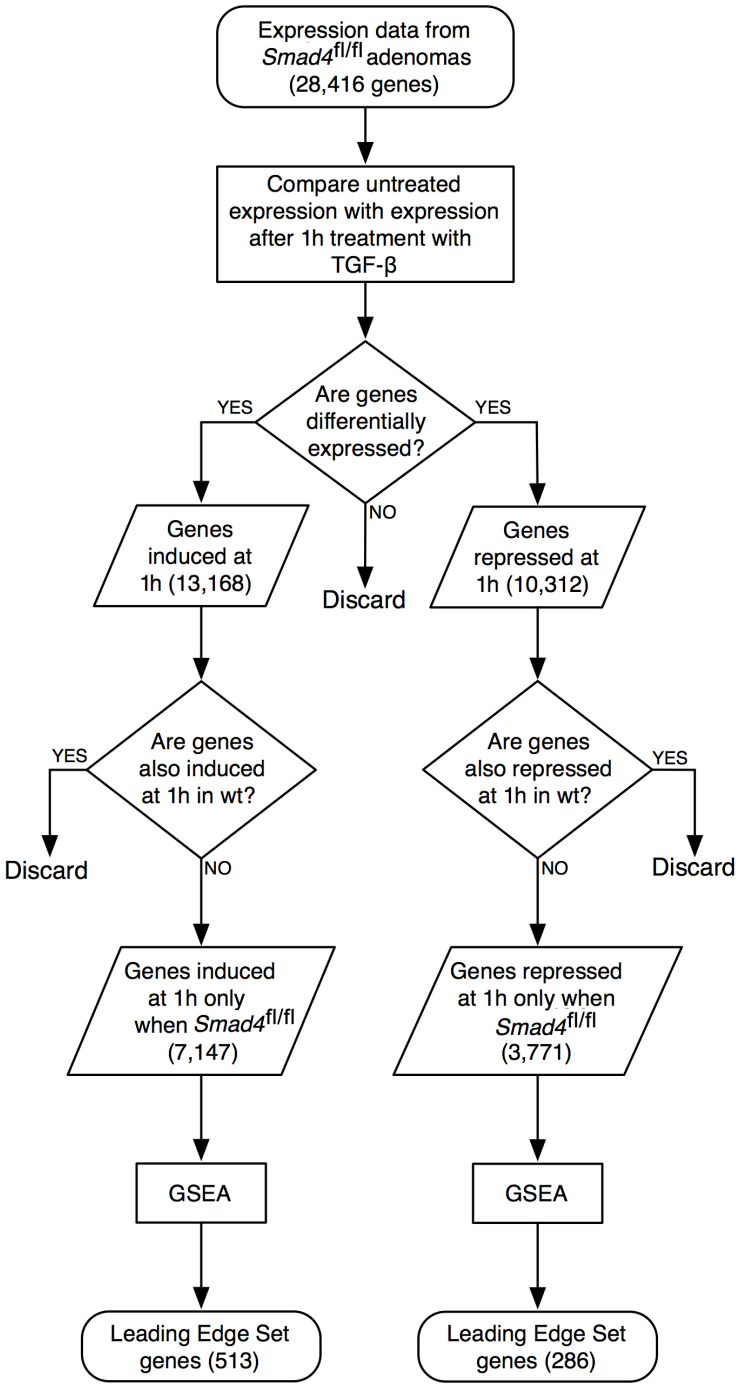

Figure 6.10: **Steps implemented for the identification of Smad4 independent genes** Flow chart shows steps implemented for the identification of Smad4 dependent genes that either suppressed or induced based on the presence or absence of Smad4 after 1h of TGF-β1 treatment.

Table 6.26: Smad4 independent genes that are expressed in *Apc*$^{fl/fl}$Smad4$^{fl/fl}$ in response to 1hr TGF-β1 treatment

	Positive regulation of response to external stimulus
Creb3	cAMP responsive element binding protein 3 [MGI:99946]
Alox5ap	arachidonate 5-lipoxygenase activating protein [MGI:107505]
Tnfsf11	tumour necrosis factor (ligand) superfamily, member 11 [MGI:1100089]
Hmgb1	high mobility group box 1 [MGI:96113]
Ccr2	chemokine (C-C motif) receptor 2 [MGI:106185]
Calr	calreticulin [MGI:88252]
Wnt5a	wingless-related MMTV integration site 5A [MGI:98958]
Akt2	thymoma viral proto-oncogene 2 [MGI:104874]
Ccr7	chemokine (C-C motif) receptor 7 [MGI:103011]
Ly86	lymphocyte antigen 86 [MGI:1321404]
Il1rl1	interleukin 1 receptor-like 1 [MGI:98427]
	Cytokinesis
Cit	citron [MGI:105313]
Kif23	kinesin family member 23 [MGI:1919069]
Racgap1	Rac GTPase-activating protein 1 [MGI:1349423]
Rab35	RAB35, member RAS oncogene family [MGI:1924657]
Ralb	v-ral simian leukemia viral oncogene homolog B (ras related) [MGI:1927244]
Anxa11	annexin A11 [MGI:108481]
Pik3c3	phosphoinositide-3-kinase, class 3 [MGI:2445019]
Bbs4	Bardet-Biedl syndrome 4 (human) [MGI:2143311]
Chmp1a	charged multivesicular body protein 1A [MGI:1920159]
	Primary cilium
Ift57	intraflagellar transport 57 [MGI:1921166]
Bbs4	Bardet-Biedl syndrome 4 (human) [MGI:2143311]
Rpgrip1	retinitis pigmentosa GTPase regulator interacting protein 1 [MGI:1932134]
Rilpl2	Rab interacting lysosomal protein-like 2 [MGI:1933112]
Cnga3	cyclic nucleotide gated channel alpha 3 [MGI:1341818]
Rapgef4	Rap guanine nucleotide exchange factor (GEF) 4 [MGI:1917723]
Pdc	phosducin [MGI:98090]
Gli3	GLI-Kruppel family member GLI3 [MGI:95729]
Ift20	intraflagellar transport 20 [MGI:1915585]
Nphp1	nephronophthisis 1 (juvenile) homolog (human) [MGI:1858233]
	ncRNA processing
Rpsa	ribosomal protein SA [MGI:105381]
Wdr4	WD repeat domain 4 [MGI:1889002]
Tsen54	tRNA splicing endonuclease 54 homolog (S. cerevisiae) [MGI:1923515]
Mettl1	methyltransferase like 1 [MGI:1339986]
Fars2	phenylalanine-tRNA synthetase 2 (mitochondrial) [MGI:1917205]
Cirh1a	cirrhosis, autosomal recessive 1A (human) [MGI:1096573]
Fbl	fibrillarin [MGI:95486]
	S-adenosylmethionine-dependent methyltransferase activity
Prmt7	protein arginine N-methyltransferase 7 [MGI:2384879]
Wdr4	WD repeat domain 4 [MGI:1889002]
Dnmt3b	DNA methyltransferase 3B [MGI:1261819]
Setd6	SET domain containing 6 [MGI:1913333]
Mepce	methylphosphate capping enzyme [MGI:106477]
Setd3	SET domain containing 3 [MGI:1289184]
Mettl1	methyltransferase like 1 [MGI:1339986]
Fbl	fibrillarin [MGI:95486]
Prmt1	protein arginine N-methyltransferase 1 [MGI:107846]
	Positive regulation of GTPase activity
Adap1	ArfGAP with dual PH domains 1 [MGI:2442201]
Arhgap24	Rho GTPase activating protein 24 [MGI:1922647]
Sgsm3	small G protein signalling modulator 3 [MGI:1916329]
Dlc1	deleted in liver cancer 1 [MGI:1354949]
Arhgef16	Rho guanine nucleotide exchange factor (GEF) 16 [MGI:2446219]
Prr5	proline rich 5 (renal) [MGI:1924714]
Axin1	axin 1 [MGI:1096327]
Rgs10	regulator of G-protein signalling 10 [MGI:1915115]
Racgap1	Rac GTPase-activating protein 1 [MGI:1349423]
Rgs2	regulator of G-protein signalling 2 [MGI:1098271]
Akt2	thymoma viral proto-oncogene 2 [MGI:104874]
Ccr7	chemokine (C-C motif) receptor 7 [MGI:103011]

Table 6.27: Smad4 independent genes that are repressed in *Apc*$^{fl/fl}$Smad4$^{fl/fl}$ in response to 1hr TGF-β1 treatment

	Cellular response to peptide, hormone stimulus, nitrogen compound
Pik3r3	phosphatidylinositol 3 kinase, regulatory subunit, polypeptide 3 (p55) [MGI:109277]
Foxo1	forkhead box O1 [MGI:1890077]
Pak1	p21 protein (Cdc42/Rac)-activated kinase 1 [MGI:1339975]
Arhgef2	rho/rac guanine nucleotide exchange factor (GEF) 2 [MGI:103264]
Kat2b	K(lysine) acetyltransferase 2B [MGI:1343094]
Irs2	insulin receptor substrate 2 [MGI:109334]
Prkcq	protein kinase C, theta [MGI:97601]
Sirt1	sirtuin 1 [MGI:2135607]
Jak2	Janus kinase 2 [MGI:96629]
Pld2	phospholipase D2 [MGI:892877]
Egr1	early growth response 1 [MGI:95295]
Rhoq	ras homolog gene family, member Q [MGI:1931553]
Mavs	mitochondrial antiviral signalling protein [MGI:2444773]
Tlr2	toll-like receptor 2 [MGI:1346060]
	Regulation of small GTPase mediated signal transduction
Cdkl5	cyclin-dependent kinase-like 5 [MGI:1278336]
Dennd2a	DENN/MADD domain containing 2A [MGI:2444961]
Ralgapa1	Ral GTPase activating protein, alpha subunit 1 [MGI:1931050]
Dock11	dedicator of cytokinesis 11 [MGI:1923224]
Mcf2l	mcf.2 transforming sequence-like [MGI:103263]
Rictor	RPTOR independent companion of MTOR, complex 2 [MGI:1926007]
Arhgef2	rho/rac guanine nucleotide exchange factor (GEF) 2 [MGI:103264]
Dock7	dedicator of cytokinesis 7 [MGI:1914549]
Amot	angiomotin [MGI:108440]
Fgd1	FYVE, RhoGEF and PH domain containing 1 [MGI:104566]
Itpkb	inositol 1,4,5-trisphosphate 3-kinase B [MGI:109235]
	RAS p21 protein activator 1 [MGI:97860]
	Axon development
Raph1	Ras association (RalGDS/AF-6) and pleckstrin homology domains 1 [MGI:1924550]
Pak1	p21 protein (Cdc42/Rac)-activated kinase 1 [MGI:1339975]
Picalm	phosphatidylinositol binding clathrin assembly protein [MGI:2385902]
Dock7	dedicator of cytokinesis 7 [MGI:1914549]
Creb1	cAMP responsive element binding protein 1 [MGI:88494]
Ank3	ankyrin 3, epithelial [MGI:88026]
Gbx2	gastrulation brain homeobox 2 [MGI:95668]
Kif5c	kinesin family member 5C [MGI:1098269]
Nefl	neurofilament, light polypeptide [MGI:97313]
Artn	artemin [MGI:1333791]
Jak2	Janus kinase 2 [MGI:96629]
Mapk8ip3	mitogen-activated protein kinase 8 interacting protein 3 [MGI:1353598]
Usp33	ubiquitin specific peptidase 33 [MGI:2159711]
	Cell leading edge
Cdkl5	cyclin-dependent kinase-like 5 [MGI:1278336]
Raph1	Ras association (RalGDS/AF-6) and pleckstrin homology domains 1 [MGI:1924550]
Acap2	ArfGAP with coiled-coil, ankyrin repeat and PH domains 2 [MGI:1925868]
Pak1	p21 protein (Cdc42/Rac)-activated kinase 1 [MGI:1339975]
Mcf2l	mcf.2 transforming sequence-like [MGI:103263]
Arhgef2	rho/rac guanine nucleotide exchange factor (GEF) 2 [MGI:103264]
Amot	angiomotin [MGI:108440]
Fgd1	FYVE, RhoGEF and PH domain containing 1 [MGI:104566]
Ptk6	PTK6 protein tyrosine kinase 6 [MGI:99683]
Pld2	phospholipase D2 [MGI:892877]
Mapk8ip3	mitogen-activated protein kinase 8 interacting protein 3 [MGI:1353598]
Rasa1	RAS p21 protein activator 1 [MGI:97860]

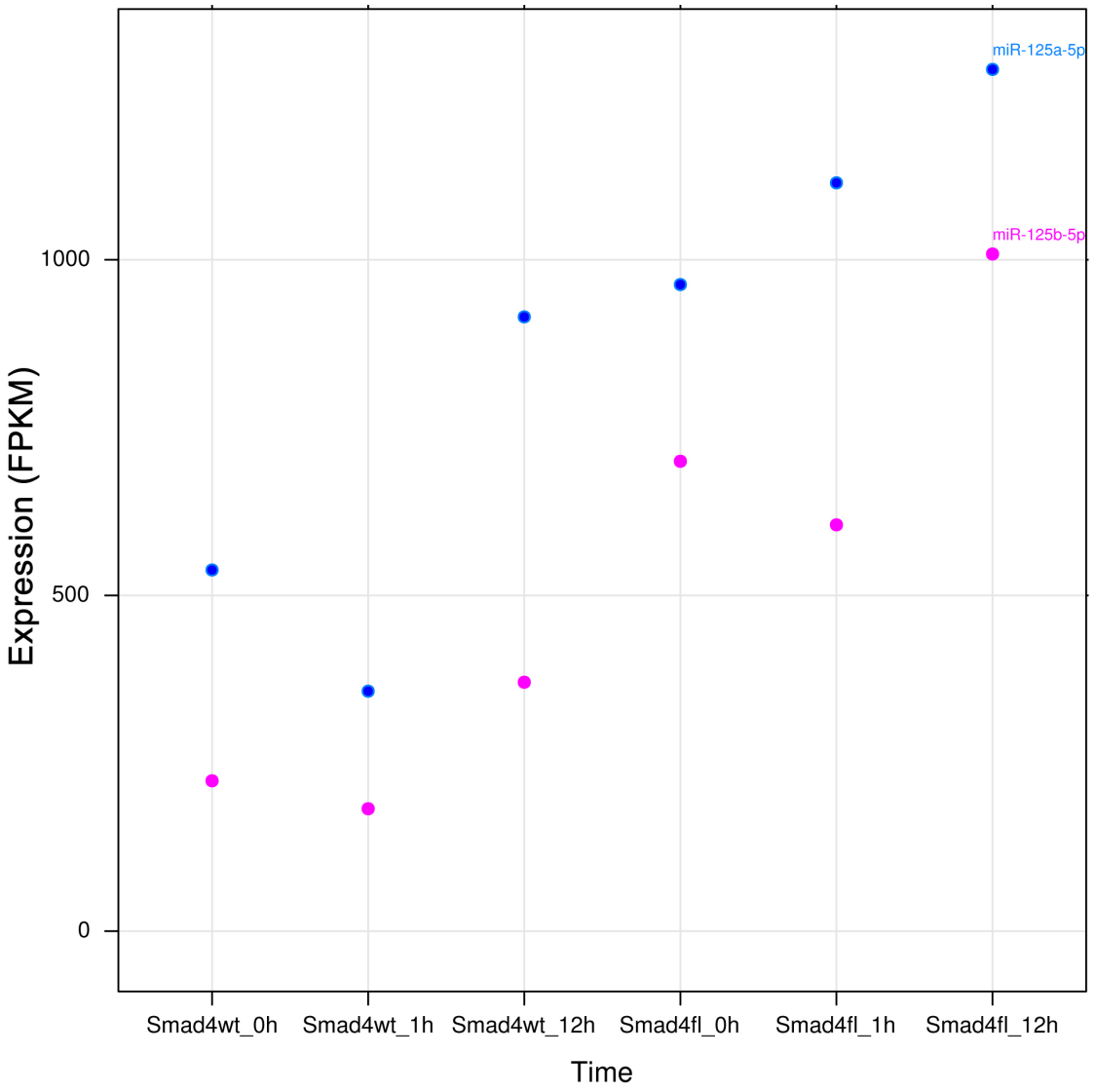

Figure 6.11: **Significant miRNA expression in adenomas**. Plot represents the expression of miRNA in *Smad4*$^{+/+}$ and *Smad4*$^{fl/fl}$ adenomas with and without TGF-β1 treatment.

6.5 Discussion

6.5.1 Differentially regulated genes at the basal level

The results of the RNA-seq experiment show several genes to be differentially regulated between *Smad4*$^{+/+}$ and *Smad4*$^{fl/fl}$ adenomas at the basal level. GSEA analysis shows an enrichment for c-Myc targets in different sets with an FDR $\geq$0.523 in *Smad4*$^{+/+}$ adenomas. The complementary analysis for *Smad4*$^{fl/fl}$ adenomas show an enrichment for TGF-β, p38-MAPK and integrin pathways with *Egr1, Tgfb1, Jun, Tnf, Foxa1, Creb1, Skil, Fos, Ddit3, Ctnnb1* and *Vegfa* being the leading edge genes. *Serpine1* and *Sox2* are among the top 50 DEG (Figure 6.2, Table6.1- 6.4). Different mucins were upregulated in the *Smad4*$^{fl/fl}$ adenomas (Figure 6.4).

6.5.1.1 c-Myc enrichment

The enrichment of *Smad4*$^{+/+}$ adenomas was mainly for c-Myc target genes with FDR $\geq$0.523. An FDR >0.25 shows biological signal as being subtle but possibly still relevant. More replicate samples would be needed to confirm the involvement of these gene sets (http://www.broadinstitute.org/cancer/software/gsea/wi- ki/index.php/FAQ). In this experiment and in this comparison the high FDR value might be related to subtle biological signal as *Apc* was deleted from both adenomas. The enrichment for c-Myc target gene was expected and is a consequence of *Apc* deletion. *Apc* deletion results in upregulation of *c-Myc* (He et al., 1998). c-Myc is required for the activation of many Wnt target genes following *Apc* loss and is required for adenoma formation (Sansom et al., 2007).

6.5.1.2 TGF-β pathway autoregulation and possible link to inflammation with Smad4 deletion

At the basal level there is enrichment for the TGF-β pathway in *Smad4*$^{fl/fl}$ adenomas with *tgfb1* as one of the common genes along with other family members such as *Skil*, *Fos*, and *Jun*. The source of TGF-β1 in tumours is variable; it might be the tumour cells and/or other cells in the tumour microenvironment (Massagué, 2008). The RNA-seq data sug-

gests that *Smad4*$^{fl/fl}$ adenomas are a source of TGF-β1 and the expression of *Serpine1*, *Jun* and *Skil* indicate that it is functional. The inability to detect an active TGF-β pathway by p-R-Smads in the *Smad4*$^{fl/fl}$ adenomas without stimulation (Figure 5.9, 5.10) might be due to the low amount of TGF-β1 produced in culture, perhaps related to the small number of adenomas in culture that was not sufficient for signal detection. Alternatively, quantification of TGF-β1 production in the culture medium on different days using ELISA should be considered. Tumour derived TGF-β might be an advantage to the tumour cells allowing them to be protected from anti-tumour immunity (Massagué, 2008). *Skil* is an oncogene and acts as a negative regulator for the TGF-β pathway (Deheuninck and Luo, 2009). *Skil* is a TGF-β target gene and its expression is reported to be Smad4 independent (Levy and Hill, 2005). Its upregulation in *Smad4*$^{fl/fl}$ is a further evidence of being Smad4 independent.

Moreover, GSE for Reactome_Response_To_Elevated_Platelet_Cytosolic_Ca2 points to an active TGF-β pathway, as the platelets are a source of TGF-β cytokine that is important in both normal wound healing and scarring (Grainger et al., 1995). The enrichment for Biocarta-P38mapk-Pathway points to the activation of non-canonical TGF-β pathway. p38 function is context dependent, it acts as tumour suppressor in normal cells and can promote survival and proliferation in cancer cells (Wagner and Nebreda, 2009). The enrichment for Pid-Integrin1-Pathway might be important for controlling the response of tumour cells to soluble growth factors and cytokines (Guo and Giancotti, 2004).

GO shows that the leading edge genes *Tgfb1, Jun, Tnf, Creb1, Fos, Ctnnb1* and *Vegfa* are involved in myeloid leukocyte differentiation and *Ddit3, Tgfb1, Tnf* and *Creb1* are involved in positive regulation of cytokine production. *Ddit3*, known as *Chop* is an interesting gene as GO shows that it is also involved in neuronal cell death. *Chop* is upregulated in endoplasmic reticulum stress-induced apoptosis (Kim et al., 2012). The function of *Ddit3* might be context dependent. A recent report showed that stromal Ddit3 is important for tumour-induced tolerance (Thevenot et al., 2014). Tumour-infiltrating myeloid-derived suppressor cells (MDSCs) expressing Ddit3 are responsible for immune inhibitory activity a process related to IL-6 production. MDSCs lacking Ddit3 are not able to produce IL-6 and have

low expression of phospho-STAT3. IL-6 overexpression restored immune-suppressive activity (Thevenot et al., 2014). Increased Chop expression was reported in colonic tumours with Duke's A and B stages compared to normal tissue (Rask et al., 2000). Low survival and aggressive tumours were reported in patients with different malignancies expressing Chop (Kim et al., 2012). In summary, Smad4 deletion is modulating the TGF-β pathway and might enhance intestinal tumorigenicity by secreting its own TGF-β1 and providing an inflammatory environment.

6.5.1.3 *Smad4* deletion increased β-*Catenin* expression

Smad4$^{fl/fl}$ gene expression at the basal level shows an upregulation in β-*catenin* (*Ctnnb1*), the central mediator of the Wnt pathway. Thus, one of the significances of Smad4 deletion in intestinal tumorigenesis is enhancing the Wnt pathway by increasing the level of β-*catenin*. As Apc is deleted in the adenomas, β-*catenin* will not be degraded by the proteasomal complex and more β-*catenin* will be available to regulate gene transcription by binding to the Tcf/Lef transcription factors (Clevers and Nusse, 2012). Genes such *Jun* and *Fos* are among the leading edge genes. *Jun* and *Fos* are also β-catenin upregulated genes (Staal et al., 2004; Herbst et al., 2014). *Jun* is also a late response gene induced in response to TGF-β1 (Levy and Hill, 2005). The increased level of β-Catenin and Wnt taget genes due to Smad4 mutation was also reported in CRC cells with Smad4 deletion (Freeman et al., 2012).

6.5.1.4 Upregulation of mucin family members in *Apc*$^{fl/fl}$*Smad4*$^{fl/fl}$

The top 50 DEG showed upregulation of *Muc2* and *Muc4*, and other mucins such as *Muc20* and *Muc1* were also overexpressed more than 2 fold (Figure 6.4). The upregulation of mucins and Muc2 was confirmed by histochemistry and IF, respectively. Muc2 was quantified by the area of Muc2 to the tumour. It was not easy to quantify the Alcian blue-PAS stain as the color of the mucins was very close to that of the tissue. Alcian blue-PAS stain gave only blue colour unlike the expected colour of a mixed blue and magenta (Bancroft,

2013). This might show that either the acidic mucin are dominant and obscure the neutral mucins or the kit used has certain problems. Thus, to exclude the latter the staining will be repeated. Adenomas with increased Muc2 expression was also observed during adenoma characterisation earlier in this project (Figure 5.2). The Smad4 mutations are known to be associated with mucinous histology (Fleming et al., 2013). The upregulation of Muc2 in CRC is mutation dependent and is reported in 11-15% of the cases at late stage (Green et al., 1993; Langner et al., 2012). It is mainly associated with MSI-H tumours (Kakar et al., 2004) and is reported in SSA/P (Delker et al., 2014). Overexpression of MUC2 has been reported in colorectal cancer with uncertainty about its role (Kufe, 2009). The upregulation of MUC2 and other mucins might suggest an increase in metastatic potential of the tumours (Bresalier et al., 1991; Sternberg et al., 1999) or the pathway regulating it is altered (Kufe, 2009).

Muc4 was also upregulated in the *Smad4*$^{fl/fl}$ adenomas. Its expression in CRC was variable among different studies (Biemer-Hüttmann et al., 1999; Shanmugam et al., 2010). Identification of patients having this mucin might be important for their management as overexpression of MUC4 is a predictor of poor survival if upregulated at early stages of tumour development (Shanmugam et al., 2010).

MUC1 and MUC6 are normally not expressed in the colonic mucosa (Taliano et al., 2013) but are upregulated in the *Smad4*$^{fl/fl}$ adenomas. MUC1 overexpression is an important predictor of the metastatic potential and prognosis of colorectal cancer (Nakamori et al., 1994; Hiraga et al., 1998). This might enhance the Wnt pathway as the cytoplasmic tail of MUC1 binds to β-catenin and is involved in the regulation of β-catenin target genes (Baldus et al., 2004; Hollingsworth and Swanson, 2004). *Muc20* is another overexpressed mucin in the the *Smad4*$^{fl/fl}$ adenoma. Its overexpression in CRC is associated with migration, invasion and marker for recurrence (Xiao et al., 2013). Muc6 is a gastric mucin showing some overexpression (0.6 fold). MUC6 and MUC5Ac are gastric mucins reported to be upregulated in CRC (Bartman et al., 1999). Interestingly, among the gastric markers there is a 17.2 fold overexpression of TFF2 (trefoil factor 2). TFF2 is overexpressed with MUC6

and MUC5AC in serrated polyps (Kim et al., 2015). Overexpression of TFF2 has been shown to promote invasion in LoVo colorectal cancer cells (Yu et al., 2015). Taken together, the RNA-seq showed for the first time several mucins to be differentially regulated with Smad4. These might provide the tumour with selective advantages that are important for invasion and metastasis. Thus, a patient profile for altered mucin might be attractive for therapeutic intervention either by of antibodies, vaccines or other therapeutic inhibitors (Kufe, 2009).

6.5.2 Normal response to TGF-β1 in Smad4$^{+/+}$ adenomas

The normal function of the TGF-β pathway has been assessed by the genes that are regulated by TGF-β1 in *Smad4*$^{+/+}$ adenomas. For instance, there is early upregulation of the TGF-β pathway regulators such as *Skil* and *Smad7*, and upregulation of apoptosis genes such as *Gadd45g*, with sustained expression of *Atf3, Junb* and *Serpine1* and late responses such as upregulation of *Ets1*, and *Itga6*. These data reflect an active normal pathway in the adenoma. The data from the RNA-seq is consistent with previous studies and have been reported several times when the TGF-β pathway is not mutated (Kowanetz et al., 2004; Levy and Hill, 2005; Nagarajan et al., 1999; Massagué and Gomis, 2006; Deheuninck and Luo, 2009). This data is not in agreement with a report that showed a different regulation for TGF-β with active Wnt signalling. This report showed a downregulation of TGF-β response genes such as *Serpine1* and *Gadd45g* when Wnt is active (Labbé et al., 2007). *Smad6* was among them but it acted as a negative regulator of the BMP pathway (Massagué et al., 2005).

6.5.3 Differential regulation of the cytostatic and apoptotic effect of TGF-β1

The RNA-seq data shows DEG for genes involved in the regulation of cell cycle, proliferation and apoptosis. In Smad4$^{+/+}$, some of these genes are early response genes such as *c-Myc, Aft3, Gadd45a, Gadd45g* and *Ddit3*. Some show transient upregulation such as *Id* family members (Table 6.5, 6.8). Downregulation of the late response genes *Birc5, E2F8,*

Aurkb, Pcna is shown in Table 6.13. The regulation of these genes is altered in *Smad4*$^{fl/fl}$ with *c-Myc* upregulated (Table 6.20), *Id* family members downregulated (Table 6.19) and *Birc5, E2F8, Aurkb*, and *Pcna* are upregulated as late response genes (Table 6.25).

Consistent with the fact that TGF-β has a cytostatic and apoptotic effect on epithelial cells, the transcriptome analysis showed early and late differential expression of genes important for this function. For instance, early downregulation of *c-Myc* and upregulation of genes involved in the apoptotic process such as *Gadd45a, Gadd45g* and *Ddit3*. The downregulation of several genes important for the cell cycle and DNA replication was a late event and might be secondary to *c-Myc* downregulation. It is reported that downregulation of *c-Myc* is an early event (Chen et al., 2002) and is required for the cytostatic effect of TGF-β1 that becomes apparent after 16h of treatment (Siegel and Massagué, 2003). c-Myc downregulation is important to deprive the cell of growth-promoting functions and to facilitate the induction of cyclin-dependent kinase inhibitors that are required for the cytostatic effect of TGF-β1 (Siegel and Massagué, 2003). It is possible also that the early response genes are TFs that are required for cytostatic effect of TGF-β1. For example, *Id* family members show an early induction with TGF-β1 followed by their repression at a later time point. Their repression is required for the cytostatic effect of TGF-β1 (Kowanetz et al., 2004). Their regulation is secondary to the early events. *Id1* repression is secondary to the upregulation of *ATF3* (Lasorella et al., 2014) or secondary to the upregulation of $p27^{Kip1}$ and $p21^{Cip1}$ (Ling et al., 2002). The downregulation of *Id2* is secondary to c-Myc downregulation (Massagué et al., 2005; Siegel and Massagué, 2003).

Gadd45a, Gadd45g and *Ddit3* are apoptotic proteins shown to be overexpressed in *Smad4*$^{+/+}$. The expression of *Gadd45a* and *Ddit3* was reported to be involved in TGF-β1 induced growth inhibition and apoptosis by upregulating the p38 MAPK pathway (Ramjaun et al., 2007; Li et al., 2015).

The cytostatic effect and apoptotic effect in response to TGF-β1 was altered in the *Smad4*$^{fl/fl}$ adenomas as shown by the RNA-seq data. *c-Myc* was upregulated in these adenomas

reflecting an altered control for TGF-β1 induced cell arrest. The early response genes responsible for apoptosis were not among the top 50 DEG or the leading edge. The late response genes were also altered. While *Smad4*$^{+/+}$ adenomas show a downregulation in genes involved in cell cycle and DNA replication, *Smad4*$^{fl/fl}$ showed an upregulation in these genes. Taken together, these expression data showed the tumour suppressor effect of TGF-β1 is altered due to faults in cytostatic response.

6.5.3.1 Novel genes in RNA-seq data

The nucleotide sequences for genes annotated as 'NA' were extracted by David Barnes, using their genomic coordinates, and these were analysed for the presence of contaminating, non-mouse sequences using BLAST. A BLAST search using all non-redundant databases failed to return any bacterial or viral hits and neither did a search using all prokaryotic genomes. Since all of the top hits from the non-redundant search were from mouse it was concluded that all of the 'NA' sequences were from the mouse genome but from unannotated regions.

6.5.3.2 Modulation of *Birc5* in response to TGF-β1

Birc5/Survivin, a Wnt target gene, is expressed in the G2/M phase of the cell cycle (Li et al., 1998). Expression data in this work shows that there is differential regulation of this gene depending on Smad4 status. This has been validated at the protein level by western blot and confocal images. The downregulation of *Survivin* has been reported in intact TGFβ pathway with similar patterns to our results (decreased at 12h and undetectable after 16h of treatment) in NRP-154 prostate cancer cells (Yang et al., 2008). The repression is reported to be Smad2 and Smad3 dependent (Yang et al., 2008). Total inhibition of *Survivin* downregulation was reported with the deletion of both Smad2 and Smad3, whereas partial inhibition was observed if each was deleted alone. It might be that Smad4 binding with both of the R-Smads is required for *Survivin* suppression and Smad4 is the limiting step. *Survivin* downregulation was also reported in intestinal organoid culture undergoing

apoptosis in response to TGF-β1 through p38 MAP kinase pathway (Wiener et al., 2014).

6.5.4 Are miRNAs contributors to intestinal tumorigenesis?

MiRNA-seq data did not show the expression of several miRNA. It might be that their contribution to intestinal pathogenesis is limited in this context. However, the ones that were upregulated, miRNA-125a and miRNA-125b (Figure 6.11) might be interesting although to date they are not reported to be involved in the TGF-β pathway. MiRNA-125a and miRNA-125b have been reported to suppress TNFAIP3 and aberrantly activate the NF-κB pathway in diffuse large B-cell lymphoma (Kim et al., 2012). GO analysis showed an anticipation of the NF-κB pathway with TGF-β1 treatment (Table 6.24).

In summary, this chapter showed that Smad4 deletion in the adenomas modulates the TGF-β pathway by upregulating an endogenous TGF-β1. This might be creating appropriate conditions for inflammation. Smad4 deletion induced expression of the stem cell marker Sox2 which might be important for reprogramming at the metastatic site. It has an effect on downregulating the cytostatic and apoptotic effect of exogenous TGF-β1. RNA-seq data shows that Smad4 mutation is predicted to affect different biological functions which might be involved in tumour progression such as epigenetic regulation of genes, cytokinesis, regulation of noncoding RNA (ncRNA) and regulation of GTPase activity. Others were upregulated in response to external stimulus such as *Ccr2* and *Ccr7* and might play role in invasion as Ccr7 was also involved in GTPase regulation. When a member of this family, Ccr1 was deleted in a *cis-Apc*$^{\Delta 716/+}$*Smad4*$^{-/+}$ mouse model, invasion was suppressed (Kitamura et al., 2007). All of these might promote tumour progression. Figure 6.12 summarises the overall change in gene expression with Smad4 knockout at the basal level and in response to TGF-β1 treatment.

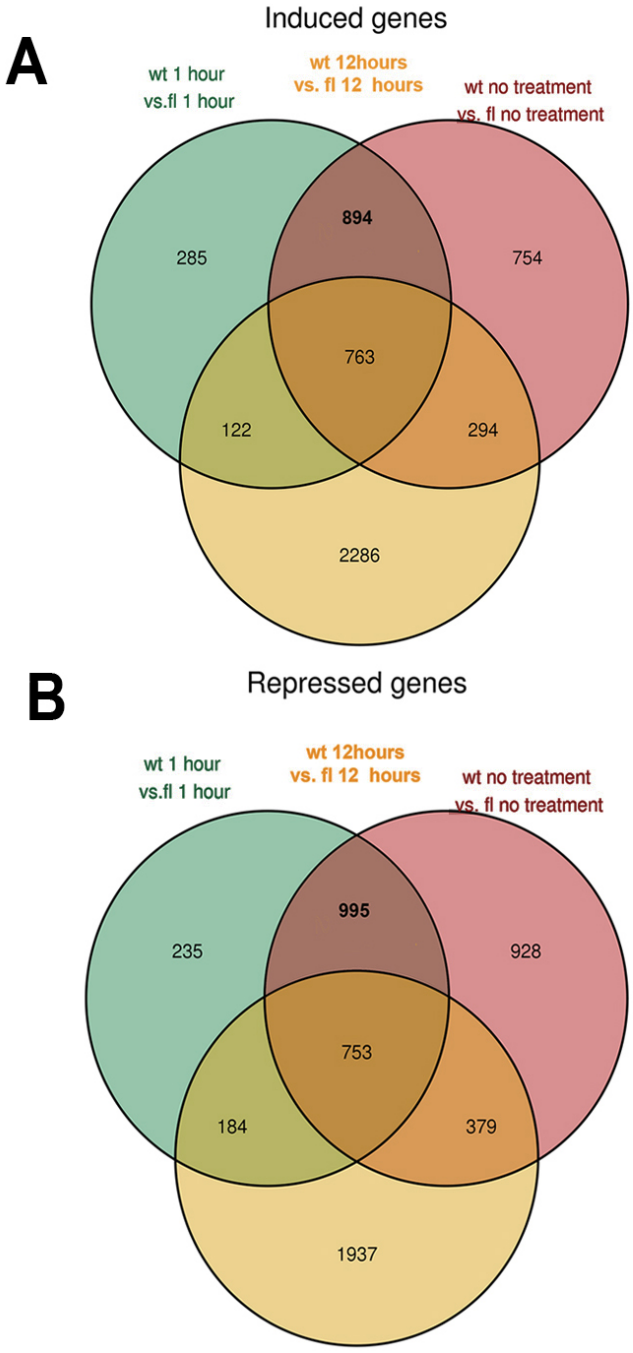

Figure 6.12: **Venn diagrams for DEG in *Smad4*$^{fl/fl}$ adenomas compared to *Smad4*$^{+/+}$ at 0h, 1h and 12h of TGF-β1**. Venn diagrams showing the overall change in gene expression at 0h, 1h and 12h of TGF-β1 (A) induced genes, (B) repressed genes in *Smad4*$^{fl/fl}$ compared to *Smad4*$^{+/+}$.

Chapter 7

Discussion and Future Directions

7.1 Summary

Data in this thesis demonstrates the role of attenuated TGF-β pathway due to Smad4 MH1 domain deletion in intestinal tumorigenesis in the context of active Wnt pathway, both *in vivo* and *in vitro*. It also demonstrates for the first time upregulation of the PI3K and RAS-MAPK/Igf2 pathways due to *Igf2r* domain 11 loss of function in the maternal allele on adenoma progression.

In vivo, Smad4 knockout resulted in altered tumour localisation with enhanced animal survival compared to controls. Inflammatory infiltrates were seen in the tumour microenvironment combined with an active TGF-β signalling as detected by nuclear p-Smad2 (Figure 3.2-3.8). *In vitro*, slow growth of *Apc*$^{fl/fl}$*Smad4*$^{fl/fl}$ adenomas that was rescued with the addition of Y-27632 (Figure 5.4). RNA-seq shows that *Smad4*$^{fl/fl}$ adenomas express *Tgfb1* together with other TGF-β target genes at the basal level, in addition to the upregulation of mucins (Table 6.1-6.4). RNA-seq data also shows that the cytostatic and apoptotic effect of the TGF-β pathway is altered with Smad4 MH1 domain knockout (Table 6.13, 6.24). This is a differential effect, however, is partial, as indicated by functional analysis on adenomas treated with TGF-β1 but is effective in maintaining Survivin expression (Figure 5.12-5.15, 6.8). With TGF-β1 treatment, adenomas acquired an EMT phenotype that is Smad4 independent with migration and motility observed in *Smad4*$^{fl/fl}$ treated adenomas. GO on RNA-seq data showed that the late response genes expressed in *Smad4*$^{+/+}$ TGF-β1 treated adenomas are important for cell-substrate adhesion, ECM organisation, cell-cell

adhesion and regulation of cell migration (Table 6.24).

Domain 11 of Igf2r binds Igf2 with high specificity, loss of function of this domain due to I1565A mutation accelerates adenoma formation with decreased survival (Figure 3.9).

7.2 Discussion and future directions

7.2.1 Altered tumour position in *Apc*$^{fl/fl}$*Smad4*$^{fl/fl}$*Lgr5-CreERT2* is a possible link to inflammation

The pattern of tumour development in *Apc*$^{fl/fl}$*Smad4*$^{fl/fl}$ mice shows that the colon is more prone to tumour initiation and progression when both of these pathways are altered. This altered position of the formed adenoma in *Apc*$^{fl/fl}$*Smad4*$^{fl/fl}$*Lgr5-CreERT2* animals is interesting and one could hypothesise that the effect might be related to the combined effect of the microenvironment and *Smad4* knockout. The work in this thesis might support this. Genetic manipulation of *Apc*$^{fl/fl}$*Smad4*$^{fl/fl}$*Villin-CreERT2* intestinal organoids *in vitro* transformed adenomas in a similar way to the *Apc*$^{fl/fl}$*Smad4*$^{+/+}$ controls (Figure 5.1), showing that gene deletion is effective and something *in vivo* is modulating it.

The *in vivo* model is more complex and might resemble more closely the human disease as the caecum comprises the first part of the colon. The microenvironment is a broad term, it includes stem cell niche, stromal compartment, immune cells and microbiota, in addition to personal lifestyle all of which might play an important role in adenoma initiation and progression. As has been discussed in section 3.5.1 there are differences in gradients of Wnt modulators such as *Grem1* and *Grem2* between the caecum and the small intestine (Leedham et al., 2012), for that, the balance between the Wnt pathway and BMP pathway at the two different anatomical areas might differ. Microbial colonisation is also different between the two anatomical areas. The bacterial density in the large intestine is approximately 10^{12} cells ml^{-1} and that of the small intestine is around 10^{2}, in line with the 12 fold increased risk of large intestinal cancer to small intestinal cancer (Tjalsma et al., 2012). Genetically modified mouse models for CRC develop significantly fewer tumours under

germ free conditions than when they are under conventional conditions. For instance, *Apc*^{Min} mice developed two fold fewer adenomas in the middle small intestine compared to the controls under conventional conditions (Dove et al., 1997). The RNA-seq data in this project shows that among the top 50 differentially expressed genes at the basal level, a downregulation of *Reg3*β by 23.2 fold, *Pla2g2a* by 8.9 fold and *Reg3*γ by 8.7 fold in the *Smad4*$^{fl/fl}$ adenomas compared to the *Smad4*$^{+/+}$ control. These genes are important for epithelial defense against bacterial invasion. It has been reported that *Reg3*β$^{-/-}$ mice have an impaired bacterial clearance of gram-negative bacteria in the Peyer's patches (Dessein et al., 2009). Reg3γ is a secreted antibacterial lectin against gram-positive bacteria that is essential for maintaining a physical barrier separating the microbiota from the small intestinal epithelial surface (Vaishnava et al., 2011). Loss of host-bacterial sequestration in *Reg3*γ$^{-/-}$ mice was associated with increased bacterial colonisation of the intestinal epithelial surface and enhanced activation of intestinal adaptive immune responses by the microbiota (Vaishnava et al., 2011). *In vivo*, Reg3γ is expressed most prominently in the distal small intestine (ileum), where it is produced by multiple epithelial lineages including enterocytes and Paneth cells (Vaishnava et al., 2011).

Pla2g2a is considered as a modulator of the Wnt pathway and *Mom1* mouse strains showed a reduced number of polyps due to increased Pla2g2a secretion (Cormier et al., 1997). It also can be considered a tumour suppressor independent of the Wnt/β-*Catenin* signalling pathway (Fijneman et al., 2008). Pla2g2a is expressed in the large intestine by the goblet cells and its secreted proteins accumulate in the mucinous gel in the crypt lumen (Fijneman et al., 2008). *Pla2g2a*$^{+}$ mouse model when bred with *Muc*$^{-/-}$ mouse model showed a reduced tumour multiplicity and tumour formation in the large intestine compared to the *Muc*$^{-/-}$ control group (Fijneman et al., 2008). Moreover, It has been reported that during the active phase of ulcerative colitis, intraluminal secretion of Pla2g2a is a host defense mechanism (Haapamäki et al., 1997) and the expression of Pla2g2a in gastric cancer may suppress progression or metastasis (Leung et al., 2002). As such, we can hypothesise that Smad4 mutation may result in impaired defense mechanisms important for adenoma formation and progression under certain conditions and anatomical areas. Such

connection is of great importance for patients management and treatment. For instance, broad spectrum antibiotics or non-steroidal anti-inflammatory drug might be considered in the treatment to keep the gut sterile from bacterial colonisation and/or reduce inflammation.

One of the main differences between mouse and human is the site of polyps formation. In mice, polyps are formed in the small intestine and in humans it is formed in the colon. Altered position in mice was achieved when *Apc*$^{\Delta 716}$ mouse model was crossed with *Cdx2*$^{-/+}$ (Aoki et al., 2003). The altered position of the tumour in the *Apc*$^{fl/fl}$*Smad4* $^{fl/fl}$ mice could be due to the same reason. The RNA-seq data at the basal level shows that the *Tff2*, *Muc2*, and *Muc4* are among the top 50 differentially expressed genes together with differences in the transcription of other mucins (Table 6.1, Figure 6.4C). Upregulation of *Tff2, Muc5AC, Muc6* and downregulation of *Muc2* has been reported in *Cdx2*^{null} small intestinal organoids (Simmini et al., 2014). Such changes transformed intestinal organoids to gastric organoids (Simmini et al., 2014). Interestingly, RNA-seq data from *Smad4*$^{fl/fl}$ intestinal organoids showed that the transcription of *Cdx2* is downregulated 1.5 fold compared to *Smad4*$^{+/+}$. It has been reported that *CDX2* is regulated by the BMP pathway in AGS human gastric carcinoma cells (Barros et al., 2008). AGS cells treated with BMP2 and BMP4 results in increased *CDX2* expression and *SMAD4* knockdown led to decreased endogenous CDX2 (Barros et al., 2008), and treatment of the SMAD4 knockdown cells with BMP2 and BMP4 unlike the wild type had no influence on CDX2 expression (Barros et al., 2008). In juvenile polyps it has been reported that *SMAD4* mutation downregulates *CDX2* expression and is responsible for the increased expression of *MUC5AC* and *MUC6* (Barros et al., 2009). Thus, one could hypothesise that Smad4 deletion has downregulated *Cdx2*. Such alternation is responsible for the altered tumour phenotype. Immunohistochemistry for tissue sections as a validation for the RNA-seq data might give a more definitive answer.

The RNA-seq data in this thesis shows a DEG at the basal level with a possible link to inflammation and has been discussed in section 6.5.1.2. Taken together, Smad4 mutations might create an environment suitable for inflammation and are important for cancer progression. This speculation requires experimental verification.

7.2.2 Are motility and migration Smad4 dependent or pathway dependent?

Apc$^{fl/fl}$*Smad4*$^{fl/fl}$ adenomas show motility and migration in Matrigel in response to TGF-β1 treatment (e.g Figure 5.19). Motility is an important feature for functional EMT as it allows the cells to invade. The debate is whether this is Smad4 dependent, pathway dependent or context dependent. This thesis shows that Smad4 deletion enhances migration in response to TGF-β1. These adenomas are growing in 3D culture that maintains tissue architecture. The ability of *Smad4*$^{fl/fl}$ to migrate suggests that it is capable of changing shape, remodelling ECM, generating force and activating small GTPase (Friedl and Alexander, 2011). EMT was observed in adenoma culture in response to TGF-β1 and RNA-seq in this project shows a differential regulation of GTPase activity with Smad4 deletion (Table 6.26 -6.27).

Another gene that might be related to motility and migration is *Serpine1*. It has been argued that motility in Smad4 knockout cells might be related to the inability of these cells to upregulate *Serpine1* induction (Levy and Hill, 2005). TGF-β1 treatment correlated with a significant increase in cell motility in part due to *Serpine1*. Cell motility is impaired in *Serpine1* deficient cells (Kutz et al., 2001). However, RNA-seq data in this project shows that *Smad4*$^{fl/fl}$ adenomas is inducing *Serpine1* at the basal level. This gene is also upregulated with TGF-β1 treatment at a late time point unlike its early induction in the presence of Smad4 (section 6.4.4.2). Thus, *Serpine1* might contribute to ECM homeostasis and cell motility (Kutz et al., 2001; Levy and Hill, 2005) but is not the main contributer.

Motility is an important aspect of cells undergoing EMT in order to invade, thus it is of great importance for patient management. For that, we need to ascertain if motility is reversible if Smad4 is re-expressed and whether it can be inhibited with certain inhibitors such as Rock inhibitors? These are questions to be answered with a complementation study using a human CRC cell line (section 7.4).

7.2.3 Is the phenotype in this study related to Smad4 MH1 deletion

The *Smad4*$^{fl/fl}$ mouse model used in this study is the first model to evaluate the function of the MH1 domain in the context of active Wnt signalling *in vivo*. It is also the first one to dissect the effect of this mutation in intestinal organoid culture with or without TGF-β1 stimulation. The effect of this mutation has been summarised in section 7.1.

One obvious difference between *Smad4*$^{fl/fl}$ and *Smad4*$^{+/+}$ is the slower sequence of events in Smad4 knockout adenomas. For example, slow growth rate (Figure 5.4), the decrease in viability and apoptotic effect of TGF-β1 (Figure 5.12, 5.13), the EMT and the time required for all of TGF-β1 treated adenomas to change in shape (Figure 5.17, 5.18) and the upregulation of *Serpine1* shown from the RNA-seq data (section 6.4.4.2). All these events occur in both adenomas but was enhanced in the presence of Smad4 suggesting that Smad4 is an accelerator although different mechanisms might also exist. The slow growth has been discussed earlier (section 5.5.2) and whether it is related to intrinsic properties of the adenomas to activate stress pathways as predicted by GO and upregulation of the TGF-β pathway at the basal level (Table 6.4) is another possibility.

There is also a possibility that these results might be related to the used concentration of TGF-β1 in this study (390pM). While most of the studies evaluating Smad4 function were mainly based on concentration between 390-780pM of TGF-β1, there is a possibility that the contradictory results is related not only to the context but also to the TGF-β1 concentration. This will be further investigated using a cell line.

The response to external TGF-β1 was also slower in the absence of Smad4. This event is reminiscent of the requirement of Smad4 in FAST-1-Smad2 complex on activin responsive element (ARE) on the *Mix2* promoter. Smad2 and FAST-1 have a ligand-stimulated affinity for one to another in the absence of Smad4 in the complex. However, this binding to ARE is not activated and not stable. The interaction of Smad4 is required to stabilise the active (DNA-binding) ARF complex (Chen et al., 1997). Thus, one could hypothesise

with this adenoma model that a similar scenario could be that activated p-R-Smad might be binding to SBE with other TF, and Smad4 is stabilising this binding to regulate gene transcription. In the absence of Smad4 another partner might bind. The recruitment of this partner might be slower possibly due to lower affinity than Smad4 binding and this might reflect the slower response of *Smad4*$^{fl/fl}$ to TGF-β1 stimulation.

Thus, the questions to be answered are: whether these phenotypic differences are related to the deletion of the MH1 domain? Or whether it is related to Smad4 mutations regardless of its site? Is the truncated form of Smad4 functional and does it interfere with the transcriptional regulation of Smad2 and Smad3? Answering these questions are important due to the diversity of *Smad4* mutations in human CRC which are shown to be missense, nonsense mutations and to a lesser extent splice site, frame-shift and in-frame insertion/deletion mutations (Fleming et al., 2013). Mutations are mainly clustered in the MH2 domain followed by the MH1 and to a lesser extent in the linker (Fleming et al., 2013).

In an attempt to start answering the previous questions and to detect if the truncated Smad4 binds to p-Smad2, p-Smad3 with pull down experiments using protein lysates from intestinal adenoma culture were came out but were not successful. The low yield of protein from adenoma culture for such experiments was a major obstacle. Owing to the difficulty in performing these experiments along with Smad4 rescue experiments using intestinal organoid culture, a cell line will be used.

7.3 Are R-Smads regulating genes in the absence of Smad4?

R-Smads are involved in signal propagation in TGF-β1 activated cells when they are phosphorylated by a type 1 receptor. The nuclear localisation of p-R-Smads in response to TGF-β1 stimuli was evident from the work in this thesis (Figure 5.9) and from others studies (Liu et al., 1997; Fink et al., 2003; Levy and Hill, 2005; Dawes et al., 2009) due to the presence of NLS in these proteins and translocation via importin7, 8 to the nucleus (Xu

et al., 2007). The nuclear localisation and EMT that was Smad4 independent raised the question of whether these R-Smads are active in signal transduction in the absence of Smad4, supported by the following reasons:

First, the presence of functional SAD in Smad3 (Wang et al., 2005). Before Wangs' study in 2005, SAD was thought to be present only in Smad4. SAD is required for the activation of Smad4-dependent signalling responses (de Caestecker et al., 1997) due to the intrinsic, p300-dependent, transcriptional activity that is important for the physical interaction between the SAD and the NH2 terminus of p300/CBP (de Caestecker et al., 2000; Chacko et al., 2001). Second, the ability of p-Smad2 to bind to p300 only on chromatin templates and not on naked DNA (Ross et al., 2006). Third, Smad3 monoubiquitination with USP15 is inhibited in Smad4 depleted cells (HaCaT and MDA-MB-321 cell lines were used as a model) (Inui et al., 2011). Fourth, the presence of R-Smad partners other than Smad4. For instance, a rapid and robust binding of R-Smads to TIF1γ in response to TGF-β in different cell types including epithelial cells (He et al., 2006). This interaction in hematopoietic stem cells can replace Smad4 and mediate erythrocyte differentiation, while Smad4 mediates growth inhibition of the same cells (He et al., 2006). In the context of mammary epithelial cells, both Smad4 and TIF1γ induce EMT. However, inactivation of TIF1γ increased the contribution of Smad4 to TGF-β1-induced EMT as detected by increased expression of EMT markers. TIF1γ silencing has no effect on TGF-β1 anti-proliferative function (Hesling et al., 2011). TIF1γ binds to the same region of *PAL1* gene promoter having the Smad binding elements (Hesling et al., 2011). Moreover, it has been reported to be an antagonist for Smad4. In the nucleus it monoubiquitinates free-Smad4 in lysine 519 and to a greater efficiency when Smad4 is in complex with Smad2 (Dupont et al., 2009). In the context of lung adenocarcinoma thyroid transcription factor-1 (TTF-1) is another partner for Smad3 and competes with Smad4 for Smad3 binding with or without TGF-β stimulation. The binding results in the transcription regulation of genes independently of Smad4 (Isogaya et al., 2014).

This evidence might lead to the hypothesise that partners other than Smad4 might bind

to the activated R-Smads in response to TGF-β1 in the context of active Wnt pathway. Luciferase repoter assays in response to TGF-β1 might give a hint for an active R-Smad in transcription. However, immunoprecipitation with p-Smad2 and p-Smad3 antibodies followed by affinity purification joined to mass spectrometry for proteomic analysis of transcription factor complexes are important to reveal these partners. Also ChIP-seq experiments for Smad2 and Smad3 binding sites and massively parallel sequencing might reveal the binding sites of these Smads on chromation and their target genes. Such approaches might open new doors to understand the paradox of the TGF-β signalling pathway for effective targeted therapy.

7.4 Future work

As has been discussed earlier, there are some questions yet to be answered. Some of them and in particular the effect of BMP signalling on adenomas, can be achieved using intestinal organoid culture. A read out of the effect can be detected using immunofluorescence with confocal microscopy and western blots. However, the complementation study will be carried out using a human CRC cell line to make the study more relevant to human cancer. Colo205 cell line that has been chosen for the complementation and functional analysis of *Smad4* mutations. Colo205 is a colon carcinoma cell line that has been established from ascites fluid obtained from a male patient with adenocarcinoma of the colon with liver metastasis (Semple et al., 1978). Colo205 has been characterised to have a deletion in exon 1-exon 4 (codon 1-904) of *Smad4* (Woodford-Richens et al., 2001; Chang et al., 2011). Exome sequencing is in agreement with the COSMIC report and showed that in addition to Smad4 deletion, Colo205 has mutations in *BRAF* (V600E), *TP53* (26 bp del) and *APC* (T1556fs (insertion A)) (Chang et al., 2011).

The complementation study aims to:

1. Rescue Smad4 loss by replacing it
2. Dissect the function of the different Smad4 domains and the effect of different mutations

in *Smad4*

3. Validation of some results from the RNA-seq experiment using the luciferase reporter assay.

Before starting thesis writing, I have characterised the Colo205 cell line (preliminary data will be shown later). I have prepared maxi preps for different luciferase (section 2.12) and pBabe-puro-Smad4-Flag plasmids following validation by DNA sequencing. I have designed some of the primers using pBabe-puro-Smad4-Flag plasmid as a back bone. A student in the lab is starting to prepare the constructs and transfect the cell line with different mutations and domain specific deletions with promising progress.

7.4.1 Preliminary results

7.4.1.1 Nuclear localisation of R-Smad and Colo205 lacks truncated Smad4

TGF-β signalling in Colo205 was determined with p-R-Smad in the absence and presence of TGF-β1 and in the presence of TGF-β1 inhibitor. TGF-β1 stimulation resulted in phosphorylation of p-Smad2 and p-Smad3 and with nuclear localisation. Nuclear localisation was prevented if cells were preincubated with SB-505124. Faint bands of p-Smad2 and p-Smad3 were seen in western blots without TGF-β1 treatment. Total R-Smads were expressed in Colo205. No truncated Smad4 protein was detected in Colo205 (Figure 7.1A-C).

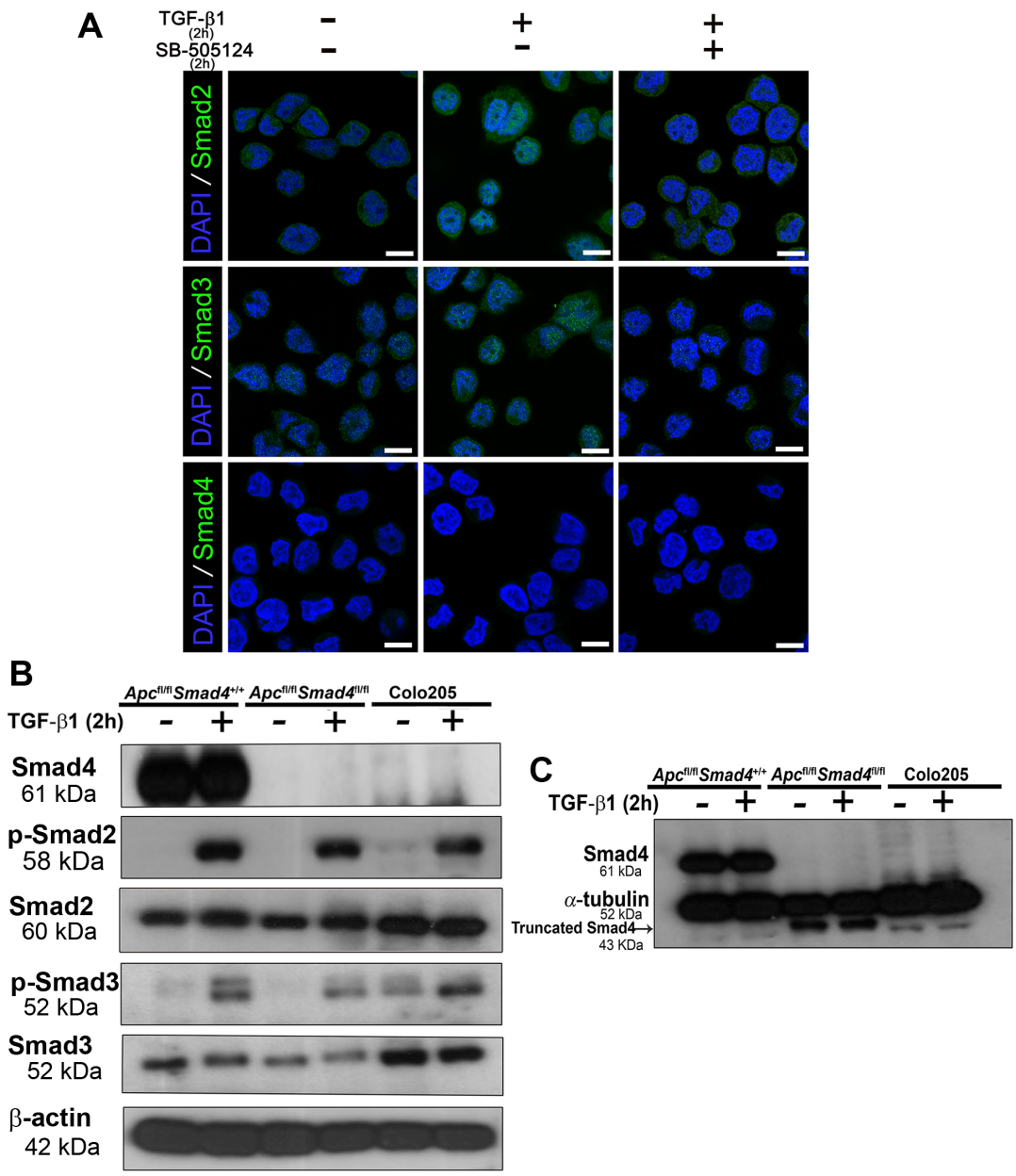

Figure 7.1: **TGF-β signalling in Colo205**. (A) Nuclear localisalion of p-Smad2 and p-Smad3 following 390pM TGF-β1 treatment for 2h. Nuclear localisation decreased when the adenomas were pre-incubated with 1μM SB-505124 for 2h. Scale bars 10μm. (B) Representative western blots of Smad4, total R-Smads, and p-Smads in Colo205 show phosphorylation of R-Smads following TGF-β1 treatment. (C) Absence of truncated Smad4 in Colo205. Positive control in B, C was *Smad4*$^{+/+}$ and *Smad4*$^{fl/fl}$ adenomas.

7.4.2 EMT, β-catenin and and Survivin in Colo205

Different EMT markers and β-catenin have been tested on Colo205 at different time points using confocal microscopy and western blots. N-cadhein, F-actin and nuclear β-catenin start to appear in confocal images after 6 days of TGF-β1 treatment. Western blots did not show any upregulation of EMT markers or an increase in β-catenin at the tested time points (Figure 7.2A-D). Survivin expression was maintained with TGF-β1 treatment (Figure 7.2E).

7.4.3 Discussion

The preliminary data shows a deletion of Smad4 protein as a result of the mutation with no truncated protein. It might be related to the absence of an open reading frame in human Smad4 gene on exon 5 as detected with *in silico* analysis. Absence of truncated Smad4 could be related to rapid degradation of mutated Smad4 in human by SCF E3 complex after being phosphorylated by JNK or p38 kinase (Liang et al., 2004) The EMT is not very clear in Colo205 in comparison with adenomas (Figure 5.17, 5.19, 5.22, 5.23). This could be related to different environments used in the experiments. Colo205 cells were growing in 2D whilst the adenomas were growing in Matrigel thus adenomas do have cell-ECM interaction unlike Colo205 cells. Also, Colo205 has mutations other than Smad4, thus the phenotype might be changed accordingly. Optimisation and different conditions will be subjects for further investigation.

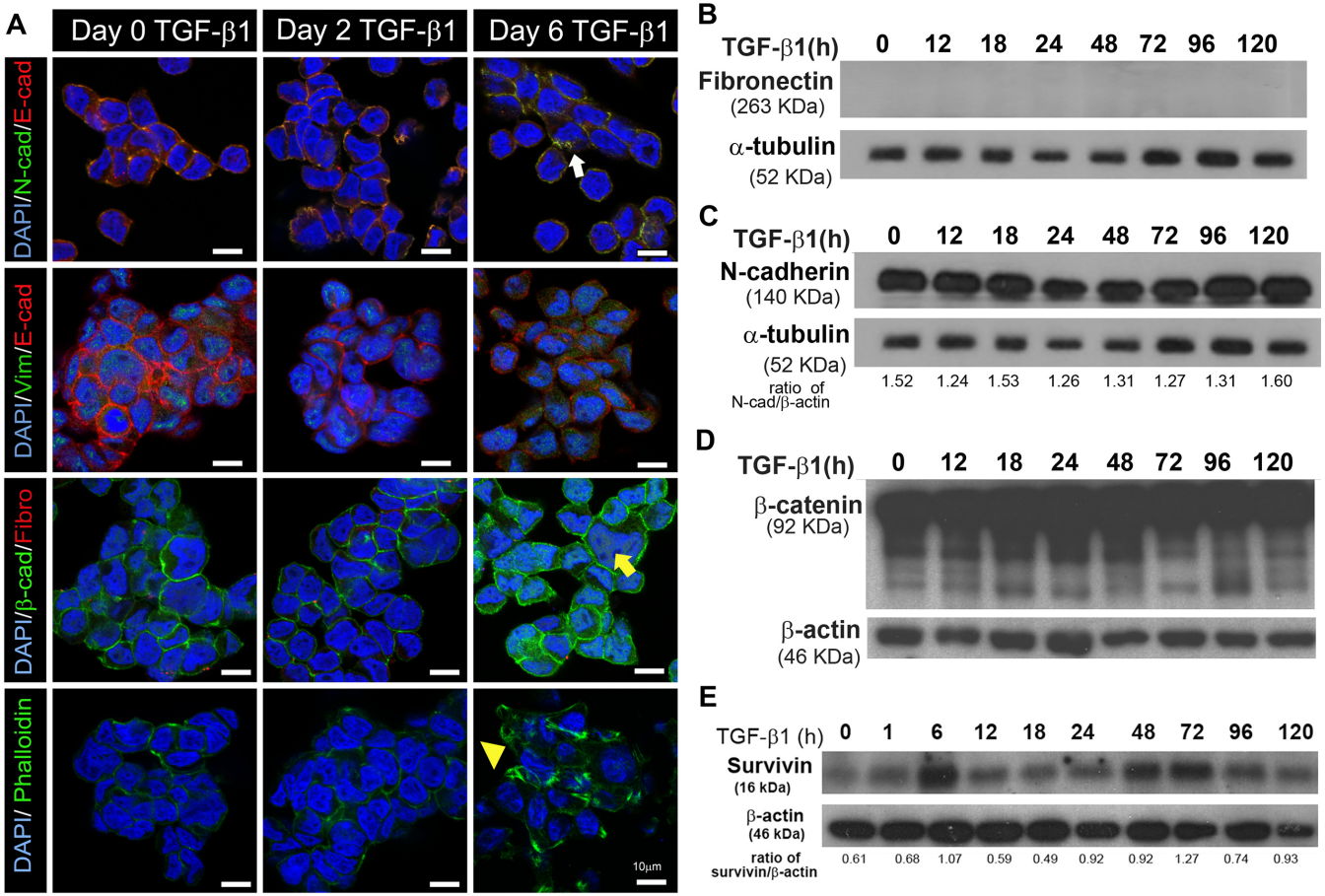

Figure 7.2: **EMT and Survivin following TGF-β1 treatment**. Colo205 treated every other day or for the time points indicated and characterised for EMT markers by confocal microscopy (A) and western blots (B-D). (E) Western blots show Survivin at different time points. Densitometric analysis was done using ImageJ and ratio of the protein/loading control is shown under the blots in C and E. Data are from one experiment. Scale bars 10μm

Appendix A

Appendix

Table A.1: PCR primers

Gene	Primers name	Sequence 5'-3'	Expected band size (bp)	Reference
Apc LoxP	APC P3	GTTCTGTATCATGGAAAGATAGGTGGTC	LoxP[1] 314 bp	(Shibata et al., 1997)
	APC P4	CACTCAAAACGCTTTTGAGGGTTG	Wt[2] 226 bp	
	APC P5	GAGTACGGGGTCTCTGTCTCAGTGAA	Rec[3] 259 bp	
Lgr5- cre	Lgr5KI/F[4]	CACTGCATTCTAGTTGTGG	positive 180 bp	(Barker et al., 2007)
	Lgr5KI/R[5]	CGGTGCCCGCAGCGAG		
Smad4	Smad4 R1	TACAAGTGCTATGTCTTCAGCG	LoxP 675 bp	(Chu et al., 2004)
	Smad4 F1(-)	CTTTTATTTTCAGATTCAGGGGTTC	Wt 625 bp	
	Smad4F2 (fl)	AAAATGGGAAAACCAACGAG	Rec 512 bp	
vil-Cre	S1X/F	GCATAACCAGTGAAACAGCATTGCTG	Positive 280 bp	(El Marjou et al., 2004)
	S1X/R	GGACATGTTCAGGGATCGCCAGGCG		
Rosa26YFP	R26g2/F	TGTTATCAGTAAGGGAGCT	Wt239 bp	(Srinivas et al., 2001)
	R26g2/R mut[6]	AAGACCGCGAAGAGTTTGT	Mut 301 bp	
	R26g2/R Wt	CACACCAGGTTAGCCTTTA		
Igf2r^{I1565A}	2RKI-37	GGTGCAGGTGTTATGACTGG	CKI 302bp	Artemis (unpublished
	2RKI-38	AGTACATCAGCCTGTATCCTGG	Wt 227bp	Hassan lab)

[1]LoxP: conditional allele,[2]Wt: wild type, [3]Rec: recombined, [4]F: forward primer,[5]R: reverse primer, [6]mut: mutant allele.

Table A.2: PCR mix, cycling conditions for genes of interest

	Gene											
	Apc		*Lgr5-Cre*		*Smad4*		*vil-Cre*		*YFP*		*Igf2r*^{I1565A}	
Reagents	Working conc.	Volume (µl)	Working conc.	Volume (µl)	Working conc.	Volume (µl)	Working conc.	Volume (µl)	Working conc.	Volume (µl)	Working conc.	Volume (µl)
Buffer	1X	2.5	1X	2.5	1X	2.5	1X	2.5	1X	2.5	1X	2.5
$MgCl_2$ (mM)	2.5	2.5	2.5	2.5	2.5	2.5	2.5	2.5	2.5	2.5	2	2
dNTP (mM)	0.4	1	0.2	0.5	0.2	0.5	0.2	0.5	0.2	0.5	0.2	0.5
Primer (µM)	0.2	0.1	0.5	0.125	0.5	0.125	0.6	0.15	0.2	0.05	0.1	0.025
ddH_2O		18.7		20.4		18.2		20.6		19.4		19.85
Taq (U/µl)	0.08	0.1	0.08	0.0625	0.08	0.0625	0.08	0.0625	0.08	0.1	0.08	0.1
PCR Conditions	Temp °C	Time sec	Temp °C	Time sec	Temp °C	Time sec	Temp °C	Time sec	Temp °C	Time sec	Temp °C	Time sec
Initial denaturation	95	180	94	180	94	180	94	180	94	420	95	300
Denaturation	95	30	94	30	94	45	94	30	94	30	95	30
Annealing	60	30	58	30	54	45	55	30	55	30	60	30
Elongation	72	60	72	30	72	45	65	60	72	30	72	30
Final elongation	72	300	72	420	72	420	72	600	72	300	72	600
Cycles*	30		35		35		53		40		35	

*: Cycles represent the repeat in the denaturation, annealing and elongation steps,

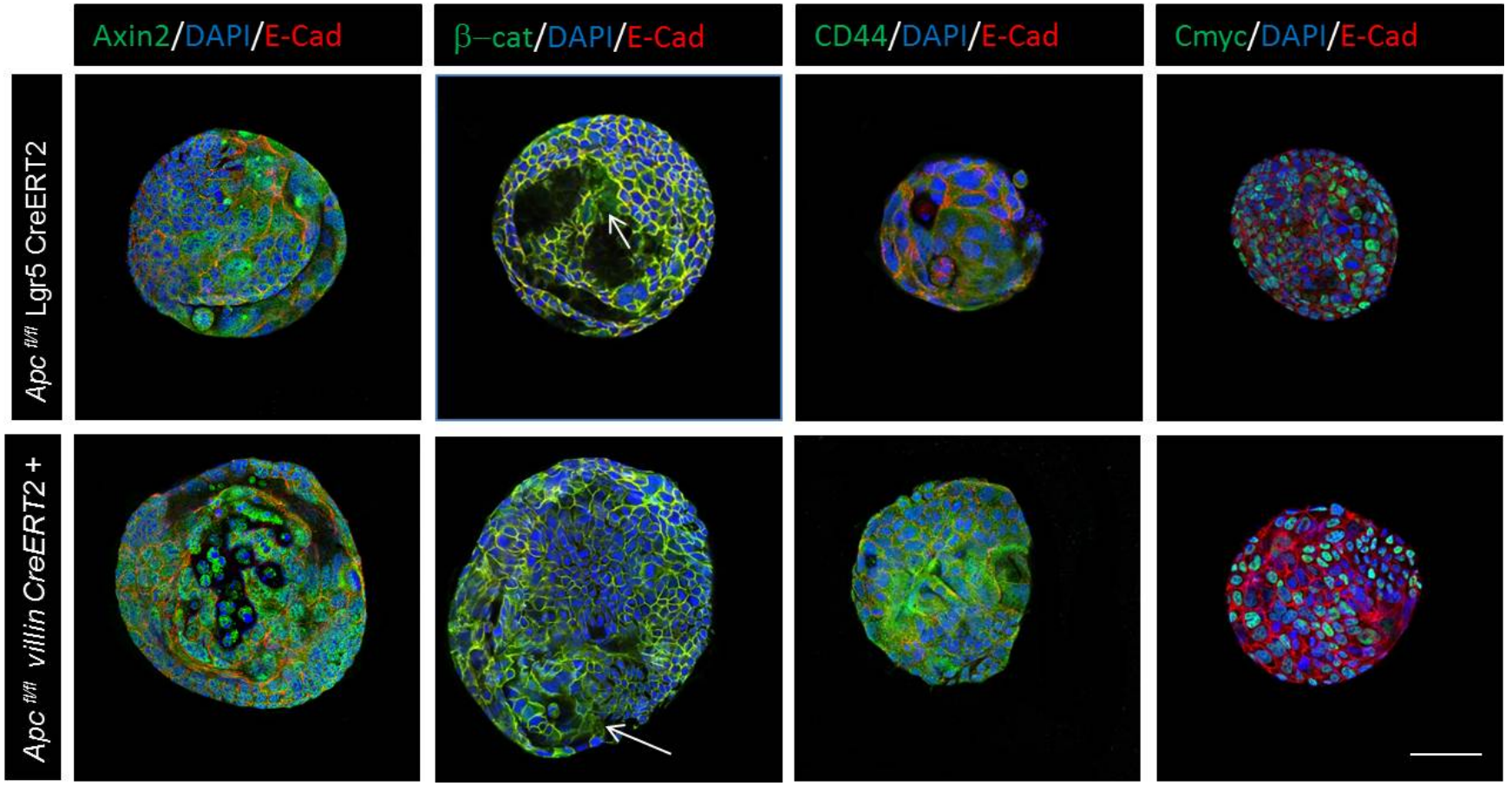

Figure A.1: **Wnt/β-catenin upregulated genes in *Apc*$^{fl/fl}$ adenomas.** Representative confocal images show Axin2, β-catenin, CD44 and c-Myc in *Apc*$^{fl/fl}$ *Lgr5-CreERT2* and *Apc*$^{fl/fl}$ *Villin-CreERT2* adenomas. White arrows point to cytoplasmic β-catenin. Scale bar 50μm.

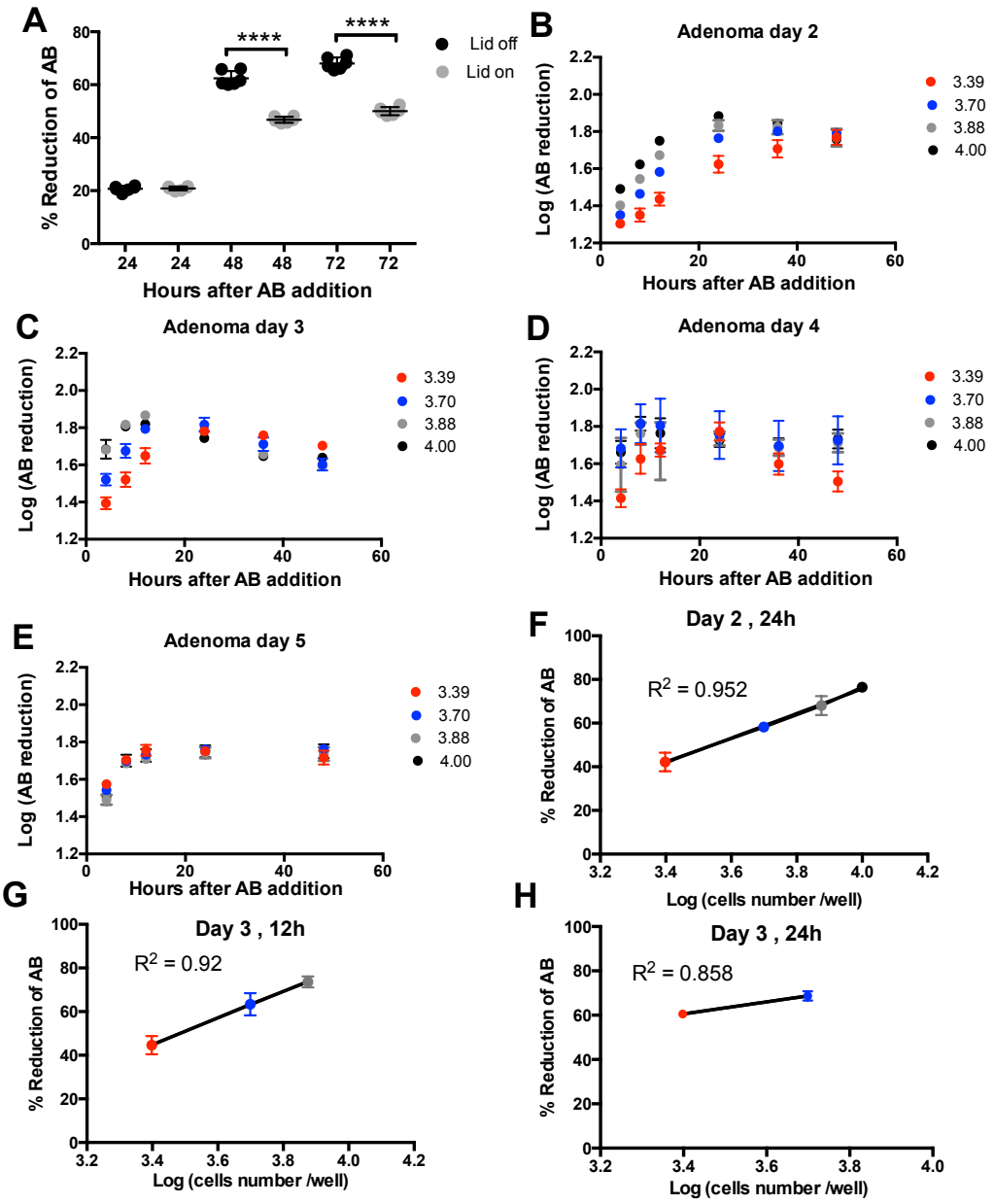

Figure A.2: **Optimisation of AB viability assay to measure adenoma growth.** (A) *Apc*$^{fl/fl}$ adenomas seeded in 96 well plates were supplemented with EGF and were incubated with AB on D2 for the indicated time points. Absorbance was measured either with the lid on or off. Statistical comparisons were performed by one-way ANOVA with Tukey's multiple comparison test **** indicates P$\leqslant$0.0001. (n=1 with 6 replicates represented by dots). Error bars represent $\pm$SD. (B-E) Adenomas were seeded in 4 different plates at different cell densities. The numbers in the graph key represent log cell number. AB was added to each plate on different days (day 2 in B, day 3 in C, day 4 in D, day 5 in E). Absorbance was measured at different time points following AB addition. (F-H) Relationship between log cell number and percent reduction in AB according to the day and time point indicated in each graph represented by R^2 (n=1, with 4 replicates per condition).

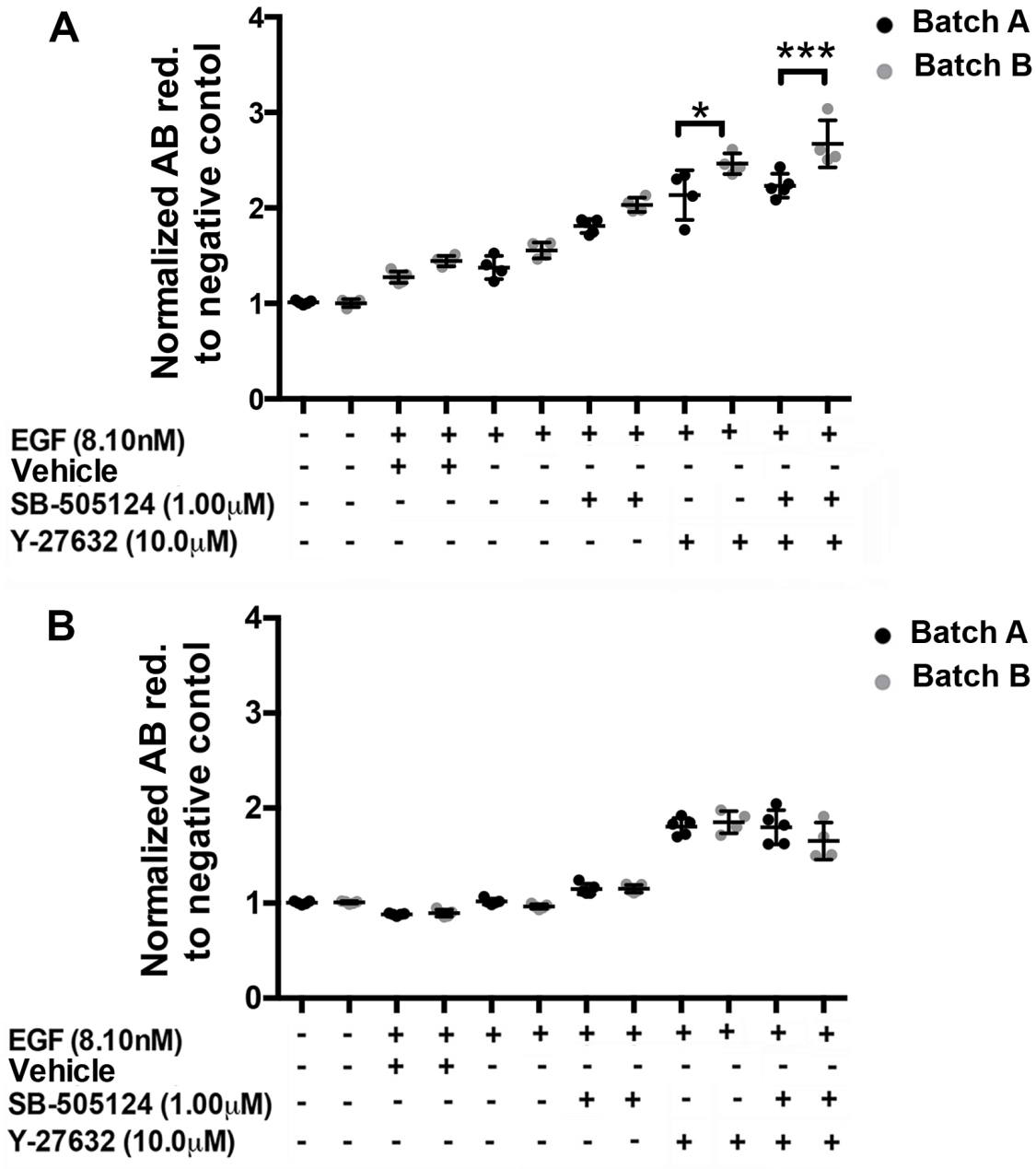

Figure A.3: **Adenoma growth is independent on Matrigel batch.** The effect of different Matrigel batches tested on adenoma growth. Cryopreserved adenomas of both genotypes were thawed and treated as detailed previously. Same sample from each genotype was embedded in 2 different batches. AB was added on D4 and measured after 24h. (n=1 with 4 replicates each condition represented by dots). Statistical analysis was performed using one-way ANOVA with Sidak's multiple comparison test **, ****P$\leqslant$0.01, P$\leqslant$0.0001, respectively.

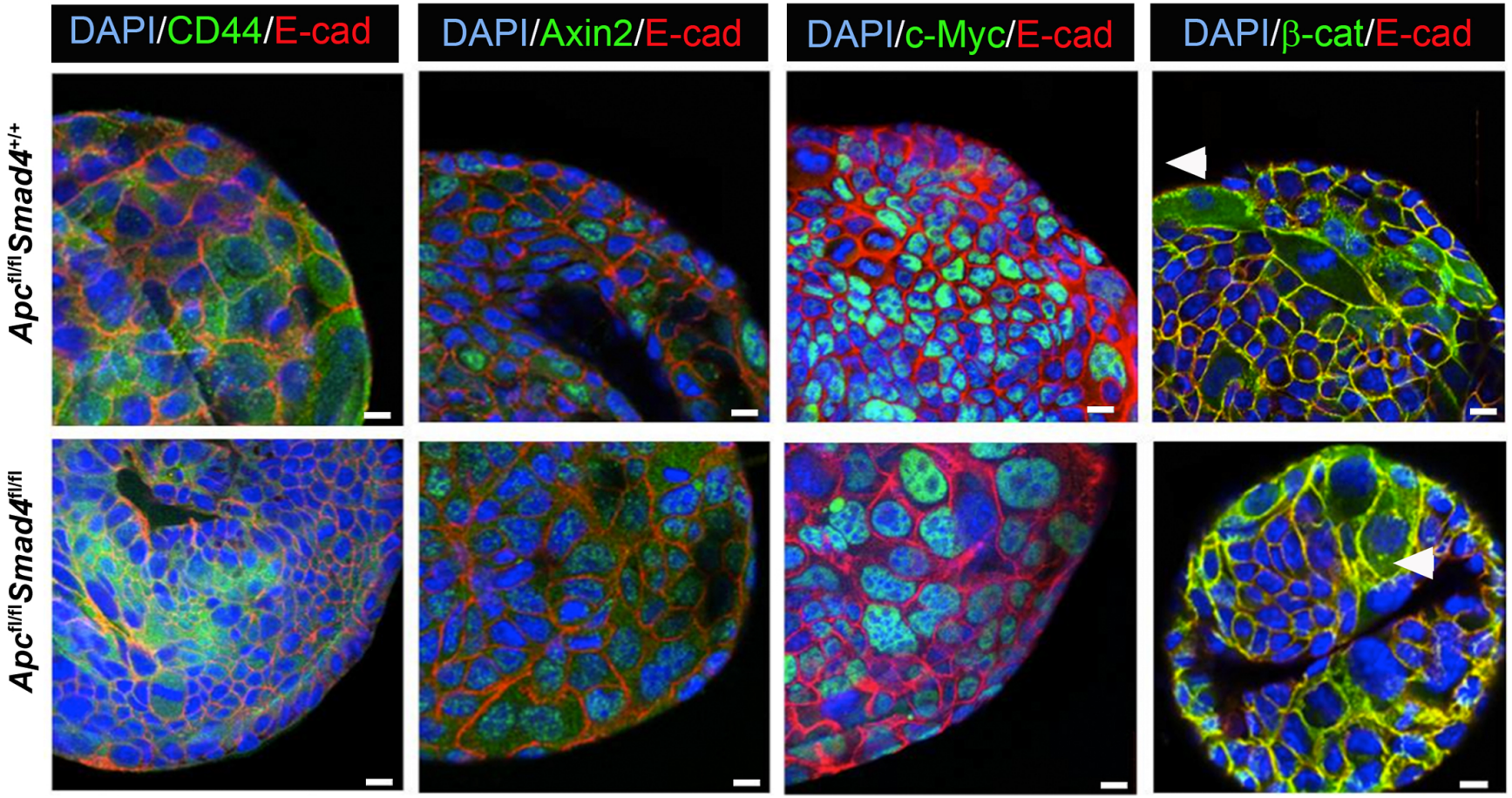

Figure A.4: **Confocal images for Wnt/β-catenin genes labelling in *Apc*$^{fl/fl}$*Smad4*$^{fl/fl}$ adenomas**. Representative confocal images showing the expression of the Wnt/β-catenin genes (CD44, Axin2, c-Myc and β-catenin) in *Smad4*$^{+/+}$ and *Smad4*$^{+/+}$ adenomas, white arrowheads represent cytoplasmic β-catenin. (n=2 with similar results). Scale bars 10μm.

References

Achyut, B. R. and L. Yang (2011). Transforming growth factor-β in the gastrointestinal and hepatic tumor microenvironment. *Gastroenterology 141*(4), 1167–1178.

Albuquerque, C., C. Breukel, R. van der Luijt, P. Fidalgo, P. Lage, F. J. Slors, C. N. Leitão, R. Fodde, and R. Smits (2002). The âĂŸjust-rightâĂŹsignaling model: Apc somatic mutations are selected based on a specific level of activation of the β-catenin signaling cascade. *Human molecular genetics 11*(13), 1549–1560.

Andreu, P., S. Colnot, C. Godard, S. Gad, P. Chafey, M. Niwa-Kawakita, P. Laurent-Puig, A. Kahn, S. Robine, C. Perret, et al. (2005). Crypt-restricted proliferation and commitment to the paneth cell lineage following apc loss in the mouse intestine. *Development 132*(6), 1443–1451.

Annes, J. P., J. S. Munger, and D. B. Rifkin (2003). Making sense of latent tgfβ activation. *Journal of cell science 116*(2), 217–224.

Aoki, K., Y. Tamai, S. Horiike, M. Oshima, and M. M. Taketo (2003). Colonic polyposis caused by mtor-mediated chromosomal instability in apc+/δ716 cdx2+/- compound mutant mice. *Nature genetics 35*(4), 323–330.

Ashcroft, G. S., X. Yang, A. B. Glick, M. Weinstein, J. J. Letterio, D. E. Mizel, M. Anzano, T. Greenwell-Wild, S. M. Wahl, C. Deng, et al. (1999). Mice lacking smad3 show accelerated wound healing and an impaired local inflammatory response. *Nature cell biology 1*(5), 260–266.

Attisano, L. and J. L. Wrana (2013). Signal integration in tgf-β, wnt, and hippo pathways. *F1000prime reports 5*.

Baldus, S. E., S. P. Mönig, S. Huxel, S. Landsberg, F.-G. Hanisch, K. Engelmann, P. M. Schneider, J. Thiele, A. H. Hölscher, and H. P. Dienes (2004). Muc1 and nuclear β-catenin are coexpressed at the invasion front of colorectal carcinomas and are both correlated with tumor prognosis. *Clinical cancer research 10*(8), 2790–2796.

Bancroft, J. D. (2013). *Histochemical techniques*. Butterworth-Heinemann.

Barker, N. (2014). Adult intestinal stem cells: critical drivers of epithelial homeostasis and regeneration. *Nature Reviews Molecular Cell Biology 15*(1), 19–33.

Barker, N., R. A. Ridgway, J. H. van Es, M. van de Wetering, H. Begthel, M. van den Born, E. Danenberg, A. R. Clarke, O. J. Sansom, and H. Clevers (2009). Crypt stem cells as the cells-of-origin of intestinal cancer. *Nature 457*(7229), 608–611.

Barker, N., J. H. van Es, J. Kuipers, P. Kujala, M. van den Born, M. Cozijnsen, A. Haegebarth, J. Korving, H. Begthel, P. J. Peters, et al. (2007). Identification of stem cells in small intestine and colon by marker gene lgr5. *Nature 449*(7165), 1003–1007.

Barros, R., N. Mendes, J. R. Howe, C. A. Reis, C. de Bolos, F. Carneiro, L. David, and R. Almeida (2009). Juvenile polyps have gastric differentiation with muc5ac expression and downregulation of cdx2 and smad4. *Histochemistry and cell biology 131*(6), 765–772.

Barros, R., B. Pereira, I. Duluc, M. Azevedo, N. Mendes, V. Camilo, R. Jacobs, P. Paulo, F. Santos-Silva, I. van Seuningen, et al. (2008). Key elements of the bmp/smad pathway co-localize with cdx2 in intestinal metaplasia and regulate cdx2 expression in human gastric cell lines. *The Journal of pathology 215*(4), 411–420.

Bartman, A. E., S. J. Serson, S. L. Ewing, G. A. Niehans, C. L. Wiehr, M. K. Evans, and S. B. Ho (1999). Aberrant expression of muc5ac and muc6 gastric mucin genes in colorectal polyps. *International journal of cancer 80*(2), 210–218.

Biemer-Hüttmann, A.-E., M. D. Walsh, M. A. McGuckin, Y. Ajioka, H. Watanabe, B. A. Leggett, and J. R. Jass (1999). Immunohistochemical staining patterns of muc1, muc2, muc4, and muc5ac mucins in hyperplastic polyps, serrated adenomas, and traditional adenomas of the colorectum. *Journal of Histochemistry & Cytochemistry 47*(8), 1039–1048.

Borrell, B. (2010). How accurate are cancer cell lines? *Nature News 463*(7283), 858–858.

Bosman, F. T., F. Carneiro, R. H. Hruban, N. D. Theise, et al. (2010). *WHO classification of tumours of the digestive system.* Number Ed. 4. World Health Organization.

Bresalier, R., Y. Niv, J. Byrd, Q.-Y. Duh, N. Toribara, R. Rockwell, R. Dahiya, and Y. Kim (1991). Mucin production by human colonic carcinoma cells correlates with their metastatic potential in animal models of colon cancer metastasis. *Journal of Clinical Investigation 87*(3), 1037.

Buchsbaum, R. J. (2007). Rho activation at a glance. *Journal of cell science 120*(7), 1149–1152.

Buess, M., L. Terracciano, J. Reuter, P. Ballabeni, J.-L. Boulay, U. Laffer, U. Metzger, R. Herrmann, and C. F. Rochlitz (2004). Amplification of ski is a prognostic marker in early colorectal cancer. *Neoplasia 6*(3), 207–212.

Butz, H., K. Rácz, L. Hunyady, and A. Patócs (2012). Crosstalk between tgf-β signaling and the microrna machinery. *Trends in pharmacological sciences 33*(7), 382–393.

Byrd, J. C. and R. S. Bresalier (2004). Mucins and mucin binding proteins in colorectal cancer. *Cancer and Metastasis Reviews 23*(1-2), 77–99.

Calon, A., E. Espinet, S. Palomo-Ponce, D. V. Tauriello, M. Iglesias, M. V. Céspedes, M. Sevillano, C. Nadal, P. Jung, X. H.-F. Zhang, et al. (2012). Dependency of colorectal cancer on a tgf-β-driven program in stromal cells for metastasis initiation. *Cancer cell 22*(5), 571–584.

Chacko, B. M., B. Qin, J. J. Correia, S. S. Lam, M. P. de Caestecker, and K. Lin (2001). The l3 loop and c-terminal phosphorylation jointly define smad protein trimerization. *Nature Structural & Molecular Biology 8*(3), 248–253.

Chang, H., D. G. Jackson, P. S. Kayne, P. B. Ross-Macdonald, R.-P. Ryseck, and N. O. Siemers (2011). Exome sequencing reveals comprehensive genomic alterations across eight cancer cell lines. *PloS one 6*(6), e21097.

Chaudhari, A. A., J.-W. Seol, S.-J. Kim, Y.-J. Lee, H.-s. Kang, I.-s. Kim, N.-S. Kim, and S.-Y. Park (2007). Reactive oxygen species regulate bax translocation and mitochondrial transmembrane potential, a possible mechanism for enhanced trail-induced apoptosis by cccp. *Oncology reports 18*(1), 71–76.

Chen, C.-R., Y. Kang, P. M. Siegel, and J. Massagué (2002). E2f4/5 and p107 as smad cofactors linking the tgfβ receptor to c-myc repression. *Cell 110*(1), 19–32.

Chen, X., M. J. Rubock, and M. Whitman (1996). A transcriptional partner for mad proteins in tgf-β signalling.

Chen, X., E. Weisberg, V. Fridmacher, M. Watanabe, G. Naco, and M. Whitman (1997). Smad4 and fast-1 in the assembly of activin-responsive factor. *Nature 389*(6646), 85–89.

Cheng, H. and C. Leblond (1974). Origin, differentiation and renewal of the four main epithelial cell types in the mouse small intestine v. unitarian theory of the origin of the four epithelial cell types. *American Journal of Anatomy 141*(4), 537–561.

Cheon, D.-J. and S. Orsulic (2011). Mouse models of cancer.

Chiang, A. C. and J. Massagué (2008). Molecular basis of metastasis. *New England Journal of Medicine 359*(26), 2814–2823.

Chu, G. C., N. R. Dunn, D. C. Anderson, L. Oxburgh, and E. J. Robertson (2004). Differential requirements for smad4 in tgfβ-dependent patterning of the early mouse embryo. *Development 131*(15), 3501–3512.

Claassen, D. A., M. M. Desler, and A. Rizzino (2009). Rock inhibition enhances the recovery and growth of cryopreserved human embryonic stem cells and human induced pluripotent stem cells. *Molecular reproduction and development 76*(8), 722–732.

Clevers, H. (2006). Wnt/β-catenin signaling in development and disease. *Cell 127*(3), 469–480.

Clevers, H. and R. Nusse (2012). Wnt/β-catenin signaling and disease. *Cell 149*(6), 1192–1205.

Consorti, F., A. Lorenzotti, G. Midiri, and M. Di Paola (2000). Prognostic significance of mucinous carcinoma of colon and rectum: A prospective case-control study. *Journal of surgical oncology 73*(2), 70–74.

Cormier, R. T., K. H. Hong, R. B. Halberg, T. L. Hawkins, P. Richardson, R. Mulherkar, W. F. Dove, and E. S. Lander (1997). Secretory phospholipase pla2g2a confers resistance to intestinal tumorigenesis. *Nature genetics 17*(1), 88–91.

Crosnier, C., D. Stamataki, and J. Lewis (2006). Organizing cell renewal in the intestine: stem cells, signals and combinatorial control. *Nature Reviews Genetics 7*(5), 349–359.

Daly, A. C., R. A. Randall, and C. S. Hill (2008). Transforming growth factor β-induced smad1/5 phosphorylation in epithelial cells is mediated by novel receptor complexes and is essential for anchorage-independent growth. *Molecular and cellular biology 28*(22), 6889–6902.

Davis, H., S. Irshad, M. Bansal, H. Rafferty, T. Boitsova, C. Bardella, E. Jaeger, A. Lewis, L. Freeman-Mills, F. C. Giner, et al. (2014). Aberrant epithelial grem1 expression initiates colonic tumorigenesis from cells outside the stem cell niche. *Nature medicine*.

Dawes, L. J., M. A. Sleeman, I. K. Anderson, J. R. Reddan, and I. M. Wormstone (2009). Tgfβ/smad4-dependent and-independent regulation of human lens epithelial cells. *Investigative ophthalmology & visual science 50*(11), 5318–5327.

de Caestecker, M. P., P. Hemmati, S. Larisch-Bloch, R. Ajmera, A. B. Roberts, and R. J. Lechleider (1997). Characterization of functional domains within smad4/dpc4. *Journal of Biological Chemistry 272*(21), 13690–13696.

de Caestecker, M. P., T. Yahata, D. Wang, W. T. Parks, S. Huang, C. S. Hill, T. Shioda, A. B. Roberts, and R. J. Lechleider (2000). The smad4 activation domain (sad) is a proline-rich, p300-dependent transcriptional activation domain. *Journal of Biological Chemistry 275*(3), 2115–2122.

de Lau, W., N. Barker, T. Y. Low, B.-K. Koo, V. S. Li, H. Teunissen, P. Kujala, A. Haegebarth, P. J. Peters, M. van de Wetering, et al. (2011). Lgr5 homologues associate with wnt receptors and mediate r-spondin signalling. *Nature 476*(7360), 293–297.

De Lau, W. B., B. Snel, and H. C. Clevers (2012). The r-spondin protein family. *Genome Biol 13*(3), 242.

De Wever, O., W. Westbroek, A. Verloes, N. Bloemen, M. Bracke, C. Gespach, E. Bruyneel, and M. Mareel (2004). Critical role of n-cadherin in myofibroblast invasion and migration in vitro stimulated by colon-cancer-cell-derived tgf-β or wounding. *Journal of cell science 117*(20), 4691–4703.

Deckers, M., M. van Dinther, J. Buijs, I. Que, C. Löwik, G. van der Pluijm, and P. ten Dijke (2006). The tumor suppressor smad4 is required for transforming growth factor β–induced epithelial to mesenchymal transition and bone metastasis of breast cancer cells. *Cancer research 66*(4), 2202–2209.

Deheuninck, J. and K. Luo (2009). Ski and snon, potent negative regulators of tgf-β signaling. *Cell research 19*(1), 47–57.

Delker, D. A., B. M. McGettigan, P. Kanth, S. Pop, D. W. Neklason, M. P. Bronner, R. W. Burt, and C. H. Hagedorn (2014). Rna sequencing of sessile serrated colon polyps identifies differentially expressed genes and immunohistochemical markers. *PloS one 9*(2), e88367.

Dennis, P. A. and D. B. Rifkin (1991). Cellular activation of latent transforming growth factor beta requires binding to the cation-independent mannose 6-phosphate/insulin-like growth factor type ii receptor. *Proceedings of the National Academy of Sciences 88*(2), 580–584.

Denoeud, F., J.-M. Aury, C. Da Silva, B. Noel, O. Rogier, M. Delledonne, M. Morgante, G. Valle, P. Wincker, C. Scarpelli, et al. (2008). Annotating genomes with massive-scale rna sequencing. *Genome Biol 9*(12), R175.

Derynck, R., R. J. Akhurst, and A. Balmain (2001). Tgf-β signaling in tumor suppression and cancer progression. *Nature genetics 29*(2), 117–129.

Dessein, R., M. Gironella, C. Vignal, L. Peyrin-Biroulet, H. Sokol, T. Secher, S. Lacas-Gervais, J. Gratadoux, F. Lafont, J. Dagorn, et al. (2009). Toll-like receptor 2 is critical for induction of reg3β expression and intestinal clearance of yersinia pseudotuberculosis. *Gut 58*(6), 771–776.

Dignass, A. U. and A. Sturm (2001). Peptide growth factors in the intestine. *European journal of gastroenterology & hepatology 13*(7), 763–770.

Donovan, E. A. and S. Kummar (2008). Role of insulin-like growth factor-1r system in colorectal carcinogenesis. *Critical reviews in oncology/hematology 66*(2), 91–98.

Dove, W. F., L. Clipson, K. A. Gould, C. Luongo, D. J. Marshall, A. R. Moser, M. A. Newton, and R. F. Jacoby (1997). Intestinal neoplasia in the apcmin mouse: independence from the microbial and natural killer (beige locus) status. *Cancer research 57*(5), 812–814.

Drost, J., R. H. van Jaarsveld, B. Ponsioen, C. Zimberlin, R. van Boxtel, A. Buijs, N. Sachs, R. M. Overmeer, G. J. Offerhaus, H. Begthel, et al. (2015). Sequential cancer mutations in cultured human intestinal stem cells. *Nature*.

Dupont, S., A. Mamidi, M. Cordenonsi, M. Montagner, L. Zacchigna, M. Adorno, G. Martello, M. J. Stinchfield, S. Soligo, L. Morsut, et al. (2009). Fam/usp9x, a deubiquitinating enzyme essential for tgfβ signaling, controls smad4 monoubiquitination. *Cell 136*(1), 123–135.

Dynkevich, Y., K. I. Rother, I. Whitford, S. Qureshi, S. Galiveeti, A. L. Szulc, A. Danoff, T. L. Breen, N. Kaviani, M. H. Shanik, et al. (2013). Tumors, igf-2, and hypoglycemia: insights from the clinic, the laboratory, and the historical archive. *Endocrine reviews 34*(6), 798–826.

Eichhorn, P. J. A. and P. V. Iyengar (2013). -ubiquitination in the tgf-β pathway. *Journal of Cancer Research and Therapeutic Oncology 1*(1), 1.

El Marjou, F., K.-P. Janssen, B. Hung-Junn Chang, M. Li, V. Hindie, L. Chan, D. Louvard, P. Chambon, D. Metzger, and S. Robine (2004). Tissue-specific and inducible cre-mediated recombination in the gut epithelium. *Genesis 39*(3), 186–193.

Elinav, E., R. Nowarski, C. A. Thaiss, B. Hu, C. Jin, and R. A. Flavell (2013). Inflammation-induced cancer: crosstalk between tumours, immune cells and microorganisms. *Nature Reviews Cancer 13*(11), 759–771.

Fearon, E. R. (2011). Molecular genetics of colorectal cancer. *Annual Review of Pathology: Mechanisms of Disease 6*, 479–507.

Ferlay, J., H.-R. Shin, F. Bray, D. Forman, C. Mathers, and D. M. Parkin (2010). Estimates of worldwide burden of cancer in 2008: Globocan 2008. *International journal of cancer 127*(12), 2893–2917.

Fijneman, R., J. Peham, M. Van de Wiel, G. Meijer, I. Matise, A. Velcich, and R. Cormier (2008). Expression of pla2g2a prevents carcinogenesis in muc2-deficient mice. *Cancer science 99*(11), 2113–2119.

Fijneman, R. J., L. K. Bade, J. R. Peham, M. A. van de Wiel, V. W. van Hinsbergh, G. A. Meijer, M. G. OâĂŹSullivan, and R. T. Cormier (2009). Pla2g2a attenuates colon tumorigenesis in azoxymethane-treated c57bl/6 mice; expression studies reveal pla2g2a target genes and pathways. *Analytical Cellular Pathology 31*(5), 345–356.

Fink, S. P., D. Mikkola, J. K. Willson, and S. Markowitz (2003). Tgf-β-induced nuclear localization of smad2 and smad3 in smad4 null cancer cell lines. *Oncogene 22*(9), 1317–1323.

Fleming, N. I., R. N. Jorissen, D. Mouradov, M. Christie, A. Sakthianandeswaren, M. Palmieri, F. Day, S. Li, C. Tsui, L. Lipton, et al. (2013). Smad2, smad3 and smad4 mutations in colorectal cancer. *Cancer research 73*(2), 725–735.

Fodde, R., W. Edelmann, K. Yang, C. van Leeuwen, C. Carlson, B. Renault, C. Breukel, E. Alt, M. Lipkin, and P. M. Khan (1994). A targeted chain-termination mutation in the mouse apc gene results in multiple intestinal tumors. *Proceedings of the National Academy of Sciences 91*(19), 8969–8973.

Fodde, R. and R. Smits (2001). Disease model: familial adenomatous polyposis. *Trends in molecular medicine 7*(8), 369–373.

Fodde, R., R. Smits, and H. Clevers (2001). Apc, signal transduction and genetic instability in colorectal cancer. *Nature Reviews Cancer 1*(1), 55–67.

Freeman, T. J., J. J. Smith, X. Chen, M. K. Washington, J. T. Roland, A. L. Means, S. A. Eschrich, T. J. Yeatman, N. G. Deane, and R. D. Beauchamp (2012). Smad4-mediated signaling inhibits intestinal neoplasia by inhibiting expression of β-catenin. *Gastroenterology 142*(3), 562–571.

Friedl, P. and S. Alexander (2011). Cancer invasion and the microenvironment: plasticity and reciprocity. *Cell 147*(5), 992–1009.

Fuda, N. J., M. B. Ardehali, and J. T. Lis (2009). Defining mechanisms that regulate rna polymerase ii transcription in vivo. *Nature 461*(7261), 186–192.

Gaarenstroom, T. and C. S. Hill (2014). Tgf-β signaling to chromatin: how smads regulate transcription during self-renewal and differentiation. In *Seminars in cell & developmental biology*, Volume 32, pp. 107–118. Elsevier.

Galdiero, M. R., E. Bonavita, I. Barajon, C. Garlanda, A. Mantovani, and S. Jaillon (2013). Tumor associated macrophages and neutrophils in cancer. *Immunobiology 218*(11), 1402–1410.

Gao, S., C. Alarcón, G. Sapkota, S. Rahman, P.-Y. Chen, N. Goerner, M. J. Macias, H. Erdjument-Bromage, P. Tempst, and J. Massagué (2009). Ubiquitin ligase nedd4l targets activated smad2/3 to limit tgf-β signaling. *Molecular cell 36*(3), 457–468.

Germain, S., M. Howell, G. M. Esslemont, and C. S. Hill (2000). Homeodomain and winged-helix transcription factors recruit activated smads to distinct promoter elements via a common smad interaction motif. *Genes & development 14*(4), 435–451.

Ghosh, P., N. M. Dahms, and S. Kornfeld (2003). Mannose 6-phosphate receptors: new twists in the tale. *Nature reviews Molecular cell biology 4*(3), 202–213.

Giles, R. H., J. H. van Es, and H. Clevers (2003). Caught up in a wnt storm: Wnt signaling in cancer. *Biochimica et Biophysica Acta (BBA)-Reviews on Cancer 1653*(1), 1–24.

Gomis, R. R., C. Alarcón, C. Nadal, C. Van Poznak, and J. Massagué (2006). C/ebpβ at the core of the tgfβ cytostatic response and its evasion in metastatic breast cancer cells. *Cancer cell 10*(3), 203–214.

Goumans, M.-J., G. Valdimarsdottir, S. Itoh, A. Rosendahl, P. Sideras, and P. ten Dijke (2002). Balancing the activation state of the endothelium via two distinct tgf-β type i receptors. *The EMBO journal 21*(7), 1743–1753.

Grainger, D. J., L. Wakefield, H. W. Bethell, R. W. Farndale, and J. C. Metcalfe (1995). Release and activation of platelet latent tgf–β in blood clots during dissolution with plasmin. *Nature medicine 1*(9), 932–937.

Green, J. B., A. E. Timmcke, W. T. Mitchell, T. C. Hicks, J. B. Gathright Jr, and J. E. Ray (1993). Mucinous carcinomaâĂŤjust another colon cancer? *Diseases of the colon & rectum 36*(1), 49–54.

Gu, A.-D., S. Zhang, Y. Wang, H. Xiong, T. A. Curtis, and Y. Y. Wan (2015). A critical role for transcription factor smad4 in t cell function that is independent of transforming growth factor β receptor signaling. *Immunity 42*(1), 68–79.

Guo, W. and F. G. Giancotti (2004). Integrin signalling during tumour progression. *Nature reviews Molecular cell biology 5*(10), 816–826.

Haapamäki, M., J. Grönroos, H. Nurmi, K. Alanen, M. Kallajoki, and T. Nevalainen (1997). Gene expression of group ii phospholipase a2 in intestine in ulcerative colitis. *Gut 40*(1), 95–101.

Hamamoto, T., H. Beppu, H. Okada, M. Kawabata, T. Kitamura, K. Miyazono, and M. Kato (2002). Compound disruption of smad2 accelerates malignant progression of intestinal tumors in apc knockout mice. *Cancer research 62*(20), 5955–5961.

Hao, H.-X., Y. Xie, Y. Zhang, O. Charlat, E. Oster, M. Avello, H. Lei, C. Mickanin, D. Liu, H. Ruffner, et al. (2012). Znrf3 promotes wnt receptor turnover in an r-spondin-sensitive manner. *Nature 485*(7397), 195–200.

Haramis, A.-P. G., H. Begthel, M. van den Born, J. van Es, S. Jonkheer, G. J. A. Offerhaus, and H. Clevers (2004). De novo crypt formation and juvenile polyposis on bmp inhibition in mouse intestine. *Science 303*(5664), 1684–1686.

Hardwick, J. C., L. L. Kodach, G. J. Offerhaus, and G. R. Van den Brink (2008). Bone morphogenetic protein signalling in colorectal cancer. *Nature Reviews Cancer 8*(10), 806–812.

Harper, J., J. L. Burns, E. J. Foulstone, M. Pignatelli, S. Zaina, and A. B. Hassan (2006). Soluble igf2 receptor rescues apcmin/+ intestinal adenoma progression induced by igf2 loss of imprinting. *Cancer research 66*(4), 1940–1948.

Hassan, A. B. (2003). Keys to the hidden treasures of the mannose 6-phosphate/insulin-like growth factor 2 receptor. *The American journal of pathology 162*(1), 3–6.

He, T.-C., A. B. Sparks, C. Rago, H. Hermeking, L. Zawel, L. T. da Costa, P. J. Morin, B. Vogelstein, and K. W. Kinzler (1998). Identification of c-myc as a target of the apc pathway. *Science 281*(5382), 1509–1512.

He, W., D. C. Dorn, H. Erdjument-Bromage, P. Tempst, M. A. Moore, and J. Massague (2006). Hematopoiesis controlled by distinct tif1γ and smad4 branches of the tgfβ pathway. *Cell 125*(5), 929–941.

He, X. C., J. Zhang, W.-G. Tong, O. Tawfik, J. Ross, D. H. Scoville, Q. Tian, X. Zeng, X. He, L. M. Wiedemann, et al. (2004). Bmp signaling inhibits intestinal stem cell self-renewal through suppression of wnt–β-catenin signaling. *Nature genetics 36*(10), 1117–1121.

Hébert, E. (2006). Mannose-6-phosphate/insulin-like growth factor ii receptor expression and tumor development. *Bioscience reports 26*, 7–17.

Heldin, C.-H. and A. Moustakas (2012). Role of smads in tgfβ signaling. *Cell and tissue research 347*(1), 21–36.

Heldin, C.-H., M. Vanlandewijck, and A. Moustakas (2012). Regulation of emt by tgfβ in cancer. *FEBS letters 586*(14), 1959–1970.

Heng, B. C., C. P. Ye, H. Liu, W. S. Toh, A. J. Rufaihah, Z. Yang, B. H. Bay, Z. Ge, H. W. Ouyang, E. H. Lee, et al. (2006). Loss of viability during freeze–thaw of intact and adherent human embryonic stem cells with conventional slow-cooling protocols is predominantly due toâŘč apoptosis rather than cellular necrosis. *Journal of biomedical science 13*(3), 433–445.

Herbst, A., V. Jurinovic, S. Krebs, S. E. Thieme, H. Blum, B. Göke, and F. T. Kolligs (2014). Comprehensive analysis of β-catenin target genes in colorectal carcinoma cell lines with deregulated wnt/β-catenin signaling. *BMC genomics 15*(1), 74.

Hesling, C., L. Fattet, G. Teyre, D. Jury, P. Gonzalo, J. Lopez, C. Vanbelle, A.-P. Morel, G. Gillet, I. Mikaelian, et al. (2011). Antagonistic regulation of emt by tif1γ and smad4 in mammary epithelial cells. *EMBO reports 12*(7), 665–672.

Heuberger, J. and W. Birchmeier (2010). Interplay of cadherin-mediated cell adhesion and canonical wnt signaling. *Cold Spring Harbor perspectives in biology 2*(2), a002915.

Hiraga, Y., S. Tanaka, K. Haruma, M. Yoshihara, K. Sumii, G. Kajiyama, F. Shimamoto, and N. Kohno (1998). Immunoreactive muc1 expression at the deepest invasive portion correlates with prognosis of colorectal cancer. *Oncology 55*(4), 307–319.

Hocevar, B. A., T. L. Brown, and P. H. Howe (1999). Tgf-β induces fibronectin synthesis through ac-jun n-terminal kinase-dependent, smad4-independent pathway. *The EMBO Journal 18*(5), 1345–1356.

Hollingsworth, M. A. and B. J. Swanson (2004). Mucins in cancer: protection and control of the cell surface. *Nature Reviews Cancer 4*(1), 45–60.

Hollnagel, A., V. Oehlmann, J. Heymer, U. Rüther, and A. Nordheim (1999). Id genes are direct targets of bone morphogenetic protein induction in embryonic stem cells. *Journal of Biological Chemistry 274*(28), 19838–19845.

Huber, M. A., N. Kraut, and H. Beug (2005). Molecular requirements for epithelial–mesenchymal transition during tumor progression. *Current opinion in cell biology 17*(5), 548–558.

Hughes, J., S. Frago, C. Bühnemann, E. J. Carter, and A. B. Hassan (2013). Maternal transmission of a humanised igf2r allele results in an igf2 dependent hypomorphic and non-viable growth phenotype. *PloS one 8*(2), e57270.

Hyytiäinen, M., C. Penttinen, and J. Keski-Oja (2004). Latent tgf-β binding proteins: extracellular matrix association and roles in tgf-β activation. *Critical reviews in clinical laboratory sciences 41*(3), 233–264.

Iacopetta, B. J., J. Welch, R. Soong, A. K. House, X.-P. Zhou, and R. Hamelin (1998). Mutation of the transforming growth factor-β type ii receptor gene in right-sided colorectal cancer: relationship to clinicopathological features and genetic alterations. *The Journal of pathology 184*(4), 390–395.

Ignotz, R. A. and J. Massague (1986). Transforming growth factor-beta stimulates the expression of fibronectin and collagen and their incorporation into the extracellular matrix. *Journal of Biological Chemistry 261*(9), 4337–4345.

Ijichi, H., M. Otsuka, K. Tateishi, T. Ikenoue, T. Kawakami, F. Kanai, Y. Arakawa, N. Seki, K. Shimizu, K. Miyazono, et al. (2004). Smad4-independent regulation of p21/waf1 by transforming growth factor-β. *Oncogene 23*(5), 1043–1051.

Ikushima, H. and K. Miyazono (2010). Tgfβ signalling: a complex web in cancer progression. *Nature Reviews Cancer 10*(6), 415–424.

Inman, G. J. (2011). Switching tgfβ from a tumor suppressor to a tumor promoter. *Current opinion in genetics & development 21*(1), 93–99.

Inman, G. J. and C. S. Hill (2002). Stoichiometry of active smad-transcription factor complexes on dna. *Journal of Biological Chemistry 277*(52), 51008–51016.

Inman, G. J., F. J. Nicolás, and C. S. Hill (2002). Nucleocytoplasmic shuttling of smads 2, 3, and 4 permits sensing of tgf-β receptor activity. *Molecular cell 10*(2), 283–294.

Inoue, Y. and T. Imamura (2008). Regulation of tgf-β family signaling by e3 ubiquitin ligases. *Cancer science 99*(11), 2107–2112.

Inui, M., A. Manfrin, A. Mamidi, G. Martello, L. Morsut, S. Soligo, E. Enzo, S. Moro, S. Polo, S. Dupont, et al. (2011). Usp15 is a deubiquitylating enzyme for receptor-activated smads. *Nature cell biology 13*(11), 1368–1375.

Isogaya, K., D. Koinuma, S. Tsutsumi, R.-A. Saito, K. Miyazawa, H. Aburatani, and K. Miyazono (2014). A smad3 and ttf-1/nkx2-1 complex regulates smad4-independent gene expression. *Cell research 24*(8), 994–1008.

Jazag, A., H. Ijichi, F. Kanai, T. Imamura, B. Guleng, M. Ohta, J. Imamura, Y. Tanaka, K. Tateishi, T. Ikenoue, et al. (2005). Smad4 silencing in pancreatic cancer cell lines using stable rna interference and gene expression profiles induced by transforming growth factor-β. *Oncogene 24*(4), 662–671.

Kakar, S., S. Aksoy, L. J. Burgart, and T. C. Smyrk (2004). Mucinous carcinoma of the colon: correlation of loss of mismatch repair enzymes with clinicopathologic features and survival. *Modern pathology 17*(6), 696–700.

Karim, B. O. and D. L. Huso (2013). Mouse models for colorectal cancer. *American journal of cancer research 3*(3), 240.

Kim, B.-G., C. Li, W. Qiao, M. Mamura, B. Kasperczak, M. Anver, L. Wolfraim, S. Hong, E. Mushinski, M. Potter, et al. (2006). Smad4 signalling in t cells is required for suppression of gastrointestinal cancer. *Nature 441*(7096), 1015–1019.

Kim, J. B. (2005). Three-dimensional tissue culture models in cancer biology. In *Seminars in cancer biology*, Volume 15, pp. 365–377. Elsevier.

Kim, J. H., K.-J. Kim, Y.-Y. Rhee, J. M. Bae, N.-Y. Cho, H. S. Lee, and G. H. Kang (2015). Gastric-type expression signature in serrated pathway-associated colorectal tumors. *Human Pathology*.

Kim, K.-A., M. Kakitani, J. Zhao, T. Oshima, T. Tang, M. Binnerts, Y. Liu, B. Boyle, E. Park, P. Emtage, et al. (2005). Mitogenic influence of human r-spondin1 on the intestinal epithelium. *Science 309*(5738), 1256–1259.

Kim, K. M., T. K. Yu, H. H. Chu, H. S. Park, K. Y. Jang, W. S. Moon, M. J. Kang, D. G. Lee, M. H. Kim, J. H. Lee, et al. (2012). Expression of er stress and autophagy-related molecules in human non-small cell lung cancer and premalignant lesions. *International Journal of Cancer 131*(4), E362–E370.

Kim, P. J., J. Plescia, H. Clevers, E. R. Fearon, and D. C. Altieri (2003). Survivin and molecular pathogenesis of colorectal cancer. *The Lancet 362*(9379), 205–209.

Kim, S.-W., K. Ramasamy, H. Bouamar, A.-P. Lin, D. Jiang, and R. C. Aguiar (2012). Microrna mir-125a and mir-125b constitutively activate the nf-κb pathway by targeting the tumor necrosis factor alpha-induced protein 3 (tnfaip3, a20). *Proceedings of the National Academy of Sciences 109*(20), 7865–7870.

Kitamura, T., K. Biyajima, M. Aoki, M. Oshima, and M. M. Taketo (2009). Matrix metalloproteinase 7 is required for tumor formation, but dispensable for invasion and fibrosis in smad4-deficient intestinal adenocarcinomas. *Laboratory Investigation 89*(1), 98–105.

Kitamura, T., K. Kometani, H. Hashida, A. Matsunaga, H. Miyoshi, H. Hosogi, M. Aoki, M. Oshima, M. Hattori, A. Takabayashi, et al. (2007). Smad4-deficient intestinal tumors recruit ccr1+ myeloid cells that promote invasion. *Nature genetics 39*(4), 467–475.

Klymkowsky, M. W. and P. Savagner (2009). Epithelial-mesenchymal transition: a cancer researcher's conceptual friend and foe. *The American journal of pathology 174*(5), 1588–1593.

Koinuma, D., S. Tsutsumi, N. Kamimura, H. Taniguchi, K. Miyazawa, M. Sunamura, T. Imamura, K. Miyazono, and H. Aburatani (2009). Chromatin immunoprecipitation on microarray analysis of smad2/3 binding sites reveals roles of ets1 and tfap2a in transforming growth factor β signaling. *Molecular and cellular biology 29*(1), 172–186.

Koo, B.-K., M. Spit, I. Jordens, T. Y. Low, D. E. Stange, M. van de Wetering, J. H. van Es, S. Mohammed, A. J. Heck, M. M. Maurice, et al. (2012). Tumour suppressor rnf43 is a stem-cell e3 ligase that induces endocytosis of wnt receptors. *Nature 488*(7413), 665–669.

Koo, B.-K., D. E. Stange, T. Sato, W. Karthaus, H. F. Farin, M. Huch, J. H. van Es, and H. Clevers (2012). Controlled gene expression in primary lgr5 organoid cultures. *Nature methods 9*(1), 81–83.

Korchynskyi, O. and P. ten Dijke (2002). Identification and functional characterization of distinct critically important bone morphogenetic protein-specific response elements in the id1 promoter. *Journal of Biological Chemistry 277*(7), 4883–4891.

Korinek, V., N. Barker, P. J. Morin, D. van Wichen, R. de Weger, K. W. Kinzler, B. Vogelstein, and H. Clevers (1997). Constitutive transcriptional activation by a β-catenin-tcf complex in apc-/- colon carcinoma. *Science 275*(5307), 1784–1787.

Kowanetz, M., U. Valcourt, R. Bergström, C.-H. Heldin, and A. Moustakas (2004). Id2 and id3 define the potency of cell proliferation and differentiation responses to transforming growth factor β and bone morphogenetic protein. *Molecular and cellular biology 24*(10), 4241–4254.

Kozak, M. M., R. von Eyben, J. Pai, S. R. Vossler, M. Limaye, P. Jayachandran, E. M. Anderson, J. L. Shaffer, T. Longacre, R. K. Pai, et al. (2015). Smad4 inactivation predicts for worse prognosis and response to fluorouracil-based treatment in colorectal cancer. *Journal of clinical pathology 68*(5), 341–345.

Krausova, M. and V. Korinek (2014). Wnt signaling in adult intestinal stem cells and cancer. *Cellular signalling 26*(3), 570–579.

Kretschmer, A., K. Moepert, S. Dames, M. Sternberger, J. Kaufmann, and A. Klippel (2003). Differential regulation of tgf-β signaling through smad2, smad3 and smad4. *Oncogene 22*(43), 6748–6763.

Kufe, D. W. (2009). Mucins in cancer: function, prognosis and therapy. *Nature Reviews Cancer 9*(12), 874–885.

Kurokawa, M., K. Mitani, K. Irie, T. Matsuyama, T. Takahashi, S. Chiba, Y. Yazaki, K. Matsumoto, and H. Hirai (1998). The oncoprotein evi-1 represses tgf-β signalling by inhibiting smad3. *Nature 394*(6688), 92–96.

Kutz, S. M., J. Hordines, P. J. McKeown-Longo, and P. J. Higgins (2001). Tgf-β1-induced pai-1 gene expression requires mek activity and cell-to-substrate adhesion. *Journal of Cell Science 114*(21), 3905–3914.

Labbé, E., L. Lock, A. Letamendia, A. E. Gorska, R. Gryfe, S. Gallinger, H. L. Moses, and L. Attisano (2007). Transcriptional cooperation between the transforming growth factor-β and wnt pathways in mammary and intestinal tumorigenesis. *Cancer research 67*(1), 75–84.

Lamouille, S., J. Xu, and R. Derynck (2014). Molecular mechanisms of epithelial–mesenchymal transition. *Nature reviews Molecular cell biology 15*(3), 178–196.

Langner, C., L. Harbaum, M. J. Pollheimer, P. Kornprat, R. A. Lindtner, A. Schlemmer, M. Vieth, and P. Rehak (2012). Mucinous differentiation in colorectal cancer–indicator of poor prognosis? *Histopathology 60*(7), 1060–1072.

Lao, V. V. and W. M. Grady (2011). Epigenetics and colorectal cancer. *Nature Reviews Gastroenterology and Hepatology 8*(12), 686–700.

Larue, L. and A. Bellacosa (2005). Epithelial–mesenchymal transition in development and cancer: role of phosphatidylinositol 3âĂš kinase/akt pathways. *Oncogene 24*(50), 7443–7454.

Lasorella, A., R. Benezra, and A. Iavarone (2014). The id proteins: master regulators of cancer stem cells and tumour aggressiveness. *Nature Reviews Cancer 14*(2), 77–91.

Lau, M., C. Stewart, Z. Liu, H. Bhatt, P. Rotwein, and C. L. Stewart (1994). Loss of the imprinted igf2/cation-independent mannose 6-phosphate receptor results in fetal overgrowth and perinatal lethality. *Genes & Development 8*(24), 2953–2963.

Leary, R. J., J. C. Lin, J. Cummins, S. Boca, L. D. Wood, D. W. Parsons, S. Jones, T. Sjöblom, B.-H. Park, R. Parsons, et al. (2008). Integrated analysis of homozygous deletions, focal amplifications, and sequence alterations in breast and colorectal cancers. *Proceedings of the National Academy of Sciences 105*(42), 16224–16229.

Lee, G. Y., P. A. Kenny, E. H. Lee, and M. J. Bissell (2007). Three-dimensional culture models of normal and malignant breast epithelial cells. *Nature methods 4*(4), 359–365.

Leedham, S. J., P. Rodenas-Cuadrado, K. Howarth, A. Lewis, S. Mallappa, S. Segditsas, H. Davis, R. Jeffery, M. Rodriguez-Justo, S. Keshav, et al. (2012). A basal gradient of wnt and stem-cell number influences regional tumour distribution in human and mouse intestinal tracts. *Gut*, gutjnl–2011.

Leung, S. Y., X. Chen, K. M. Chu, S. T. Yuen, J. Mathy, J. Ji, A. S. Chan, R. Li, S. Law, O. G. Troyanskaya, et al. (2002). Phospholipase a2 group iia expression in gastric adenocarcinoma is associated with prolonged survival and less frequent metastasis. *Proceedings of the National Academy of Sciences 99*(25), 16203–16208.

Levy, L. and C. S. Hill (2005). Smad4 dependency defines two classes of transforming growth factor β (tgf-β) target genes and distinguishes tgf-β-induced epithelial-mesenchymal transition from its antiproliferative and migratory responses. *Molecular and cellular biology 25*(18), 8108–8125.

Li, D., N. Kang, J. Ji, and Q. Zhan (2015). Brca1 regulates transforming growth factor-β (tgf-β1) signaling through gadd45a by enhancing the protein stability of smad4. *Molecular Oncology*.

Li, F., G. Ambrosini, E. Y. Chu, J. Plescia, S. Tognin, P. C. Marchisio, and D. C. Altieri (1998). Control of apoptosis and mitotic spindle checkpoint by survivin. *Nature 396*(6711), 580–584.

Li, V. S. and H. Clevers (2012). In vitro expansion and transplantation of intestinal crypt stem cells. *Gastroenterology 143*(1), 30–34.

Li, V. S., S. S. Ng, P. J. Boersema, T. Y. Low, W. R. Karthaus, J. P. Gerlach, S. Mohammed, A. J. Heck, M. M. Maurice, T. Mahmoudi, et al. (2012). Wnt signaling through inhibition of β-catenin degradation in an intact axin1 complex. *Cell 149*(6), 1245–1256.

Li, X., L. Nadauld, A. Ootani, D. C. Corney, R. K. Pai, O. Gevaert, M. A. Cantrell, P. G. Rack, J. T. Neal, C. W. Chan, et al. (2014). Oncogenic transformation of diverse gastrointestinal tissues in primary organoid culture. *Nature medicine 20*(7), 769–777.

Li, Z., X. Dong, Z. Wang, W. Liu, N. Deng, Y. Ding, L. Tang, T. Hla, R. Zeng, L. Li, et al. (2005). Regulation of pten by rho small gtpases. *Nature cell biology 7*(4), 399–404.

Liang, M., Y.-Y. Liang, K. Wrighton, D. Ungermannova, X.-P. Wang, F. C. Brunicardi, X. Liu, X.-H. Feng, and X. Lin (2004). Ubiquitination and proteolysis of cancer-derived smad4 mutants by scfskp2. *Molecular and cellular biology 24*(17), 7524–7537.

Liang, Y.-Y., F. C. Brunicardi, and X. Lin (2009). Smad3 mediates immediate early induction of id1 by tgf-β. *Cell research 19*(1), 140–148.

Lim, S. K. and F. M. Hoffmann (2006). Smad4 cooperates with lymphoid enhancer-binding factor 1/t cell-specific factor to increase c-myc expression in the absence of tgf-β signaling. *Proceedings of the National Academy of Sciences 103*(49), 18580–18585.

Ling, M., X. Wang, S. Tsao, and Y. Wong (2002). Down-regulation of id-1 expression is associated with tgfβ1-induced growth arrest in prostate epithelial cells. *Biochimica et Biophysica Acta (BBA)-General Subjects 1570*(3), 145–152.

Liu, F., C. Pouponnot, and J. Massagué (1997). Dual role of the smad4/dpc4 tumor suppressor in tgfβ-inducible transcriptional complexes. *Genes & development 11*(23), 3157–3167.

Liu, I. M., S. H. Schilling, K. A. Knouse, L. Choy, R. Derynck, and X.-F. Wang (2009). Tgfβ-stimulated smad1/5 phosphorylation requires the alk5 l45 loop and mediates the pro-migratory tgfβ switch. *The EMBO Journal 28*(2), 88–98.

Liu, W., X. Dong, M. Mai, R. S. Seelan, K. Taniguchi, K. K. Krishnadath, K. C. Halling, J. M. Cunningham, C. Qian, E. Christensen, et al. (2000). Mutations in axin2 cause colorectal cancer with defective mismatch repair by activating β-catenin/tcf signalling. *Nature genetics 26*(2), 146–147.

Ludwig, T., J. Eggenschwiler, P. Fisher, A. J. D'Ercole, M. L. Davenport, and A. Efstratiadis (1996). Mouse mutants lacking the type 2 igf receptor (igf2r) are rescued from perinatal lethality inigf2andigf1rnull backgrounds. *Developmental biology 177*(2), 517–535.

Luo, K. (2004). Ski and snon: negative regulators of tgf-β signaling. *Current opinion in genetics & development 14*(1), 65–70.

Lustig, B., B. Jerchow, M. Sachs, S. Weiler, T. Pietsch, U. Karsten, M. van de Wetering, H. Clevers, P. M. Schlag, W. Birchmeier, et al. (2002). Negative feedback loop of wnt signaling through upregulation of conductin/axin2 in colorectal and liver tumors. *Molecular and cellular biology 22*(4), 1184–1193.

MacPhee, M., K. P. Chepenik, R. A. Liddell, K. K. Nelson, L. D. Siracusa, and A. M. Buchberg (1995). The secretory phospholipase a2 gene is a candidate for the mom1 locus, a major modifier of apcmin-induced intestinal neoplasia. *Cell 81*(6), 957–966.

Maher, C. A., C. Kumar-Sinha, X. Cao, S. Kalyana-Sundaram, B. Han, X. Jing, L. Sam, T. Barrette, N. Palanisamy, and A. M. Chinnaiyan (2009). Transcriptome sequencing to detect gene fusions in cancer. *Nature 458*(7234), 97–101.

March, H. N., A. G. Rust, N. A. Wright, J. ten Hoeve, J. de Ridder, M. Eldridge, L. van der Weyden, A. Berns, J. Gadiot, A. Uren, et al. (2011). Insertional mutagenesis identifies multiple networks of cooperating genes driving intestinal tumorigenesis. *Nature genetics 43*(12), 1202–1209.

Martin-Ibanez, R., C. Unger, A. Strömberg, D. Baker, J. Canals, and O. Hovatta (2008). Novel cryopreservation method for dissociated human embryonic stem cells in the presence of a rock inhibitor. *Human Reproduction 23*(12), 2744–2754.

Massagué, J. (1998). Tgf-β signal transduction. *Annual review of biochemistry 67*(1), 753–791.

Massagué, J. (2008). Tgfβ in cancer. *Cell 134*(2), 215–230.

Massagué, J. (2012). Tgfβ signalling in context. *Nature reviews Molecular cell biology 13*(10), 616–630.

Massagué, J. et al. (1997). Repression of the cdk activator cdc25a and cell-cycle arrest by cytokine tgf-β in cells lacking the cdk inhibitor p15. *Nature 387*(6631), 417–422.

Massagué, J. and R. R. Gomis (2006). The logic of tgfβ signaling. *FEBS letters 580*(12), 2811–2820.

Massagué, J., J. Seoane, and D. Wotton (2005). Smad transcription factors. *Genes & development 19*(23), 2783–2810.

Matano, M., S. Date, M. Shimokawa, A. Takano, M. Fujii, Y. Ohta, T. Watanabe, T. Kanai, and T. Sato (2015). Modeling colorectal cancer using crispr-cas9-mediated engineering of human intestinal organoids. *Nature medicine*.

Matheson, J. (2012). *E-Cadherin loss of function in the murine intestine*. Ph. D. thesis, University of Oxford.

McCart, A. E., N. K. Vickaryous, and A. Silver (2008). Apc mice: models, modifiers and mutants. *Pathology-Research and Practice 204*(7), 479–490.

McKinsey, T. A. and D. A. Kass (2007). Small-molecule therapies for cardiac hypertrophy: moving beneath the cell surface. *Nature Reviews Drug Discovery 6*(8), 617–635.

Medema, J. P. and L. Vermeulen (2011). Microenvironmental regulation of stem cells in intestinal homeostasis and cancer. *Nature 474*(7351), 318–326.

Miyaki, M., T. Iijima, M. Konishi, K. Sakai, A. Ishii, M. Yasuno, T. Hishima, M. Koike, N. Shitara, T. Iwama, et al. (1999). Higher frequency of smad4 gene mutation in human colorectal cancer with distant metastasis. *Oncogene 18*(20), 3098–3103.

Miyoshi, H. and T. S. Stappenbeck (2013). In vitro expansion and genetic modification of gastrointestinal stem cells in spheroid culture. *Nature protocols 8*(12), 2471–2482.

Montojo, J., K. Zuberi, H. Rodriguez, G. D. Bader, and Q. Morris (2014). Genemania: fast gene network construction and function prediction for cytoscape. *F1000Research 3*.

Morin, P. J., A. B. Sparks, V. Korinek, N. Barker, H. Clevers, B. Vogelstein, and K. W. Kinzler (1997). Activation of β-catenin-tcf signaling in colon cancer by mutations in β-catenin or apc. *Science 275*(5307), 1787–1790.

Moser, A. R., E. M. Mattes, W. F. Dove, M. J. Lindstrom, J. D. Haag, and M. N. Gould (1993). Apcmin, a mutation in the murine apc gene, predisposes to mammary carcinomas and focal alveolar hyperplasias. *Proceedings of the National Academy of Sciences 90*(19), 8977–8981.

Moser, A. R., H. C. Pitot, and W. F. Dove (1990). A dominant mutation that predisposes to multiple intestinal neoplasia in the mouse. *Science 247*(4940), 322–324.

Mulherkar, R., R. Rao, L. Rao, V. Patki, V. Chauhan, and M. G. Deo (1993). Enhancing factor protein from mouse small intestines belongs to the phospholipase a2 family. *FEBS letters 317*(3), 263–266.

Muñoz, N. M., M. Upton, A. Rojas, M. K. Washington, L. Lin, A. Chytil, E. G. Sozmen, B. B. Madison, A. Pozzi, R. T. Moon, et al. (2006). Transforming growth factor β receptor type ii inactivation induces the malignant transformation of intestinal neoplasms initiated by apc mutation. *Cancer research 66*(20), 9837–9844.

Nagarajan, R. P., J. Zhang, W. Li, and Y. Chen (1999). Regulation of smad7 promoter by direct association with smad3 and smad4. *Journal of Biological Chemistry 274*(47), 33412–33418.

Nakamori, S., D. M. Ota, K. R. Cleary, K. Shirotani, and T. Irimura (1994). Muc1 mucin expression as a marker of progression and metastasis of human colorectal carcinoma. *GASTROENTEROLOGY-BALTIMORE THEN PHILADELPHIA- 106*, 353–353.

Network, C. G. A. et al. (2012). Comprehensive molecular characterization of human colon and rectal cancer. *Nature 487*(7407), 330–337.

Nicolas, F. J. and C. S. Hill (2003). Attenuation of the tgf-β-smad signaling pathway in pancreatic tumor cells confers resistance to tgf-β-induced growth arrest. *Oncogene 22*(24), 3698–3711.

Nieto, M. A. (2002). The snail superfamily of zinc-finger transcription factors. *Nature reviews Molecular cell biology 3*(3), 155–166.

Nishisho, I., Y. Nakamura, Y. Miyoshi, Y. Miki, H. Ando, A. Horii, K. Koyama, J. Utsunomiya, S. Baba, and P. Hedge (1991). Mutations of chromosome 5q21 genes in fap and colorectal cancer patients. *Science 253*(5020), 665–669.

Nusse, R. (2012). Wnt signaling. *Cold Spring Harbor perspectives in biology 4*(5), a011163.

Ootani, A., X. Li, E. Sangiorgi, Q. T. Ho, H. Ueno, S. Toda, H. Sugihara, K. Fujimoto, I. L. Weissman, M. R. Capecchi, et al. (2009). Sustained in vitro intestinal epithelial culture within a wnt-dependent stem cell niche. *Nature medicine 15*(6), 701–706.

Orsulic, S. and M. Peifer (1996). An in vivo structure-function study of armadillo, the beta-catenin homologue, reveals both separate and overlapping regions of the protein required for cell adhesion and for wingless signaling. *The Journal of cell biology 134*(5), 1283–1300.

Oshima, M., H. Oshima, K. Kitagawa, M. Kobayashi, C. Itakura, and M. Taketo (1995). Loss of apc heterozygosity and abnormal tissue building in nascent intestinal polyps in mice carrying a truncated apc gene. *Proceedings of the National Academy of Sciences 92*(10), 4482–4486.

Pan, Q., O. Shai, L. J. Lee, B. J. Frey, and B. J. Blencowe (2008). Deep surveying of alternative splicing complexity in the human transcriptome by high-throughput sequencing. *Nature genetics 40*(12), 1413–1415.

Peinado, H., D. Olmeda, and A. Cano (2007). Snail, zeb and bhlh factors in tumour progression: an alliance against the epithelial phenotype? *Nature Reviews Cancer 7*(6), 415–428.

Pierreux, C. E., F. J. Nicolás, and C. S. Hill (2000). Transforming growth factor β-independent shuttling of smad4 between the cytoplasm and nucleus. *Molecular and cellular biology 20*(23), 9041–9054.

Pohl, M., Y. Radacz, N. Pawlik, A. Schoeneck, S. E. Baldus, J. Munding, W. Schmiegel, I. Schwarte-Waldhoff, and A. Reinacher-Schick (2010). Smad4 mediates mesenchymal–epithelial reversion in sw480 colon carcinoma cells. *Anticancer research 30*(7), 2603–2613.

Pollak, M. (2008). Insulin and insulin-like growth factor signalling in neoplasia. *Nature Reviews Cancer 8*(12), 915–928.

Porter, E., C. Bevins, D. Ghosh, and T. Ganz (2002). The multifaceted paneth cell. *Cellular and molecular life sciences CMLS 59*(1), 156–170.

Powell, S. M., N. Zilz, Y. Beazer-Barclay, T. M. Bryan, S. R. Hamilton, S. N. Thibodeau, B. Vogelstein, and K. W. Kinzler (1992). Apc mutations occur early during colorectal tumorigenesis. *Nature 359*(6392), 235–237.

Prince, S. N., E. J. Foulstone, O. J. Zaccheo, C. Williams, and A. B. Hassan (2007). Functional evaluation of novel soluble insulin-like growth factor (igf)-ii–specific ligand traps based on modified domain 11 of the human igf2 receptor. *Molecular cancer therapeutics 6*(2), 607–617.

Ramjaun, A., S. Tomlinson, A. Eddaoudi, and J. Downward (2007). Upregulation of two bh3-only proteins, bmf and bim, during tgfβ-induced apoptosis. *Oncogene 26*(7), 970–981.

Rampersad, S. N. (2012). Multiple applications of alamar blue as an indicator of metabolic function and cellular health in cell viability bioassays. *Sensors 12*(9), 12347–12360.

Randall, R. A., S. Germain, G. J. Inman, P. A. Bates, and C. S. Hill (2002). Different smad2 partners bind a common hydrophobic pocket in smad2 via a defined proline-rich motif. *The EMBO journal 21*(1-2), 145–156.

Rask, K., M. Thörn, F. Pontén, W. Kraaz, K. Sundfeldt, L. Hedin, and S. Enerbäck (2000). Increased expression of the transcription factors ccaat-enhancer binding protein-b (c/ebb) and c/ebpζ (chop) correlate with invasiveness of human colorectal cancer. *International journal of cancer 86*(3), 337–343.

Rizk, P. and N. Barker (2012). Gut stem cells in tissue renewal and disease: methods, markers, and myths. *Wiley Interdisciplinary Reviews: Systems Biology and Medicine 4*(5), 475–496.

Rodrigues, P., I. Macaya, S. Bazzocco, R. Mazzolini, E. Andretta, H. Dopeso, S. Mateo-Lozano, J. Bilić, F. Cartón-García, R. Nieto, et al. (2014). Rhoa inactivation enhances wnt signalling and promotes colorectal cancer. *Nature communications 5*.

Ross, S., E. Cheung, T. G. Petrakis, M. Howell, W. L. Kraus, and C. S. Hill (2006). Smads orchestrate specific histone modifications and chromatin remodeling to activate transcription. *The EMBO journal 25*(19), 4490–4502.

Sancho, E., E. Batlle, and H. Clevers (2004). Signaling pathways in intestinal development and cancer. *Annu. Rev. Cell Dev. Biol. 20*, 695–723.

Sangiorgi, E. and M. R. Capecchi (2008). Bmi1 is expressed in vivo in intestinal stem cells. *Nature genetics 40*(7), 915–920.

Sansom, O. (2009). *Advances in Experimental Medicine and Biology*, Volume 656, Chapter Tissue-Specific Tumour Suppression by APC.

Sansom, O. J., V. S. Meniel, V. Muncan, T. J. Phesse, J. A. Wilkins, K. R. Reed, J. K. Vass, D. Athineos, H. Clevers, and A. R. Clarke (2007). Myc deletion rescues apc deficiency in the small intestine. *Nature 446*(7136), 676–679.

Sansom, O. J., K. R. Reed, A. J. Hayes, H. Ireland, H. Brinkmann, I. P. Newton, E. Batlle, P. Simon-Assmann, H. Clevers, I. S. Nathke, et al. (2004). Loss of apc in vivo immediately perturbs wnt signaling, differentiation, and migration. *Genes & development 18*(12), 1385–1390.

Sato, T. and H. Clevers (2013). *Primary mouse small intestinal epithelial cell cultures*. Springer.

Sato, T., D. E. Stange, M. Ferrante, R. G. Vries, J. H. Van Es, S. Van den Brink, W. J. Van Houdt, A. Pronk, J. Van Gorp, P. D. Siersema, et al. (2011). Long-term expansion of epithelial organoids from human colon, adenoma, adenocarcinoma, and barrett's epithelium. *Gastroenterology 141*(5), 1762–1772.

Sato, T., J. H. van Es, H. J. Snippert, D. E. Stange, R. G. Vries, M. van den Born, N. Barker, N. F. Shroyer, M. van de Wetering, and H. Clevers (2011). Paneth cells constitute the niche for lgr5 stem cells in intestinal crypts. *Nature 469*(7330), 415–418.

Sato, T., R. G. Vries, H. J. Snippert, M. van de Wetering, N. Barker, D. E. Stange, J. H. van Es, A. Abo, P. Kujala, P. J. Peters, et al. (2009). Single lgr5 stem cells build crypt villus structures in vitro without a mesenchymal niche. *Nature 459*(7244), 262–265.

Scandura, J. M., P. Boccuni, J. Massagué, and S. D. Nimer (2004). Transforming growth factor β-induced cell cycle arrest of human hematopoietic cells requires p57kip2 up-regulation. *Proceedings of the National Academy of Sciences of the United States of America 101*(42), 15231–15236.

Schmierer, B. and C. S. Hill (2007). Tgfβ–smad signal transduction: molecular specificity and functional flexibility. *Nature Reviews Molecular Cell Biology 8*(12), 970–982.

Schneider, C. A., W. S. Rasband, and K. W. Eliceiri (2012). Nih image to imagej: 25 years of image analysis. *Nature methods 9*(7), 671–675.

Semple, T. U., L. A. Quinn, L. K. Woods, and G. E. Moore (1978). Tumor and lymphoid cell lines from a patient with carcinoma of the colon for a cytotoxicity model. *Cancer research 38*(5), 1345–1355.

Seoane, J., H.-V. Le, L. Shen, S. A. Anderson, and J. Massagué (2004). Integration of smad and forkhead pathways in the control of neuroepithelial and glioblastoma cell proliferation. *Cell 117*(2), 211–223.

Seshagiri, S., E. W. Stawiski, S. Durinck, Z. Modrusan, E. E. Storm, C. B. Conboy, S. Chaudhuri, Y. Guan, V. Janakiraman, B. S. Jaiswal, et al. (2012). Recurrent r-spondin fusions in colon cancer. *Nature 488*(7413), 660–664.

Shanmugam, C., N. C. Jhala, V. R. Katkoori, W. Wan, S. Meleth, W. E. Grizzle, and U. Manne (2010). Prognostic value of mucin 4 expression in colorectal adenocarcinomas. *Cancer 116*(15), 3577–3586.

Shi, Y. and J. Massagué (2003). Mechanisms of tgf-β signaling from cell membrane to the nucleus. *Cell 113*(6), 685–700.

Shi, Y., Y.-F. Wang, L. Jayaraman, H. Yang, J. Massagué, and N. P. Pavletich (1998). Crystal structure of a smad mh1 domain bound to dna: insights on dna binding in tgf-β signaling. *Cell 94*(5), 585–594.

Shibata, H., K. Toyama, H. Shioya, M. Ito, M. Hirota, S. Hasegawa, H. Matsumoto, H. Takano, T. Akiyama, K. Toyoshima, et al. (1997). Rapid colorectal adenoma formation initiated by conditional targeting of the apc gene. *Science 278*(5335), 120–123.

Siegel, P. M. and J. Massagué (2003). Cytostatic and apoptotic actions of tgf-β in homeostasis and cancer. *Nature Reviews Cancer 3*(11), 807–820.

Simmini, S., M. Bialecka, M. Huch, L. Kester, M. van de Wetering, T. Sato, F. Beck, A. van Oudenaarden, H. Clevers, and J. Deschamps (2014). Transformation of intestinal stem cells into gastric stem cells on loss of transcription factor cdx2. *Nature communications 5*.

Sirard, C., J. L. de la Pompa, A. Elia, A. Itie, C. Mirtsos, A. Cheung, S. Hahn, A. Wakeham, L. Schwartz, S. E. Kern, et al. (1998). The tumor suppressor gene smad4/dpc4 is required for gastrulation and later for anterior development of the mouse embryo. *Genes & development 12*(1), 107–119.

Sirard, C., S. Kim, C. Mirtsos, P. Tadich, P. A. Hoodless, A. Itié, R. Maxson, J. L. Wrana, and T. W. Mak (2000). Targeted disruption in murine cells reveals variable requirement for smad4 in transforming growth factor β-related signaling. *Journal of Biological Chemistry 275*(3), 2063–2070.

Sleeman, J. P. and J. P. Thiery (2011). Snapshot: The epithelial-mesenchymal transition. *Cell 145*(1), 162–162.

Smit, M. A., T. R. Geiger, J.-Y. Song, I. Gitelman, and D. S. Peeper (2009). A twist-snail axis critical for trkb-induced epithelial-mesenchymal transition-like transformation, anoikis resistance, and metastasis. *Molecular and cellular biology 29*(13), 3722–3737.

Smits, R., M. F. Kielman, C. Breukel, C. Zurcher, K. Neufeld, S. Jagmohan-Changur, N. Hofland, J. van Dijk, R. White, W. Edelmann, et al. (1999). Apc1638t: a mouse model delineating critical domains of the adenomatous polyposis coli protein involved in tumorigenesis and development. *Genes & development 13*(10), 1309–1321.

Sodir, N. M., X. Chen, R. Park, A. E. Nickel, P. S. Conti, R. Moats, J. R. Bading, D. Shibata, and P. W. Laird (2006). Smad3 deficiency promotes tumorigenesis in the distal colon of apcmin/+ mice. *Cancer Research 66*(17), 8430–8438.

Souza, R. F., R. Appel, J. Yin, S. Wang, K. N. Smolinski, J. M. Abraham, T.-T. Zou, Y.-Q. Shi, J. Lei, J. Cottrell, et al. (1996). Microsatellite instability in the insulin–like growth factor ii receptor gene in gastrointestinal tumours. *Nature genetics 14*(3), 255–257.

Spagnuolo, G., V. DâĂŹAntò, C. Cosentino, G. Schmalz, H. Schweikl, and S. Rengo (2006). Effect of n-acetyl-l-cysteine on ros production and cell death caused by hema in human primary gingival fibroblasts. *Biomaterials 27*(9), 1803–1809.

Srinivas, S., T. Watanabe, C.-S. Lin, C. M. William, Y. Tanabe, T. M. Jessell, and F. Costantini (2001). Cre reporter strains produced by targeted insertion of eyfp and ecfp into the rosa26 locus. *BMC developmental biology 1*(1), 4.

Staal, F. J., F. Weerkamp, M. R. Baert, C. M. van den Burg, M. van Noort, E. F. de Haas, and J. J. van Dongen (2004). Wnt target genes identified by dna microarrays in immature cd34+ thymocytes regulate proliferation and cell adhesion. *The Journal of Immunology 172*(2), 1099–1108.

Starr, T. K., R. Allaei, K. A. Silverstein, R. A. Staggs, A. L. Sarver, T. L. Bergemann, M. Gupta, M. G. O'Sullivan, I. Matise, A. J. Dupuy, et al. (2009). A transposon-based genetic screen in mice identifies genes altered in colorectal cancer. *Science 323*(5922), 1747–1750.

Stemmer, V., B. De Craene, G. Berx, and J. Behrens (2008). Snail promotes wnt target gene expression and interacts with β-catenin. *Oncogene 27*(37), 5075–5080.

Sternberg, L. R., J. C. Byrd, C. K. Yunker, S. Dudas, V. K. Hoon, and R. S. Bresalier (1999). Liver colonization by human colon cancer cells is reduced by antisense inhibition of muc2 mucin synthesis. *Gastroenterology 116*(2), 363–371.

Su, L.-K., K. W. Kinzler, B. Vogelstein, A. C. Preisinger, A. R. Moser, C. Luongo, K. A. Gould, and W. F. Dove (1992). Multiple intestinal neoplasia caused by a mutation in the murine homolog of the apc gene. *Science 256*(5057), 668–670.

Subramanian, A., P. Tamayo, V. K. Mootha, S. Mukherjee, B. L. Ebert, M. A. Gillette, A. Paulovich, S. L. Pomeroy, T. R. Golub, E. S. Lander, et al. (2005). Gene set enrichment analysis: a knowledge-based approach for interpreting genome-wide expression profiles. *Proceedings of the National Academy of Sciences of the United States of America 102*(43), 15545–15550.

Tachibana, C. (2015). Transcriptomics today: Microarrays, rna-seq, and more. *Science 349*(6247), 544–546.

Takaku, K., H. Miyoshi, A. Matsunaga, M. Oshima, N. Sasaki, and M. M. Taketo (1999). Gastric and duodenal polyps in smad4 (dpc4) knockout mice. *Cancer research 59*(24), 6113–6117.

Takaku, K., M. Oshima, H. Miyoshi, M. Matsui, M. F. Seldin, and M. M. Taketo (1998). Intestinal tumorigenesis in compound mutant mice of both dpc4 (smad4) and apc genes. *Cell 92*(5), 645–656.

Taketo, M. M. (2012). Roles of stromal microenvironment in colon cancer progression. *Journal of biochemistry 151*(5), 477–481.

Taliano, R. J., M. LeGolvan, and M. B. Resnick (2013). Immunohistochemistry of colorectal carcinoma: current practice and evolving applications. *Human pathology 44*(2), 151–163.

Ten Dijke, P., M.-J. Goumans, F. Itoh, and S. Itoh (2002). Regulation of cell proliferation by smad proteins. *Journal of cellular physiology 191*(1), 1–16.

Tetsu, O. and F. McCormick (1999). β-catenin regulates expression of cyclin d1 in colon carcinoma cells. *Nature 398*(6726), 422–426.

Thevenot, P. T., R. A. Sierra, P. L. Raber, A. A. Al-Khami, J. Trillo-Tinoco, P. Zarreii, A. C. Ochoa, Y. Cui, L. Del Valle, and P. C. Rodriguez (2014). The stress-response sensor chop regulates the function and accumulation of myeloid-derived suppressor cells in tumors. *Immunity 41*(3), 389–401.

Thiery, J. P., H. Acloque, R. Y. Huang, and M. A. Nieto (2009). Epithelial-mesenchymal transitions in development and disease. *cell 139*(5), 871–890.

Thiery, J. P. and J. P. Sleeman (2006). Complex networks orchestrate epithelial–mesenchymal transitions. *Nature reviews Molecular cell biology 7*(2), 131–142.

Thuault, S., U. Valcourt, M. Petersen, G. Manfioletti, C.-H. Heldin, and A. Moustakas (2006). Transforming growth factor-β employs hmga2 to elicit epithelial–mesenchymal transition. *The Journal of cell biology 174*(2), 175–183.

Tian, H., B. Biehs, S. Warming, K. G. Leong, L. Rangell, O. D. Klein, and F. J. de Sauvage (2011). A reserve stem cell population in small intestine renders lgr5-positive cells dispensable. *Nature 478*(7368), 255–259.

Tjalsma, H., A. Boleij, J. R. Marchesi, and B. E. Dutilh (2012). A bacterial driver–passenger model for colorectal cancer: beyond the usual suspects. *Nature Reviews Microbiology 10*(8), 575–582.

Trapnell, C., A. Roberts, L. Goff, G. Pertea, D. Kim, D. R. Kelley, H. Pimentel, S. L. Salzberg, J. L. Rinn, and L. Pachter (2012). Differential gene and transcript expression analysis of rna-seq experiments with tophat and cufflinks. *Nature protocols 7*(3), 562–578.

Truett, G., P. Heeger, R. Mynatt, A. Truett, J. Walker, and M. Warman (2000). Preparation of pcr-quality mouse genomic dna with hot sodium hydroxide and tris (hotshot). *Biotechniques 29*(1), 52–54.

Tsukazaki, T., T. A. Chiang, A. F. Davison, L. Attisano, and J. L. Wrana (1998). Sara, a fyve domain protein that recruits smad2 to the tgfβ receptor. *Cell 95*(6), 779–791.

Vaishnava, S., M. Yamamoto, K. M. Severson, K. A. Ruhn, X. Yu, O. Koren, R. Ley, E. K. Wakeland, and L. V. Hooper (2011). The antibacterial lectin regiiiγ promotes the spatial segregation of microbiota and host in the intestine. *Science 334*(6053), 255–258.

Valcourt, U., M. Kowanetz, H. Niimi, C.-H. Heldin, and A. Moustakas (2005). Tgf-β and the smad signaling pathway support transcriptomic reprogramming during epithelial-mesenchymal cell transition. *Molecular biology of the cell 16*(4), 1987–2002.

van der Flier, L. G. and H. Clevers (2009). Stem cells, self-renewal, and differentiation in the intestinal epithelium. *Annual review of physiology 71*, 241–260.

van Iterson, M., S. Bervoets, E. J. de Meijer, H. P. Buermans, P. ACâĂŹt Hoen, R. X. Menezes, and J. M. Boer (2013). Integrated analysis of microrna and mrna expression: adding biological significance to microrna target predictions. *Nucleic acids research 41*(15), e146–e146.

Varelas, X., R. Sakuma, P. Samavarchi-Tehrani, R. Peerani, B. M. Rao, J. Dembowy, M. B. Yaffe, P. W. Zandstra, and J. L. Wrana (2008). Taz controls smad nucleocytoplasmic shuttling and regulates human embryonic stem-cell self-renewal. *Nature cell biology 10*(7), 837–848.

Vecsey-Semjen, B., K.-F. Becker, A. Sinski, E. Blennow, I. Vietor, K. Zatloukal, H. Beug, E. Wagner, and L. A. Huber (2002). Novel colon cancer cell lines leading to better understanding of the diversity of respective primary cancers. *Oncogene 21*(30), 4646–4662.

Vermeulen, L. and H. J. Snippert (2014). Stem cell dynamics in homeostasis and cancer of the intestine. *Nature Reviews Cancer 14*(7), 468–480.

Vijayachandra, K., W. Higgins, J. Lee, and A. Glick (2009). Induction of p16ink4a and p19arf by tgfβ1 contributes to growth arrest and senescence response in mouse keratinocytes. *Molecular carcinogenesis 48*(3), 181–186.

Vincent, T., E. P. Neve, J. R. Johnson, A. Kukalev, F. Rojo, J. Albanell, K. Pietras, I. Virtanen, L. Philipson, P. L. Leopold, et al. (2009). A snail1–smad3/4 transcriptional repressor complex promotes tgf-β mediated epithelial–mesenchymal transition. *Nature cell biology 11*(8), 943–950.

Voorneveld, P. W., L. L. Kodach, R. J. Jacobs, N. Liv, A. C. Zonnevylle, J. P. Hoogenboom, I. Biemond, H. W. Verspaget, D. W. Hommes, K. de Rooij, et al. (2014). Loss of smad4 alters bmp signaling to promote colorectal cancer cell metastasis via activation of rho and rock. *Gastroenterology 147*(1), 196–208.

Wagner, E. F. and Á. R. Nebreda (2009). Signal integration by jnk and p38 mapk pathways in cancer development. *Nature Reviews Cancer 9*(8), 537–549.

Wakefield, L. M. and C. S. Hill (2013). Beyond tgfβ: roles of other tgfβ superfamily members in cancer. *Nature Reviews Cancer 13*(5), 328–341.

Walther, A., E. Johnstone, C. Swanton, R. Midgley, I. Tomlinson, and D. Kerr (2009). Genetic prognostic and predictive markers in colorectal cancer. *Nature Reviews Cancer 9*(7), 489–499.

Wang, G., J. Long, I. Matsuura, D. He, and F. Liu (2005). The smad3 linker region contains a transcriptional activation domain. *Biochem. J 386*, 29–34.

Wang, W.-C., F.-M. Lin, W.-C. Chang, K.-Y. Lin, H.-D. Huang, and N.-S. Lin (2009). mirexpress: analyzing high-throughput sequencing data for profiling microrna expression. *BMC bioinformatics 10*(1), 328.

Wang, Z., M. Gerstein, and M. Snyder (2009). Rna-seq: a revolutionary tool for transcriptomics. *Nature Reviews Genetics 10*(1), 57–63.

Wang, Z.-Q., M. R. Fung, D. P. Barlow, and E. F. Wagner (1994). Regulation of embryonic growth and lysosomal targeting by the imprintedigf2/mpr gene.

Watanabe, K., M. Ueno, D. Kamiya, A. Nishiyama, M. Matsumura, T. Wataya, J. B. Takahashi, S. Nishikawa, S.-i. Nishikawa, K. Muguruma, et al. (2007). A rock inhibitor permits survival of dissociated human embryonic stem cells. *Nature biotechnology 25*(6), 681–686.

Watanabe, M., N. Masuyama, M. Fukuda, and E. Nishida (2000). Regulation of intracellular dynamics of smad4 by its leucine-rich nuclear export signal. *EMBO reports 1*(2), 176–182.

Wheelock, M. J., Y. Shintani, M. Maeda, Y. Fukumoto, and K. R. Johnson (2008). Cadherin switching. *Journal of cell science 121*(6), 727–735.

Wielenga, V. J., R. Smits, V. Korinek, L. Smit, M. Kielman, R. Fodde, H. Clevers, and S. T. Pals (1999). Expression of cd44 in apc and tcfmutant mice implies regulation by the wnt pathway. *The American journal of pathology 154*(2), 515–523.

Wiener, Z., A. M. Band, P. Kallio, J. Högström, V. Hyvönen, S. Kaijalainen, O. Ritvos, C. Haglund, O. Kruuna, S. Robine, et al. (2014). Oncogenic mutations in intestinal adenomas regulate bim-mediated apoptosis induced by tgf-β. *Proceedings of the National Academy of Sciences 111*(21), E2229–E2236.

Winesett, M. P., G. W. Ramsey, and J. A. Barnard (1996). Cancer biology: Type ii tgfβ receptor expression in intestinal cell lines and in the intestinal tract. *Carcinogenesis 17*(5), 989–995.

Wolfrum, S., A. Dendorfer, Y. Rikitake, T. J. Stalker, Y. Gong, R. Scalia, P. Dominiak, and J. K. Liao (2004). Inhibition of rho-kinase leads to rapid activation of phosphatidylinositol 3-kinase/protein kinase akt and cardiovascular protection. *Arteriosclerosis, thrombosis, and vascular biology 24*(10), 1842–1847.

Woodford-Richens, K., A. Rowan, P. Gorman, S. Halford, D. Bicknell, H. Wasan, R. Roylance, W. Bodmer, and I. Tomlinson (2001). Smad4 mutations in colorectal cancer probably occur before chromosomal instability, but after divergence of the microsatellite instability pathway. *Proceedings of the National Academy of Sciences 98*(17), 9719–9723.

Wrana, J. L. (2013). Signaling by the tgfβ superfamily. *Cold Spring Harbor perspectives in biology 5*(10), a011197.

Wrana, J. L., L. Attisano, J. Cárcamo, A. Zentella, J. Doody, M. Laiho, X.-F. Wang, and J. Massague (1992). Tgfβ signals through a heteromeric protein kinase receptor complex. *Cell 71*(6), 1003–1014.

Wylie, A. A., D. J. Pulford, A. J. McVie-Wylie, R. A. Waterland, H. K. Evans, Y.-T. Chen, C. M. Nolan, T. C. Orton, and R. L. Jirtle (2003). Tissue-specific inactivation of murine m6p/igf2r. *The American journal of pathology 162*(1), 321–328.

Xi, Q., W. He, X. H.-F. Zhang, H.-V. Le, and J. Massagué (2008). Genome-wide impact of the brg1 swi/snf chromatin remodeler on the transforming growth factor β transcriptional program. *Journal of Biological Chemistry 283*(2), 1146–1155.

Xiao, X., L. Wang, P. Wei, Y. Chi, D. Li, Q. Wang, S. Ni, C. Tan, W. Sheng, M. Sun, et al. (2013). Role of muc20 overexpression as a predictor of recurrence and poor outcome in colorectal cancer. *J Transl Med 11*, 151.

Xiao, Z., R. Latek, and H. F. Lodish (2003). An extended bipartite nuclear localization signal in smad4 is required for its nuclear import and transcriptional activity. *Oncogene 22*(7), 1057–1069.

Xiao, Z., X. Liu, Y. I. Henis, and H. F. Lodish (2000). A distinct nuclear localization signal in the n terminus of smad 3 determines its ligand-induced nuclear translocation. *Proceedings of the National Academy of Sciences 97*(14), 7853–7858.

Xu, L., Y. Kang, S. Çöl, and J. Massagué (2002). Smad2 nucleocytoplasmic shuttling by nucleoporins can/nup214 and nup153 feeds tgfβ signaling complexes in the cytoplasm and nucleus. *Molecular cell 10*(2), 271–282.

Xu, L., X. Yao, X. Chen, P. Lu, B. Zhang, and Y. T. Ip (2007). Msk is required for nuclear import of tgf-β/bmp-activated smads. *The Journal of cell biology 178*(6), 981–994.

Yamada, K. M. and E. Cukierman (2007). Modeling tissue morphogenesis and cancer in 3d. *Cell 130*(4), 601–610.

Yamazaki, K., Y. Masugi, K. Effendi, H. Tsujikawa, N. Hiraoka, M. Kitago, M. Shinoda, O. Itano, M. Tanabe, Y. Kitagawa, et al. (2014). Upregulated smad3 promotes epithelial–mesenchymal transition and predicts poor prognosis in pancreatic ductal adenocarcinoma. *Laboratory Investigation 94*(6), 683–691.

Yang, B., H. Guo, Y. Zhang, L. Chen, D. Ying, and S. Dong (2011). Microrna-145 regulates chondrogenic differentiation of mesenchymal stem cells by targeting sox9. *PloS one 6*(7), e21679.

Yang, J., K. Song, T. L. Krebs, M. W. Jackson, and D. Danielpour (2008). Rb/e2f4 and smad2/3 link survivin to tgf-β-induced apoptosis and tumor progression. *Oncogene 27*(40), 5326–5338.

Yang, T., J. L. Owen, Y. L. Lightfoot, M. P. Kladde, and M. Mohamadzadeh (2013). Microbiota impact on the epigenetic regulation of colorectal cancer. *Trends in molecular medicine 19*(12), 714–725.

Yoo, J., M. Ghiassi, L. Jirmanova, A. G. Balliet, B. Hoffman, A. J. Fornace, D. A. Liebermann, E. P. Böttinger, and A. B. Roberts (2003). Transforming growth factor-β-induced apoptosis is mediated by smad-dependent expression of gadd45b through p38 activation. *Journal of Biological Chemistry 278*(44), 43001–43007.

Young, M., L. Ordonez, and A. R. Clarke (2013). What are the best routes to effectively model human colorectal cancer? *Molecular oncology 7*(2), 178–189.

Yu, G., P. Jiang, Y. Xiang, Y. Zhang, Z. Zhu, C. Zhang, S. Lee, W. Lee, and Y. Zhang (2015). Increased expression of protease-activated receptor 4 and trefoil factor 2 in human colorectal cancer. *PloS one 10*(4).

Zaina, S. and S. Squire (1998). The soluble type 2 insulin-like growth factor (igf-ii) receptor reduces organ size by igf-ii-mediated and igf-ii-independent mechanisms. *Journal of Biological Chemistry 273*(44), 28610–28616.

Zambelli, F., G. Pesole, and G. Pavesi (2009). Pscan: finding over-represented transcription factor binding site motifs in sequences from co-regulated or co-expressed genes. *Nucleic acids research 37*(suppl 2), W247–W252.

Zawel, L., J. Le Dai, P. Buckhaults, S. Zhou, K. W. Kinzler, B. Vogelstein, and S. E. Kern (1998). Human smad3 and smad4 are sequence-specific transcription activators. *Molecular cell 1*(4), 611–617.

Zhang, B., X. Chen, S. Bae, K. Singh, M. Washington, and P. Datta (2014). Loss of smad4 in colorectal cancer induces resistance to 5-fluorouracil through activating akt pathway. *British journal of cancer 110*(4), 946–957.

Zhang, B., S. K. Halder, N. D. Kashikar, Y.-J. Cho, A. Datta, D. L. Gorden, and P. K. Datta (2010). Antimetastatic role of smad4 signaling in colorectal cancer. *Gastroenterology 138*(3), 969–980.

Zhao, S., K. Venkatasubbarao, J. W. Lazor, J. Sperry, C. Jin, L. Cao, and J. W. Freeman (2008). Inhibition of stat3tyr705 phosphorylation by smad4 suppresses transforming growth factor β–mediated invasion and metastasis in pancreatic cancer cells. *Cancer Research 68*(11), 4221–4228.

Zhong, X., A. C. Chung, H.-Y. Chen, X.-M. Meng, and H. Y. Lan (2011). Smad3-mediated upregulation of mir-21 promotes renal fibrosis. *Journal of the American Society of Nephrology 22*(9), 1668–1681.

Zhou, S., P. Buckhaults, L. Zawel, F. Bunz, G. Riggins, J. Le Dai, S. E. Kern, K. W. Kinzler, and B. Vogelstein (1998). Targeted deletion of smad4 shows it is required for transforming growth factor β and activin signaling in colorectal cancer cells. *Proceedings of the National Academy of Sciences 95*(5), 2412–2416.

Zhu, Y., J. A. Richardson, L. F. Parada, and J. M. Graff (1998). Smad3 mutant mice develop metastatic colorectal cancer. *Cell 94*(6), 703–714.

Zi, Z., D. A. Chapnick, and X. Liu (2012). Dynamics of tgf-β/smad signaling. *FEBS letters 586*(14), 1921–1928.